The University of Sheffield

Faculty of Engineering

Department of Materials Science and Engineering

Development of 3D vascularised cancer models

Caitlin E Jackson

A thesis submitted in fulfilment of the requirements for the degree of

Doctor of Philosophy

Submitted: September 2023

Abstract

Cancer is a becoming a huge social and economic burden on society, being the most significant barrier to life expectancy in the 21st century. One of the most significant difficulties to finding efficient therapies for specific cancers, such as breast cancer, is the efficiency and ease of drug development and testing. Micro-physiological systems (MPS) are under development to mimic the structural and biological complexity of human tissue, thus, becoming increasingly popular as an alternative to animal testing for pharmaceuticals.

High molecular weight polycaprolactone methacrylate (PCL-M) was used to fabricate polymerised high internal phase emulsions (polyHIPEs) scaffolds to support 3D breast cancer (MDA-MB-231) cell culture within MPS. The effect of varying production parameters on the polyHIPE properties was assessed. MDA-MB-231 cells were used to assess cell growth on PCL-M polyHIPE scaffolds. An *ex-ovo* chick chorioallantoic membrane (CAM) assay was used to assess the biocompatibility and potential for vascular invasion.

We demonstrated the tenability of the properties of the polyHIPEs via varying production processes. *Ex-ovo* CAM assays identified the scaffolds as bioinert. Further studies identified breast cancer cell seeded gelatin-containing PCL-M polyHIPE scaffolds as promising substrates to support angiogenesis. Furthermore, in vitro assessment of cell growth showed promising potential for the use of PCL-M polyHIPEs to support breast cancer cell growth. This indicates that PCL-M polyHIPE scaffolds show promise as a substrate for MPS to study 3D breast cancer cell culture with potential for vascularisation.

The project also included an industrial element, with research undertaken at GlaxoSmithKline. This research focussed on developing an *in vitro* vascularised tumour model for oncology applications, initially using histology and fluorescence microscopy to characterise tumour spheroids before integration within a commercial MPS to assess tumour-vascular connection and the capability of the system to assess the efficacy of two common oncology therapies.

Acknowledgements

Firstly, I would like to thank everyone who has contributed to and supported me along my PhD journey, without which I would not have enjoyed my time and achieved such success.

I am sincerely grateful to my primary supervisor, Professor Frederik Claeyssens, for unwavering support and trust through all my work. Your breadth and depth of knowledge will forever amaze me and thank you for answering all my questions with the utmost patience and insight. To my secondary supervisors, Dr Nicola Green and Dr William English, thank you for your ongoing support, your knowledge and critical feedback have been invaluable.

Thank you to the EPSRC and CDT for advanced biomedical materials for providing the opportunity to complete this journey. With extra recognition to the CDT for providing a series of workshops and away events which have helped me to build my skills as a researcher beyond the laboratory.

I would like to thank all my collaborators in my research articles for your dedicated expertise, training and support. Special thanks to my co-author Rachel Furmidge, working alongside each other was an absolute joy and you continually inspired me with your ideas. Moreover, thank you to all the members of the Kroto laboratory for uplifting support and friendship throughout my journey. In particular, thank you to David Ramos-Rodriguez, Ana Maria Sandoval Castellanos, Maria Velazquez de la Paz, Colin Sherborne and Nicholas Farr for helping me get settled in Kroto and taking the time to train and support me. Further thanks to Mina Aleemardani and Victoria Workman for continued support and advice throughout my time.

Thank you to GlaxoSmithKline for allowing me the opportunity to join the Complex In Vitro Models team for 6 months, I learned a great deal and my time with you was invaluable. Furthermore, I am very grateful to have met a wonderful colleague and friend within the field, thank you Pelin Candarlioglu for your drive, determination and ongoing support within my PhD and more.

Throughout my journey my fiancé, Samuel Williams, and family have stood next to me steadfast in their support. Thank you for your all love, support, patience and unwavering belief in my abilities. You are truly appreciated, never change.

Academic Outputs

Publications

Jackson CE, Johnson LSJ, Williams DA, Laasch HU, Edwards DW, Harvey AG. A viewpoint on material and design considerations for oesophageal stents with extended lifetime. Journal of Materials Science 2022 57(1):3–26. doi: 10.1007/S10853-021-06700-9

Pashneh-Tala S, Field J, Fornesa B, Colomer MM, **Jackson CE**, Balcells M, Martorell J, Claeyssens F. Versatile, elastomeric and degradable polyHIPEs of poly(glycerol sebacate)-methacrylate and their application in vascular graft tissue-engineering. Materials Today Advances 2023 20. doi: 10.1016/j.mtadv.2023.100432

Albu IA, Downs-Ford R, Furmidge R, **Jackson CE**, Morgan A, Nathan K, Osmani Y, Patel A, Pennington CEW, Weller R, Whalley T, Harvey AG. Controversies and scandals as an RRI teaching and learning tool: Beyond inspiring. Journal of Responsible Innovation 2024 (*Under Review*)

<u>From PhD Thesis</u>

Published

Jackson CE, Ramos-Rodriguez DH, Farr NTH, English WR, Green NH, Claeyssens F. Development of PCL PolyHIPE Substrates for 3D Breast Cancer Cell Culture. Bioengineering 2023 10(5):522. doi: 10.3390/bioengineering10050522.

Jackson CE*, Furmidge R*****, Velazquez de la Paz MF, Workman VL, Green NH, Reilly GC, Hearnden V, Claeyssens F. Surfactant-Free Gelatin-Stabilised Biodegradable Polymerised High Internal Phase Emulsions with Macroporous Structures. Frontiers Chemistry 2023 11. doi: 10.3389/fchem.2023.1236944

Jackson CE, Doyle I, Khan H, Williams SF, Dikici BA, Barajas Ledesma E, Bryant HE, English WR, Green NH, Claeyssens F. Gelatin-containing Porous Polycaprolactone PolyHIPEs as Substrates for 3D Breast Cancer Cell Culture and Vascular Infiltration. Frontiers in Bioengineering and Biotechnology 2023 11. doi: 10.3389/fbioe.2023.1321197

(* co-first authors)

Jackson CE, Lam NL, Macdougall CE, Grandhi TSP, Chenoweth H, Miller BR, Kaprowicz R, Gales TL, Candarlioglu PL. Development of an in vitro vascularised tumour model for oncology applications. Cells 2024

Jackson CE, Green NH, English WR, Claeyssens F. The use of microphysiological systems to model metastatic cancer. Biofabrication 2024

Presentations

Jackson CE, English WR, Green NH, Claeyssens F. (2020) Lab-based produced vascularised tissue for in vitro lab-on-a-chip models of healthy and diseased tissue. Flash Presentation. Virtual Meeting of future leaders in regenerative medicine: Joint CDT conference *(3rd Place for Flash Poster Presentation)*

Jackson CE. (2020) Responsible Research and Innovation. Oral Presentation. Virtual research in progress seminar.

Jackson CE, English WR, Green NH, Claeyssens F. (2020) Lab-based produced vascularised tissue for in vitro lab-on-a-chip models of diseased tissue. Oral Presentation. Advanced Biomedical Materials CDT Annual Conference, Manchester, UK.

Jackson CE, English WR, Green NH, Claeyssens F. (2021) Lab-based produced vascularised tissue for *in vitro* lab-on-a-chip models of metastatic cancer. Poster Presentation. Virtual Meeting of future leaders in regenerative medicine: Joint CDT conference.

Jackson CE, English WR, Green NH, Claeyssens F. (2021) Lab-based produced vascularised tissue for *in vitro* lab-on-a-chip models of metastatic cancer. Poster Presentation. BioMedEng 2021. Sheffield, UK.

Jackson CE, Furmidge R, English WR, Bryant HE, Green NH, Claeyssens F. (2022) Lab-based produced vascularised tissue for in vitro lab-on-a-chip models of metastatic cancer. Oral Presentation. Advanced Biomedical Materials CDT Annual Conference, Sheffield, UK.

Jackson CE, Furmidge R, English WR, Bryant HE, Green NH, Claeyssens F. (2022) Lab-based produced vascularised tissue for in vitro lab-on-a-chip models of metastatic cancer. Oral Presentation. BiTEG 2022, York, UK.

Jackson CE, English WR, Green NH, Claeyssens F. (2023) Production of porous polycaprolactone polyHIPEs as substrates for *in vitro* 3D breast cancer cell culture. Poster Presentation. TERMIS. Manchester, UK.

Jackson CE, Furmidge R, English WR, Bryant HE, Green NH, Claeyssens F. (2023) Production of porous polycaprolactone polyHIPEs as substrates for *in vitro* 3D breast cancer cell culture. Poster Presentation. Microphysiological Systems World Summit. Berlin, Germany.

Awards

2020. Virtual Meeting of future leaders in regenerative medicine, 3rd Place for Flash Presentation.

2023. Recognition as an Associate Fellow of the Higher Education Academy (AFHEA).

Industrial Placement

Visiting PhD Student, Complex In Vitro Models, GlaxoSmithKline, Stevenage, UK, January 2022-July 2022.

Table of Contents

List of Abbreviations

2D	2 dimensional
3D	3 dimensional
AAc	Acrylic acid
AM	Additive manufacturing
ANOVA	Analysis of variance
ATR	Attentuated total reflection
CAF	Cancer-associated fibroblast
CAM	Chick chorioallantoic membrane
CAR-T	Chimeric antigen receptor
CO$_2$	Carbon Dioxide
CSC	Cancer stem-like cells
CTC	Circulating tumour cell
DCM	Dichloromethane
dH$_2$0	Deionised water
DLD	Deterministic lateral displacement
DMEM	Dulbecco`s Modified Eagle Media
DNA	Deoxyribonucleic acid
ECM	Extracellular matrix
EDD	Embryonic development day
EDTA	Ethylenediaminetetraacetic acid
ELISA	Enzyme-linked immunosorbent assay
EMT	Epithelial-mesenchymal transition
EPCAM	Epithelial cell adhesion molecule
ETD	Everhart–Thornley detector
FCS	Fetal calf serum
FDA	Food and Drug Administration
FRP	Free radical polymerisation
FTIR	Fourier transform infrared
GEMM	Genetically Engineered Mouse Models
GFP	Green fluorescent protein
H&E	Haematoxylin & Eosin

HIPE	High internal phase emulsion
HUVEC	Human umbilical vein endothelial cells
IgG	Isotype control
IMS	Industrial methylated spirit
MMPs	Matrix metalloproteinases
MPS	Microphysiological systems
NET	Neutrophil extracellular trap
NMR	Nuclear magnetic resonance
PBS	Phosphate buffer saline
PCL	Polycaprolactone
PCL-M	4-arm polycaprolactone methacrylate
PDMS	Polydimethylsiloxane
PEG	Poly(ethylene glycol)
PGA	Polyglycolic acid
PGPR	Polyglycerol polyricinoleate
PGS	Polyglycerol sebacate
PGS-M	Polyglycerol sebacate-methacrylate
PI	Photoinitiator
PLA	Polylactic acid
PLGA	Polylactic-co-glycolic acid
PMMA	Polymethyl methacrylate
PolyHIPE	Polymerised high internal phase emulsion
PRP	Platelet-rich plasma
PS	Penicillin/streptomycin
PU	Polyurethane
PVA	Polyvinyl alcohol
RGD	Arginine–glycine–aspartic acid
RR	Resazurin reduction
RT	Room temperature
SE	Standard error of mean
SEM	Scanning electron microscopy
SLA	Stereolithography
TCP	Tissue culture plastic

TE	Tissue engineering
TLD	Through lens detector
TME	Tumour microenvironment
VEGF	Vascular endothelial growth factor
ULA	Ultra-low adhesive
UTS	Ultimate tensile strength
UV	Ultraviolet
XPS	X-ray photoelectron spectroscopy

CHAPTER 1. Introduction

1.1 Thesis Outline

This thesis describes the fabrication and optimisation of high molecular weight polycaprolactone-methacrylate (PCL-M) emulsion templated structures to support 3D cell culture of breast cancer cells and vascular ingrowth.

Chapter 1 is composed of 2 literature reviews, the first review outlines our current understanding of metastatic cancer and the *in vitro* models that have been explored within the research field to study and observe cancer metastasis. The second review focuses on the material, design and fabrication considerations for tissue engineered scaffolds. Chapter 2 describes the fabrication of PCL-M scaffolds and initial mechanical, chemical and *in vitro* characterisation. Chapter 3, continues the optimisation of PCL-M scaffolds developing a fabrication technique to produce scaffolds with larger pores more suited for supporting vascularisation. In Chapter 4 the gelatin-containing PCL-M scaffolds previously optimised are characterised mechanically, chemically, *in vitro* and *ex ovo* to assess the capability of 3D cell culture and vascular in growth. In the next chapter, a commercially available microphysiological system was utilised to develop a vascularised tumour model. The capability of the model to study cancer therapies effects was further investigated. Finally, Chapter 6 provides an overall conclusion and future considerations for the PCL-M work discussed in this thesis.

Chapter 1-5 of this thesis are published/submitted articles to peer-reviewed journals. Each chapter has been presented as the entirety of each article. The work submitted is my own, except where the work has formed a jointly authored publication. The contribution of each author is stated below.

Chapter 1: Review Article (*Under Review*)

The use of microphysiological systems to model metastatic cancer, Jackson CE, Green NH, English WR, Claeyssens F. (2024) Biofabrication

Author contributions: CEJ completed the literature review and wrote the manuscript. NHG, WRE and FC provided feedback and edited the manuscript.

Chapter 2: Published Research Article

Development of PCL PolyHIPE Substrates for 3D Breast Cancer Cell Culture, Jackson CE, Ramos-Rodriguez DH, Farr NTH, English WR, Green NH, Claeyssens F. (2023) Bioengineering 10(5):522. doi: 10.3390/bioengineering10050522.

Author contributions: CEJ was the key contributor to experimental design, analysis, acquisition, and interpretation of data, statistical analysis and wrote the manuscript. DHR-R and NTHF provided additional specialist support with investigation and analysis techniques and reviewed and edited the manuscript. WRE, NHG and FC provided project supervision and reviewed and edited the manuscript.

Chapter 3: Published Research Article

Surfactant-Free Gelatin-Stabilised Biodegradable Polymerised High Internal Phase Emulsions with Macroporous Structures, Jackson CE*, Furmidge R*, Velazquez de la Paz MF, Workman VL, Green NH, Reilly GC, Hearnden V, Claeyssens F. (2023) Frontiers in Chemistry 11. doi: 10.3389/fchem.2023.1236944

Author contributions: CEJ was the key contributor to experimental design, analysis, acquisition, and interpretation of data, statistical analysis and wrote the manuscript alongside RF. CEJ was responsible for all work corresponding to PCL-M whilst RF was similarly responsible for any work corresponding to PGS-M. MFV provided additional support with an investigation and analysis technique and reviewed and edited the manuscript. VLW, NHG, GCR, VH and FC provided project supervision and reviewed and edited the manuscript.

Chapter 4: Research Article (*Under Review*)

Development of an in vitro vascularised tumour model for oncology applications, Jackson CE, Lam NL, Macdougall CE, Grandhi TSP, Chenoweth H, Miller BR, Kaprowicz R, Gales TL, Candarlioglu PL. (2024) Cells

Author contributions: CEJ was the key contributor to experimental design, analysis, acquisition, and interpretation of data, statistical analysis and wrote the manuscript. NLL, CEM, TSPG, HC, RK and TLG provided additional support with investigation and analysis techniques and reviewed and edited the manuscript. BRM provided additional specialised support with statistical analysis and supplied the accompanying information for the manuscript. CEM and PL provided project supervision and critically reviewed and edited the manuscript.

Chapter 5: Published Research Article

Gelatin-containing Porous Polycaprolactone PolyHIPEs as Substrates for 3D Breast Cancer Cell Culture and Vascular Infiltration, Jackson CE, Doyle I, Khan H, Williams SF, Dikici BA, Barajas Ledesma E, Bryant HE, English WR, Green NH, Claeyssens F. (2023) Frontiers in Bioengineering and Biotechnology 11. doi: 10.3389/fbioe.2023.1321197

Author contributions: CEJ was the key contributor to experimental design, analysis, acquisition, and interpretation of data, statistical analysis and wrote the manuscript. ID and HK provided additional support with investigation and reviewed the manuscript. SFW provided additional specialist support with investigation and analysis techniques and reviewed and edited the manuscript. BAD provided specialised support with an analysis technique and reviewed and edited the manuscript. EBL, HEB, WRE, NHG and FC provided project supervision and reviewed and edited the manuscript.

1.2 Literature Review Part 1: The use of microphysiological systems to model metastatic cancer

The use of microphysiological systems to model metastatic cancer

Abstract

Cancer is one of the leading causes of death in the 21st century with metastasis of cancer attributing to 90% of cancer-related deaths. Therefore, to improve patient outcomes there is an increased demand for better preclinical models to increase the success of translation of oncological therapies to clinic. Current traditional static *in vitro* models lack a perfusable network which is critical to overcome the diffusional mass transfer limit to provide a mechanism for the exchange of essential nutrients and waste removal and increase their physiological relevance. Furthermore, these models lack cellular heterogeneity and key components of the immune system and tissue microenvironment. This review explores rapidly developing strategies utilising perfusable microphysiological systems (MPS) for investigating cancer cell metastasis. In this review we initially outline the mechanism of cancer metastasis, highlighting key steps and identifying the current gaps in our understanding of the metastatic cascade before describing traditional *in vitro* models and their limitations. This review then focuses on the development of increasingly complex MPS systems and how these can be used to model different aspects of the metastatic cascade individually and in combination.

Introduction

Cancer is one of the leading causes of death worldwide, presenting as an ever current, ongoing challenge, being the most significant barrier to increasing life expectancy in the 21st century [1], [2]. Cancer is a huge social and economic burden on modern society, with an estimated 1 in 3 people to be diagnosed with cancer within their lifetime [3]. In order to overcome the multitude of challenges cancer poses, many different disciplines of research have come together worldwide to further develop techniques for prevention, diagnosis and treatment.

Moreover, a significant challenge faced by cancer researchers in this field is the need for sufficient platforms to test potential therapies and to improve the ease and efficiency of drug development. For studies of metastasis, the current standard is to use *in vivo* animal models, predominantly mice. These provide biophysical conditions comparable to human tissue and can replicate all aspects of the metastatic cascade, or select steps. For example, metastasis can be studied from primary tumours to the secondary, metastatic site through implantation of cancer cells, tumour tissue or the use of Genetically Engineered Mouse Models (GEMM) or just transit through the circulation to secondary sites by intravenous or intracardiac injection [4]–[6]. However, there are high cost, time and ethical implications associated with animal studies. Furthermore, there is a very low success rate (8% on average) of translation to clinical cancer trials from animal studies [7]. One of the most significant problems to overcome in the use of *in vivo* models is their limitations in the replication of heterogeneity of cancer in the clinical setting. Even a single cancer type, defined histologically in combination with molecular markers, will show significant levels of inter patient and intra tumoral molecular heterogeneity that has a significant impact on response to therapy and propensity to metastasise in an individual patient [8]. This is driving changes in the approach to cancer drug discovery to develop model systems that can rapidly assess the impact of cancer heterogeneity on drug response and ultimately improve the probability of successful translation into the clinical setting.

This review firstly discusses the steps of the metastatic cascade, highlighting the gaps in the current knowledge and understanding of the cascade. We then introduce the role of *in vitro* models, briefly describing 2D assays and circulating tumour cell (CTC) models which mainly focus on investigating individual steps of the metastatic cascade. Further discussion moves into detailing the latest microphysiological systems (MPS) which are capable of investigating multiple components of the cascade, summarising the key strengths and weaknesses of each

design. Finally, this review highlights the crucial design requirements that must be met and challenges that must be overcome to better recapitulate *in vivo* conditions within *in vitro* models and ensure wider adoption of MPS.

Cancer and Metastatic Cells

Metastasis is the detachment, migration and colonisation of tumour cells from the bulk of the primary mass to a secondary site, either in the surrounding or distant tissue from the primary site [9]. Due to such a large association with cancer mortalities, it is important to gain a deeper understanding of cancer metastasis and to identify potential drug targets to reduce it.

Metastatic cells originate from mutated cells (tumour cells). Cellular mutations may occur spontaneously during mitosis due to instability in base pairs or DNA replication errors. Alternatively, exposure to environmental factors may induce mutations, such as; ultraviolet light or chemical carcinogens [10]–[12]. Most mutated cells undergo apoptosis (pre-programmed cell death). However, in a small number of cases, apoptosis is suppressed and the mutated cells proliferate at an unregulated, increased rate, forming a neoplasm which may develop into a tumorous mass [13]. In addition, the process is further accelerated if stromal cells are affected by the mutation. This is due to increased expression of growth factors within the tumour, such as; transforming growth factor, and vascular endothelial growth factor (VEGF) [14]. Increased VEGF supports the formation of vascular networks, further supporting and accelerating the growth of a tumour by providing a source of oxygen and nutrients [15].

Metastatic cells demonstrate high levels of heterogeneity within cell populations [16]. There are 3 mechanisms described in literature to explain the high levels of heterogeneity within metastatic populations; i) clonal evolution, ii) cancer stem-like cells (CSC) model and iii) cancer stem-like cell plasticity model [17]. Clonal evolution describes a mechanism which follows the basic principle of Darwin's evolutionary theory, in which there are genetic and/or epigenetic changes in individual cells within populations which result in natural selection of the 'fittest' clone [18]. The model suggests there is numerous occurrences of mutations with successive clonal dominance, otherwise known as selective sweeps, in which the dominant clone is the one which can best survive and thrive within the specific tumour microenvironment [19]. The (CSC) model describes a sub-population of cancer cells which possess stem-like properties and functions [20], including self-renewing abilities and can initiate and maintain long-term tumour growth [17]. The CSC plasticity model proposes that clonal evolution and the CSC model are not mutually exclusive [21]. It is suggested that due to the high plasticity

of cancer cells they are capable of transitioning between non-CSC and CSC states dependent on the specific chemical and mechanical cues from the tissue microenvironment [22].

Metastatic Cascade

Metastasis of primary tumours occurs via three routes; blood vessels, lymphatic vessels, and serosal surfaces [23]. In addition, cancer can be divided into three categories based on their cell lineage: carcinomas (epithelial), sarcomas (mesenchymal) and leukaemias and lymphomas (blood and lymph tissue respectively) [24], each of which metastasise via different routes. The majority of cancers (90%) are carcinomas, which commonly metastasise via lymphatic vessels. Sarcomas, bone and soft tissue malignancies metastasise via blood vessels and few malignancies via serosal surfaces, i.e. the outer lining of organs and body cavities of the abdomen and chest [25].

The process of metastasis is not yet fully understood. However, it has been defined by a cascade of steps: loss of cellular adhesion, increase in cell movement and invasiveness, intravasation (entry into the circulatory system), extravasation (exit from the circulatory system) and colonisation at a secondary site (**Figure 1**) [13], [26].
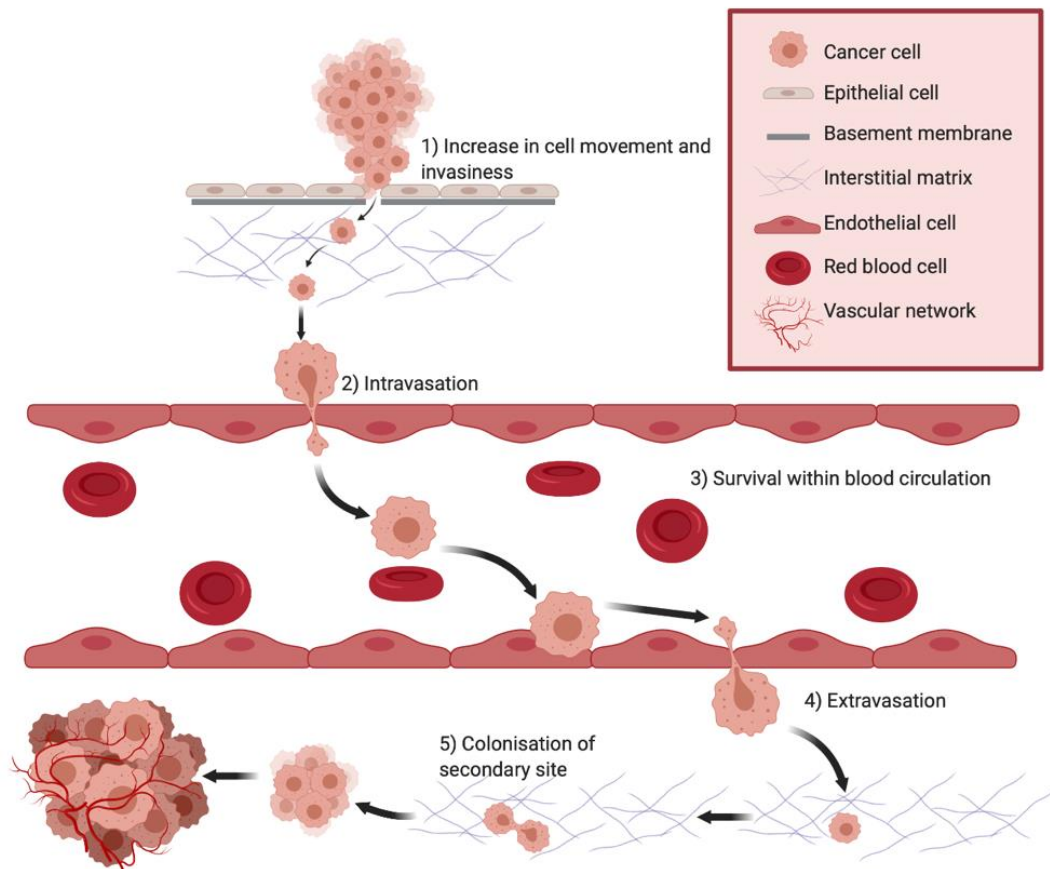

Figure 1. Cascade of steps outlining the process of cancer cell metastasis. Created with BioRender.com

Metastatic cell invasion follows the disaggregation of metastatic cells from the primary tumour via the breakdown of cellular adhesions [27]. Within carcinomas, the epithelial cells must first undergo epithelial-mesenchymal transition (EMT) before the process of invasion can occur [28], [29]. Undergoing this process leads to a loss of the main epithelial cell adhesion mediator, E-cadherin [27]–[29]. Complementary to this, Perl et al. reported evidence of a causal link between the loss of the E-cadherin adhesion mediator and the progression from benign adenoma to malignant carcinoma *in vivo* [30]. Furthermore, through a collagen invasion assay, Frixen et al. found that E-cadherin expressing cells were largely non-invasive compared to E-cadherin deficient cells, which were considerably more invasive [31]. It is important to note that EMT is not always towards fully mesenchymal phenotype and may only be a partial transition [17] and it is thought sarcomas also go through a similar process called the metastable phenotype [32]. Aiello et al. show how partial EMT phenotypes promote collective tumour cell migration and clusters of CTCs to form [33]. Furthermore, due to the high plasticity of cancer cells, EMT is a reversible process and as such allows them to switch between proliferative to invasive phenotypes when necessary [34]. The progression of EMT, whether it be partial or full impacts tumour growth and metastasis differently depending on the tumour type and stage of tumour progression [17].

During invasion metastatic cells penetrate through the basal lamina of surrounding tissue via adhesion to and digestion of the ECM components, including collagen (type IV) and laminin [26], [35]. ECM degradation is mediated by actin-rich membrane protrusions formed by metastatic cells, known as invadopodia [36], [37]. These protrusions mediate ECM degradation by localised proteolytic activity of matrix metalloproteinases (MMPs) [36]. Liotta et al. report a positive correlation between the activity of type IV collagenase (a member of the MMP family) and metastatic cell invasion [38]. Following partial degradation of the ECM, metastatic cells form pseudopodia in response to the expression of epidermal growth factor from tumour associated macrophages [37]. Pseudopodia attach to collagen fibrils in the ECM and facilitate the movement of metastatic cells through ECM, whilst also allowing the metastatic cells to squeeze between other cells present in the surrounding tissue [39]. Interestingly, Shankar et al. reported a link between pseudopodia dynamics and EMT [28]. The authors further suggested targeting the molecules crucial for the formation of pseudopodia to potentially reverse EMT, inducing mesenchymal-epithelial transition. Thus, inhibiting the potential of malignant cells to metastasise.

Metastatic cells transverse through the ECM towards the blood and lymphatic vessels via different migratory modes [40]. Hematogenous intravasation (via the blood vessels) is

generally the most common pathway for entry into the circulatory system. However, the lymphatic system eventually drains into venous circulation [41], [42]. The mechanism for metastatic cells to undergo hematogenous and lymphatic intravasation differs due to the vessels' structural differences [42]. Blood vessels have tight endothelial junctions compared to lymphatic vessels. Thus, lymphatic vessels are defined as 'leaky' in comparison, reducing the barriers for intravasation [41].

Once in circulation, metastatic cells are known as circulating tumour cells (CTCs), of which less than 0.01% survive. This is due to applied shear stress from the blood circulation and the presence of immune cells, particularly natural killer cells [42], [43]. However, there is an increased chance of survival in lymphatic vessels due to reduced shear stress, as a result of the significantly reduced flow in lympathic vessels [41], [44]. Metastatic cells can employ protective methods once in circulation. In 1968, Gasic et al. first reported one such method of protection, the formation of tumour cell-platelet microaggregates which physically shielded the metastatic cells from the shear stress and immune cells [45]. Egan et al. have since demonstrated this phenomenon, reporting a decrease in shear induced membrane damage of ovarian cancer cells in the presence of platelets than compared to in the absence of platelets [46].

In recent years it has also been suggested that the presence of neutrophils could play an active role in CTC extravasation [47], [48]. Yang et al. show how neutrophil extracellular traps (NETs) are present in the liver metastasis of breast and colon cancer [49]. Furthermore, the DNA component in these NETs act as a chemoattractant to CTCs, helping facilitate cancer metastasis. Cancer cell plasticity can also play a significant role in CTC survival in response to capillary-induced restriction [48]. Nuclear deformation is a critical process that can enable CTCs to successfully transit through capillary beds towards optimal sites of extravasation [50]. Yamauchi et al. showed how fibrosarcoma cells are capable of elongating 4× their normal length and increased the length of their nuclei 1.6× to allow survival and transit through capillaries [51]. Furthermore, evidence has been found to show that CTCs can regulate cell stiffness and are able to soften to migrate through confined spaces [52]. Such extensive cell deformations can cause the CTCs to undergo hybrid EMT in response to the mechanical stimuli [53].

Following CTC survival, cells must undergo extravasation, whilst it is not as well defined as intravasation, it involves cellular adhesion to the endothelium, penetration of the cell through the endothelial barrier and trans-endothelial migration. This process is facilitated by platelets and results in metastatic cells reaching the underlying tissue [54], [55]. Leong et al. utilised

high-resolution time-lapse imaging to further investigate the extravasation process [56]. The study found that the predominant mode of extravasation for metastatic cells is paracellular migration. In which the metastatic cells migrate between two endothelial cells, disrupting the inter-endothelial cell-cell junctions by extending invadopodia through the endothelium at the junctions. In addition, there are two further modes of migration through the endothelium; transcellular migration, metastatic cells migrate through the endothelium cells, and mosaic process, metastatic cell becomes a part of the endothelial layer for a short time (up to 24 hours) [57].

Following extravasation, migration of metastatic cells towards the secondary site occurs via similar methods described previously for invasion [58]. The metastatic cells rapidly proliferate at the secondary site, initially forming a micro-metastasis (0.2-2 mm) [59], [60]. Following further proliferation and angiogenesis the colony develops into a macro-metastasis (>2 mm) [59]. Unfortunately, the success of treatment after the establishment of a metastatic colony in a secondary site is greatly reduced. With significantly decreased responses to drug treatments, surgery is often the only viable treatment. Furthermore, the presence of CTCs in the circulatory system may lead to the formation of colonies in multiple sites, thus resulting in a poorer patient prognosis.

Modes of Migration

Metastatic cells migrate via 3 modes: single cells, loosely attached cell streams and well-organised multi-cellular collections (**Figure 2**) [40], [61]. The mode of migration is dependent on cell phenotype and the surrounding ECM [61]. Single cell migration is further divided into amoeboid (rapid single cell crawling) and mesenchymal cell phenotype migration [40]. Cells which migrate via amoeboid migration have a rounded or ellipsoid morphology, lack mature focal adhesions and constantly change shape during motion [40], [62]. Amoeboid migration can again be subdivided into two modes of migration. The first is rounded cells which form blebs (small spherical protrusions) using cytoplasmic pressure, exerting a pushing motion to squeeze and migrate through the ECM [62]–[64]. This mode does not involve any adhesion or pulling on the surrounding substrate, leaving the ECM intact. The second mode occurs in elongated amoeboid cells which produce actin-rich filopodia that weakly adhere to the surrounding substrate via actin-protein binding, resulting in a gliding motion [62], [65]. Amoeboid migration utilises the use of protrusions instead of the attachment and contraction of lamellipodia to the ECM. Thus, this is the fastest mode of migration, with speeds between 0.4 and 5 μm min^{-1} [66]. In addition, Denais et al. demonstrated the ability of amoeboid cells

to undergo nuclear envelope rupture and self-repair to facilitate migration through tight interstitial spaces within dense ECM [67].
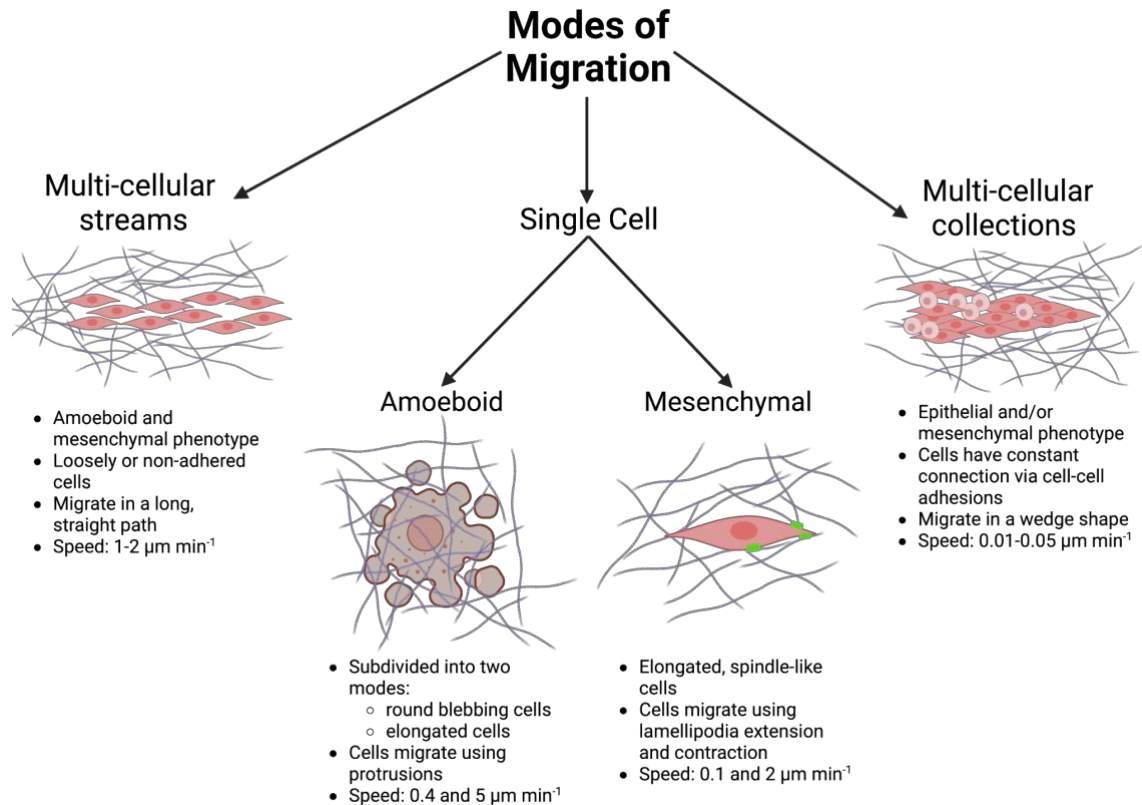

Figure 2. Metastatic cells modes of migration. Single-cell amoeboid migration: Blebby, spherical protrusions used to push and squeeze through the ECM. Single-cell mesenchymal migration: Spindle-like cells using strong integrin-mediated adhesions (green) to adhere and migrate through the ECM. Multi-cellular stream migration: Loosely- or non-adhered cells migrating in the same direction. Collective migration: Epithelial and/or mesenchymal phenotypes migrate in the same direction with constant cell-cell contact. Created with BioRender.com

Mesenchymal migration is commonly observed in connective-tissue tumours [68]. Single cell mesenchymal migration is characterised by elongated, spindle-like cell morphologies with cells utilising lamellipodia to form strong integrin-mediated adhesions to the ECM [68], [69]. This migration mode is not a smooth continuous process, the leading edge of the cell moves via the lamellipodia extensions followed by contraction of the trailing edge [70], [71]. Focal contacts form and turnover within 10-120 minutes, thus resulting in a slow migration speed, ranging from 0.1-2 μm min^{-1} [68].

Multi-cellular streams are often formed of mesenchymal or amoeboid phenotypes, which are either loosely- or non-adhered cells, migrating along the same pathway [72]. It is often

observed that cell streams have longer, straighter pathways than single cell migration and typically migrate at a speed of 1-2 μm min^{-1} [66]. Patsialou et al. reported a significant correlation between multicellular streaming and metastatic cell intravasation and increased levels of CTCs in the blood within primary human breast tumours [73].

The final mode, collective migration, is formed of either epithelial and/or mesenchymal phenotypes [66]. All the cells migrate in the same direction with constant contact with the neighbouring cell due to the retention of cell-cell adhesions [72]. The cell collections may migrate in a wedge shape with a singular leader cell or in a broader, irregular shape with a multi-cellular leading row [74]. In addition, the phenotypes may differ between the leading and following cells. Collective migration is the slowest mode of migration with a typical speed ranging from 0.01-0.05 μm min^{-1} [66].

Microenvironment

The tumour microenvironment plays an integral role in maintaining normal cell function and behaviour and can have a significant impact on cancer development [75], [76]. The tissue microenvironment is composed of; tumour cells, stromal cells, such as fibroblasts, endothelial cells and infiltrated immune cells [77].

As briefly mentioned, the tumour microenvironment plays a key role in the EMT. The tumour microenvironment provides signals to cancer cells and due the high plasticity of cancer cells, these signals can result in full, partial or reversal of the EMT [17]. Furthermore, the tumour microenvironment is involved in therapy-induced plasticity, in which cancer-associated fibroblasts (CAFs), a stromal cell population in the tumour microenvironment, have been well-documented in promoting therapy resistance [77]. Factors produced by CAFs can activate stem-like associated pathways promoting a shift in tumour cells to CSCs, correlating with poor patient prognosis [20], [78], [79].

A significant element of the microenvironment is the ECM. The ECM is comprised of multiple components: proteins, glycoproteins, proteoglycans and polysaccharides which form both the basement membrane and the interstitial matrix (**Figure 3**) [76], [80]. Collagen is the most abundant protein in the human body and collagen fibres are the most substantial component of the ECM, ranging from 50-500 nm in diameter [81]. In addition, it has been increasingly reported to have a significant impact on tumour progression [76], [82]–[85].
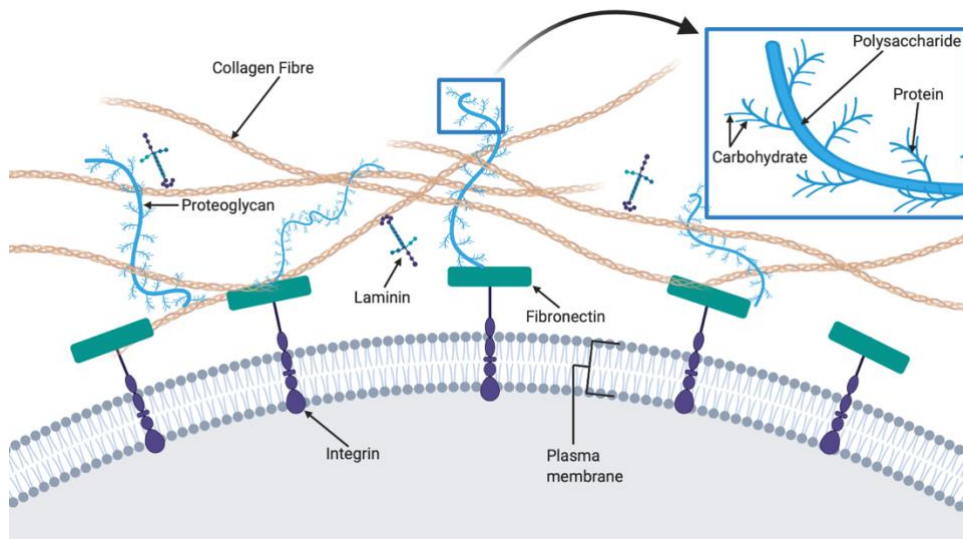
Figure 3. Extracellular matrix and cell membrane, demonstrating the position and structure of the extracellular matrix components. Created with BioRender.com

Provenzano et al. reported dense, highly linear and oriented collagen type I fibres aligned perpendicular and radially to tumorous breast tissue [82]. Furthermore, invasive metastatic cells in direct contact with the collagen fibres were observed to be migrating across the fibres via amoeboid migration. By comparing the collagen alignment in tumorous breast tissue to normal breast tissue, this study provides evidence that strongly indicates the ability of cancer cells to trigger collagen fibril reorganisation into a radial alignment, aiding metastatic cell invasion. Moreover, Ramaswamy et al. described the increased expression of genes encoding type I collagens (COL1A1 and COL1A2) within tumours with metastatic potential [86]. The reorganisation and increased formation of collagen type I and III results in the gradual stiffening of the ECM [76], [87]. This leads to increased tension in the tissue which can affect cell differentiation and gene expression. Potentially, this then promotes increased tumour growth and metastatic potential, resulting in a poorer prognosis for patients [76], [86], [88].

In-vitro models to study cancer metastasis

Two-dimensional *in vitro* assays

The focus of this review is on rapidly developing 3D models rather than conventional 2D models and further in depth discussion on 2D models can be found in many previous reviews [89]–[92]. Briefly, 2D *in vitro* assays mainly focus on investigating cellular mode of migration. 2D assays use cells cultured on flat surfaces, most simply and commonly a petri dish or well plate. There are numerous 2D *in vitro* assays for cell migration, including; the

wound healing/scratch assay [93], [94], the nest/fence assay [93], [95], the micro-carrier bead assay [89], and the transwell migration assay [94] (**Figure 4**).
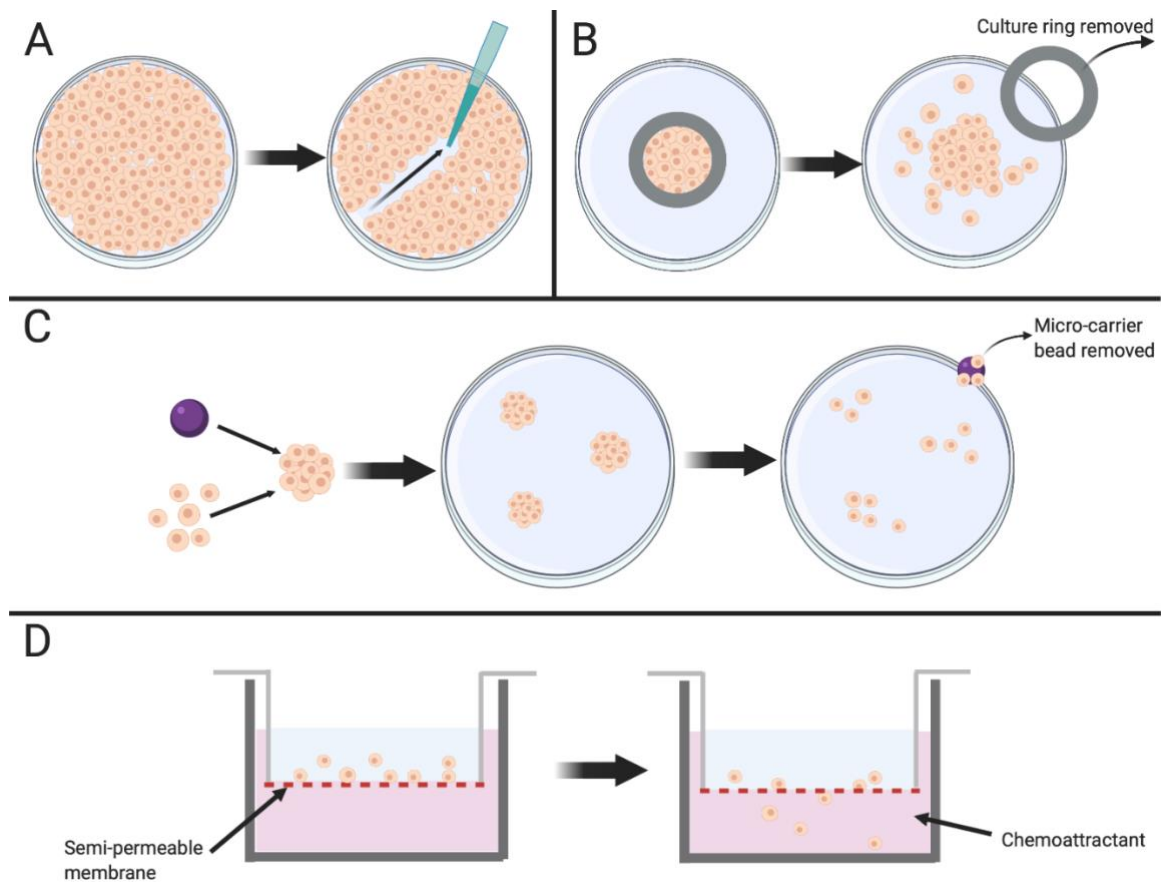

Figure 4. 2D migrations assays. A) Wound healing assay, a scratch is made through a confluent layer of cells using a pipette tip, cells migrate inwards to close the gap. B) Nest assay, cells are cultured within a culture ring to form a confluent layer. The ring is removed and cells migrate outwards. C) Micro-carrier bead assay, cells are cultured onto micro-carrier beads and placed in a petri dish. After a set period of time the beads are removed and cells that have migrated are left on the dish. D) Boyden chamber migration assay, cells are placed in the upper compartment and migrate through a semi-permeable membrane due to a chemoattractant. Created with BioRender.com

The wound healing assay has been utilised to study melanoma cell migration by Freitas et al. [96]. Whilst it provides an inexpensive and simple method, in which single cell morphological changes, such as formation of lamellipodia, can be analysed throughout the migration which can indicate any impaired or enhanced cell types [97]. However, the assay lacks a chemotactic gradient and the scratch can be filled by proliferating cells rather than

migrating cells, and unless cell proliferation is inhibited there are likely to be inaccuracies in any collected data [98].

The nest assay better recapitulates the migration of cells from dense tissues such as tumours [93], thus can be used to investigate and observe cell behaviours when migrating away from such dense populations. Further improvements can be made by including a Matrigel overlay to better represent tumour ingrowth into surrounding tissue *in vivo* [99]. However, migration rates may decrease after a period of normal migration as cell density rapidly decreases as the nest empties.

A micro-carrier assay observes cell migration from carrier beads to a 2D surface [89]. However, although the cells migrate outward from a central location similar to a tumour, they are migrating from a monolayer and not a dense collection as customary within a tumour.

In the transwell migration assay, also known as the Boyden chamber migration assay, cells are positioned in the upper compartment and migrate through the membrane to the lower compartment as a result of a chemotactic gradient [94], comparable to a leaky endothelium or lymphatic vessel. Joeckel et al. demonstrated the use of a simple transwell migration assay to assess the metastatic potential of renal cancer cells [100], showing a 20-fold increase in the migration of metastasised cells compared to non-metastasised patient cells. The assay supports the analysis of a range of cell phenotypes [101], however, it is a simplistic model and therefore has reduced physiological relevance [102]. Collective cell migration cannot be analysed and single cells cannot be visualised [99].

Circulating Tumour Cells

Given their importance in metastasis, the isolation of CTCs is critical for the study of the metastatic ability of cancer cells and are key indicators in a patient's blood for the presence of metastatic tumours [103]. A variety of methods follow similar aims to target, isolate, count and characterise CTCs. CellSearch is an FDA-approved lab-on-a-chip device that is used as a prognostic tool for breast, prostate and colorectal cancer [104]. The device uses antibodies that are able to specifically identify and bind to epithelial cell adhesion molecule (EpCAM) expressing CTCs, which are further magnetically isolated, stained and counted (**Figure 5**) [105]. Allard et al. presented an initial study using CellSearch, investigating the efficacy of identifying CTCs to further identify the presence of metastatic carcinomas [106]. The study found the presence of CTCs was extremely rare in healthy patients and patients with non-malignant diseases (1/344 patients ≥2 CTCs/7.5 ml of blood). However, for patients with metastatic carcinomas there was a wide range of frequencies of CTCs. Nevertheless Rao et al.

reported a 10-fold decrease of EpCAM expression in CTCs compared to tumour tissue from the primary and secondary sites [107], suggesting that the expression of EpCAM is dependent upon the local microenvironment. In addition, reduced expression in CTCs may lead to reduced accuracy within the CellSearch device. CellSearch amplifies the magnetic load per antigen using avidin/biotin chemistry in order to reduce the effect of reduced EpCAM expression in CTCs [105].
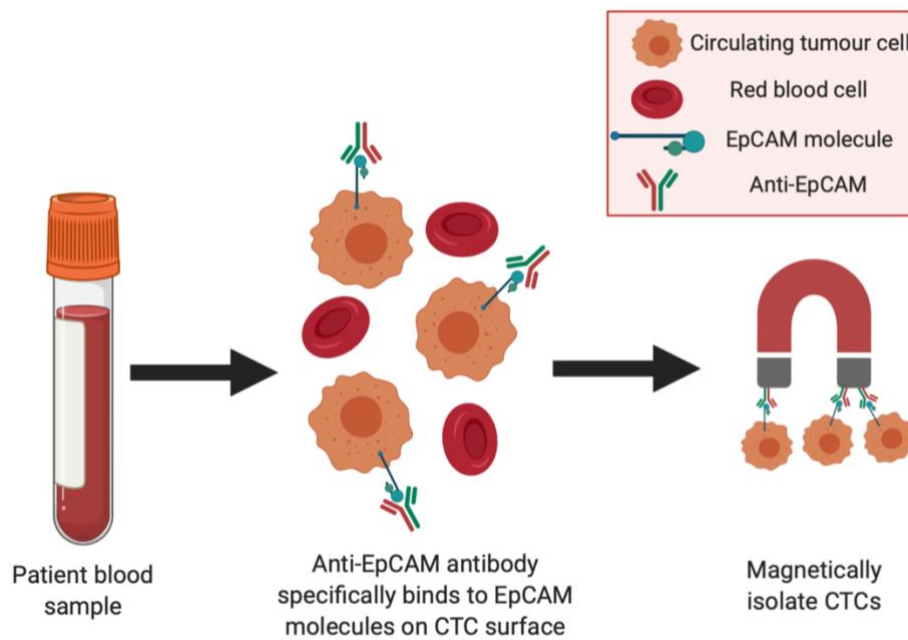

Figure 5. Simplified process diagram of the CellSearch CTC capture system. Created with BioRender.com

ScreenCell and Rarecell are antibody-free devices which feature track-etched polycarbonate filters in order to sieve and isolate the CTCs due to their large size [108]. Mu et al. demonstrated successful, simple and effective isolation of CTCs and CTC-clusters using ScreenCell [109]. The authors further reported isolation of single cells for genetic characterisation by the combination of ScreenCell filtration with the DEPArray system. The DEPArray system consists of a digital sorter combining microfluidics and microelectronics in order to isolate single CTCs for further analysis [110]. Filtration methods overcome the challenges associated with reduced EpCAM expression and can detect whole cell populations which could be missed by CellSearch. This includes populations that have undergone EMT, these cells lose the expression of epithelial markers through the EMT process [108]. Conversely, filtration methods may miss cells which are smaller than 12 μm in diameter whereas CellSearch detects cells between 4-18 μm [111].

Microfluidic deterministic lateral displacement (DLD) is an alternative filtration method for the capture and isolation of CTCs [112]. The method comprises blood flow through an array of microposts, where each row of posts is laterally offset from the previous row and post separation reduces in each successive row, simulating *in vivo* bifurcations [113]. Cells below a critical diameter pass through the array whilst CTCs are arrested within the device and thus are separated from the sample (**Figure 6**). Loutherback et al. demonstrated the ability of the DLD array to isolate CTCs from a blood sample with >85% efficiency, with no effect on cell viability [114]. Furthermore, Au et al. reported 99% efficiency by using a two-stage DLD device [115]. The first stage captures larger CTC clusters via 'standard DLD' whilst the second stage uses asymmetric posts with height restrictions to capture smaller clusters. Although this two-stage process increases the capture efficiency compared to 'standard' DLD, cell viability is reduced due to physical damage to the cells, reported at 87% at its lowest.
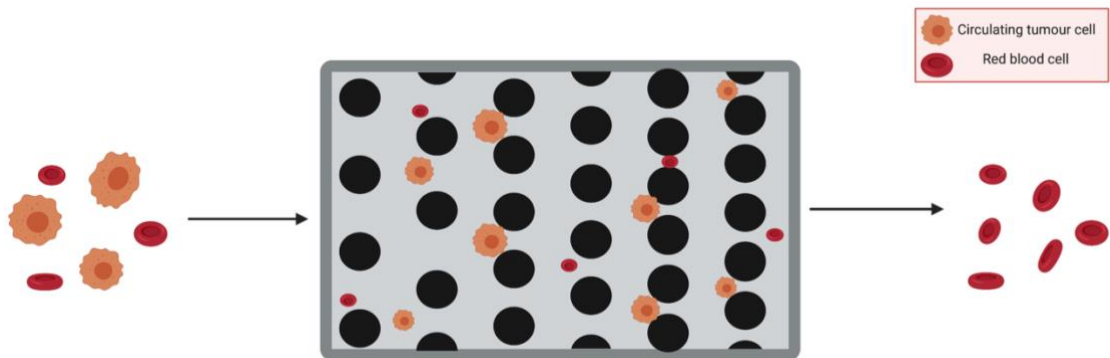

Figure 6. Simplified process diagram of a lateral displacement filtration in which CTCs are captured within the device between the micropillars whilst red blood cells pass through freely. Created with BioRender.com

Microphysiological Systems

Cells *in vivo* have a three-dimensional (3D) geometry, supported by a complex extracellular matrix (ECM). However, cells *in vitro* are commonly cultured in two-dimensional (2D) monolayers. Whilst 2D assays provide quick, easily repeatable and simple models, they lack the complexity to recapitulate *in vivo* microenvironments. The lack of cell-cell and cell-matrix signalling pathways reduces physiochemical cues. Thus, resulting in a negative effect on cell identity and behaviour, further impacting cell growth and function [116], [117]. However, *in vitro* models that can perform to a similar standard to *in vivo* models result in reductions in cost, time and ethical challenges that are normally associated with *in vivo* models. Microphysiological systems (MPSs), also known as complex *in vitro* models, lab-on-a-chip or

organ-on-a-chip models, are rapidly developing to mimic human physiology and disease [118], [119]. MPS models are capable of studying cell-cell interactions and cell-ECM interactions within a 3D microenvironment with an improved semblance of *in vivo* biophysical and chemical properties. There are many different designs for MPS which can be divided into 3 themes; single chip designs, well-plate designs and connected chamber designs (**Figure 7**). 3D models can also be divided based on the culture conditions into 3 subclasses; suspension cultures or non-adherent plates, cultures in gel-like medium and cultures on scaffolds [120]. Many 3D models commonly use scaffolds (natural or synthetic) combined with human cells to support the growth and expansion of new tissue structures [121]. In addition, many include the use of growth factors or biophysical conditions to further enhance cell growth within the scaffold and integration. Cells, scaffolds and growth factors/growth stimulating conditions are often referred to as the tissue engineering (TE) triad [122].
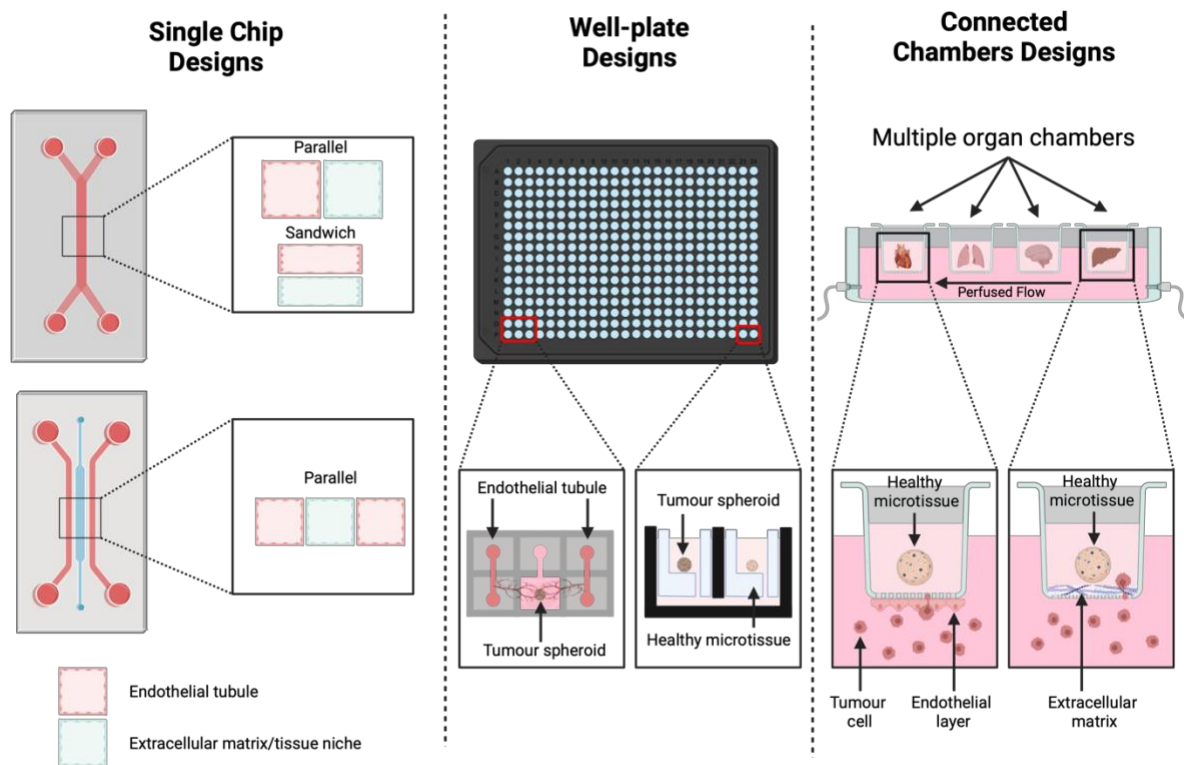

Figure 7. Simplified diagrams demonstrating examples of microphysiological system designs within the 3 different themes; single chip designs, well-plate designs and connected chambers designs.

The successful use of TE constructs in clinical applications is limited due to poor vascularisation within the tissue [123]. The constructs are restricted to 100-200 µm tissue

thickness due to diffusional mass transfer limitations. Constructs with a thickness greater than 200 μm fail due to ischemia and cell death within the tissue [124]. Vascularisation of *in vitro* models provides access to nutrients and removal of waste for cells within the bulk of the constructs. Therefore, by improving vascularisation culture times can be extended and the culture conditions more accurately simulate *in vivo* conditions. Consequently, there is a large emphasis on promoting vasculogenesis within models to improve accuracy and increase the information gained from *in vitro* models over a longer period. Kameda et al. developed a model which utilised removable membranes to enable direct contact between tissue and an on-chip vascular bed [125]. This model allows for vascular bed formation without the need of angiogenic factors released from the tissue. Thus, the model can be utilised to study the interaction of vasculature with any 3D tissue, independent of whether it secretes angiogenic factors. However, the model is cultured under static conditions and thus lacks active perfusion of nutrients through the vascular network. Alternatively, Chesnais et al. developed a fully-perfusable vascularised platform which was matrix-free [126]. The model was capable of studying vascular remodelling of capillaries over two weeks. Whilst, this model is not as flexible to the inclusion of 3D tissues as the previously presented model, it could be used successfully as a cancer model to investigate circulating tumour cell transit and/or arrest within capillaries.

MPSs are a relevantly recent development in the modelling of biological systems. Many models are currently in development, however there are a small number of fully developed MPS platforms that are commercially available. One such platform widely used is Mimetas. Mimetas provides a range of 3D platforms depending on the application. Each platform is constructed of chips, with each chip consisting of 2-3 different channels/chambers separated via a phase guide and an ECM bed within one of the chambers in the individual chips. The platform uses a rocker to provide bi-directional flow through the channels within the chips. Lanz et al. utilised the Mimetas platform to demonstrate the use of an MPS for therapy selection for triple negative breast cancer [127]. The model improved 3D cell culture viability via constant media perfusion and showed successful compatibility with dissected tumour tissue. Furthermore, the study highlighted the potential for MPS systems to be used within personalised medicines for drug selection and the prediction of patient response.

Mimetas platforms provide microfluidic MPSs within standardised 384-well plates that can be easily imaged on existing imaging systems and require little extra specialised equipment to utilise the platform. However, the use of bi-directional flow is not appropriate for all applications, such as models of the blood-brain barrier [128].

Emulate Bio is a commercially available platform that utilises a uni-directional flow. The platform consists of an organ chip with two distinct channels separated by a thin, flexible, porous PDMS membrane. Whilst the platform requires specialised equipment, the system can exert mechanical forces on each chip. Strelez et al. successfully utilised the Emulate system and demonstrated the ability to tune the tissue microenvironment to assess the invasive capabilities of colorectal cancer [129]. To improve the physiological relevance to the tumour microenvironment within the intestine, peristalsis-like mechanical forces were applied across the endothelial:epithelial interface. These forces stimulated the epithelial cells to form 3D structures and further differentiate into the 4 intestinal lineages.

Similar to Mimetas and Emulate, many MPS systems are based on a design of multiple microchannels with an ECM component (Matrigel, hydrogel or collagen gel) incorporated in one of the compartments. Toh et al. developed an MPS using a microchannel divided into three smaller channels via micro-pillars [130]. Cancer cells were seeded and cultured into the central channel, forming tumour aggregates. A 3D collagen barrier, resembling the dense basement membrane of the ECM, was formed around these tumour aggregates. The migration and invasion of tumour cells from the aggregates through the collagen membrane to the outer channels via chemo-attractant stimulation was observed in real time. This method allows for the study of cancer cell migration at high spatial and temporal resolution whilst better mimicking the 3D tumour microenvironment than with the previously mentioned CTC devices.

SynVivo have developed an alternative to the common design strategy which consists of microchannels separating independent compartments. SynTumor is a 3D tumour model which uses scans of vascular networks to generate a chip which incorporates geometrically and spatially relevant vascular beds with additional space for tissue or tumour sections [131]. Pradhan et al. utilised this model to culture breast cancer cells and stromal fibroblasts in adjoining tissue compartments which were separated by an interstitial space containing pores to mimic leaky vasculature *in vivo*. The study was able to investigate the efficacy of anti-cancer drugs under dynamic flow conditions.

It has been shown that many types of cancer frequently metastasise towards specific target organs within the body. For example; breast cancer metastasises towards the brain, liver, lung and bone [132]–[134], colorectal cancer towards the liver and lungs [135] and lung cancer to the brain, bone, liver, lymph nodes and adrenal glands [132], [136], [137].

Berisini et al. demonstrated the use of a tri-culture system, composed of 3 media channels, to observe the effect of osteo-cell conditioned microenvironment on the extravasation of metastatic breast cancer cells (MDA-MB-231) [138]. Cancer cells transmigrated through an

endothelial layer into the osteo-cell conditioned regions, resulting in the formation of micrometastases within these regions. Additionally, the model was able to identify key molecular pathways for the process of extravasation involving breast cancer cell surface receptor CXCR2 and bone secreted chemokine CXCL5.

A similar device composed of 3 hydrogel channels within a PDMS chip has been developed by Chen et al. to study extravasation [139]. Human umbilical vein endothelial cells and lung fibroblasts were used to establish vascular and tissue microenvironments in the channels respectively. The device successfully monitored the extravasation of breast cancer cells (MDA-MB-231) from a perfused flow within the vascular channel into the ECM compartment. The model was capable of differentiating between the tumour cell migrating via paracellular migration versus transcellular migration. Furthermore, extracellular proteins could be observed such as F-actin, VE cadherin and focal adhesion proteins. However, the authors do note the model is not capable of fully recapitulating the *in vivo* microenvironment as a range of additional cell populations, such as stromal cells and immune cells would be required.

An alternative device design has been developed by Skardal et al., composed of two chambers, independently housing gut and liver constructs, connected by fluid flow in series investigating metastasis of colorectal cancer [140]. Each construct is composed of representative host tissue cells, suspended within hyaluronic acid-based hydrogels. The liver construct is composed of HepG2 cells whilst the gut construct is composed of INT-407 cells and colon carcinoma cells (HCT-116) which formed tumour aggregates. Observations found the tumour aggregates grew before undergoing dissemination from the gut construct and migrating to the liver construct via the circulation system. However, whilst this does allow modelling of two independent organ constructs, the model lacks a full recapitulation of *in vivo*-like function due to the simplistic cell encapsulation within the hydrogel and a lack of endothelial barriers to model extravasation and intravasation.

Similar to Skardal et al., Xu et al. demonstrate the use of a multi-organ-on-a-chip platform to investigate the metastasis of lung cancer to three target organs [141]. The PDMS chip is composed of an upstream lung compartment separated via PDMS microporous membranes from three downstream brain, bone and liver compartments. The study observed the formation of a tumour mass and increased invasive capacity following EMT. Furthermore, the model was able to investigate the effect of cancer cell metastasis within the cell populations in the downstream compartments, observing the overexpression of specific proteins: CXCR4, RANKL and AFP. Whilst PDMS is a good candidate for MPS due to its transparent, gas permeable and biocompatible properties, it also has disadvantages [142], [143]. A key issue of

PDMS in MPS is the absorption of small molecules onto the surface of the PDMS, which can have a profound effect on the outcome of drug screening studies as highlighted by Toepke and Beebe [144].

Therefore, there has been focussed development on the fabrication of MPSs using alternative materials to PDMS. The commercial LiverChip from CN Bio is a hepatic PDMS-free model and was the first MPS validated for the study of metastatic behaviour [145]. Clark et al. demonstrated the use of the LiverChip to investigate the dormant-emergent progression of metastatic breast cancer [146]. The chip is a 12 unit-platform with two connected chambers for media and cell-seeded polystyrene scaffolds. The study presented a complete complement of liver cells, including immune/inflammatory cells cultured alongside breast cancer. Over a period of a month, the model allowed researchers to observe breast cancer cells spontaneously entering quiescent dormancy and becoming resistant to chemotherapies before re-emerging from dormancy following an inflammatory stimulus. However, the scaffolds used within this system require precoating with collagen type I before cell seeding. The use of collagen-based ECM gels within MPSs can lead to potential issues relating to protein impurities, pathogen transmission and batch-to-batch variability, affecting experimental reproducibility [147]–[149].

Scaffold designs such as the polyurethane (PU) foams (open porosity >70%) developed by Angeloni et al. could provide synthetic substrates for improved recapitulation of the microenvironment within an MPS [150]. The scaffolds remove the need for Matrigel or similar collagen-based ECM gels required by many other platforms to provide a suitable tissue microenvironment. The PU foam was shown to be a suitable scaffold to produce a biomimetic bone microenvironment for the co-culture of human osteoblasts and breast cancer tumour cells (MCF7). Results showed increased levels of osteopontin when osteoblasts were cultured within the PU foams compared to TCP. Furthermore, sites of MCF7 metastatic formation were observed within the PU foams when co-cultured with osteoblasts, resulting in desorption of calcium and phosphorus particles and modelling the negative effects of metastatic growth on bone ECM. However, many models are now moving past co-culture with an emphasis on increasing the complexity of systems to recapitulate the cancer microenvironment more fully.

Regier et al. demonstrated the difference in gene expression between mono-, bi- and tri-culture within an MPS system [151]. The study highlighted that the co-culture of three cell types more strongly alters cell type-, time- and complexity-dependent gene expression than if models that are limited to only two cell types. In addition, it showed how varying the complexity of microenvironments within MPS models affects the response of tumour and

stromal cells. Thus, expanding past conventional bi-cultures towards heterotypic cultures is crucial.

Fluid flow is another factor that can affect the response of cells to the microenvironment. Cancer cells experience fluid flow, either blood or interstitial, throughout all steps in the metastasis cascade [152]. Polacheck et al. developed an MPS to study the effect of interstitial flows on breast cancer cells within a 3D collagen type I matrix [153]. The model is composed of two media channels on either side of a central channel containing MDA-MB-231 cells embedded within a collagen type I hydrogel. A flow field was produced through the collagen gel by creating a higher fluid pressure in one channel than the other. The model identified key molecular biophysical mechanisms that lead to protrusion formation on the upstream side of the cell when exposed to high rates of interstitial flow (4.6 μm s^{-1}).

Further effects of interstitial fluid flow on the mode of cell migration were observed within a model developed by Huang et al. [154]. The device was composed of three parallel cell channels separated by polydimethylsiloxane ridges with a fluid flow (2 μm s^{-1}) channel perpendicular to the cell channels. The model showed that the cells exhibited both amoeboid and mesenchymal migration modes. However, the influence of interstitial flow promoted the migration of the cells towards amoeboid mode. It was suggested this was due to the interstitial flow washing away fibronectin, an important molecule in cell adhesion, vital for mesenchymal migration. Further observation showed that the addition of exogenous fibronectin promoted cell migration via the mesenchymal model. Additionally, the model demonstrated that increasing interstitial flow increases the migration speed but decreases unidirectional migration.

Moreover, matrix stiffness is an additional factor within the microenvironment that can have a significant impact on the metastatic ability of cancer cells. Pathak et al. developed an MPS to study the independent impacts of stiffness and pore size [155]. The device contains microfluidic channels of varying widths (10-40 μm) and stiffnesses (0.4-120 kPa) formed via polymerisation and gelation of polyacrylamide hydrogels. The authors reported a decrease in glioma cell migration speed with increasing pore size at a fixed stiffness. However, at a fixed pore size the relationship between migration speed and stiffness varied. This suggests that pore size can significantly affect migration speed but also affects the way matrix stiffness controls migration speed.

Future Direction of MPSs

This review focuses on the importance of further understanding the metastatic cascade. There are many models available to study individual aspects of the cascade however there are few that study more than one stage in the process [16]. A key area of the metastatic cascade which needs better understanding is the extravasation of metastatic cells to a secondary site, particularly investigating the diverse role of capillaries in the cascade. To model this complex process, model development needs to focus on better recapitulating vascularisation, including the capillary microenvironment. It is known that cancers have highly heterogeneous populations and therefore future models need to reflect this key feature. Inclusion of patient derived spheroids or organoids would better reflect cancer heterogeneity and introduce clonal variations within cultures. Furthermore, whilst there are many model systems which compose of multiple organ constructs future work should focus on tailoring these constructs to better represent different microenvironments connected within a vascular network. The inclusion of biomaterials, particularly porous biomaterials, could provide a novel approach to easily tune different microenvironments within MPSs.

Current designs of MPSs, as presented above, mainly focus on the use of simplistic compartmentalised systems. There is a wealth of information and knowledge gained from these systems regarding a vast array of factors that influence the cancer microenvironment and thus the behaviour of cancer. It is crucial to utilise this wealth of knowledge to further drive and inform future MPS model designs towards heterotypic cultures forming complex microenvironments. Furthermore, it is key to better recapitulate the tumour microenvironment by focussing on more wholly representing the ECM, tuning the mechanical properties, incorporating CSCs, stromal cells and immune cells. These systems could better recapitulate the tumour microenvironment which strongly influences the potential and mechanism of cancer cells to metastasise. Ronaldson-Bouchard et al. have developed a microfluidic system composed of 4 organ tissue niches connected via a vascular flow and separated by semi-permeable endothelial membrane [156]. The 4 organ niches are representative of heart, bone, liver and skin and via the use of human induced pluripotent stem cells and stromal cells, physiological ECM in each compartment was matured by 4-6 weeks. Models such as this, which provide multiple tissue niches composed of numerous cell types all connected via a perfusable flow channel lined with endothelial cells are critical in developing improved cancer models which better recapitulate the *in vivo* microenvironment.

More broadly, there is a need to encourage industry to progress from the use of MPSs for internal project decisions to the use of MPSs for regulatory progression. Following the Modernization Act 2.0, signed in December 2022, the FDA no longer requires animal testing for the progression of drug candidates to clinical trials [157]. However, no MPS data have been used within regulatory applications to progress to clinical trials [158]. To ensure further adoption of MPSs it is crucial to overcome key challenges currently associated with the use of these models. The majority of current models are proof of concept, costly, time consuming and with no single cell culture media optimal for the co-culture of all cell types needed to fully recapitulate the *in vivo* microenvironment. Furthermore, improvement in throughput and automation of these models is essential to allow for sufficient data collection for model validation, without which the wide industrial adoption of MPSs will not occur.

Whilst there are still many associated challenges with MPSs, there are several driving forces to encourage the adoption of MPSs. The current cost and time for drug discovery and development is high to which development of robust and reproducible models is key. Furthermore, the introduction of the 3Rs principles (replacement, reduction, and refinement) concerning animal research is a critical social and regulatory pressure promoting the development and use of MPSs.

Conflicts of Interest: The authors declare no conflict of interest.

References

[1] R. L. Siegel, K. D. Miller, and A. Jemal, "Cancer statistics, 2020," *CA Cancer J Clin*, vol. 70, no. 1, pp. 7–30, Jan. 2020, doi: 10.3322/caac.21590.

[2] F. Bray, J. Ferlay, I. Soerjomataram, R. L. Siegel, L. A. Torre, and A. Jemal, "Global cancer statistics 2018: GLOBOCAN estimates of incidence and mortality worldwide for 36 cancers in 185 countries," *CA Cancer J Clin*, vol. 68, no. 6, 2018, doi: 10.3322/caac.21492.

[3] M. Laudicella, B. Walsh, E. Burns, and P. C. Smith, "Cost of care for cancer patients in England: evidence from population-based patient-level data," *Br J Cancer*, vol. 114, no. 11, pp. 1286–1292, May 2016, doi: 10.1038/bjc.2016.77.

[4] L. Gomez-Cuadrado, N. Tracey, R. Ma, B. Qian, and V. G. Brunton, "Mouse models of metastasis: progress and prospects," *Dis Model Mech*, vol. 10, no. 9, pp. 1061–1074, Sep. 2017, doi: 10.1242/DMM.030403.

[5] M. V. Céspedes, I. Casanova, M. Parreño, and R. Mangues, "Mouse models in oncogenesis and cancer therapy," *Clinical and Translational Oncology*, vol. 8, no. 5, pp. 318–329, 2006, doi: 10.1007/s12094-006-0177-7.

[6] P. D. Bos, D. X. Nguyen, and J. Massagué, "Modeling metastasis in the mouse," *Curr Opin Pharmacol*, vol. 10, no. 5, pp. 571–577, Oct. 2010, doi: 10.1016/J.COPH.2010.06.003.

[7]   I. W. Mak, N. Evaniew, and M. Ghert, "Lost in translation: animal models and
        clinical trials in cancer treatment," *American Journal of Translation Research*,
        vol. 6, no. 2, pp. 114–118, 2014, Accessed: Jul. 31, 2023. [Online]. Available:
        www.ajtr.org

[8]   I. Dagogo-Jack and A. T. Shaw, "Tumour heterogeneity and resistance to cancer
        therapies," *Nat Rev Clin Oncol*, vol. 15, no. 2, pp. 81–94, 2018, doi:
        10.1038/nrclinonc.2017.166.

[9]   H. Lodish, A. Berk, S. Zipursky, and et al, "Section 24.1, Tumor Cells and the
        Onset of Cancer ," in *Molecular Cell Biology* , 4th ed.New York: Freeman, W.
        H., 2000.

[10]   H. Lodish, A. Berk, S. L. Zipursky, P. Matsudaira, D. Baltimore, and J. Darnell,
        "Mutations: Types and Causes," in *Molecular Cell Biology. 4th edition.*, New
        York: W. H. Freeman, 2000.

[11]   G. I. Evan and K. H. Vousden, "Proliferation, cell cycle and apoptosis in
        cancer," *Nature*, vol. 411, no. 6835, pp. 342–348, May 2001, doi:
        10.1038/35077213.

[12]   T. A. Brown, "Mutation, Repair and Recombination," in *Genomes*, 2nd
        ed.Oxford: Wiley-Liss, 2002.

[13]   R. M. Bremnes *et al.*, "The Role of Tumor Stroma in Cancer Progression and
        Prognosis: Emphasis on Carcinoma-Associated Fibroblasts and Non-small Cell
        Lung Cancer," *Journal of Thoracic Oncology*, vol. 6, no. 1, pp. 209–217, Jan.
        2011, doi: 10.1097/JTO.0B013E3181F8A1BD.

[14]   N. A. Bhowmick, E. G. Neilson, and H. L. Moses, "Stromal fibroblasts in
        cancer initiation and progression," *Nature*, vol. 432, no. 7015, pp. 332–337,
        Nov. 2004, doi: 10.1038/nature03096.

[15]   G. P. Gupta and J. Massagué, "Cancer metastasis: building a framework.," *Cell*,
        vol. 127, no. 4, pp. 679–95, Nov. 2006, doi: 10.1016/j.cell.2006.11.001.

[16]   L. A. Hapach, J. A. Mosier, W. Wang, and C. A. Reinhart-King, "Engineered
        models to parse apart the metastatic cascade," *NPJ Precis Oncol*, vol. 3, no. 1,
        p. 20, 2019, doi: 10.1038/s41698-019-0092-3.

[17]   V. da Silva-Diz, L. Lorenzo-Sanz, A. Bernat-Peguera, M. Lopez-Cerda, and P.
        Muñoz, "Cancer cell plasticity: Impact on tumor progression and therapy
        response," *Semin Cancer Biol*, vol. 53, pp. 48–58, Dec. 2018, doi:
        10.1016/J.SEMCANCER.2018.08.009.

[18]   M. Greaves and C. C. Maley, "Clonal evolution in cancer," *Nature 2012
        481:7381*, vol. 481, no. 7381, pp. 306–313, Jan. 2012, doi:
        10.1038/nature10762.

[19]   I. Bozic *et al.*, "Accumulation of driver and passenger mutations during tumor
        progression," *Proc Natl Acad Sci U S A*, vol. 107, no. 43, pp. 18545–18550,
        Oct. 2010, doi: 10.1073/PNAS.1010978107/SUPPL_FILE/APPENDIX.PDF.

[20]   A. Z. Ayob and T. S. Ramasamy, "Cancer stem cells as key drivers of tumour
        progression," *Journal of Biomedical Science 2018 25:1*, vol. 25, no. 1, pp. 1–18,
        Mar. 2018, doi: 10.1186/S12929-018-0426-4.

[21]   C. E. Meacham and S. J. Morrison, "Tumour heterogeneity and cancer cell
        plasticity," *Nature 2013 501:7467*, vol. 501, no. 7467, pp. 328–337, Sep. 2013,
        doi: 10.1038/nature12624.

[22]   M. Carla Cabrera, R. E. Hollingsworth, and E. M. Hurt, "Cancer stem cell
        plasticity and tumor hierarchy," *World J Stem Cells*, vol. 7, no. 1, pp. 27–36,
        Jan. 2015, doi: 10.4252/wjsc.v7.i1.27.

[23] S. Senapati, R. K. Singh, and S. K. Batra, "Tumor microenvironment: blood vascular system in cancer metastasis," in *Systems Biology of Cancer*, S. Thiagalingam, Ed., Cambridge University Press, 2015, pp. 309–319.

[24] G. Cooper, "The Development and Causes of Cancer," in *The Cell: A Molecular Approach*, 2nd Editio.Sunderland (MA): Sinauer Associates, 2000.

[25] M. Bacac and I. Stamenkovic, "Metastatic Cancer Cell," *Annual Review of Pathology: Mechanisms of Disease*, vol. 3, no. 1, pp. 221–247, Feb. 2008, doi: 10.1146/annurev.pathmechdis.3.121806.151523.

[26] L. A. Liotta, P. S. Steeg, and W. G. Stetler-Stevenson, "Cancer metastasis and angiogenesis: An imbalance of positive and negative regulation," *Cell*, vol. 64, no. 2, pp. 327–336, Jan. 1991, doi: 10.1016/0092-8674(91)90642-C.

[27] J. Behrens, "The role of cell adhesion molecules in cancer invasion and metastasis," *Breast Cancer Res Treat*, vol. 24, no. 3, pp. 175–184, Oct. 1993, doi: 10.1007/BF01833258.

[28] J. Shankar, A. Messenberg, J. Chan, T. M. Underhill, L. J. Foster, and I. R. Nabi, "Pseudopodial Actin Dynamics Control Epithelial-Mesenchymal Transition in Metastatic Cancer Cells," *Cancer Res*, vol. 70, no. 9, pp. 3780–3790, May 2010, doi: 10.1158/0008-5472.CAN-09-4439.

[29] J. P. Thiery, H. Acloque, R. Y. J. Huang, and M. A. Nieto, "Epithelial-mesenchymal transitions in development and disease.," *Cell*, vol. 139, no. 5, pp. 871–90, Nov. 2009, doi: 10.1016/j.cell.2009.11.007.

[30] A.-K. Perl, P. Wilgenbus, U. Dahl, H. Semb, and G. Christofori, "A causal role for E-cadherin in the transition from adenoma to carcinoma," *Nature*, vol. 392, no. 6672, pp. 190–193, Mar. 1998, doi: 10.1038/32433.

[31] U. H. Frixen *et al.*, "E-cadherin-mediated cell-cell adhesion prevents invasiveness of human carcinoma cells," *Journal of Cell Biology*, vol. 113, no. 1, pp. 173–185, 1991, doi: 10.1083/jcb.113.1.173.

[32] G. Sannino, A. Marchetto, T. Kirchner, and T. G. P. Grünewald, "Epithelial-to-Mesenchymal and Mesenchymal-to-Epithelial Transition in Mesenchymal Tumors: A Paradox in Sarcomas?," *Cancer Res*, vol. 77, no. 17, pp. 4556–4561, Aug. 2017, doi: 10.1158/0008-5472.CAN-17-0032.

[33] N. M. Aiello *et al.*, "EMT Subtype Influences Epithelial Plasticity and Mode of Cell Migration Developmental Cell Article EMT Subtype Influences Epithelial Plasticity and Mode of Cell Migration," *Dev Cell*, vol. 45, pp. 681-695.e4, 2018, doi: 10.1016/j.devcel.2018.05.027.

[34] T. Brabletz, "EMT and MET in Metastasis: Where Are the Cancer Stem Cells?," *Cancer Cell*, vol. 22, pp. 699–701, Dec. 2012, doi: 10.1016/j.ccr.2012.11.009.

[35] S. Dedhar and R. Saulnier, "Alterations in integrin receptor expression on chemically transformed human cells: Specific enhancement of laminin and collagen receptor complexes," *Journal of Cell Biology*, vol. 110, no. 2, pp. 481–489, 1990, doi: 10.1083/jcb.110.2.481.

[36] H. Yamaguchi, "Pathological roles of invadopodia in cancer invasion and metastasis," *Eur J Cell Biol*, vol. 91, no. 11–12, pp. 902–907, Nov. 2012, doi: 10.1016/J.EJCB.2012.04.005.

[37] J. J. Bravo-Cordero, L. Hodgson, and J. Condeelis, "Directed cell invasion and migration during metastasis.," *Curr Opin Cell Biol*, vol. 24, no. 2, pp. 277–83, Apr. 2012, doi: 10.1016/j.ceb.2011.12.004.

[38] L. A. Liotta, K. Tryggvason, S. Garbisa, I. Hart, C. M. Foltz, and S. Shafie, "Metastatic potential correlates with enzymatic degradation of basement

membrane collagen," *Nature*, vol. 284, no. 5751, pp. 67–68, 1980, doi: 10.1038/284067a0.

[39] K. Wolf and P. Friedl, "Mapping proteolytic cancer cell-extracellular matrix interfaces," *Clin Exp Metastasis*, vol. 26, no. 4, pp. 289–298, Jul. 2009, doi: 10.1007/s10585-008-9190-2.

[40] P. Friedl and K. Wolf, "Plasticity of cell migration: a multiscale tuning model.," *J Cell Biol*, vol. 188, no. 1, pp. 11–9, Jan. 2010, doi: 10.1083/jcb.200909003.

[41] S. Y. Wong and R. O. Hynes, "Lymphatic or hematogenous dissemination: How does a metastatic tumor cell decide?," *Cell Cycle*, vol. 5, no. 8, pp. 812–817, Apr. 2006, doi: 10.4161/cc.5.8.2646.

[42] S. P. H. Chiang, R. M. Cabrera, and J. E. Segall, "Tumor cell intravasation," *Am J Physiol Cell Physiol*, vol. 311, no. 1, pp. C1–C14, Jul. 2016, doi: 10.1152/ajpcell.00238.2015.

[43] J. A. Joyce and J. W. Pollard, "Microenvironmental regulation of metastasis.," *Nat Rev Cancer*, vol. 9, no. 4, pp. 239–52, Apr. 2009, doi: 10.1038/nrc2618.

[44] K. Alitalo and P. Carmeliet, "Molecular mechanisms of lymphangiogenesis in health and disease," *Cancer Cell*, vol. 1, no. 3, pp. 219–227, Apr. 2002, doi: 10.1016/S1535-6108(02)00051-X.

[45] G. J. Gasic, T. B. Gasic, and C. C. Stewart, "Antimetastatic effects associated with platelet reduction.," *Proc Natl Acad Sci U S A*, vol. 61, no. 1, pp. 46–52, 1968, doi: 10.1073/pnas.61.1.46.

[46] K. Egan, N. Cooke, and D. Kenny, "Living in shear: Platelets protect cancer cells from shear induced damage," *Clin Exp Metastasis*, vol. 31, no. 6, pp. 697–704, Jun. 2014, doi: 10.1007/S10585-014-9660-7/FIGURES/4.

[47] B. M. Szczerba *et al.*, "Neutrophils escort circulating tumour cells to enable cell cycle progression," *Nature 2019 566:7745*, vol. 566, no. 7745, pp. 553–557, Feb. 2019, doi: 10.1038/s41586-019-0915-y.

[48] J. Perea Paizal, S. H. Au, and C. Bakal, "Squeezing through the microcirculation: survival adaptations of circulating tumour cells to seed metastasis," *Br J Cancer*, vol. 124, no. 1, p. 58, Jan. 2021, doi: 10.1038/S41416-020-01176-X.

[49] L. Yang *et al.*, "DNA of neutrophil extracellular traps promotes cancer metastasis via CCDC25," *Nature 2020 583:7814*, vol. 583, no. 7814, pp. 133–138, Jun. 2020, doi: 10.1038/s41586-020-2394-6.

[50] Y. Xia *et al.*, "Nucleus of Circulating Tumor Cell Determines Its Translocation Through Biomimetic Microconstrictions and Its Physical Enrichment by Microfiltration," *Small*, vol. 14, no. 44, p. 1802899, Nov. 2018, doi: 10.1002/SMLL.201802899.

[51] K. Yamauchi *et al.*, "Real-time In vivo Dual-color Imaging of Intracapillary Cancer Cell and Nucleus Deformation and Migration," *Cancer Res*, vol. 65, no. 10, pp. 4246–4252, May 2005, doi: 10.1158/0008-5472.CAN-05-0069.

[52] C. Rianna, M. Radmacher, and S. Kumar, "Direct evidence that tumor cells soften when navigating confined spaces," *Mol Biol Cell*, vol. 31, no. 16, pp. 1726–1734, Jul. 2020, doi: 10.1091/MBC.E19-10-0588/ASSET/IMAGES/LARGE/MBC-31-1726-G007.JPEG.

[53] H. A. Cognart, J. L. Viovy, and C. Villard, "Fluid shear stress coupled with narrow constrictions induce cell type-dependent morphological and molecular changes in SK-BR-3 and MDA-MB-231 cells," *Sci Rep*, vol. 10, no. 1, pp. 1–14, Apr. 2020, doi: 10.1038/s41598-020-63316-w.

[54] B. Strilic and S. Offermanns, "Intravascular Survival and Extravasation of Tumor Cells," *Cancer Cell*, vol. 32, no. 3, pp. 282–293, Sep. 2017, doi: 10.1016/j.ccell.2017.07.001.

[55] D. Stegner, S. Dütting, and B. Nieswandt, "Mechanistic explanation for platelet contribution to cancer metastasis," *Thromb Res*, vol. 133, no. SUPPL. 2, pp. S149–S157, May 2014, doi: 10.1016/S0049-3848(14)50025-4.

[56] H. S. Leong *et al.*, "Invadopodia Are Required for Cancer Cell Extravasation and Are a Therapeutic Target for Metastasis," *Cell Rep*, vol. 8, no. 5, pp. 1558–1570, Sep. 2014, doi: 10.1016/j.celrep.2014.07.050.

[57] P. L. Tremblay, J. Huot, and F. A. Auger, "Mechanisms by which E-Selectin Regulates Diapedesis of Colon Cancer Cells under Flow Conditions," *Cancer Res*, vol. 68, no. 13, pp. 5167–5176, Jul. 2008, doi: 10.1158/0008-5472.CAN-08-1229.

[58] F. van Zijl, G. Krupitza, and W. Mikulits, "Initial steps of metastasis: cell invasion and endothelial transmigration.," *Mutat Res*, vol. 728, no. 1–2, pp. 23–34, 2011, doi: 10.1016/j.mrrev.2011.05.002.

[59] K. Naidoo and S. E. Pinder, "Micro- and macro-metastasis in the axillary lymph node: A review," *The Surgeon*, vol. 15, no. 2, pp. 76–82, Apr. 2017, doi: 10.1016/J.SURGE.2016.07.002.

[60] P. Hermanek, R. V. P. Hutter, L. H. Sobin, and C. Wittekind, "Classification of isolated tumor cells and micrometastasis," *Cancer*, vol. 86, no. 12, pp. 2668–2673, Dec. 1999, doi: 10.1002/(SICI)1097-0142(19991215)86:12<2668::AID-CNCR11>3.0.CO;2-R.

[61] P. Friedl, S. Borgmann, and E. B. Bröcker, "Amoeboid leukocyte crawling through extracellular matrix: lessons from the Dictyostelium paradigm of cell movement.," *J Leukoc Biol*, vol. 70, no. 4, pp. 491–509, Oct. 2001, doi: 10.1189/jlb.70.4.491.

[62] T. Lämmermann and M. Sixt, "Mechanical modes of 'amoeboid' cell migration," *Curr Opin Cell Biol*, vol. 21, no. 5, pp. 636–644, Oct. 2009, doi: 10.1016/J.CEB.2009.05.003.

[63] G. Charras and E. Paluch, "Blebs lead the way: how to migrate without lamellipodia," *Nat Rev Mol Cell Biol*, vol. 9, no. 9, pp. 730–736, Sep. 2008, doi: 10.1038/nrm2453.

[64] O. T. Fackler and R. Grosse, "Cell motility through plasma membrane blebbing.," *J Cell Biol*, vol. 181, no. 6, pp. 879–84, Jun. 2008, doi: 10.1083/jcb.200802081.

[65] K. Yoshida and T. Soldati, "Dissection of amoeboid movement into two mechanically distinct modes," *J Cell Sci*, vol. 119, no. 18, pp. 3833–3844, Sep. 2006, doi: 10.1242/jcs.03152.

[66] A. G. Clark and D. M. Vignjevic, "Modes of cancer cell invasion and the role of the microenvironment," *Curr Opin Cell Biol*, vol. 36, pp. 13–22, Oct. 2015, doi: 10.1016/J.CEB.2015.06.004.

[67] C. M. Denais *et al.*, "Nuclear envelope rupture and repair during cancer cell migration.," *Science*, vol. 352, no. 6283, pp. 353–8, Apr. 2016, doi: 10.1126/science.aad7297.

[68] P. Friedl and K. Wolf, "Tumour-cell invasion and migration: diversity and escape mechanisms," *Nat Rev Cancer*, vol. 3, no. 5, pp. 362–374, May 2003, doi: 10.1038/nrc1075.

[69] K. M. Yamada and M. Sixt, "Mechanisms of 3D cell migration," *Nat Rev Mol Cell Biol*, vol. 20, no. 12, pp. 738–752, Dec. 2019, doi: 10.1038/s41580-019-0172-9.

[70] E. Zamir *et al.*, "Dynamics and segregation of cell-matrix adhesions in cultured fibroblasts," *Nat Cell Biol*, vol. 2, no. 4, pp. 191–6, Apr. 2000.

[71] C. Ballestrem, B. Hinz, B. A. Imhof, and B. Wehrle-Haller, "Marching at the front and dragging behind: Differential αVβ3-integrin turnover regulates focal adhesion behavior," *Journal of Cell Biology*, vol. 155, no. 7, pp. 1319–1332, Dec. 2001, doi: 10.1083/jcb.200107107.

[72] P. Friedl and S. Alexander, "Cancer Invasion and the Microenvironment: Plasticity and Reciprocity," *Cell*, vol. 147, no. 5, pp. 992–1009, Nov. 2011, doi: 10.1016/J.CELL.2011.11.016.

[73] A. Patsialou *et al.*, "Intravital multiphoton imaging reveals multicellular streaming as a crucial component of in vivo cell migration in human breast tumors," *Intravital*, vol. 2, no. 2, p. e25294, Apr. 2013, doi: 10.4161/intv.25294.

[74] A. A. Khalil and P. Friedl, "Determinants of leader cells in collective cell migration," *Integrative Biology*, vol. 2, no. 11–12, p. 568, Nov. 2010, doi: 10.1039/c0ib00052c.

[75] P. Lu, V. M. Weaver, and Z. Werb, "The extracellular matrix: a dynamic niche in cancer progression.," *J Cell Biol*, vol. 196, no. 4, pp. 395–406, Feb. 2012, doi: 10.1083/jcb.201102147.

[76] M. Egeblad, M. G. Rasch, and V. M. Weaver, "Dynamic interplay between the collagen scaffold and tumor evolution," *Curr Opin Cell Biol*, vol. 22, no. 5, pp. 697–706, Oct. 2010, doi: 10.1016/j.ceb.2010.08.015.

[77] S. Shen and J. Clairambault, "Cell plasticity in cancer cell populations [version 1; peer review: 2 approved]," *F1000Research 2020*, vol. 9, no. F1000 Faculty Rev, p. 635, Jun. 2020, doi: 10.12688/f1000research.24803.1.

[78] M. R. Junttila and F. J. De Sauvage, "Influence of tumour micro-environment heterogeneity on therapeutic response," *Nature*, vol. 501, no. 7467, pp. 346–354, Sep. 2013, doi: 10.1038/nature12626.

[79] S. I. Grivennikov, F. R. Greten, and M. Karin, "Immunity, Inflammation, and Cancer," *Cell*, vol. 140, no. 6, pp. 883–899, Mar. 2010, doi: 10.1016/J.CELL.2010.01.025.

[80] S. Özbek, P. G. Balasubramanian, R. Chiquet-Ehrismann, R. P. Tucker, and J. C. Adams, "The evolution of extracellular matrix," *Mol Biol Cell*, vol. 21, no. 24, pp. 4300–4305, Dec. 2010, doi: 10.1091/mbc.E10-03-0251.

[81] I. O. Smith, X. H. Liu, L. A. Smith, and P. X. Ma, "Nanostructured polymer scaffolds for tissue engineering and regenerative medicine," *Wiley Interdiscip Rev Nanomed Nanobiotechnol*, vol. 1, no. 2, pp. 226–236, Mar. 2009, doi: 10.1002/wnan.26.

[82] P. P. Provenzano, K. W. Eliceiri, J. M. Campbell, D. R. Inman, J. G. White, and P. J. Keely, "Collagen reorganization at the tumor-stromal interface facilitates local invasion.," *BMC Med*, vol. 4, no. 1, p. 38, Dec. 2006, doi: 10.1186/1741-7015-4-38.

[83] S. Nallanthighal, J. P. Heiserman, and D.-J. Cheon, "The Role of the Extracellular Matrix in Cancer Stemness," *Front Cell Dev Biol*, vol. 7, p. 86, Jul. 2019, doi: 10.3389/fcell.2019.00086.

[84] C. Walker, E. Mojares, and A. Del Río Hernández, "Role of extracellular matrix in development and cancer progression," *Int J Mol Sci*, vol. 19, no. 10, Oct. 2018, doi: 10.3390/ijms19103028.

[85]   E. Henke, R. Nandigama, and S. Ergün, "Extracellular Matrix in the Tumor Microenvironment and Its Impact on Cancer Therapy," *Front Mol Biosci*, vol. 6, no. 160, Jan. 2020, doi: 10.3389/fmolb.2019.00160.

[86]   S. Ramaswamy, K. N. Ross, E. S. Lander, and T. R. Golub, "A molecular signature of metastasis in primary solid tumors," 2002, doi: 10.1038/ng1060.

[87]   M. J. Paszek *et al.*, "Tensional homeostasis and the malignant phenotype," *Cancer Cell*, vol. 8, no. 3, pp. 241–254, Sep. 2005, doi: 10.1016/j.ccr.2005.08.010.

[88]   M. J. Paszek and V. M. Weaver, "The tension mounts: Mechanics meets morphogenesis and malignancy," *J Mammary Gland Biol Neoplasia*, vol. 9, no. 4, pp. 325–342, Oct. 2004, doi: 10.1007/s10911-004-1404-x.

[89]   C. Decaestecker, O. Debeir, P. Van Ham, and R. Kiss, "Can anti-migratory drugs be screened in vitro? A review of 2D and 3D assays for the quantitative analysis of cell migration," *Med Res Rev*, vol. 27, no. 2, pp. 149–176, Mar. 2007, doi: 10.1002/med.20078.

[90]   F. Entschladen *et al.*, "Analysis methods of human cell migration," *Exp Cell Res*, vol. 307, pp. 418–426, 2005, doi: 10.1016/j.yexcr.2005.03.029.

[91]   N. Kramer *et al.*, "In vitro cell migration and invasion assays," *Mutation Research/Reviews in Mutation Research*, vol. 752, no. 1, pp. 10–24, 2013, doi: https://doi.org/10.1016/j.mrrev.2012.08.001.

[92]   W. J. Ashby and A. Zijlstra, "Established and novel methods of interrogating two-dimensional cell migration," *Integrative Biology*, vol. 4, no. 11, pp. 1338–1350, Oct. 2012, doi: 10.1039/c2ib20154b.

[93]   W. J. Ashby and A. Zijlstra, "Established and novel methods of interrogating two-dimensional cell migration.," *Integr Biol (Camb)*, vol. 4, no. 11, pp. 1338–50, Nov. 2012, doi: 10.1039/c2ib20154b.

[94]   C. R. Justus, N. Leffler, M. Ruiz-Echevarria, and L. V Yang, "In vitro cell migration and invasion assays.," *J Vis Exp*, no. 88, Jun. 2014, doi: 10.3791/51046.

[95]   L. J. Wager, R. Z. Murray, E. W. Thompson, and D. I. Leavesley, "A fence barrier method of leading edge cell capture for explorative biochemical research," *Cell Adh Migr*, vol. 11, no. 5–6, pp. 496–503, Sep. 2017, doi: 10.1080/19336918.2016.1269997.

[96]   J. T. Freitas, I. Jozic, and B. Bedogni, "Wound Healing Assay for Melanoma Cell Migration," *Methods in Molecular Biology*, vol. 2265, pp. 65–71, 2021, doi: 10.1007/978-1-0716-1205-7_4/FIGURES/2.

[97]   Y. Zhang *et al.*, "Comparative study of 3D morphology and functions on genetically engineered mouse melanoma cells," *Integrative Biology*, vol. 4, no. 11, p. 1428, Oct. 2012, doi: 10.1039/c2ib20153d.

[98]   J. E. N. Jonkman *et al.*, "An introduction to the wound healing assay using live-cell microscopy," *Cell Adh Migr*, vol. 8, no. 5, pp. 440–451, Sep. 2014, doi: 10.4161/cam.36224.

[99]   Y. Kam, A. Karperien, B. Weidow, L. Estrada, A. R. Anderson, and V. Quaranta, "Nest expansion assay: A cancer systems biology approach to in vitro invasion measurements," *BMC Res Notes*, vol. 2, p. 130, 2009, doi: 10.1186/1756-0500-2-130.

[100] E. Joeckel *et al.*, "High calcium concentration in bones promotes bone metastasis in renal cell carcinomas expressing calcium-sensing receptor," *Mol Cancer*, vol. 13, no. 1, pp. 1–11, Feb. 2014, doi: 10.1186/1476-4598-13-42.

[101] S. Bersini, J. S. Jeon, M. Moretti, and R. D. Kamm, "In vitro models of the metastatic cascade: from local invasion to extravasation.," *Drug Discov Today*, vol. 19, no. 6, pp. 735–42, Jun. 2014, doi: 10.1016/j.drudis.2013.12.006.

[102] M. E. Katt, A. L. Placone, A. D. Wong, Z. S. Xu, and P. C. Searson, "In vitro tumor models: Advantages, disadvantages, variables, and selecting the right platform," *Front Bioeng Biotechnol*, vol. 4, no. FEB, p. 12, Feb. 2016, doi: 10.3389/fbioe.2016.00012.

[103] L. Zhou, D. T. Dicker, E. Matthew, W. S. El-Deiry, and R. K. Alpaugh, "Circulating tumor cells: silent predictors of metastasis.," *F1000Res*, vol. 6, 2017, doi: 10.12688/f1000research.11313.1.

[104] L. Wang, P. Balasubramanian, A. P. Chen, S. Kummar, Y. A. Evrard, and R. J. Kinders, "Promise and limits of the CellSearch platform for evaluating pharmacodynamics in circulating tumor cells," *Semin Oncol*, vol. 43, no. 4, pp. 464–475, Aug. 2016, doi: 10.1053/j.seminoncol.2016.06.004.

[105] S. F. Moussavi-Harami, K. B. Wisinski, and D. J. Beebe, "Circulating Tumor Cells in Metastatic Breast Cancer: A Prognostic and Predictive Marker.," *J Patient Cent Res Rev*, vol. 1, no. 2, pp. 85–92, 2014, doi: 10.17294/2330-0698.1017.

[106] W. J. Allard *et al.*, "Tumor cells circulate in the peripheral blood of all major carcinomas but not in healthy subjects or patients with nonmalignant diseases," *Clinical Cancer Research*, vol. 10, no. 20, pp. 6897–6904, Oct. 2004, doi: 10.1158/1078-0432.CCR-04-0378.

[107] C. Rao *et al.*, "Expression of epithelial cell adhesion molecule in carcinoma cells present in blood and primary and metastatic tumors," *Int J Oncol*, vol. 27, no. 1, pp. 49–57, Jul. 2005, doi: 10.3892/ijo.27.1.49.

[108] C. Dolfus, N. Piton, E. Toure, and J.-C. Sabourin, "Circulating tumor cell isolation: the assets of filtration methods with polycarbonate track-etched filters.," *Chin J Cancer Res*, vol. 27, no. 5, pp. 479–87, Oct. 2015, doi: 10.3978/j.issn.1000-9604.2015.09.01.

[109] Z. Mu *et al.*, "Abstract P2-02-14: Detection and characterization of CTCs isolated by ScreenCell®-Filtration in metastatic breast cancer," in *Cancer Research*, American Association for Cancer Research (AACR), Feb. 2016, pp. P2-02-14-P2-02–14. doi: 10.1158/1538-7445.sabcs15-p2-02-14.

[110] M. Di Trapani, N. Manaresi, and G. Medoro, "DEPArray™ system: An automatic image-based sorter for isolation of pure circulating tumor cells," *Cytometry Part A*, vol. 93, no. 12, pp. 1260–1266, Dec. 2018, doi: 10.1002/cyto.a.23687.

[111] M. G. Krebs *et al.*, "Analysis of circulating tumor cells in patients with non-small cell lung cancer using epithelial marker-dependent and -independent approaches," *Journal of Thoracic Oncology*, vol. 7, no. 2, pp. 306–315, Feb. 2012, doi: 10.1097/JTO.0b013e31823c5c16.

[112] D. Holmes *et al.*, "Separation of blood cells with differing deformability using deterministic lateral displacement," *Interface Focus*, vol. 4, no. 6, Dec. 2014, doi: 10.1098/rsfs.2014.0011.

[113] Y. Chen *et al.*, "Rare cell isolation and analysis in microfluidics.," *Lab Chip*, vol. 14, no. 4, pp. 626–45, Feb. 2014, doi: 10.1039/c3lc90136j.

[114] K. Loutherback, J. D'Silva, L. Liu, A. Wu, R. H. Austin, and J. C. Sturm, "Deterministic separation of cancer cells from blood at 10 mL/min," *AIP Adv*, vol. 2, no. 4, 2012, doi: 10.1063/1.4758131.

[115] S. H. Au *et al.*, "Microfluidic isolation of circulating tumor cell clusters by size and asymmetry," *Sci Rep*, vol. 7, no. 1, pp. 1–10, Dec. 2017, doi: 10.1038/s41598-017-01150-3.

[116] E. Knight, B. Murray, R. Carnachan, and S. Przyborski, "Alvetex®: Polystyrene Scaffold Technology for Routine Three Dimensional Cell Culture," in *Methods in molecular biology (Clifton, N.J.)*, Humana Press, 2011, pp. 323–340. doi: 10.1007/978-1-60761-984-0_20.

[117] W. Asghar, R. El Assal, H. Shafiee, S. Pitteri, R. Paulmurugan, and U. Demirci, "Engineering cancer microenvironments for in vitro 3-D tumor models," *Materials Today*, vol. 18, no. 10. Elsevier, pp. 539–553, Dec. 01, 2015. doi: 10.1016/j.mattod.2015.05.002.

[118] C. M. Leung *et al.*, "A guide to the organ-on-a-chip," *Nature Reviews Methods Primers 2022 2:1*, vol. 2, no. 1, pp. 1–29, May 2022, doi: 10.1038/s43586-022-00118-6.

[119] S. Abdulghani and G. R. Mitchell, "Biomaterials for in situ tissue regeneration: A review," *Biomolecules*, vol. 9, no. 11, p. 750, Nov. 2019, doi: 10.3390/biom9110750.

[120] M. Kapałczyńska *et al.*, "2D and 3D cell cultures – a comparison of different types of cancer cell cultures," *Arch Med Sci*, vol. 14, no. 4, p. 910, 2018, doi: 10.5114/AOMS.2016.63743.

[121] F. J. O'Brien, "Biomaterials & scaffolds for tissue engineering," *Materials Today*, vol. 14, no. 3. Elsevier B.V., pp. 88–95, Mar. 01, 2011. doi: 10.1016/S1369-7021(11)70058-X.

[122] B. P. Chan and K. W. Leong, "Scaffolding in tissue engineering: General approaches and tissue-specific considerations," *European Spine Journal*, vol. 17, no. SUPPL. 4, p. 479, Dec. 2008, doi: 10.1007/s00586-008-0745-3.

[123] G. Yang, B. Mahadik, J. Y. Choi, and J. P. Fisher, "Vascularization in tissue engineering: fundamentals and state-of-art," *Progress in Biomedical Engineering*, vol. 2, no. 1, p. 012002, Jan. 2020, doi: 10.1088/2516-1091/AB5637.

[124] M. Sarker, X. B. Chen, and D. J. Schreyer, "Experimental approaches to vascularisation within tissue engineering constructs," *J Biomater Sci Polym Ed*, vol. 26, no. 12, pp. 683–734, Aug. 2015, doi: 10.1080/09205063.2015.1059018.

[125] Y. Kameda *et al.*, "Three-dimensional tissue model in direct contact with an on-chip vascular bed enabled by removable membranes," *Lab Chip*, vol. 22, no. 3, pp. 641–651, Feb. 2022, doi: 10.1039/d1lc00751c.

[126] F. Chesnais *et al.*, "Continuously perfusable, customisable, and matrix-free vasculature on a chip platform," *Lab Chip*, vol. 23, no. 4, pp. 761–772, Feb. 2023, doi: 10.1039/D2LC00930G.

[127] H. L. Lanz *et al.*, "Therapy response testing of breast cancer in a 3D high-throughput perfused microfluidic platform," *BMC Cancer*, vol. 17, no. 1, Nov. 2017, doi: 10.1186/S12885-017-3709-3.

[128] W. Wei, F. Cardes, A. Hierlemann, and M. M. Modena, "3D In Vitro Blood-Brain-Barrier Model for Investigating Barrier Insults," *Advanced Science*, vol. 10, no. 11, p. 2205752, Apr. 2023, doi: 10.1002/ADVS.202205752.

[129] C. Strelez *et al.*, "Human colorectal cancer-on-chip model to study the microenvironmental influence on early metastatic spread," *iScience*, vol. 24, no. 5, p. 102509, May 2021, doi: 10.1016/J.ISCI.2021.102509.

[130] Y.-C. Toh, A. Raja, H. Yu, and D. van Noort, "A 3D Microfluidic Model to Recapitulate Cancer Cell Migration and Invasion.," *Bioengineering (Basel)*, vol. 5, no. 2, Apr. 2018, doi: 10.3390/bioengineering5020029.

[131] "SynTumor 3D Cancer Model | SynVivo." https://www.synvivobio.com/syntumor/#1588022204361-a177b155-1008 (accessed Jul. 31, 2023).

[132] F. Macedo *et al.*, "Bone Metastases: An Overview," *Oncol Rev*, vol. 11, no. 1, Mar. 2017, doi: 10.4081/ONCOL.2017.321.

[133] O. J. Scully, B.-H. Bay, G. Yip, and Y. Yu, "Breast Cancer Metastasis," *Cancer Genomics - Proteomics*, vol. 9, no. 5, pp. 311 LP – 320, Sep. 2012.

[134] A. J. Minn *et al.*, "Distinct organ-specific metastatic potential of individual breast cancer cells and primary tumors," *J Clin Invest*, vol. 115, no. 1, pp. 44–55, Jan. 2005, doi: 10.1172/JCI22320.

[135] D. A. August, R. T. Ottow, and P. H. Sugarbaker, "Clinical perspective of human colorectal cancer metastasis," *Cancer and Metastasis Reviews*, vol. 3, no. 4, pp. 303–324, 1984, doi: 10.1007/BF00051457.

[136] H. H. Popper, "Progression and metastasis of lung cancer," 2016, doi: 10.1007/s10555-016-9618-0.

[137] M. Riihimäki *et al.*, "Metastatic sites and survival in lung cancer," *Lung Cancer*, vol. 86, no. 1, pp. 78–84, 2014, doi: https://doi.org/10.1016/j.lungcan.2014.07.020.

[138] S. Bersini *et al.*, "A microfluidic 3D in vitro model for specificity of breast cancer metastasis to bone," *Biomaterials*, vol. 35, no. 8, pp. 2454–2461, Mar. 2014, doi: 10.1016/J.BIOMATERIALS.2013.11.050.

[139] M. B. Chen, J. A. Whisler, J. Fröse, C. Yu, Y. Shin, and R. D. Kamm, "On-chip human microvasculature assay for visualization and quantitation of tumor cell extravasation dynamics," *Nat Protoc*, vol. 12, no. 5, p. 865, May 2017, doi: 10.1038/NPROT.2017.018.

[140] A. Skardal, M. Devarasetty, S. Forsythe, A. Atala, and S. Soker, "A reductionist metastasis-on-a-chip platform for in vitro tumor progression modeling and drug screening," *Biotechnol Bioeng*, vol. 113, no. 9, pp. 2020–2032, Sep. 2016, doi: 10.1002/BIT.25950.

[141] Z. Xu *et al.*, "Design and Construction of a Multi-Organ Microfluidic Chip Mimicking the in vivo Microenvironment of Lung Cancer Metastasis," *ACS Appl Mater Interfaces*, vol. 8, no. 39, pp. 25840–25847, 2016, doi: 10.1021/acsami.6b08746.

[142] R. Mukhopadhyay, "When PDMS isn't the best," *Anal Chem*, vol. 79, no. 9, pp. 3249–3253, May 2007, doi: 10.1021/AC071903E/ASSET/AC071903E.FP.PNG_V03.

[143] K. Raj M and S. Chakraborty, "PDMS microfluidics: A mini review," *J Appl Polym Sci*, vol. 137, no. 27, p. 48958, Jul. 2020, doi: 10.1002/APP.48958.

[144] M. W. Toepke and D. J. Beebe, "PDMS absorption of small molecules and consequences in microfluidic applications," *Lab Chip*, vol. 6, no. 12, pp. 1484–1486, Nov. 2006, doi: 10.1039/B612140C.

[145] A. M. Clark, B. Ma, D. Lansing Taylor, L. Griffith, and A. Wells, "Liver metastases: Microenvironments and ex-vivo models," *Exp Biol Med*, vol. 241, pp. 1639–1652, 2016, doi: 10.1177/1535370216658144.

[146] A. M. Clark *et al.*, "A model of dormant-emergent metastatic breast cancer progression enabling exploration of biomarker signatures," *Molecular and*

Cellular Proteomics, vol. 17, no. 4, pp. 619–630, Apr. 2018, doi: 10.1074/mcp.RA117.000370.

[147] B. Aldemir Dikici, C. Sherborne, G. C. Reilly, and F. Claeyssens, "Emulsion templated scaffolds manufactured from photocurable polycaprolactone," *Polymer (Guildf)*, vol. 175, pp. 243–254, Jun. 2019, doi: 10.1016/j.polymer.2019.05.023.

[148] S. Bhatia, "Natural Polymers vs Synthetic Polymer," in *Natural Polymer Drug Delivery Systems: Nanoparticles, Plants, and Algae*, S. Bhatia, Ed., Cham: Springer International Publishing, 2016, pp. 95–118. doi: 10.1007/978-3-319-41129-3_3.

[149] S. S. Shetye, K. S. Miller, J. E. Hsu, and L. J. Soslowsky, "7.18 Materials in Tendon and Ligament Repair," P. B. T.-C. B. I. I. Ducheyne, Ed., Oxford: Elsevier, 2017, pp. 314–340. doi: https://doi.org/10.1016/B978-0-12-803581-8.09252-3.

[150] V. Angeloni *et al.*, "Polyurethane foam scaffold as in vitro model for breast cancer bone metastasis," *Acta Biomater*, vol. 63, pp. 306–316, Nov. 2017, doi: 10.1016/J.ACTBIO.2017.09.017.

[151] M. C. Regier *et al.*, "Transitions from mono- to co- to tri-culture uniquely affect gene expression in breast cancer, stromal, and immune compartments," *Biomed Microdevices*, vol. 18, no. 4, 2016, doi: 10.1007/s10544-016-0083-x.

[152] Y.-H. V. Ma, K. Middleton, L. You, and Y. Sun, "A review of microfluidic approaches for investigating cancer extravasation during metastasis," *Microsyst Nanoeng*, vol. 4, no. 1, pp. 1–13, Apr. 2018, doi: 10.1038/micronano.2017.104.

[153] W. J. Polacheck, A. E. German, A. Mammoto, D. E. Ingber, and R. D. Kamm, "Mechanotransduction of fluid stresses governs 3D cell migration," *Proc Natl Acad Sci U S A*, vol. 111, no. 7, pp. 2447–2452, Feb. 2014, doi: 10.1073/PNAS.1316848111/SUPPL_FILE/SM03.MOV.

[154] Y. L. Huang, C. K. Tung, A. Zheng, B. J. Kim, and M. Wu, "Interstitial flows promote amoeboid over mesenchymal motility of breast cancer cells revealed by a three dimensional microfluidic model," *Integrative Biology (United Kingdom)*, vol. 7, no. 11, pp. 1402–1411, Nov. 2015, doi: 10.1039/c5ib00115c.

[155] A. Pathak and S. Kumar, "Independent regulation of tumor cell migration by matrix stiffness and confinement," *Proc Natl Acad Sci U S A*, vol. 109, no. 26, pp. 10334–10339, 2012, doi: 10.1073/pnas.1118073109/-/DCSupplemental.

[156] K. Ronaldson-Bouchard *et al.*, "A multi-organ chip with matured tissue niches linked by vascular flow," *Nature Biomedical Engineering 2022 6:4*, vol. 6, no. 4, pp. 351–371, Apr. 2022, doi: 10.1038/s41551-022-00882-6.

[157] J. J. Han, "FDA Modernization Act 2.0 allows for alternatives to animal testing," *Artif Organs*, vol. 47, no. 3, pp. 449–450, Mar. 2023, doi: 10.1111/AOR.14503.

[158] U. Marx *et al.*, "Biology-inspired microphysiological systems to advance patient benefit and animal welfare in drug development," *ALTEX*, vol. 37, no. 3, pp. 365–394, 2020, doi: 10.14573/ALTEX.2001241.

1.3 Literature Review Part 2: Tissue engineering scaffold considerations and methods of fabrication

Tissue engineering scaffold considerations and methods of fabrication

Microphysiological systems (MPSs), commonly known as organ-on-a-chip constructs, offer an *in vitro* alternative to *in vivo* animal models. A successful MPS is commonly composed of human derived cells and a scaffold. Scaffolds are biomaterials that are used to provide structural and functional support for cell attachment and growth [1], [2]. It is becoming increasingly apparent that there is a need to improve scaffold design to overcome the diffusional mass transfer limit, to supply oxygen and nutrients to the cells within the scaffold whilst also facilitating waste removal [3].

There are many ways to approach this challenge, for example, scaffolds can be fabricated with a pre-determined transport network which requires no further supporting cells to allow for mass diffusion or cells can be spatially organised within a scaffold to ensure they are within the diffusional mass transfer limit (<200 µm) from fresh media [4]. Alternatively, the scaffold can be designed to support vascularisation alongside standard cell culture [5]. Scaffolds utilised in these systems are required to either provide a vascularised network or induce and support vascularisation into the scaffold from a pre-existing vascular network. The former requires a scaffold with a pre-determined transport network which can be lined with endothelial cells to artificially create a vascular network whilst the latter requires a simpler design in which the bulk of scaffold is accessible to infiltrating vessels which form a vascular network [6]. These scaffolds can also incorporate inducing factors, such as chemokines and angiogenic factors, or cells which produce inducing factors. For example, most tumour cells express vascular endothelial growth factor (VEGF) thus they are commonly utilised in cancer models to induce and support vascularisation. Furthermore, scaffolds which are capable of modelling vascularisation are key within MPS to fundamentally support 3D cell culture but to also better recapitulate *in vivo* conditions. For example, in cancer research there is a need to better model the metastatic cascade of which a vascular network is critical to investigate intravasation, circulating tumour cells and extravasation, of which the latter is poorly defined [7].

This literature review further highlights and explores the methods mentioned above to improve scaffold design. Furthermore, in the variety of scaffolds presented in literature there are many design considerations, including; material selection, porosity, interconnectivity and fabrication method, each of which are outlined in further detail in individual sections of this chapter.

1 Material Selection

The choice of scaffold material is dependent upon the scaffold application and thus the intended function. Certain materials are more suited for specific purposes, for example a material that provides structural support may not be well suited to provide drug-delivering functionalities. Scaffold materials are either natural or synthetic and can further be subcategorised as polymer, ceramic or a composite of the two [8]. However, ceramics are generally used in bone tissue engineering (TE) and not used in soft TE [9]–[12] therefore ceramics are not discussed in further detail in this review. Natural scaffolds are better able to provide the correct architecture for cells to sufficiently attach and proliferate however batch-to-batch variability is common [13], and there are additional risks such as pathogen transmission and protein impurities which can lead to an undesirable immune response [14]. On the other hand, whilst synthetic scaffolds do not replicate the exact architecture of the tissue, they remove the risk of pathogen transmission and protein impurities. Additionally, they provide an inexpensive, mechanically and chemically tuneable method for the reproducible production of tissue scaffolds [15]. Moreover, synthetic polymers are often used due to their low cost and ease of availability and production scale up [16], all of which are desirable material characteristics for MPS models.

1.1 Natural Polymers

Natural polymers can be classified into two types: protein-based and polysaccharide polymers [17], [18]. Commonly used natural protein-based polymers include collagen, fibrin, fibrinogen and silk fibroin [17], [19]. Fabricating a scaffold using natural collagen can improve cell interactions and adhesion to a scaffold as it provides the natural architecture at the macroscopic and/or microscopic scale depending on the processing technique. Collagen is widely used in hydrogels to provide both macroscopic and microscopic architecture, including the presentation of receptor-binding ligands which allows for proteolytic remodelling and degradation by cells, an advantageous feature for biodegradable scaffolds [20]. Matthews et al. developed collagen scaffolds with nanofibers using electrospinning techniques, utilising the microscopic architecture of collagen [21]. Electrospinning collagen with hexafluoro-2-propanol solvent produced 100 nm fibres with the periodic 67 nm banding pattern which is observed in native, interstitial fibroblast-deposited collagen. Offeddu et al. fabricated collagen scaffolds using freeze-drying techniques, reporting an increase in scaffold stiffness with increasing collagen concentration [22]. Furthermore, Benning et al. found that fibrin and

collagen to be the most suitable bioinks for the inkjet printing of endothelial cells to produce pre-vascularised constructs, with good printability and support for vasculogenesis [23].

However, although pure collagen scaffolds provide favourable biological properties, the mechanical and structural properties of these scaffolds are poor. Native collagen is naturally crosslinked both between the chains in the triple helix and between each triple helix strand via one of two mechanisms, enzymatically controlled or spontaneous, non-specific series of reactions, mainly with glucose-derived molecules, which form in turn advanced glycation end products (AGEs) [24]. Physical and chemical treatments, such as ultraviolet [25] or gamma irradiation [26], glutaraldehyde [27], [28] and 1-ethyl-3-(3-dimethylaminopropyl)-carbodiimide hydrochloride treatments [29], can be used to replicate this natural mechanism to form inter-molecular collagen crosslinks, improving the mechanical properties [30].

Commonly used natural polysaccharide polymers include chitosan, hyaluronic acid, alginate and cellulose [18], [31]. Many natural polysaccharide polymers have been reported to be used within TE scaffolds to induce and support vasculogenesis. Hyaluronic acid has been reported to be capable of inducing soft tissue regeneration when combined with recombinant gelatin [32]. Tuin et al. reports that the hyaluronic acid within the gel functions as the scaffold whilst the incorporated recombinant gelatin is the component that induces tissue formation and ECM deposition, resulting in vascularisation and integration of the gel with the surrounding tissue. Furthermore, Gerecht-Nir et al. reported the use of alginate, to study the ability of 3D porous alginate scaffolds to provide a conducive environment for the culture and growth of human embryonic stem cells [33]. The scaffolds had pore sizes ranging from 50-200 mm with a porosity of 90%. Results showed the scaffolds were able to facilitate the aggregation of human embryonic stem cells and form tube-like structures *in vivo*. To further enhance vascularisation, growth factors such as VEGF can be incorporated into alginate scaffolds, as described by Drury and Mooney [34].

In addition, chitosan has been widely studied for vascularisation within tissue engineering due to its significant wound healing capabilities. Whilst promoting wound healing, chitosan is also antimicrobial, biodegradable and non-toxic [35]. Chevrier et al. presented *in vitro* and *in vivo* studies assessing the effect of injectable chitosan platelet-rich plasma (PRP) implants on cell recruitment and vascularisation [36]. The chitosan loaded PRP implants showed increased capability to induce cell recruitment and vascularisation compared to the pure PRP implants.

1.2   Synthetic Polymers

A wide range of synthetic polymers have been used to produce a variety of scaffolds for tissue engineering applications including polyethylene gycol (PEG), polylactic acid (PLA), polycaprolactone (PCL), polyglycolic acid (PGA), polylactic-co-glycolic acid (PLGA) and polystyrene [18], [19], [31].

Wu et al. developed PGA scaffolds (97% porosity), seeded with human periodontal ligaments cells which can support vascular ingrowth following implantation on an established vascular network, they demonstrated the use of these scaffolds in mice models [37]. Results showed increased mRNA expression of collagen type I and III and fibronectin. In addition, 14 days post implantation in mice, staining showed the scaffolds were well vascularised, suggesting PGA scaffolds are a feasible material for tissue regeneration. Alternatively, Shinoka et al. demonstrated the effectiveness of PGA scaffolds, seeded with bovine artery cells to artificially create a vascular network before implantation, as pulmonary artery conduits [38]. Following 11 weeks after implantation in ovine models, the scaffolds fully degraded and were replaced by new tissue, which had 73.9% collagen content compared to the collagen content of native tissue. Histological analysis found elastic fibres were present in the media layer of the vessel scaffolds. Furthermore, the scaffolds showed an increase in diameter following implantation, suggesting growth and development of ECM and endothelial lining.

Many 3D testing platforms, such as Alvetex, use polystyrene as an inert, non-degradable material [31]. The scaffolds are generally simple and cheap to produce and provide a consumable product with a long shelf life, a significant benefit in comparison to other polymers [39]. However, the biodegradation of PCL is relatively slow (>1 year) compared to other polymers, such as polylactides and polyglycolides (2-4 months complete resorption). Thus, it is an ideal candidate for longer-term scaffolds, implants, drug delivery applications or testing platforms, such as substrates that can easily integrate within MPS models. Additionally, PCL has many other beneficial characteristics including FDA approval, low cost and ease of manufacture and manipulation, as presented by Woodruff et al. [40]. Aldemir Dikici et al. presented a novel bilayer PCL scaffold to guide bone regeneration comprised of a composite structure of a PCL polymerised high internal phase emulsion (polyHIPE) layer below an electrospun PCL layer [41]. The study found the PCL electrospun layer limited cell infiltration for up to 4 weeks whilst the porous polyHIPE layer supported cell infiltration and blood vessel ingrowth through the pores (average diameter ~34 μm). These results demonstrate the capability of a PCL polyHIPE to promote vascularisation, whilst an electrospun PCL layer can

be used as a soft tissue barrier to prevent cell invasion. A soft tissue barrier mimic such as this one may have potential use to mimic the basement membrane barrier that metastatic cells must pass through during intravasation.

Similar to the aims within this project, Rijal et al. assessed the use of synthetic polymeric scaffolds for breast cancer tumour models, focusing on PCL as well as PLGA, to study tumour cell viability, morphology, proliferation and response to anticancer drugs [16]. The study used a modified gas foaming method and demonstrated the successful use of PLGA, PCL and PLGA/PCL scaffolds for 3D tissue cultures. The model observed cancer cell migration and interactions within the scaffold pores whilst providing a standardised testing platform, reducing the large variations commonly observed between animal models. However, the authors importantly note that these 3D synthetic polymer systems cannot recreate all features of native tumour tissue, such as interstitial fluid flow and the range of cell types and cell-cell signalling pathways present *in vivo*.

PCL is hydrophobic which can adversely affect cell interactions with the material surface. Many studies have attempted to improve this property by blending PCL with natural polymers. A recent study by Gniesmer et al. modified PCL electrospun scaffolds with chitosan to create a scaffold to support vascular ingrowth [42]. The unmodified PCL scaffolds showed increased porosity and pore size compared to the chitosan scaffolds (80.61% vs. 76.21% and 9.19 μm vs. 8.16 μm respectively). However, the chitosan modification resulted in a significant increase in vascularisation when compared to unmodified PCL scaffolds in a rat model. This is most likely due to the crystallisation of chitosan on the surface increasing the hydrophilicity and surface roughness, thus enhancing cell adhesion and growth as recently demonstrated by de Cassan et al. [43].

Alternative commonly used methods to improve the hydrophilicity of PCL include plasma and protein coatings. Cools et al. used acrylic acid plasma coating to stimulate cell migration of osteoblasts and improved attachment and migration of adipose derived mesenchymal stem cells through a 3D printed PCL scaffold [44]. Similarly, Siri et al. demonstrated the use of air plasma improved cell adhesion to electrospun PCL fibres by 66% [45]. When further combining the plasma treatment with laminin, a common ECM protein, cell adhesion improved up to 84% compared to non-treated PCL electrospun fibres.

2 Porosity and Pore Size

It is important to consider the scaffold porosity and pore size; these factors can have a significant influence on cellular behaviour and processes that occur within a scaffold. In

particular, to enable the infiltration and formation of a vascular network to increase tissue thickness and cell culture period, pore size is a key factor for the success of neo-vascular formation within a scaffold. Current knowledge understands the optimal pore size for vascularisation to be at least 250 µm [4].

The pore size of a scaffold can be classified into three groups: nano-pores/nano-roughness <100 nm, micro-pores/micro-roughness 100 nm–100 µm and macro-pores/macro-roughness 100 µm-millimetres [46], [47]. Macro-pores enable vascularisation and neo-vascularisation, whilst micropores enable cell infiltration into the scaffold and nanopores enhance cell attachment and the formation of collagen fibres and ECM [46], [48], [49]. Therefore, it is often vitally important for a range of pore sizes to be present within a scaffold to form a successfully functioning biomimetic scaffold.

A study by Druecke et al. supports this understanding, observing a significantly higher functional vessel density in large pore sizes (250-300 µm) compared to smaller and medium pore sizes (20-75 µm and 75-212 µm respectively) [50]. However, many studies report high functional capillary density sufficient for vascular invasion in smaller pore sizes. Klenke et al. observed significantly higher functional capillary density in pore sizes ranging from 140-280 µm [51]. Similarly, Chiu et al., studied the effect of pore size in PEG hydrogels on vascularisation [52], reporting that pore sizes ranging from 100-150 µm had significantly greater vascular invasion after two weeks compared to smaller pore sizes ranging from 25-100 µm. Interestingly, after three weeks there was no significant difference in vascular invasion in pore sizes ranging from 100-150 µm and 50-100 µm. With the results showing that the pores could support mature vascular formation through the bulk of the material. However, there was significant difference when comparing the largest and smallest pore sizes (100-150 µm vs. 25-50 µm), with the 25-50 µm sized pores only able to support vascularised tissue formation on the external surface of the scaffold.

In addition, when determining scaffold porosity and pore size, cell type and required cell behaviour are additional factors that need to be considered. Bružauskaitė et al. summarised that smaller cell types require smaller pore sizes to reduce unwanted cell migration and therefore improve cell attachment to the scaffold [46].

It is important to note that pore size is not the only significant factor for vascularisation. A secondary significant factor is pore interconnectivity, ensuring cells are within 200 µm of a blood supply and therefore the mass transfer of oxygen and nutrients can occur [53]. Additionally, interconnectivity is important in order for cell migration to occur, a vital mechanism for vascularisation, and is inhibited if pores are poorly/not interconnected [4], [54].

3 Methods of Scaffold Fabrication

Porous 3D scaffolds in TE are popular and are increasingly needed to overcome the limit of diffusional mass transfer. As well as ensuring delivery of cell nutrients, porous interconnected scaffolds allow for increased cell ingrowth. In addition, within TE recapitulation of the ECM via the fabrication of porous, interconnected scaffolds has been widely researched in order to successfully mimic the *in vivo* microenvironment and to stimulate formation of natural ECM components by cells seeded within the scaffold. Many fabrication techniques are utilised in order to achieve high porosity and interconnectivity within TE scaffolds, including: particle leaching, solvent casting, freeze-drying, gas foaming, electrospinning, emulsion templating, additive manufacturing and thermal-induced phase separation, all of which are discussed in detail within numerous literature reviews [55]–[58].

3.1 Particle Leaching

In 1994, Mikos et al. reported on a particulate leaching method to prepare highly porous biodegradable polymer membranes, solvent casting/particulate leaching [59]. The method involved casting a mixture of biodegradable polymer solvent solution (poly(L-lactic acid)/chloroform solution) with water-soluble salt particles into a selected shape (**Figure 1**), resulting in a porous membrane with median pore sizes up to 150 μm. However, salt distribution is uneven throughout the membrane [60]. In addition, due to mixing the salt particles and the polymer in a liquid state, the salt particles become completely enveloped in the polymer solution, reducing pore interconnections and thus removing the ease and ability to wash out the salt particles, limiting the thickness of the membranes to 500-2000 μm [60]. Overcoming this limitation, Mikos et al. followed on to report the preparation of 3D biodegradable foams by laminating the particle leached membranes [61].
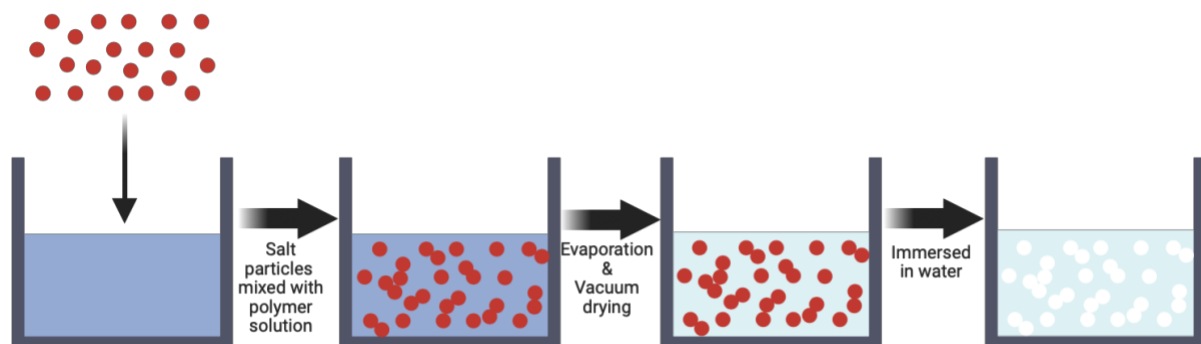
Figure 1. Solvent casting/particulate leaching, water soluble salt particles are mixed into a polymer solution and cast into a mould. The solvent is removed via evaporation and vacuum

drying. The salt particles are leached out by immersing the scaffold in water, resulting in a porous polymer scaffold. Created with BioRender.com.

In 2002, Liao et al. demonstrated a novel method to manufacture 3D biodegradable porous polymer scaffolds without the need for lamination of multiple layers [60]. The study mixed the biodegradable polymer and the salt in solid phase, solvent merging/particulate leaching. The solid phase mixture is placed into the mould, the solvent is added to dissolve and merge the polymer phase under negative pressure. A non-solvent is introduced to solidify the polymer followed by water to wash out the salt particles. The technique enabled manufacture of a 3D (70 mm diameter and 40 mm thickness) porous (>85 vol%) and interconnected polymer scaffold, with pore sizes ranging from 250-500 μm.

However, throughout literature solvent casting/particulate leaching is a more commonly used technique. In a recent study, Sola et al. used solvent casting/particulate leaching methods to successfully produce 3D polymethyl methacrylate (PMMA) and polyurethane (PU) scaffolds [62]. The scaffolds were porous and well interconnected, with porosity reported to range from 82.1 vol% to 91.3 vol%. The study used a mixture of fine- and coarse-grained salt powders to increase the control of the final scaffold pore size. Results observed sufficient cell colonisation within the centre of the scaffolds with the presence of regular cytoskeleton and focal adhesion where cells attached to the scaffold, demonstrating that the scaffold allowed for cells and nutrients to migrate and diffuse respectively into the bulk of the material. In addition, Sin et al. demonstrated a modified solvent casting/particulate leaching method which involved an additional centrifuge step [63]. The additional step improved the uniform distribution of particulates, leading to improvements in pore and interconnectivity uniformity. The PU scaffolds showed high porosity (92%) with average pore sizes of 250 μm. Additionally, it was shown that highly porous and interconnected scaffolds could be obtained at high polymer concentrations (20%). Moreover, this modified method allowed for sample thicknesses of up to 8 mm compared to the conventional solvent casting/particulate leaching method which is reported to be limited to <4 mm [64]. This vast increase in sample thickness is due to the ability to more densely pack the salt particles via the centrifugation step [63].

Similarly, Gong et al. presented a modified solvent casting/particulate leaching method in which vacuum volatilization is used to vastly reduce processing time [65]. The PLA scaffolds were reported to have high porosity (>89%). When compared with conventional solvent casting/particulate leaching it was shown that this modified method could fabricate thicker scaffolds more efficiently.

Overall, it can be summarised from literature that scaffold porosity, interconnectivity and pore size are all dependent on the particulate size. In addition, the uniformity and packing of the particulates in the polymer solvent solution is an additional factor for scaffold porosity and interconnectivity.

3.2   Gas Foaming Technology

Gas foaming was first introduced by Mooney et al. [66] in 1996 as a novel method to fabricate 3D porous polymer scaffolds and has since become a very popular technique to fabricate TE porous scaffolds. The study reported the fabrication of biodegradable polymer macroporous sponges by saturating solid discs of poly(D,L-lactic-co-glycolic acid) with high pressure carbon dioxide (CO_2) (**Figure 2**). The resulting sponges were highly porous (up to 93%) with pore sizes of approximately 100 μm. Furthermore, in 2000 Nam et al. introduced a modified gas foaming method using ammonium bicarbonate salt particles [67]. The modified method casted ammonium bicarbonate salt particles in a poly-L-lactic acid-solvent gel into a mould. Immersion of the mould in a hot water solution triggered the release of ammonia and CO_2, resulting in the formation and expansion of pores. The resulting scaffolds had high porosity and interconnectivity with macropores ranging from 300-400 μm. This modified method allows for the fabrication of many different moulded shapes due to the easy handling and manipulation of the polymer-salt paste.
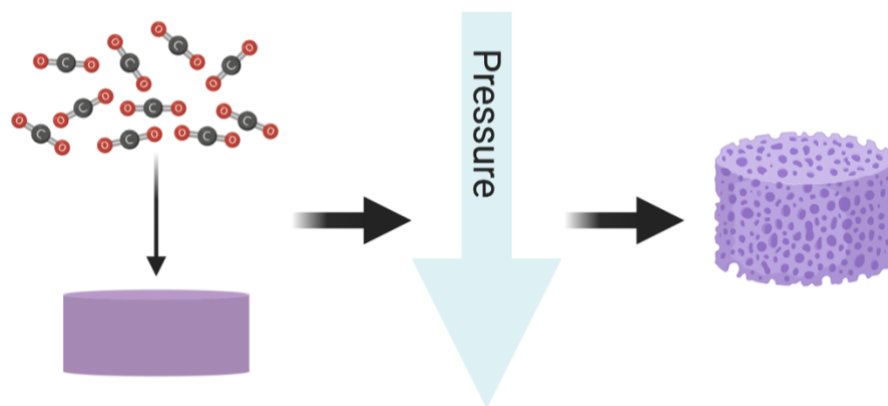
Figure 2. Gas Foaming, a polymer disc is saturated with CO_2. By reducing pressure, the dissolved CO_2 becomes thermodynamically unstable causing nucleation and growth of the CO_2 gas cells, resulting in a highly porous polymer scaffold. Created with BioRender.com.

Annabi et al. reported the fabrication of porous scaffolds by gas foaming heterogeneous blends, using a PCL/elastin composite blend to fabricate a porous, interconnected scaffold [68]. Fabrication of the scaffold was a two-step process. Porous PCL scaffolds were fabricated using

gas foaming/particulate leaching. The initial PCL scaffolds had average pore sizes of 540 μm with high interconnectivity. The scaffolds were further permeated with elastin and crosslinked with glutaraldehyde under high pressure CO_2. The study showed that the addition of elastin improves the water uptake properties of the initial PCL scaffold. In addition, initial *in vitro* studies demonstrated successful adhesion and proliferation of articular cartilage chondrocytes within the composite scaffold.

In 2015, Poursamar et al. reported a modified, *in situ* gas foaming technique to fabricate porous gelatin scaffolds, utilising the intrinsic foaming ability of gelatin when exposed to CO_2, stabilised by crosslinking with glutaraldehyde [69]. The study used sodium hydrogen carbonate as the foaming agent and acetic acid was added to the gelatin solution shortly after moulding. The chemical reaction between acetic acid and sodium hydrogen carbonate salt particles releases CO_2 and initiates the formation of porous gelatin scaffolds. The average pore size was dependent on the concentration of glutaraldehyde used (280 μm and 550 μm for 0.5% v/v and 1.0% v/v respectively). The study also indicated that increased glutaraldehyde concentration increased pore interconnectivity and scaffold compression strength. However, the tensile strength of the scaffold only increased up to 0.5% v/v glutaraldehyde. Poursamar et al. continued their work later reporting on an improved technique of *in situ* gas foaming for skin tissue engineering applications [70]. The study fabricated porous gelatin scaffolds with improved tensile strength by reducing the pore size. In order to reduce the pore size, the chemical reaction, and thus the gas released, occurred outside the mould. This allowed for the released gas to be vented off and reduce over-pressurisation within the gelatin, reducing the formation of macropores. The tensile strength of the scaffolds increased by approximately 45-fold when compared to the gelatin scaffolds in the previous study (239.48 kPa vs. 5.37 kPa).

One of the main advantages when using the gas foaming methods is the absence of solvents and thus removing the toxic effects any residual solvent may have on cellular activity within a scaffold [57], [71]–[73].

3.3 Electrospinning

The origins of electrospinning dates back to 1902, when Cooley and Morton each published patents, reporting two methods of electrically dispersing fluids [74], [75]. The electrospinning technique used today emerged many decades later (**Figure 3**). In 1969, Taylor reported the formation of electrically driven jets of glycerin, a viscous fluid [76]. The study

reported jets with 20 μm diameters and 5 cm in length. High voltages were introduced in the late 1990s, producing fibres with less than 5 μm diameters [77]–[79].
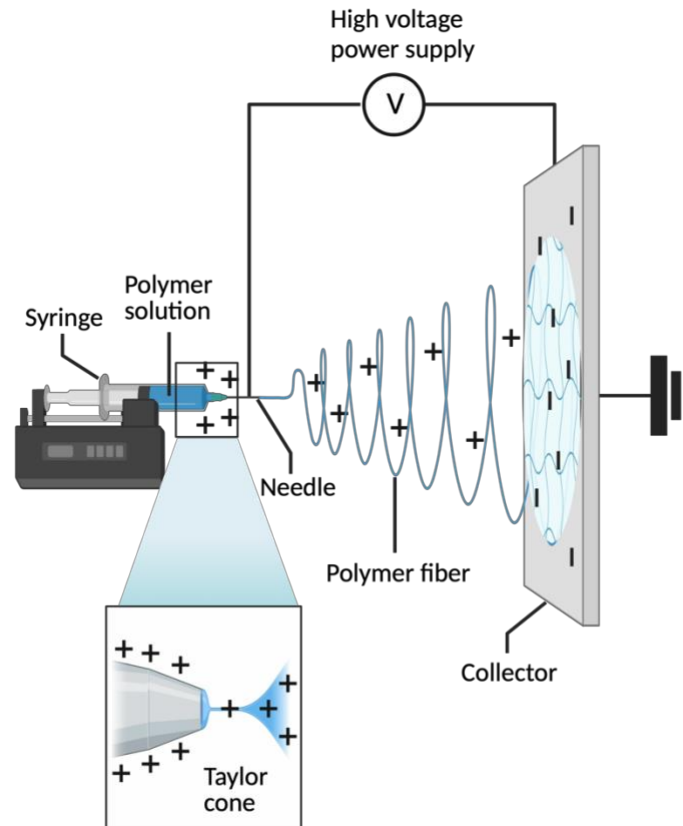

Figure 3. Electrospinning set-up, a high voltage is applied across a metallic needle tip, forming a polymer jet when the electrical force from the applied voltage overcomes the surface tension of the polymer solution within the needle tip. The resultant force causes the spherical droplet to form a conical shape (Taylor cone) in which the polymer jet is formed. The resulting micro or nanofibers are attracted to and collected on a metallic rotating or static collector which is electrically grounded [79], [80]. Created with BioRender.com.

Electrospinning is a versatile technique which up to now has been used with approximately 100 polymers, both natural and synthetic [81]. However, there are many parameters affecting the fabrication of electrospun nanofibers: applied voltage, distance between the needle and collector (working distance), flow rate, needle diameter, solvent, polymer concentration, viscosity, solution conductivity, humidity and temperature [80]–[82].

Fibrous electrospun scaffolds provide micro- and nano-scale structures that are well interconnected, mimicking the natural ECM in tissue [83]. Sisson et al. reported the effect of electrospun fibre diameter on scaffold porosity. Gelatin scaffolds with large and small fibre diameters (600 nm and 110 nm respectively) were electrospun by varying the acetic acid:ethyl

acetate:water ratio and the gelatin concentration (25% w/w and 10% w/w respectively). The larger fibre scaffolds had pore sizes 10-fold greater than the small fibre scaffolds (10.7 μm^2 vs. 1.0 μm^2). Initial *in vitro* studies found cell penetration depth of the large fibre scaffolds was up to 50 μm whilst the small fibre scaffolds showed poor cell invasion with cells penetrating up to 18 μm. In addition, metabolic activity of the cells in the large fibre scaffold was significantly higher at day 7 compared to the small fibre scaffolds. Indicating that fibre diameter has a significant impact on porosity and pore size and thus the cellular behaviour within the scaffold.

3.4 Additive Manufacturing

Additive manufacturing (AM) is an umbrella term that describes a range of techniques that transform digital design files into functional products [84]. These techniques include: solid free-form fabrication, stereolithography, fused deposition modelling, selective laser sintering, 3D printing and bioprinting, as outlined in the review of Eltom et al.[55].

Within TE, additive manufacturing techniques are utilised in order to achieve macropores within a scaffold, a significant feature to allow vascularisation to occur with TE scaffolds. Pashneh-Tala et al. demonstrate the use of selective photocuring to develop porous poly(glycerol sebacate)-methacrylate scaffolds from digital designs [85].

In addition, techniques such as stereolithography (SLA) overcome the wastage of material associated with subtractive manufacturing whilst enabling the fabrication of scaffolds at a high resolution [55]. SLA utilises UV light for photopolymerisation of liquid-based resins, first reported by Kodama in 1981 [86]. More recently, Melchiorri et al. fabricated a poly(propylene fumarate) vascular graft using digital light processing SLA [87]. Mechanical testing of the grafts showed properties comparable to native vessels commonly used in vascular grafts. In addition, initial *in vitro* tests showed good cell viability on the graft surfaces.

Furthermore, using SLA, Melchels et al. fabricated porous polymer scaffolds using PCL- and PLA-based resins [88]. The resulting mechanical properties of the scaffolds were comparable with the finite element predictions indicating this technique is an accurate method to prepare high resolution polymer TE scaffolds. High resolution of SLA, due to the small width and high control of the light source, is an advantage widely noted throughout literature [89], [90].

3.5 High Internal Phase Emulsion Templating

An emerging method to achieve a porous and well interconnected scaffold is by synthesising porous emulsion-templated polymers using high internal phase emulsions, commonly known as polyHIPEs [15], [91], [92]. The synthesis process involves mixing two immiscible liquids/phases, the internal phase is dispersed in a continuous, connected external phase in the presence of an emulsifier, commonly a surfactant, which stabilises the emulsion (**Figure 4**). An emulsion is classified as a high internal phase emulsion (HIPE) when the volume of the internal phase is greater than 74.05% [15], [91], [93] and is formed of the external phase enveloping the dispersed internal phase droplets. The continuous phase is then polymerised resulting in a polyHIPE. Multiple polymerisation techniques can we utilised within polyHIPEs, including; atom transfer radical polymerisation, reversible-addition-fragmentation chain-transfer, ring opening metathesis polymerisation, click polymerisation [94] and free-radical polymerisation [95]. The porosity and interconnectivity of polyHIPE scaffolds have been shown to be affected by many variables, including; temperature, surfactant type/quality, stirring speed and the internal phase volume [96].
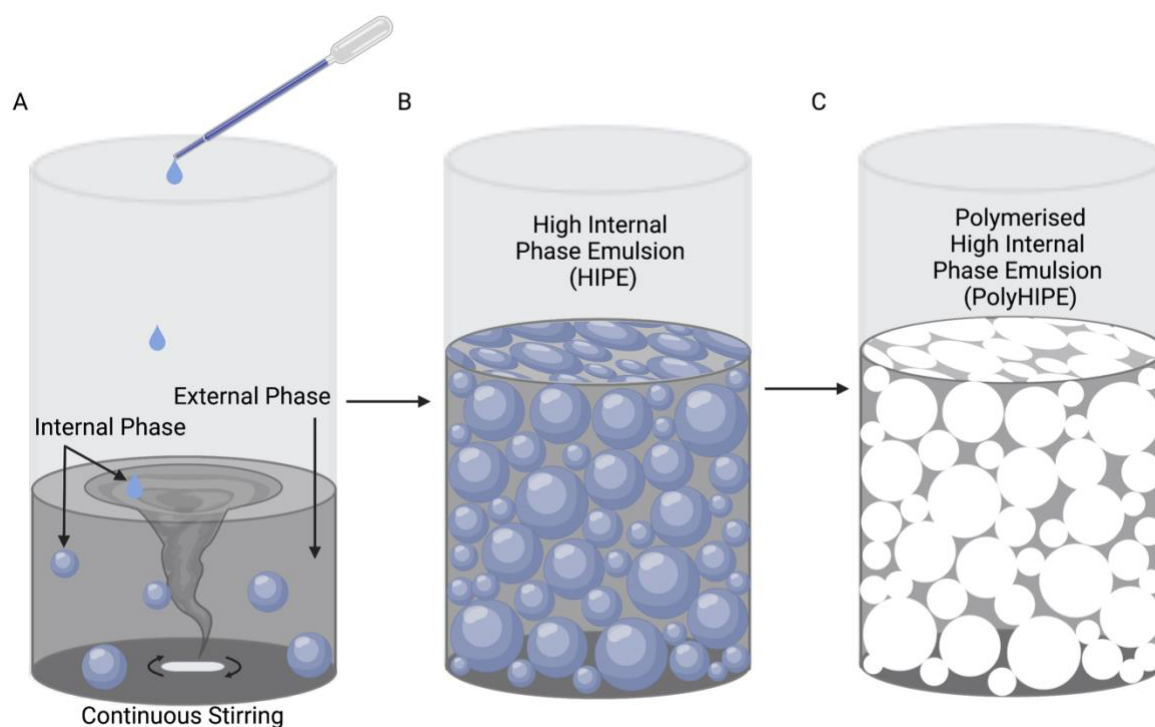
Figure 4. Schematic diagram representing the basic process of PolyHIPE fabrication. A) The external phase enveloped the dispersed internal phase droplets. B) The external phase envelopes rupture at the thinnest sections, the internal phase transforms into a continuous

connected phase. C) The internal phase is removed, resulting in a porous, interconnected polymer scaffold. Image sourced from Jackson et al. [97].

As polyHIPEs have an internal phase content >74% this can often lead to materials with relatively low crush strengths and Young's modulus, reducing the range of suitable applications [91]. Therefore, many studies focus on improving the mechanical properties of polyHIPEs. Jing et al. presented a polystyrene polyHIPE scaffold with increased strength via the incorporation of UPy groups (2-Ureido-4[1H] pyrimidinone) and quadruple hydrogen bond functionality [98]. Incorporation of the UPy groups allowed for controlled porous morphology of the scaffold with porosity as high as 92%. Whilst the quadruple hydrogen bond reinforced the scaffold, resulting in increased Young's modulus to 28.5 MPa, a 50% improvement in comparison to pure polystyrene polyHIPE.

Sun et al. studied the effectiveness of polystyrene polyHIPE scaffolds, investigating the application of the scaffolds for cytotoxicity testing of cigarette smoke [99]. The polystyrene scaffolds showed high porosity (89.8-95.3%) and interconnectivity with pore sizes ranging from 6.5-12 μm, depending upon the water-in-oil ratio (W/O) of the polyHIPE. However, *in vitro* analysis found that scaffolds with greater W/O ratio better promoted cell proliferation due to higher porosity, interconnectivity and pore size. Results showed lower levels of smoke cytotoxicity on carcinomic human alveolar basal epithelial cells in the 3D polystyrene polyHIPE system than the 2D culture platform. Further demonstrating the greater effectiveness of 3D models compared to 2D models to mimic the native *in vivo* microenvironment.

Alvetex is a current gold-standard polyHIPE-based scaffold widely used in *in vitro* assays to study cell growth, differentiation and function [39]. It is a rigid highly porous (90%) polystyrene scaffold [100], formed by polymerisation in a biphasic emulsion. The HIPE consists of an aqueous and non-aqueous monomer/surfactant phase, resulting in a polyHIPE with a homogeneous porous structure. Costello et al. engineered a multilayer skin equivalent via incorporating the Alvetex membrane [101]. The Alvetex membrane formed the dermal component of the skin by seeding it with fibroblasts. The membrane allowed the fibroblasts to establish and generate ECM proteins (collagen and elastin). Using Alvetex within this study removed the need to incorporate exogeneous collagen and supported cell differentiation and stratification. Furthermore, a recent study by Porcelli et al. used Alvetex scaffolds to provide a 3D scaffold for the investigation of the resistance of anti-cancer drugs via the activation mast cells [102]. Metastatic cells were seeded and cultured on Alvetex over 7 days, the scaffolds

provided a platform to successfully investigate the anti-cancer drugs enabling the discovery of the role mast cells in resistance to the drugs.

Due to its popularity and success, the performance of newly developed scaffolds is often compared to Alvetex. A recent study by Aldemir Dikici et al. investigated the effect of incorporating two solvents into the fabrication of PCL polyHIPEs in order to reduce the polymer viscosity for successful fabrication, comparing the cell culture performance to Alvetex [15]. 4-arm polycaprolactone methacrylate (PCL-M) HIPEs and open porous PCL-M polyHIPEs were successfully fabricated with a chloroform/toluene blend, increasing the capability of pore size tunability. When compared to Alvetex the PCL-M scaffolds performed to a similar level in cell culture and ingrowth, demonstrating the success of PCL polyHIPE for cell culture applications. Dikici et al. continued their work investigating the use of these PCL-M polyHIPEs to support angiogenesis, demonstrating successful vascular ingrowth into the polyHIPE scaffolds using a chorioallantoic membrane (CAM) assay [103]–[106].

Similarly, Paterson et al. used the CAM assay to demonstrate how porous microspheres fabricated using HIPEs successfully supported angiogenesis [107]. They observed further improvement in angiogenesis within the polyHIPE microspheres when seeded with human embryonic stem cell-derived mesenchymal progenitor cells.

Overall, the ability to control and influence the pore size and morphology with polyHIPEs, by altering one or more variables, whilst maintaining high porosity and interconnectivity makes high internal phase emulsion templating a popular technique for producing TE scaffolds suitable for vascularisation.

3.6   Hybrid Techniques

Each of the techniques above faces limitations when applied to specific applications. To overcome these limitations, forming 'hybrid' techniques by combining two or more techniques is a popular method. For example, small pore sizes reducing cell infiltration is one of the main reported limitations for electrospun porous scaffolds [81], [83], [108]. Therefore, many studies report the use of modified electrospinning methods incorporating: salt leaching, sacrificial fibres, nano- and micro-diameter fibres, cryogenic electrospinning, a liquid bath collector, ultrasonication, gas foaming, electrospinning/electrospraying and custom-made collectors [109]–[117]. Tuzlakoglu reported a nano- and micro-fibrous combination scaffold design to overcome this limitation [117]. The combined scaffold is fabricated from a wet spun microfiber (100 μm diameter) scaffold in which nanofibers (400 nm diameter) were collected using

electrospinning techniques. The microfibres ensure sufficient pore size within the structure for cell migration whilst the nanofibers allow for improved cell adhesion and proliferation [108]. In addition, Nam et al. reported a salt leaching/electrospinning method to increase pore size [116]. A solution of 12 wt.% PCL was electrospun with deposition of salt crystals into the polymer fibre jet via a sheath surrounding the needle. The salt crystals were leached out with water, resulting in a porous PCL scaffold with average fibre diameters of 740 nm and pore sizes of 100-200 μm. Initial *in vitro* studies observed cell penetration of up to 4 mm with 70% cell coverage on the scaffolds.

Closed pore or reduced pore interconnectivity in gas foamed fabricated scaffolds has often been reported, thus gas foaming is commonly combined with particulate leaching methods to improve interconnectivity [57], [68], [72], [118].

Many techniques are often combined with additive manufacturing techniques to create scaffolds with defined macro-geometry and microporosity. The above-mentioned study by Pashneh-Tala et al. combined selective photocuring with porogen leaching [85]. Selective photocuring controls the macro-geometry of the scaffold whilst porogen leaching incorporates micropores within the scaffold. Johnson et al. combined micro-stereolithography with emulsion templating resulting in the fabrication of porous acrylate-based polyHIPEs [119]. Similarly, micro-stereolithography defined the microgeometry and emulsion templating produced the microporosity within the scaffold. More recently, Huang et al. used E-jet 3D printing and electrospinning techniques to fabricate a triple-layered PCL vascular graft [120]. The graft consisted of a highly aligned 3D printed interior layer, a dense electrospun middle layer and an outer layer composed of mixed fibres by electrospraying. The combination of techniques provided a suitable internal environment for enhanced proliferation and migration whilst retaining good mechanical properties.

4   Conclusion

To summarise, the increasing rate of TE development is leading to significant improvements in 3D *in vitro* models with TE constructs integrated within MPS are becoming increasingly popular for modelling tumours. However, vascularisation of MPS models must be significantly improved in order to extend the cell culture time and tissue thickness that can be modelled *in vitro*. Porous, interconnected scaffolds hold promise in providing a solution to overcome the diffusional mass transfer limit capable of supporting 3D cell culture and vascular ingrowth. There are many fabrication techniques for porous polymers that have been developed since the early 1900s. High internal phase emulsion templating is a more recently developed

technique which shows promise for the fabrication of highly porous, interconnected and tuneable scaffolds. With studies demonstrating increased vasculature in polymer scaffolds allowing for increased culture time due to the delivery and removal of nutrients and waste respectively. In these studies, sufficient vasculature allows for further in-depth *in vitro* studies with increased accuracy, offering key insight on cell behaviour which can provide greater insight into cancer targeting therapies, critical for pharmaceutical drug development. Furthermore, models that can utilise such technology lead to a reduction in high cost and ethical implications that are associated with *in vivo* animal testing.

5   References

[1]   B. P. Chan and K. W. Leong, "Scaffolding in tissue engineering: General approaches and tissue-specific considerations," *European Spine Journal*, vol. 17, no. SUPPL. 4, p. 479, Dec. 2008, doi: 10.1007/s00586-008-0745-3.

[2]   J. N. Fu *et al.*, "Scaffold-Based Tissue Engineering Strategies for Osteochondral Repair," *Front Bioeng Biotechnol*, vol. 9, p. 812383, Jan. 2022, doi: 10.3389/FBIOE.2021.812383/BIBTEX.

[3]   M. Lovett, K. Lee, A. Edwards, and D. L. Kaplan, "Vascularization Strategies for Tissue Engineering," *Tissue Eng Part B Rev*, vol. 15, no. 3, pp. 353–370, Sep. 2009, doi: 10.1089/TEN.TEB.2009.0085.

[4]   J. Rouwkema, N. C. Rivron, and C. A. van Blitterswijk, "Vascularization in tissue engineering," *Trends Biotechnol*, vol. 26, no. 8, pp. 434–441, Aug. 2008, doi: 10.1016/j.tibtech.2008.04.009.

[5]   S. G. Anthon and K. P. Valente, "Vascularization Strategies in 3D Cell Culture Models: From Scaffold-Free Models to 3D Bioprinting," *Int J Mol Sci*, vol. 23, no. 23, Dec. 2022, doi: 10.3390/IJMS232314582.

[6]   N. K. Mekala, R. R. Baadhe, and R. Potumarthi, "Mass transfer aspects of 3D cell cultures in tissue engineering," *Asia-Pacific Journal of Chemical Engineering*, vol. 9, no. 3, pp. 318–329, May 2014, doi: 10.1002/APJ.1800.

[7]   X. Cheng and K. Cheng, "Visualizing cancer extravasation: from mechanistic studies to drug development," *Cancer and Metastasis Reviews*, vol. 40, pp. 71–88, Mar. 2021, doi: 10.1007/S10555-020-09942-2/FIGURES/3.

[8]   Y. Khan, M. J. Yaszemski, A. G. Mikos, and C. T. Laurencin, "Tissue Engineering of Bone: Material and Matrix Considerations," *The Journal of Bone and Joint Surgery-American Volume*, vol. 90, no. Suppl 1, pp. 36–42, Feb. 2008, doi: 10.2106/JBJS.G.01260.

[9]   L. C. Gerhardt *et al.*, "The pro-angiogenic properties of multi-functional bioactive glass composite scaffolds," *Biomaterials*, vol. 32, no. 17, pp. 4096–4108, Jun. 2011, doi: 10.1016/j.biomaterials.2011.02.032.

[10]   B. Huang, G. Caetano, C. Vyas, J. J. Blaker, C. Diver, and P. Bártolo, "Polymer-ceramic composite scaffolds: The effect of hydroxyapatite and β-tri-calcium phosphate," *Materials*, vol. 11, no. 1, Jan. 2018, doi: 10.3390/ma11010129.

[11]   Y. M. Khan, E. K. Cushnie, J. K. Kelleher, and C. T. Laurencin, "In situ synthesized ceramic-polymer composites for bone tissue engineering: Bioactivity and degradation studies," *J Mater Sci*, vol. 42, no. 12, pp. 4183–4190, Jun. 2007, doi: 10.1007/s10853-006-0636-0.

[12]   A. Gloria, R. De Santis, and L. Ambrosio, "Polymer-based composite scaffolds for tissue engineering," *Journal of Applied Biomaterials and Biomechanics*, vol. 8, no. 2, pp. 57–67, May 2010, doi: 10.1177/228080001000800201.

[13]   P. B. Malafaya, G. A. Silva, and R. L. Reis, "Natural-origin polymers as carriers and scaffolds for biomolecules and cell delivery in tissue engineering applications," *Adv Drug Deliv Rev*, vol. 59, no. 4–5, pp. 207–233, May 2007, doi: 10.1016/J.ADDR.2007.03.012.

[14]   M. S. B. Reddy, D. Ponnamma, R. Choudhary, and K. K. Sadasivuni, "A Comparative Review of Natural and Synthetic Biopolymer Composite Scaffolds," *Polymers (Basel)*, vol. 13, no. 7, p. 1105, Apr. 2021, doi: 10.3390/POLYM13071105.

[15]   B. Aldemir Dikici, C. Sherborne, G. C. Reilly, and F. Claeyssens, "Emulsion templated scaffolds manufactured from photocurable polycaprolactone," *Polymer (Guildf)*, vol. 175, pp. 243–254, Jun. 2019, doi: 10.1016/j.polymer.2019.05.023.

[16] G. Rijal, C. Bathula, and W. Li, "Application of Synthetic Polymeric Scaffolds in Breast Cancer 3D Tissue Cultures and Animal Tumor Models," *Int J Biomater*, vol. 2017, 2017, doi: 10.1155/2017/8074890.

[17] S. H. Hsu, K. C. Hung, and C. W. Chen, "Biodegradable polymer scaffolds," *J Mater Chem B*, vol. 4, no. 47, pp. 7493–7505, Nov. 2016, doi: 10.1039/c6tb02176j.

[18] M. Sarker, X. B. Chen, and D. J. Schreyer, "Experimental approaches to vascularisation within tissue engineering constructs," *J Biomater Sci Polym Ed*, vol. 26, no. 12, pp. 683–734, Aug. 2015, doi: 10.1080/09205063.2015.1059018.

[19] F. J. O'Brien, "Biomaterials & scaffolds for tissue engineering," *Materials Today*, vol. 14, no. 3. Elsevier B.V., pp. 88–95, Mar. 01, 2011. doi: 10.1016/S1369-7021(11)70058-X.

[20] I. M. El-Sherbiny and M. H. Yacoub, "Hydrogel scaffolds for tissue engineering: Progress and challenges," *Glob Cardiol Sci Pract*, vol. 2013, no. 3, p. 316, Sep. 2013, doi: 10.5339/GCSP.2013.38.

[21] J. A. Matthews, G. E. Wnek, D. G. Simpson, and G. L. Bowlin, "Electrospinning of collagen nanofibers," *Biomacromolecules*, vol. 3, no. 2, pp. 232–238, 2002, doi: 10.1021/bm015533u.

[22] G. S. Offeddu, J. C. Ashworth, R. E. Cameron, and M. L. Oyen, "Multi-scale mechanical response of freeze-dried collagen scaffolds for tissue engineering applications," *J Mech Behav Biomed Mater*, vol. 42, pp. 19–25, Feb. 2015, doi: 10.1016/j.jmbbm.2014.10.015.

[23] L. Benning *et al.*, "Assessment of hydrogels for bioprinting of endothelial cells," *J Biomed Mater Res A*, vol. 106, no. 4, pp. 935–947, Apr. 2018, doi: 10.1002/jbm.a.36291.

[24] M. Meyer, "Processing of collagen based biomaterials and the resulting materials properties," *Biomed Eng Online*, vol. 18, no. 1, pp. 1–74, Mar. 2019, doi: 10.1186/s12938-019-0647-0.

[25] K. S. Weadock, E. J. Miller, L. D. Bellincampi, J. P. Zawadsky, and M. G. Dunn, "Physical crosslinking of collagen fibers: comparison of ultraviolet irradiation and dehydrothermal treatment," *J Biomed Mater Res*, vol. 29, no. 11, pp. 1373–1379, 1995, doi: 10.1002/JBM.820291108.

[26] T. Takitoh, M. Bessho, M. Hirose, H. Ohgushi, H. Mori, and M. Hara, "Gamma-cross-linked nonfibrillar collagen gel as a scaffold for osteogenic differentiation of mesenchymal stem cells," *J Biosci Bioeng*, vol. 119, no. 2, pp. 217–225, Feb. 2015, doi: 10.1016/J.JBIOSC.2014.07.008.

[27] J. M. Ruijgrok, J. R. De Wijn, and M. E. Boon, "Optimizing glutaraldehyde crosslinking of collagen: effects of time, temperature and concentration as measured by shrinkage temperature," *Journal of Materials Science: Materials in Medicine 1994 5:2*, vol. 5, no. 2, pp. 80–87, Feb. 1994, doi: 10.1007/BF00121695.

[28] Y. Y. Peng, V. Glattauer, and J. A. M. Ramshaw, "Stabilisation of Collagen Sponges by Glutaraldehyde Vapour Crosslinking," *Int J Biomater*, vol. 2017, 2017, doi: 10.1155/2017/8947823.

[29] S. N. Park, J. C. Park, H. O. Kim, M. J. Song, and H. Suh, "Characterization of porous collagen/hyaluronic acid scaffold modified by 1-ethyl-3-(3-dimethylaminopropyl)carbodiimide cross-linking," *Biomaterials*, vol. 23, no. 4, pp. 1205–1212, Feb. 2002, doi: 10.1016/S0142-9612(01)00235-6.

[30] C. Dong and Y. Lv, "Application of collagen scaffold in tissue engineering: Recent advances and new perspectives," *Polymers (Basel)*, vol. 8, no. 2, 2016, doi: 10.3390/polym8020042.

[31] W. Asghar, R. El Assal, H. Shafiee, S. Pitteri, R. Paulmurugan, and U. Demirci, "Engineering cancer microenvironments for in vitro 3-D tumor models," *Materials Today*, vol. 18, no. 10. Elsevier, pp. 539–553, Dec. 01, 2015. doi: 10.1016/j.mattod.2015.05.002.

[32] A. Tuin, J. Zandstra, S. G. Kluijtmans, J. B. Bouwstra, M. C. Harmsen, and M. J. A. van Luyn, "Hyaluronic acid-recombinant gelatin gels as a scaffold for soft tissue regeneration," *Eur Cell Mater*, vol. 24, pp. 320–330, 2012, doi: 10.22203/eCM.v024a23.

[33] S. Gerecht-Nir, S. Cohen, A. Ziskind, and J. Itskovitz-Eldor, "Three-dimensional porous alginate scaffolds provide a conducive environment for generation of well-vascularized embryoid bodies from human embryonic stem cells," *Biotechnol Bioeng*, vol. 88, no. 3, pp. 313–320, Nov. 2004, doi: 10.1002/bit.20248.

[34] J. L. Drury and D. J. Mooney, "Hydrogels for tissue engineering: Scaffold design variables and applications," *Biomaterials*, vol. 24, no. 24, pp. 4337–4351, Nov. 2003, doi: 10.1016/S0142-9612(03)00340-5.

[35] M. A. Matica, F. L. Aachmann, A. Tøndervik, H. Sletta, and V. Ostafe, "Chitosan as a wound dressing starting material: Antimicrobial properties and mode of action," *Int J Mol Sci*, vol. 20, no. 23, pp. 1–33, 2019, doi: 10.3390/ijms20235889.

[36] A. Chevrier *et al.*, "Injectable chitosan-platelet-rich plasma implants to promote tissue regeneration: in vitro properties, in vivo residence, degradation, cell recruitment and vascularization," *J Tissue Eng Regen Med*, vol. 12, no. 1, pp. 217–228, Jan. 2018, doi: 10.1002/term.2403.

[37] Y. Wu, H. Xia, B. Zhang, Y. Zhao, and Y. Wang, "Assessment of polyglycolic acid scaffolds for periodontal ligament regeneration," *Biotechnology & Biotechnological Equipment*, vol. 32, no. 3, pp. 701–706, May 2018, doi: 10.1080/13102818.2018.1437358.

[38] T. Shinoka *et al.*, "Creation of viable pulmonary artery autografts through tissue engineering," *Journal of Thoracic and Cardiovascular Surgery*, vol. 115, no. 3, pp. 536–546, Mar. 1998, doi: 10.1016/S0022-5223(98)70315-0.

[39] E. Knight, B. Murray, R. Carnachan, and S. Przyborski, "Alvetex®: Polystyrene Scaffold Technology for Routine Three Dimensional Cell Culture," in *Methods in molecular biology (Clifton, N.J.)*, Humana Press, 2011, pp. 323–340. doi: 10.1007/978-1-60761-984-0_20.

[40] M. A. Woodruff and D. W. Hutmacher, "The return of a forgotten polymer - Polycaprolactone in the 21st century," *Progress in Polymer Science (Oxford)*, vol. 35, no. 10, pp. 1217–1256, 2010, doi: 10.1016/j.progpolymsci.2010.04.002.

[41] B. A. Dikici, S. Dikici, G. C. Reilly, S. MacNeil, and F. Claeyssens, "A Novel Bilayer Polycaprolactone Membrane for Guided Bone Regeneration: Combining Electrospinning and Emulsion Templating," *Materials*, vol. 12, no. 16, p. 2643, 2019, doi: 10.3390/MA12162643.

[42] S. Gniesmer *et al.*, "In vivo analysis of vascularization and biocompatibility of electrospun polycaprolactone fibre mats in the rat femur chamber," *J Tissue Eng Regen Med*, vol. 13, no. 7, p. term.2868, May 2019, doi: 10.1002/term.2868.

[43] D. de Cassan *et al.*, "Attachment of nanoparticulate drug-release systems on poly(ε-caprolactone) nanofibers via a graftpolymer as interlayer," *Colloids Surf B Biointerfaces*, vol. 163, pp. 309–320, Mar. 2018, doi: 10.1016/j.colsurfb.2017.12.050.

[44] P. Cools, H. Declercq, R. Ghobeira, R. Morent, and N. De Geyter, "Acrylic acid plasma coatings for enhanced cell migration in PCL 3D additive manufactured scaffolds," *Surf Coat Technol*, vol. 350, pp. 925–935, Sep. 2018, doi: 10.1016/J.SURFCOAT.2018.03.067.

[45] S. Siri, P. Wadbua, V. Amornkitbamrung, N. Kampa, and S. Maensiri, "Surface modification of electrospun PCL scaffolds by plasma treatment and addition of adhesive protein to promote fibroblast cell adhesion," *https://doi.org/10.1179/026708310X12798718274070*, vol. 26, no. 11, pp. 1292–1297, Nov. 2013, doi: 10.1179/026708310X12798718274070.

[46] I. Bružauskaitė, D. Bironaitė, E. Bagdonas, and E. Bernotienė, "Scaffolds and cells for tissue regeneration: different scaffold pore sizes—different cell effects," *Cytotechnology*, vol. 68, no. 3, pp. 355–369, 2016, doi: 10.1007/s10616-015-9895-4.

[47] B. Vagaská, L. Bačáková, E. Filová, and K. Balík, "Osteogenic cells on bio-inspired materials for bone tissue engineering," *Physiol Res*, vol. 59, no. 3, pp. 309–322, 2010.

[48] I. O. Smith, X. H. Liu, L. A. Smith, and P. X. Ma, "Nanostructured polymer scaffolds for tissue engineering and regenerative medicine," *Wiley Interdiscip Rev Nanomed Nanobiotechnol*, vol. 1, no. 2, pp. 226–236, Mar. 2009, doi: 10.1002/wnan.26.

[49] K. Zhang, Y. Fan, N. Dunne, and X. Li, "Effect of microporosity on scaffolds for bone tissue engineering," *Regen Biomater*, vol. 5, no. 2, pp. 115–124, Mar. 2018, doi: 10.1093/rb/rby001.

[50] D. Druecke *et al.*, "Neovascularization of poly(ether ester) block-copolymer scaffoldsin vivo: Long-term investigations using intravital fluorescent microscopy," *J Biomed Mater Res*, vol. 68A, no. 1, pp. 10–18, Jan. 2004, doi: 10.1002/jbm.a.20016.

[51] F. M. Klenke, Y. Liu, H. Yuan, E. B. Hunziker, K. A. Siebenrock, and W. Hofstetter, "Impact of pore size on the vascularization and osseointegration of ceramic bone substitutesin vivo," *J Biomed Mater Res A*, vol. 85A, no. 3, pp. 777–786, Jun. 2008, doi: 10.1002/jbm.a.31559.

[52] Y. C. Chiu *et al.*, "The role of pore size on vascularization and tissue remodeling in PEG hydrogels," *Biomaterials*, vol. 32, no. 26, pp. 6045–6051, Sep. 2011, doi: 10.1016/j.biomaterials.2011.04.066.

[53] B. Dhandayuthapani, Y. Yoshida, T. Maekawa, and D. S. Kumar, "Polymeric scaffolds in tissue engineering application: A review," *Int J Polym Sci*, vol. 2011, no. ii, 2011, doi: 10.1155/2011/290602.

[54] S. Yang, K.-F. Leong, Z. M. E. Du, and C.-K. Chua, "The Design of Scaffolds for Use in Tissue Engineering. Part I. Traditional Factors," Mary Ann Liebert, Inc, 2001.

[55] A. Eltom, G. Zhong, and A. Muhammad, "Scaffold Techniques and Designs in Tissue Engineering Functions and Purposes: A Review," *Advances in Materials Science and Engineering*, vol. 2019, 2019, doi: 10.1155/2019/3429527.

[56] D. W. Hutmacher, "Scaffold design and fabrication technologies for engineering tissues - State of the art and future perspectives," *J Biomater Sci Polym Ed*, vol. 12, no. 1, pp. 107–124, 2001, doi: 10.1163/156856201744489.

[57] D. W. Hutmacher, T. B. F. Woodfield, and P. D. Dalton, "Scaffold Design and Fabrication," in *Tissue Engineering*, Elsevier, 2014, pp. 311–346. doi: 10.1016/B978-0-12-420145-3.00010-9.

[58] P. Zhao, H. Gu, H. Mi, C. Rao, J. Fu, and L.-S. Turng, "Fabrication of scaffolds in tissue engineering: A review", doi: 10.1007/s11465-018-0496-8.

[59] A. G. Mikos *et al.*, "Preparation and characterization of poly(l-lactic acid) foams," *Polymer (Guildf)*, vol. 35, no. 5, pp. 1068–1077, Mar. 1994, doi: 10.1016/0032-3861(94)90953-9.

[60] C.-J. Liao, C.-F. Chen, J.-H. Chen, S.-F. Chiang, Y.-J. Lin, and K.-Y. Chang, "Fabrication of porous biodegradable polymer scaffolds using a solvent merging/particulate leaching method," *J Biomed Mater Res*, vol. 59, no. 4, pp. 676–681, Mar. 2002, doi: 10.1002/jbm.10030.

[61] A. G. Mikos, G. Sarakinos, S. M. Leite, J. P. Vacant, and R. Langer, "Laminated three-dimensional biodegradable foams for use in tissue engineering," *Biomaterials*, vol. 14, no. 5, pp. 323–330, Apr. 1993, doi: 10.1016/0142-9612(93)90049-8.

[62] A. Sola *et al.*, "Development of solvent-casting particulate leaching (SCPL) polymer scaffolds as improved three-dimensional supports to mimic the bone marrow niche," *Materials Science and Engineering C*, vol. 96, pp. 153–165, Mar. 2019, doi: 10.1016/j.msec.2018.10.086.

[63] D. C. Sin *et al.*, "Polyurethane (PU) scaffolds prepared by solvent casting/particulate leaching (SCPL) combined with centrifugation," *Materials Science and Engineering C*, vol. 30, no. 1, pp. 78–85, 2010, doi: 10.1016/j.msec.2009.09.002.

[64] B. Stevens, Y. Yang, A. Mohandas, B. Stucker, and K. T. Nguyen, "A review of materials, fabrication methods, and strategies used to enhance bone regeneration in engineered bone tissues," *J Biomed Mater Res B Appl Biomater*, vol. 85B, no. 2, pp. 573–582, May 2008, doi: 10.1002/jbm.b.30962.

[65] X. Gong *et al.*, "Fabrication of poly(lactic acid) scaffolds by a modified solvent casting/porogen leaching method," *E-Polymers*, no. 113, pp. 1–9, 2010, doi: 10.1515/epoly.2010.10.1.1264.

[66] D. J. Mooney, D. F. Baldwin, N. P. Suh, J. P. Vacanti, and R. Langer, "Novel approach to fabricate porous sponges of poly(D,L-lactic-co-glycolic acid) without the use of organic solvents," *Biomaterials*, vol. 17, no. 14, pp. 1417–1422, 1996, doi: 10.1016/0142-9612(96)87284-X.

[67] Y. S. Nam, J. J. Yoon, and T. G. Park, "A novel fabrication method of macroporous biodegradable polymer scaffolds using gas foaming salt as a porogen additive," *J Biomed Mater Res*, vol. 53, no. 1, pp. 1–7, Jan. 2000, doi: 10.1002/(SICI)1097-4636(2000)53:1<1::AID-JBM1>3.0.CO;2-R.

[68] N. Annabi, A. Fathi, S. M. Mithieux, P. Martens, A. S. Weiss, and F. Dehghani, "The effect of elastin on chondrocyte adhesion and proliferation on poly (e{open}-caprolactone)/elastin composites," *Biomaterials*, vol. 32, no. 6, pp. 1517–1525, Feb. 2011, doi: 10.1016/j.biomaterials.2010.10.024.

[69] S. A. Poursamar, J. Hatami, A. N. Lehner, C. L. Da Silva, F. C. Ferreira, and A. P. M. Antunes, "Gelatin porous scaffolds fabricated using a modified gas foaming technique: Characterisation and cytotoxicity assessment," *Materials Science and Engineering C*, vol. 48, pp. 63–70, Mar. 2015, doi: 10.1016/j.msec.2014.10.074.

[70] S. A. Poursamar, J. Hatami, A. N. Lehner, C. L. da Silva, F. C. Ferreira, and A. P. M. Antunes, "Potential application of gelatin scaffolds prepared through in situ gas foaming in skin tissue engineering," *International Journal of Polymeric Materials and Polymeric Biomaterials*, vol. 65, no. 6, pp. 315–322, Apr. 2016, doi: 10.1080/00914037.2015.1119688.

[71] D. Gorth and T. J. Webster, "Matrices for tissue engineering and regenerative medicine," in *Biomaterials for Artificial Organs*, Elsevier Inc., 2010, pp. 270–286. doi: 10.1533/9780857090843.2.270.

[72] P. Carter and N. Bhattarai, "Bioscaffolds: Fabrication and Performance," in *Engineered Biomimicry*, Elsevier Inc., 2013, pp. 161–188. doi: 10.1016/B978-0-12-415995-2.00007-6.

[73] E. M. Prieto and S. A. Guelcher, "Tailoring properties of polymeric biomedical foams," in *Biomedical Foams for Tissue Engineering Applications*, Elsevier Ltd., 2014, pp. 129–162. doi: 10.1533/9780857097033.1.129.

[74] J. F. Cooley, "Appartus for Electrically Dispersed Fluids," 692631, Feb. 04, 1902

[75] W. Morton, "Method of dispersing fluids.," 705691, Jul. 29, 1902

[76] G. I. Taylor, "Electrically driven jets," *Proceedings of the Royal Society of London. A. Mathematical and Physical Sciences*, vol. 313, no. 1515, pp. 453–475, Dec. 1969, doi: 10.1098/rspa.1969.0205.

[77] G. Srinivasan and D. H. Reneker, "Structure and morphology of small diameter electrospun aramid fibers," *Polym Int*, vol. 36, no. 2, pp. 195–201, Feb. 1995, doi: 10.1002/pi.1995.210360210.

[78] X. Fang and D. H. Reneker, "DNA fibers by electrospinning," *J Macromol Sci Phys*, vol. 36, no. 2, pp. 169–173, 1997, doi: 10.1080/00222349708220422.

[79] J.-S. Kim and D. H. Reneker, "Polybenzimidazole nanofiber produced by electrospinning," *Polym Eng Sci*, vol. 39, no. 5, pp. 849–854, May 1999, doi: 10.1002/pen.11473.

[80] Z.-M. Huang, Y.-Z. Zhang, M. Kotaki, and S. Ramakrishna, "A review on polymer nanofibers by electrospinning and their applications in nanocomposites," *Compos Sci Technol*, vol. 63, no. 15, pp. 2223–2253, Nov. 2003, doi: 10.1016/S0266-3538(03)00178-7.

[81] A. Haider, S. Haider, and I.-K. Kang, "A comprehensive review summarizing the effect of electrospinning parameters and potential applications of nanofibers in biomedical and biotechnology," *Arabian Journal of Chemistry*, vol. 11, no. 8, pp. 1165–1188, Dec. 2018, doi: 10.1016/J.ARABJC.2015.11.015.

[82] M. Mirjalili and S. Zohoori, "Review for application of electrospinning and electrospun nanofibers technology in textile industry," *J Nanostructure Chem*, vol. 6, no. 3, pp. 207–213, Sep. 2016, doi: 10.1007/s40097-016-0189-y.

[83] I. Jun, H. S. Han, J. R. Edwards, and H. Jeon, "Electrospun fibrous scaffolds for tissue engineering: Viewpoints on architecture and fabrication," *Int J Mol Sci*, vol. 19, no. 3, Mar. 2018, doi: 10.3390/ijms19030745.

[84] H. Bikas, P. Stavropoulos, and G. Chryssolouris, "Additive manufacturing methods and modeling approaches: A critical review," *International Journal of Advanced Manufacturing Technology*, vol. 83, no. 1–4, pp. 389–405, Jul. 2016, doi: 10.1007/s00170-015-7576-2.

[85] S. Pashneh-Tala, R. Moorehead, and F. Claeyssens, "Hybrid manufacturing strategies for tissue engineering scaffolds using methacrylate functionalised poly(glycerol sebacate)," *J Biomater Appl*, vol. 34, no. 8, pp. 1114–1130, Mar. 2020, doi: 10.1177/0885328219898385.

[86] H. Kodama, "Automatic method for fabricating a three-dimensional plastic model with photo-hardening polymer," *Review of Scientific Instruments*, vol. 52, no. 11, pp. 1770–1773, Nov. 1981, doi: 10.1063/1.1136492.

[87] A. J. Melchiorri *et al.*, "3D-Printed Biodegradable Polymeric Vascular Grafts," *Adv Healthc Mater*, vol. 5, no. 3, pp. 319–325, Feb. 2016, doi: 10.1002/adhm.201500725.

[88] F. P. W. Melchels, K. Bertoldi, R. Gabbrielli, A. H. Velders, J. Feijen, and D. W. Grijpma, "Mathematically defined tissue engineering scaffold architectures prepared by stereolithography," *Biomaterials*, vol. 31, no. 27, pp. 6909–6916, Sep. 2010, doi: 10.1016/j.biomaterials.2010.05.068.

[89] D. G. Tamay, T. D. Usal, A. S. Alagoz, D. Yucel, N. Hasirci, and V. Hasirci, "3D and 4D printing of polymers for tissue engineering applications," *Front Bioeng Biotechnol*, vol. 7, no. JUL, p. 164, Jul. 2019, doi: 10.3389/fbioe.2019.00164.

[90] K. Ji *et al.*, "Application of 3D printing technology in bone tissue engineering," *Biodes Manuf*, vol. 1, no. 3, pp. 203–210, Sep. 2018, doi: 10.1007/s42242-018-0021-2.

[91] M. S. Silverstein, "PolyHIPEs: Recent advances in emulsion-templated porous polymers," *Prog Polym Sci*, vol. 39, no. 1, pp. 199–234, Jan. 2014, doi: 10.1016/j.progpolymsci.2013.07.003.

[92] N. R. Cameron, "High internal phase emulsion templating as a route to well-defined porous polymers," *Polymer (Guildf)*, vol. 46, no. 5, pp. 1439–1449, Feb. 2005, doi: 10.1016/J.POLYMER.2004.11.097.

[93] M. S. Silverstein, N. R. (Neil R. Cameron, and P. Krajnc, "Colloidal Templating," in *Porous Polymers*, M. S. Silverstein, N. R. (Neil R. Cameron, and M. A. Hillmyer, Eds., John Wiley & Sons, 2011, pp. 119–172.

[94] S. Kramer, N. R. Cameron, and P. Krajnc, "Porous Polymers from High Internal Phase Emulsions as Scaffolds for Biological Applications," *Polymers (Basel)*, vol. 13, no. 11, 2021, doi: 10.3390/POLYM13111786.

[95] R. Furmidge *et al.*, "Surfactant-free gelatin-stabilised biodegradable polymerised high internal phase emulsions with macroporous structures," *Front Chem*, vol. 11, Aug. 2023, doi: 10.3389/FCHEM.2023.1236944.

[96] R. S. Moglia, J. L. Holm, N. A. Sears, C. J. Wilson, D. M. Harrison, and E. Cosgriff-Hernandez, "Injectable polyHIPEs as high-porosity bone grafts," *Biomacromolecules*, vol. 12, no. 10, pp. 3621–3628, Oct. 2011, doi: 10.1021/bm2008839.

[97] C. E. Jackson, D. H. Ramos-Rodriguez, N. T. H. Farr, W. R. English, N. H. Green, and F. Claeyssens, "Development of PCL PolyHIPE Substrates for 3D Breast Cancer Cell Culture," *Bioengineering 2023, Vol. 10, Page 522*, vol. 10, no. 5, p. 522, 2023, doi: 10.3390/BIOENGINEERING10050522.

[98] G. Jing *et al.*, "Synthesis and properties of polystyrene-based polyHIPEs reinforced with quadruple hydrogen bond functionality," *Journal of Polymer Research*, vol. 22, no. 8, pp. 1–11, Aug. 2015, doi: 10.1007/s10965-015-0791-6.

[99] P. Sun *et al.*, "Preparation of PolyHIPE Scaffolds for 3D Cell Culture and the Application in Cytotoxicity Evaluation of Cigarette Smoke," *Polymers (Basel)*, vol. 11, no. 6, p. 959, Jun. 2019, doi: 10.3390/polym11060959.

[100] Reprocell USA Inc., "REPROCELL Brand: Alvetex." https://www.reprocell.com/brand-alvetex-i26 (accessed Jul. 10, 2020).

[101] L. Costello *et al.*, "Engineering a multilayered skin equivalent: The importance of endogenous extracellular matrix maturation to provide robustness and reproducibility," in *Methods in Molecular Biology*, Humana Press Inc., 2019, pp. 107–122. doi: 10.1007/978-1-4939-9473-1_9.

[102] L. Porcelli *et al.*, "CAFs and TGF-β Signaling Activation by Mast Cells Contribute to Resistance to Gemcitabine/Nabpaclitaxel in Pancreatic Cancer," *Cancers (Basel)*, vol. 11, no. 3, p. 330, Mar. 2019, doi: 10.3390/cancers11030330.

[103] B. A. Dikici, S. Dikici, G. C. Reilly, S. MacNeil, and F. Claeyssens, "A novel bilayer polycaprolactone membrane for guided bone regeneration: Combining electrospinning and emulsion templating," *Materials*, vol. 12, no. 16, p. 2643, Aug. 2019, doi: 10.3390/ma12162643.

[104] B. Aldemir Dikici, G. C. Reilly, and F. Claeyssens, "Boosting the Osteogenic and Angiogenic Performance of Multiscale Porous Polycaprolactone Scaffolds by in Vitro Generated Extracellular Matrix Decoration," *ACS Appl Mater Interfaces*, vol. 12, no. 11, pp. 12510–12524, 2020, doi: 10.1021/ACSAMI.9B23100/ASSET/IMAGES/LARGE/AM9B23100_0008.JPEG.

[105] S. Dikici *et al.*, "Assessment of the Angiogenic Potential of 2-Deoxy-D-Ribose Using a Novel in vitro 3D Dynamic Model in Comparison With Established in vitro Assays," *Front Bioeng Biotechnol*, vol. 7, p. 451, Jan. 2020, doi: 10.3389/FBIOE.2019.00451/BIBTEX.

[106] S. Dikici, B. Aldemir Dikici, S. Macneil, and F. Claeyssens, "Decellularised extracellular matrix decorated PCL PolyHIPE scaffolds for enhanced cellular activity,

integration and angiogenesis," *Biomater Sci*, vol. 9, no. 21, pp. 7297–7310, Oct. 2021, doi: 10.1039/D1BM01262B.

[107] T. E. Paterson *et al.*, "Porous microspheres support mesenchymal progenitor cell ingrowth and stimulate angiogenesis," *APL Bioeng*, vol. 2, no. 2, p. 26103, Jun. 2018, doi: 10.1063/1.5008556/23015.

[108] J. Wu and Y. Hong, "Enhancing cell infiltration of electrospun fibrous scaffolds in tissue regeneration," *Bioact Mater*, vol. 1, no. 1, pp. 56–64, Sep. 2016, doi: 10.1016/j.bioactmat.2016.07.001.

[109] Y. H. Lee *et al.*, "Electrospun dual-porosity structure and biodegradation morphology of Montmorillonite reinforced PLLA nanocomposite scaffolds," *Biomaterials*, vol. 26, no. 16, pp. 3165–3172, Jun. 2005, doi: 10.1016/j.biomaterials.2004.08.018.

[110] B. A. Blakeney *et al.*, "Cell infiltration and growth in a low density, uncompressed three-dimensional electrospun nanofibrous scaffold," *Biomaterials*, vol. 32, no. 6, pp. 1583–1590, Feb. 2011, doi: 10.1016/j.biomaterials.2010.10.056.

[111] R. Hashizume *et al.*, "Morphological and mechanical characteristics of the reconstructed rat abdominal wall following use of a wet electrospun biodegradable polyurethane elastomer scaffold," *Biomaterials*, vol. 31, no. 12, pp. 3253–3265, Apr. 2010, doi: 10.1016/j.biomaterials.2010.01.051.

[112] J. B. Lee *et al.*, "Highly porous electrospun nanofibers enhanced by ultrasonication for improved cellular infiltration," *Tissue Eng Part A*, vol. 17, no. 21–22, pp. 2695–2702, Nov. 2011, doi: 10.1089/ten.tea.2010.0709.

[113] W. Yang, F. Yang, Y. Wang, S. K. Both, and J. A. Jansen, "In vivo bone generation via the endochondral pathway on three-dimensional electrospun fibers," *Acta Biomater*, vol. 9, no. 1, pp. 4505–4512, Jan. 2013, doi: 10.1016/j.actbio.2012.10.003.

[114] M. Simonet, O. D. Schneider, P. Neuenschwander, and W. J. Stark, "Ultraporous 3D polymer meshes by low-temperature electrospinning: Use of ice crystals as a removable void template," *Polym Eng Sci*, vol. 47, no. 12, pp. 2020–2026, Dec. 2007, doi: 10.1002/pen.20914.

[115] B. M. Baker *et al.*, "The potential to improve cell infiltration in composite fiber-aligned electrospun scaffolds by the selective removal of sacrificial fibers," *Biomaterials*, vol. 29, no. 15, pp. 2348–2358, May 2008, doi: 10.1016/j.biomaterials.2008.01.032.

[116] J. Nam, Y. Huang, S. Agarwal, and J. Lannutti, "Improved cellular infiltration in electrospun fiber via engineered porosity," *Tissue Eng*, vol. 13, no. 9, pp. 2249–2257, Sep. 2007, doi: 10.1089/ten.2006.0306.

[117] K. Tuzlakoglu, M. I. Santos, N. Neves, and R. L. Reis, "Design of Nano- and Microfiber Combined Scaffolds by Electrospinning of Collagen onto Starch-Based Fiber Meshes: A Man-Made Equivalent of Natural Extracellular Matrix," *Tissue Eng Part A*, vol. 17, no. 3–4, pp. 463–473, Feb. 2011, doi: 10.1089/ten.tea.2010.0178.

[118] A. Salerno, M. Oliviero, E. Di Maio, S. Iannace, and P. A. Netti, "Design of porous polymeric scaffolds by gas foaming of heterogeneous blends," *J Mater Sci Mater Med*, vol. 20, no. 10, pp. 2043–2051, Oct. 2009, doi: 10.1007/s10856-009-3767-4.

[119] D. W. Johnson, C. Sherborne, M. P. Didsbury, C. Pateman, N. R. Cameron, and F. Claeyssens, "Macrostructuring of emulsion-templated porous polymers by 3D laser patterning," *Advanced Materials*, vol. 25, no. 23, pp. 3178–3181, Jun. 2013, doi: 10.1002/adma.201300552.

[120] R. Huang *et al.*, "Triple-Layer Vascular Grafts Fabricated by Combined E-Jet 3D Printing and Electrospinning," *Ann Biomed Eng*, vol. 46, no. 9, pp. 1254–1266, Sep. 2018, doi: 10.1007/s10439-018-2065-z.

1.4   Research Aim and Objective

The main aim of the project presented in this thesis was to develop a substrate suitable for 3D cancer culture and vascular infiltration with potential to be used within a microphysiological system (MPS) to study cancer metastasis.

Each chapter focuses on the following aims and objectives in order to achieve the main aim:

1. Chapter 1 is composed of two literature reviews which investigate:
   a) The role of microphysiological systems to study metastatic cancer
   b) The considerations and methods of fabrication required for a successful tissue engineered scaffold.
      Whilst high molecular weight polycaprolactone methacrylate (PCL-M) was used within this project the reviews cover a breadth of MPS models and scaffold materials and fabrication methods within the research field that can be utilised to construct an effective *in vitro* model.

2. The primary aim of chapter 2 focuses on developing a substrate suitable for 3D cancer cell culture, this was achieved by:
   a) Investigating the effect of mixing speed on PCL-M polyHIPE pore size and interconnectivity and any resulting changes in mechanical properties.
   b) Studying the effect of plasma and fibronectin coating on scaffold hydrophilicity and the effect of such coating on cell response.
   c) Performing initial biocompatibility testing using triple negative breast cancer cells *in vitro* and an *ex ovo* chick chorioallontoic membrane (CAM) assay.

3. Chapter 3 focused on developing a fabrication technique to increase pore size of the PCL-M polyHIPEs. This was achieved by:
   a) Investigating the effect of incorporating gelatin within the internal phase of the PCL-M emulsion.
   b) Optimising the effect of gelatin on the pore size by altering the concentration of gelatin within the internal phase and studying the effect on the mechanical properties of the resulting scaffolds.
   c) Studying the long-term stability of PCL-M polyHIPEs fabricated with gelatin in the internal phase.

4. Using the fabrication technique optimised in chapter 3, chapter 4 focuses on investigating 3D cell culture and vascular in-growth within the gelatin-containing PCL-M substrate. This was achieved by:

    a) Investigating the mechanical and chemical environment of the 3D environment of the cells within the PCL-M substrate.

    b) Quantifying cell metabolic activity and expression of vascular endothelial growth factor on the gelatin-containing PCL-M polyHIPEs.

    c) Utilising the CAM assay to assess vascular ingrowth into the PCL-M substrates with the additional influence of breast cancer cells within the scaffold.

5. Chapter 5 describes the development of an in vitro vascularised tumour model using a commercially available MPS system for oncology applications. This was achieved by:

    a) Characterising colon adenocarcinoma spheroids up to 10 days in culture, to assess parameters such as; growth, proliferative regions and hypoxic characteristics

    b) Utilising a commercially available vascularised MPS to investigate spheroid/vascular connection.

    c) Studying the effect of antibody-based anti-angiogenic cancer therapies on the spheroid/vascular system.

    d) Investigating the efficacy of CAR-T cell therapy treatments within the system and the translatability of the model to clinic.

6. Chapter 6 discusses the conclusions and future direction of the use of PCL-M polyHIPEs within MPS.

CHAPTER 2. Development of PCL PolyHIPE Substrates for 3D Breast Cancer Cell Culture

Article

Development of PCL PolyHIPE Substrates for 3D Breast Cancer Cell Culture

Caitlin E. Jackson [1,2], David H. Ramos-Rodriguez [3], Nicholas T. H. Farr [1,2], William R. English [4], Nicola H. Green [1,2] and Frederik Claeyssens [1,2,*]

1   Materials Science and Engineering, The Kroto Research Institute, University of Sheffield, Sheffield S3 7HQ, UK
2   Insigneo Institute for In Silico Medicine, The Pam Liversidge Building, University of Sheffield, Sheffield S1 3JD, UK
3   Department of Orthopaedic Surgery, UC Davis Health, Sacramento, CA 95817, USA
4   Norwich Medical School, University of East Anglia, Norwich NR3 7TJ, UK
*   Correspondence: f.claeyssens@sheffield.ac.uk

Abstract: Cancer is a becoming a huge social and economic burden on society, becoming one of the most significant barriers to life expectancy in the 21st century. In particular, breast cancer is one of the leading causes of death for women. One of the most significant difficulties to finding efficient therapies for specific cancers, such as breast cancer, is the efficiency and ease of drug development and testing. Tissue-engineered (TE) *in vitro* models are rapidly developing as an alternative to animal testing for pharmaceuticals. Additionally, porosity included within these structures overcomes the diffusional mass transfer limit whilst enabling cell infiltration and integration with surrounding tissue. Within this study, we investigated the use of high-molecular-weight polycaprolactone methacrylate (PCL–M) polymerised high-internal-phase emulsions (polyHIPEs) as a scaffold to support 3D breast cancer (MDA-MB-231) cell culture. We assessed the porosity, interconnectivity, and morphology of the polyHIPEs when varying mixing speed during formation of the emulsion, successfully demonstrating the tunability of these polyHIPEs. An *ex ovo* chick chorioallantoic membrane assay identified the scaffolds as bioinert, with biocompatible properties within a vascularised tissue. Furthermore, *in vitro* assessment of cell attachment and proliferation showed promising potential for the use of PCL polyHIPEs to support cell growth. Our results demonstrate that PCL polyHIPEs are a promising material to support cancer cell growth with tuneable porosity and interconnectivity for the fabrication of perfusable 3D cancer models.

Keywords: polycaprolactone; polyHIPE; tissue engineering; CAM assay; breast cancer

1. Introduction

Breast cancer is a leading cause of death for women [1], with an estimated 51,400 new diagnoses of ductal carcinoma in the US in 2022 [2]. MDA-MB-231 cell line (isolated from a patient with invasive ductal carcinoma) is a metastatic, triple-negative (ER, PR, and HER), and E-cadherin-negative breast cancer [3]. It is a cell line commonly used to model late-stage breast cancer. MDA-MB-231 cells have been shown to be invasive *in vitro* and spontaneously metastasise in *in vivo* models [4–6]. This is a well-defined and frequently used cell line that can be used to develop relevant 3D *in vitro* models for assessing drug efficacy, a research area that is increasingly needing further development. Currently, there is a >96% failure rate of potential drug candidates for breast cancer in clinical trials, driven by a lack of translatability of *in vitro* efficacy *in vivo* [1]. *In vitro* drug screening platforms that closely mimic *in vivo* models can reduce the use of *in vivo* animal models, reducing high cost, time, and ethical implications. Tissue-engineered (TE) *in vitro* models are rapidly developing for many applications including drug discovery, toxicity testing, and disease modelling [7]. Incorporating a porous structure into a TE model is a popular technique to

overcome the diffusional mass transfer limit whilst enabling cell infiltration and integration with surrounding tissue [8]. This is an alternative to commonly used spheroidal cultures, where the porous scaffold provides a conducive environment for 3D culture. Previous studies highlight that a pore size of ~40 μm and a porosity of 90% is suitable for cell ingrowth for a variety of cell types [9–11], while our approach also enables the pore size and overall porosity to be tuned. This scaffold approach is open to 3D cell culture of all cell types and enables easier co-culture compared to spheroidal cultures where the use of specific cell types can be limited. In addition, the porous structure can provide a scaffold to stimulate the production of extracellular matrix (ECM) components by cells, resulting in ECM recapitulation within the model [12]. The ECM is a significant element of the tissue microenvironment and plays an integral role in maintaining normal cell function and behaviour, and can have a significant impact on cancer development [13,14].

Both natural and synthetic polymers are materials commonly used in the fabrication of TE scaffolds. Whilst natural polymers recapitulate the chemistry and architecture needed for cell attachment and growth [15], there are many associated disadvantages such as batch-to-batch variability, risk of pathogen transmission, and the potential of containing protein impurities [16–18]. In contrast, TE scaffolds produced from synthetic polymers are inexpensive to manufacture, possess tuneable chemical and mechanical properties, and can be reproduced accurately without the concern of polymer batch variation.

In order to incorporate porosity into a polymer-based scaffold, various manufacturing techniques have been applied, including particle leaching, solvent casting, gas foaming, and additive manufacturing, as detailed in numerous reviews [8,19–22]. Recently, high-internal-phase emulsion (HIPE) templating has become an emerging technique to produce TE scaffolds with multiple advantageous properties [23–25]. The scaffolds can be produced via inexpensive production methods, while the porosity can be tuned controllably. Emulsion-templated scaffolds provide high porosity and interconnectivity, enabling mass transport of nutrients and waste, cell migration, and potential vascularisation via co-culture with endothelial cells [24]. In addition, the scaffolds are highly tuneable, enabling the production of TE models for specific applications [26].

Emulsion templating involves the mixing of two immiscible phases, where an internal phase (water) is dispersed within an external continuous phase (polymer) in the presence of an emulsifier, commonly a surfactant, to stabilise the emulsion (Figure 1). When the volume of the internal phase is greater than 74.05%, an emulsion is classified as a HIPE. The process of emulsion templating is well-documented in numerous studies and reviews [25–28].

Alvetex is a current gold-standard polystyrene polyHIPE-based scaffold widely used in *in vitro* assays to study cell growth, differentiation, and function [7]. Thus, the performance of novel scaffolds is often compared to Alvetex. A recent study by Aldemir Dikici et al. [23] compared Alvetex to four-arm methacrylated polycaprolactone polyHIPE scaffolds, demonstrating a similar level of performance in cell culture and ingrowth.

Polycaprolactone (PCL) has many beneficial characteristics including FDA approval, low-cost, and ease of manufacture and manipulation, as presented by Woodruff et al. [29].

In addition, the biodegradation of PCL is relatively slow (>1 year) compared to other polymers, such as polylactides (2–4 months complete resorption) and polyglycolides (weeks to months for complete resorption) [30]. Thus, it is an ideal candidate for longer-term scaffolds, implants, drug delivery applications, or testing platforms and models. PCL has a lower Young's modulus than polystyrene (350 MPa versus 3.4 GPa), which makes it a more suitable material for soft tissue models. PCL has been used in a range of TE applications including bone [31,32], skin [33], cartilage [34], vascular [35], tendon, and ligament engineering [29].

In this study, we investigated the use of emulsion templating to manufacture a porous PCL scaffold, where high-internal-phase emulsion templating was combined with high-molecular-weight four-arm polycaprolactone methacrylate (PCL–M) to fabricate highly porous and interconnected polyHIPEs. The effect of mixing speed and post-processing washing cycles on the polyHIPEs structural and mechanical properties was investigated.

The surfaces of the scaffolds were functionalised via air and acrylic acid plasma treatment and initial *in vitro* cell viability and proliferation within the scaffolds was analysed via a resazurin reduction assay. Furthermore, an *ex ovo* chorioallantoic membrane (CAM) assay was used to investigate the biocompatibility of PCL–M polyHIPEs within an *in vivo* vascularised tissue.
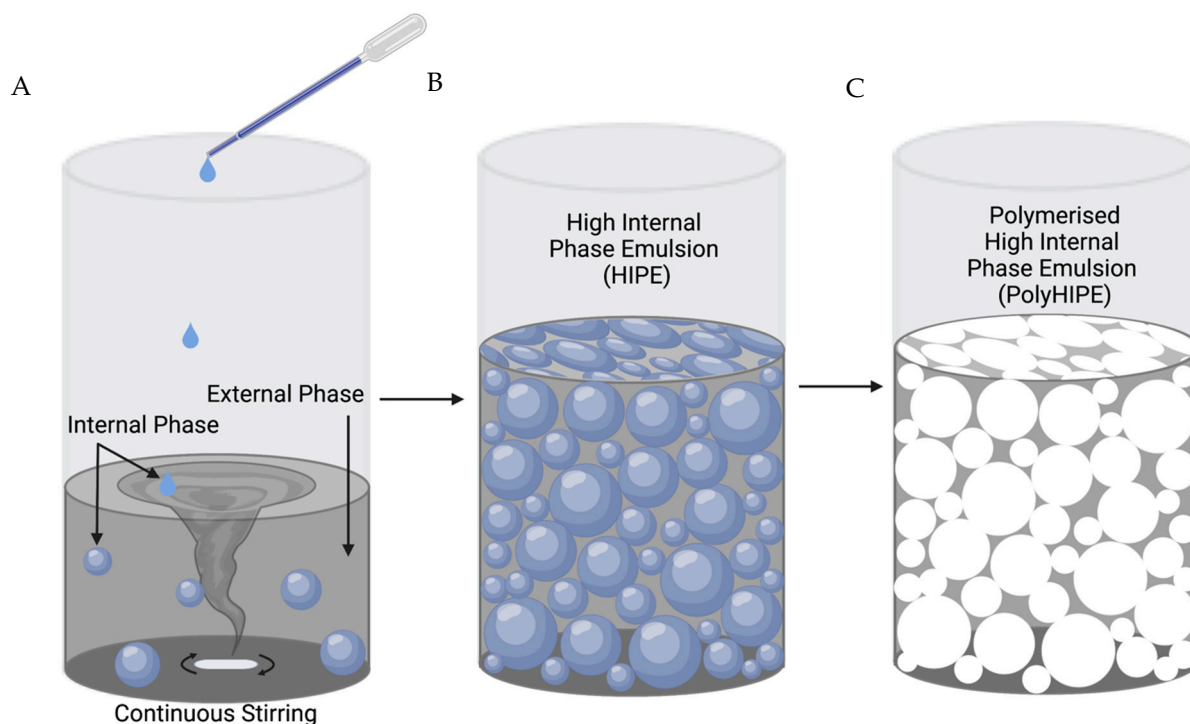

Figure 1. Process to fabricate polymerised high-internal-phase emulsions (polyHIPEs). (**A**) Addition of an internal phase, drop-wise, into a continuous external phase. (**B**) The external phase ruptures at the thinnest sections, transforming the internal phase into a continuous connected phase. (**C**) The external phase is solidified via polymerisation and the internal phase is removed, resulting in a porous, interconnected polymer structure. Created with BioRender.com.

2. Materials

Photoinitiator (PI) (2,4,6-Trimethylbenzoyl Phosphine Oxide/2-Hydroxy-2- Methyl-propiophenone), SLYGARD 184 Silicone elastomer base and silicone elastomer curing agent, Dulbecco's modified Eagle media (DMEM), fetal bovine serum (FBS), penicillin/streptomycin (PS), l-glutamine, trypsin, paraformaldehyde, and resazurin sodium salt were purchased from Sigma Aldrich. Chloroform, toluene, ethanol, and methanol were purchased from Fisher Scientific. Fibronectin was purchased from YO Proteins. The surfactant, Hypermer B246, was purchased from Croda. High-molecular-weight four-arm polycaprolactone methacrylate (PCL–M, 20,000 g/mol) was synthesised in the laboratory (a general synthesis method is given in [23]).

3. Methods

3.1. Preparation of PCL–M Emulsions

Unless stated otherwise, the amounts of PCL–M (0.40 g), surfactant (0.04 g), photoinitiator (0.03 g), solvent blend (60 wt% chloroform and 40 wt% toluene, 0.60 g), and water (2 mL) were kept constant in each batch of emulsion. This resulted in an internal phase volume of 83% *w/w*. PCL–M and the surfactant were added to a glass vial, heated to dissolve the surfactant, and left to cool. Photoinitiator and the solvent blend were added to the PCL–M–surfactant mixture. The vial was protected from light and the contents were mixed (200–800 rpm) using a magnetic stirrer (20 mm × 7 mm) for 3 min at 37 °C. Once

homogeneity was reached, water was added dropwise within 3 min and the emulsion was further mixed for 5 min.

3.2. Polymerisation of PCL–M Emulsions

Samples were either polymerised in a 2 mL syringe or in a silicone mould. For scaffolds with a 6.5 mm diameter, the PCL–M emulsion was loaded into a 2 mL syringe. Samples for mechanical testing, a dog-bone-shaped silicone mould (thickness (T): 3 mm, gage length (G): 13.5 mm, and width overall: 5.7 mm) was made using silicone elastomer base mixed with silicone elastomer curing agent (10:1 ratio). The two reagents were mixed for 5 min before being poured into a petri dish, forming a layer sufficiently covering the acrylic dog-bone, and left in an oven for 12 h to cure at 60 °C. The PCL–M emulsion was syringed into the dog-bone-shaped mould. All samples were cured for 5 min on both sides using the OmniCure Series 1000 system (100 W, Lumen Dynamics, Mississauga, ON, Canada), with 18 W/cm^2 reported light density and spectral output from 250–600 nm. The resulting polyHIPEs were removed from the syringe or mould and washed in 100% methanol for 3 days, changing the methanol after each 24 h period. Following this, the samples were washed in water for 3 days, changing the water after each 24 h period, removing contaminants such as surfactant, solvent, and uncured emulsion. The samples were then removed from the water and left to dry in a vacuum oven at room temperature overnight.

3.3. Assessment of PCL–M PolyHIPEs Porosity by SEM

To observe and analyse the micro-porosity of the polyHIPE samples, scaffolds polymerised using the 2 mL syringe were sliced into 1 mm thick discs using a vibrating microtome (5100 mz, Campden Instruments, Loughborough, UK). The vibratome frequency, amplitude, and speed were set at 80 Hz, 1.50 mm, and 0.10 mm/s, respectively. The porosity and morphology of the polyHIPEs were analysed using a scanning electron microscope (SEM, Helios G4 CXe PFIB DualBeam, Thermo Fisher Scientific, Eindhoven, The Netherlands). Samples were not subject to deposition of conductive coatings (e.g., gold or carbon), in contrast to usual SEM analysis practice for polymers. To avoid surface charging and damage to the sample, a low accelerating voltage of 1 kV with typical vacuum pressure of 10^{-5} mbar at a working distance of 3 mm was applied. Working with low acceleration voltage allows for accurate visualisation of pore size and morphology of non-conductive materials such as the PCL polyHIPE substrates without the need of a metal coating [36]. An Everhart–Thornley detector (ETD) was used for low magnification images and a through lens detector (TLD) was used for high magnification images. The SEM images were used to calculate the average pore size, window size, and degree of openness. The diameter of pores and windows were measured using ImageJ v. 1.48 from the National Institutes of Health (NIH, Bethesda, MD, USA). The pores were selected by placing a 12 square grid over the image and measuring the pore diameters that were in contact with the grid. A correction factor $(2/\sqrt{3})$ was applied to adjust for the assumption that each pore was exactly bisected. The correction factor evaluates the average of the ratio R/r, where R is the actual pore diameter and r is the measured diameter of the pore, further detailed in [37]. The windows were selected by measuring any window that was found within a pore in contact with the grid. Histograms of the pore and window size were created using GraphPad (GraphPad Prism, Version 9.4.1, San Diego, CA, USA). Data points that lay outside the mean ± 3 standard deviations (1.64% of total data set) were classed as outliers and removed from the dataset. These outliers were considered to be caused by air bubbles from transfer of the emulsion to the mould.

3.4. Mechanical Characterisation

The elastic modulus of the PCL–M was calculated using tensile testing (MultiTest 2.5–dV Mecmesin, Slinfold, UK). The MultiTest 2.5 was equipped with 25 N and 250 N load cells that were utilised to characterise PCL–M polyHIPEs and bulk polymer, respectively. PCL–M emulsions and bulk polymer were cured in tensile test pieces and clamped between

the two grips. The tensile tests were performed on each sample at a rate of 1 mm/min until the samples failed. The elastic modulus was calculated from the gradient of the initial linear region of the stress–strain curve for each sample. The ultimate tensile strength was measured at the point at which the samples withstood the maximum stress. Maximum elongation was the defined as the percentage elongation at the time the samples broke.

3.5. Surface Wettability of PCL–M polyHIPE

Water contact angle measurements were used to analyse and quantify the hydrophilicity of PCL–M bulk and polyHIPE disc surfaces. A disc silicone mould was made using silicone elastomer base mixed with silicone elastomer curing agent (10:1 ratio). The two reagents were mixed for 5 min before being poured into a petri dish, forming a layer sufficiently covering acrylic discs, and left in an oven at 60 °C for 12 h to cure. PCL–M bulk discs were produced by heating PCL–M in a glass vial until the polymer melted. Then, 5 wt% of PI was added to the PCL–M and thoroughly mixed. The discs were injected into the silicon mould and cured on both sides for 5 min using the OmniCure Series 1000 system. The discs were treated with air and acrylic acid plasma for durations of 2 and 30 min, respectively. The sessile drop method with deionised water was used to measure the contact angle on the functionalised polyHIPE and bulk PCL–M discs (diameter 6.5 mm and 15 mm, respectively) using a contact angle goniometer (Goniometer FTÅ 200) paired with First Ten Angstroms (FTA) software. The mean reported from each variable was acquired from three surface locations.

3.6. Assessment of Surface Functionalisation of PCL–M Scaffolds

X-ray photoelectron spectroscopy (XPS) was used to assess the surface functionalisation of PCL–M polyHIPE scaffolds following plasma coating with air and acrylic acid and/or fibronectin coating. Samples were analysed using a Kratos AXIS Ultra DLD instrument (Department of Chemistry, the University of Sheffield, UK). Spectra were recorded using a monochromatized Al Kα X-ray source (1486.6 eV) operating at a power of 150 W. An internal flood gun was used to reduce the charging of the sample during irradiation. Each sample was analysed at an emission angle normal to the sample surface. Data processing, analysis, and charge correction were carried out using Casa XPS software (Casa Software Ltd., Teignmouth, UK). Component peaks within the recorded C(1s) spectra were deconvoluted and fitted to an asymmetric Lorentzian line-shape (model LA with parameters α = β = 1.53 and m = 243). The aliphatic hydrocarbon component of the C(1s) was set to 285.0 eV as an internal reference.

3.7. General Cell Culture

MDA-MB-231 cells (triple-negative breast cancer cell line) [38] were used to evaluate the proliferation and morphology of cancer cells with PCL–M polyHIPE scaffolds. The MDA-MB-231 cells were purchased from Merck (ECACC) and transduced to express luciferase2 and mStrawberry by transfection with a transposon and the transposase PiggyBac using methodology developed previously [39]. The cells were transduced and selected with puromycin, stocks frozen within 5 passages, and then used within 30 passages of receipt from ECACC. The cells were thawed, transferred to media (DMEM supplemented with 10% FBS, 1% PS, 1% L-glutamine), and centrifuged at 95 g for 5 min. The cell pellet was resuspended in fresh media with 1 µg/mL puromycin and cultured until 90% confluence with media changes every 3 days. Puromycin was removed from the media 24 h before each experiment.

3.8. Scaffold Fabrication for Cell Culture

To initially characterise cell–scaffold interactions, polyHIPE discs (6 mm diameter and 1 mm depth) were used. To sterilise, all scaffolds were washed in methanol followed by PBS. Scaffolds were treated for 24 h before cell culture using air plasma or acrylic acid (AAc) plasma (in house set-up as described in [40]). Air plasma was applied to the scaffold

discs with a power of 50 W for 2 min. AAc plasma was applied to the scaffold discs with a power of 10 W for 30 min. Following this, the scaffolds were placed in a 24 well-plate and soaked in one of two conditions; phosphate-buffered saline (PBS) or fibronectin (10 μg/mL) for 12 h in an incubator at 37 °C and 5% CO_2.

3.9. MDA-MB-231 Cell Seeding on PCL–M polyHIPE Scaffolds

Once reaching 90% confluency, cells were detached from the cell culture flask using trypsin. After 4 min, the trypsin was neutralised with cell culture media (ratio of 1:2), followed by centrifugation ($95 \times g$ for 5 min), and resuspended in fresh media before counting using the trypan blue exclusion method to assess cell viability. The pre-soaking solutions were removed from the scaffolds and 25 μL of MDA-MB-231 cells at 1×10^6 cells/mL were transferred onto each scaffold and left for 1 h in the incubator (37 °C and 5% CO_2) to allow cell attachment. After 1 h, a further 25 μL of MDA-MB-231 cells at 1×10^6 cells/mL were transferred onto the second side of the scaffolds and left for an additional 1 h in the incubator. After 1 h, fresh media was placed in each well and incubated for 7 days.

3.10. Cell Viability on PCL–M polyHIPE Scaffolds

The viability of cells on the scaffold was assessed using the resazurin reduction (RR) assay. For this, 1 mM resazurin stock solution was diluted in cell culture media to form a 10% *v/v* resazurin working solution. The media was removed and discarded from each well and a further 1 mL of the working solution was added to each well. The well plate was protected from light and incubated for 4 h at 37 °C. An orbital rocker (30 rpm) was used in the incubator to ensure full penetration of the resazurin working solution. A total of 200 μL was taken, in triplicate, from each scaffold and transferred to a 96 well-plate. A spectrofluorometer (BioTek ELx800, Agilent BioTek, Santa Clara, CA, USA) was used to read the fluorescence of each well at an excitation wavelength of 540 nm and an emission wavelength of 630 nm. The working solution was removed from the scaffolds and each scaffold was further washed with PBS twice before adding fresh cell culture media and continuing incubation. The assay was performed at day 1 and repeated at day 3 and 7.

3.11. CAM Assay

The *ex ovo* chick chorioallantoic membrane (CAM) assay as described by Ramos-Rodriquez et al. [33] was used to study potential toxic effects of the samples within a developing vascular system. Briefly, pathogen-free fertilised eggs (Gallus domesticus), obtained from Henry Stewart & Co. (Fakenham, UK), were cleaned with 20% *v/v* industrial methylated spirits (IMS) and incubated in a humidified hatching incubator (Rcom King Suro Max-20, P&T Poultry, Powys, Wales, UK) at 38 °C for 3 days. On day 3, the eggs were cracked into sterile 100 mL weighing boats with 3 mL of PBS + 1% *v/v* penicillin–streptomycin solution (100 IU/mL–100 mg/mL). The eggs were further incubated at 38 °C in a humidified cell culture incubator (Binder, Tuttlingen, Germany). On day 7, the sterilised 200 μm sectioned polyHIPE discs were implanted within the boundaries of the CAM and incubated for a further 5 days. On day 11, the CAM was imaged using a digital camera and MicroCapture software (version 2.0). Moisturising cream (Lacura, Atherstone, UK) was injected into the surrounding area of the sample to provide contrast between blood vessels and the sample. The vascular density of the CAM was further analysed from the images using the vessel analysis ImageJ plugin. Following imaging, all embryos were sacrificed by the end of day 11 of embryonic development. All embryos were incubated and handled under the guidelines of the Home Office, UK.

3.12. Statistical Analysis

Statistical analysis was carried out using analysis software GraphPad Prism (Version 9.4.1, San Diego, CA, USA). All data was analysed using one-way or two-way analysis of variance (ANOVA) followed by Games–Howell ($n > 50$) and Dunnett T3 ($n < 50$) multiple

comparisons tests. Error bars on graphs indicate standard deviation and all *n* values are given in figure captions where relevant.

4. Results

4.1. Manufacturing and Assessment of PCL–M polyHIPEs Porosity

The ratio of the volume of the internal phase (water) to the total volume (water and polymer) results in a polyHIPE scaffold with an internal phase volume of 83%. The porosity of the PCL–M polyHIPEs is greatly affected by the mixing speed used during the manufacturing of the emulsion. The mean diameter of pores (D) within the polyHIPE significantly decreases from 55 ± 22 μm at 200 rpm to 29 ± 10 μm at 400 rpm (Figure 2A). Following a similar trend, there is a further significant decrease in the mean pore diameter from 400 rpm to 9 ± 3 μm at 600 rpm. Following 600 rpm, any increase in mixing speed does not result in a significant decrease in pore size. However, the structure of the pores is affected, with the morphology of the pores becoming distorted and disorganised. Similarly, the window size within the polyHIPEs decreases with increasing mixing speed, with a significant decrease in mean window diameter (d) from 200 rpm to 400 rpm to 600 rpm (11 ± 5 μm, 6 ± 3 μm, and 2 ± 1 μm, respectively) (Figure 2B). The literature describes the fact that pore sizes >10 μm are required for cell attachment and infiltration [41]. Thus, further analysis of pores was limited to scaffolds fabricated at 200 and 400 rpm.
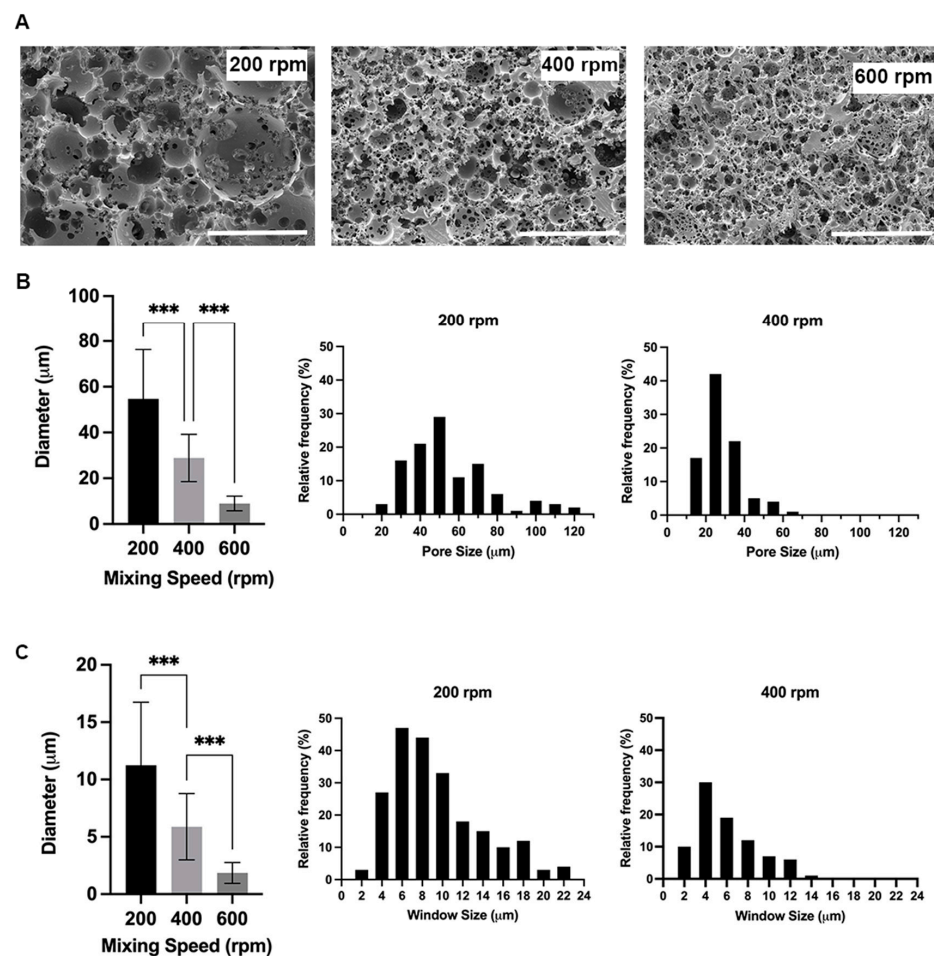
Figure 2. PCL–M polyHIPEs fabricated using different mixing speeds. (**A**) SEM images demonstrating the changes in polyHIPE pore size and morphology due to varying mixing speed (scalebar represents 100 μm). The addition of the internal phase to the external phase affects (**B**) the pore and (**C**) window size (mean +SD, *n* = 72 and 82, respectively, *** *p* < 0.001), and the relative frequency and distribution of pore and window sizes.

High variability is observed in pore and window size in scaffolds when mixing at 200 and 400 rpm. Whilst the average pore sizes are measured at 55 ± 22 μm and 29 ± 10 μm at 200 and 400 rpm, respectively, the pores range from 22–117 μm and 12–63 μm, respectively (Figure 2B). Furthermore, the interconnections between pores averages 11 ± 5 μm and 6 ± 3 μm; however, they range from 3–26 μm and 2–14 μm for 200 and 400 rpm, respectively (Figure 2A,B). The degree of interconnectivity (d/D) is not affected by changing the mixing speed and remains at 0.2.

4.2. Mechanical Characterisation of PCL–M polyHIPEs

Tensile tests were conducted on PCL–M polyHIPE under both washed and unwashed conditions and on bulk PCL–M. The stiffness is measured at 0.03 ± 0.01 MPa, 2.38 ± 0.66 MPa, and 7.07 ± 1.09 MPa for unwashed PCL–M polyHIPE, washed PCL–M polyHIPE, and bulk PCL–M, respectively (Figure 3A). The ultimate tensile strength increases from the unwashed to washed polyHIPE scaffold and then further increases for bulk PCL–M, measuring 0.04 ± 0.02 MPa, 0.25 ± 0.05 MPa, and 1.88 ± 0.51 MPa, respectively (Figure 3B). The maximum elongation of the scaffolds decreases significantly from unwashed to washed polyHIPE ($107 \pm 24\%$ and $39 \pm 11\%$, respectively) (Figure 3C). However, there is no significant change in maximum elongation observed between washed polyHIPE scaffolds and bulk PCL–M ($39 \pm 11\%$ and $42 \pm 14\%$, respectively). Therefore, the washing process of the PCL–M polyHIPE scaffolds has a significant effect on the mechanical properties of the material.

4.3. Effect of Washing

The polyHIPE scaffold must undergo post-processing washing cycles to remove remaining solvent, surfactant, and initiator before they are further utilised for cell culture. The washing cycle is observed to affect the size of the scaffolds, resulting in a significant decrease in scaffold diameter from 8.0 mm to 6.5 mm (Figure 4A). A 20% decrease is measured in both scaffold diameter and length, demonstrating that the effect of washing on the polyHIPE scaffolds is isotropic (Figure 4B). The compressive stiffness of the unwashed samples was unable to be quantified as the value was under the detection limit for a 25 N strain gauge. However, a significant increase in stiffness post-washing is clearly observed using calibrated weights (Figure 4C).

4.4. Surface Wettability of PCL–M polyHIPE

The surfaces of both washed PCL–M polyHIPEs and bulk PCL–M were functionalised using air plasma and acrylic acid (AAc) plasma treatment. Under all conditions (control, air, and AAc plasma treatment), bulk PCL–M is more hydrophilic than the comparative PCL–M polyHIPE scaffolds. There is a decrease in contact angle from polyHIPE to bulk PCL–M of 53°, 51°, and 37° across the three conditions; control, air, and AAc plasma treatment, respectively (Figure 5A). Both air and AAc plasma treatment result in a significant decrease in surface contact angle for PCL–M polyHIPEs (Figure 5B), with air plasma treatment yielding the most effective reduction in surface contact angle for both PCL–M polyHIPEs and bulk PCL–M from $124° \pm 6°$ and $71° \pm 4°$ to $99° \pm 6°$ and $48° \pm 7°$, respectively.

4.5. Surface Functionalisation of PCL–M Scaffolds

The polyHIPE scaffolds were also analysed via X-ray photoelectron spectroscopy (XPS). The survey scan reveals 24 at% oxygen and 76 at% carbon for the four-arm caprolactone methacrylate, close to the theoretically expected ratio of 25/75 at%. Air plasma coating introduces a small amount of nitrogen on the surface (~1%), while the carbon to oxygen ratio remains mainly unchanged for both air and acrylic acid coating. Importantly, all fibronectin-coated samples exhibit an increased amount of nitrogen on the surface, from 3.25 at% nitrogen for a non-plasma-coated PCL–M surface, to 5.32 at% for an air-plasma-treated surface and 6.33 at% for an acrylic-acid-plasma-treated surface. This indicates that the protein coating present on all fibronectin-coated surfaces has an affect while acrylic acid

and air plasma increase protein attachment. A high-resolution scan of the carbon 1s region reveals a change in surface functional groups depending on the treatments highlighted in Table 1. Combining the information from the survey and high-resolution scans reveals the following notable trends; (i) both air and acrylic acid treatment increase the amount of hydroxyl and carboxyl surface moieties, while (ii) both amine and amide moieties are observed when coating with fibronectin.
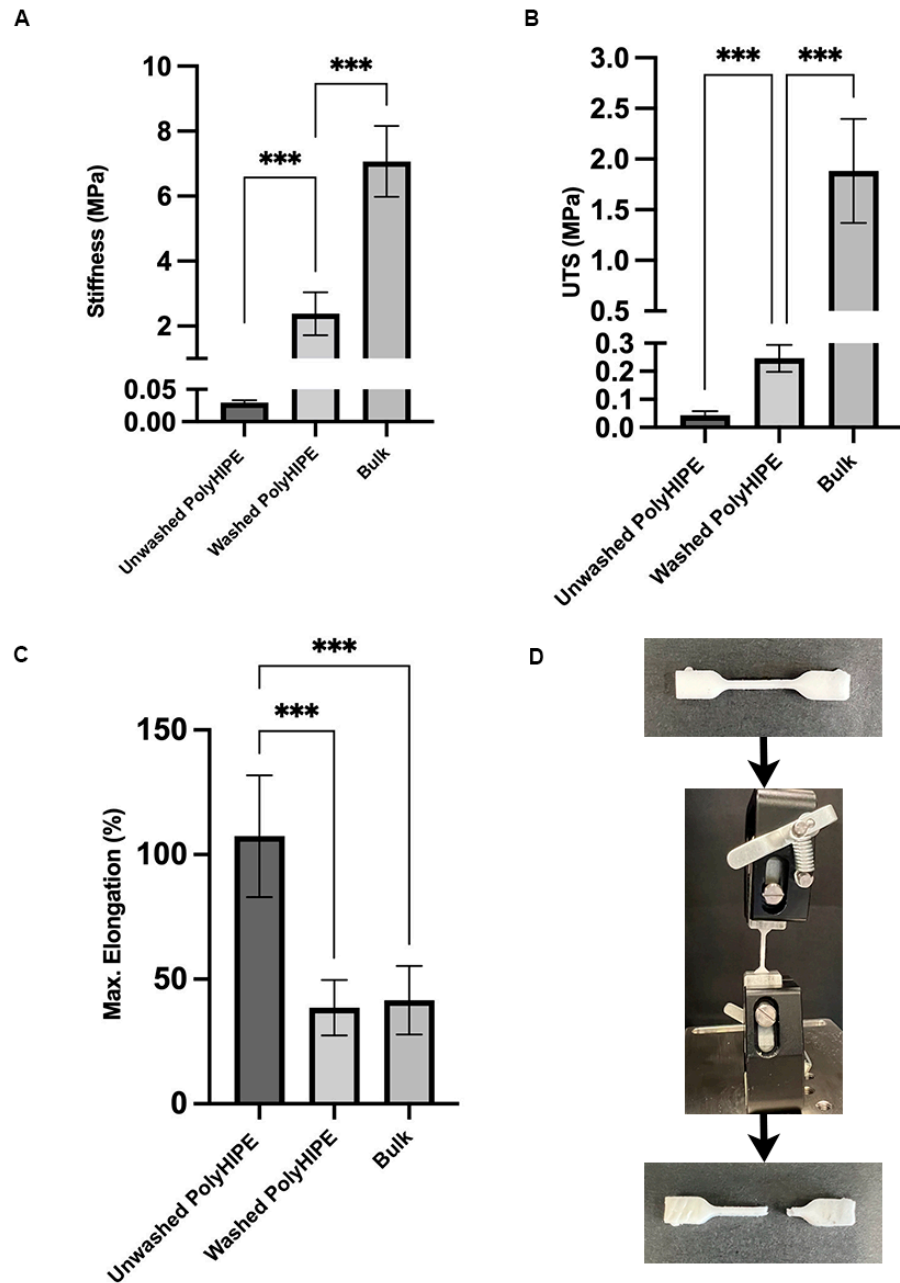

Figure 3. Mechanical properties of PCL–M polyHIPEs under two conditions (washed and unwashed) and bulk PCL–M. (**A**) Stiffness, (**B**) ultimate tensile strength (UTS), and (**C**) maximum elongation of the polyHIPE and bulk scaffolds (mean +SD, N = 3, *n* = 5, *** *p* < 0.001). (**D**) A polyHIPE sample before and after tensile testing, demonstrating the common region of failure when the material broke.
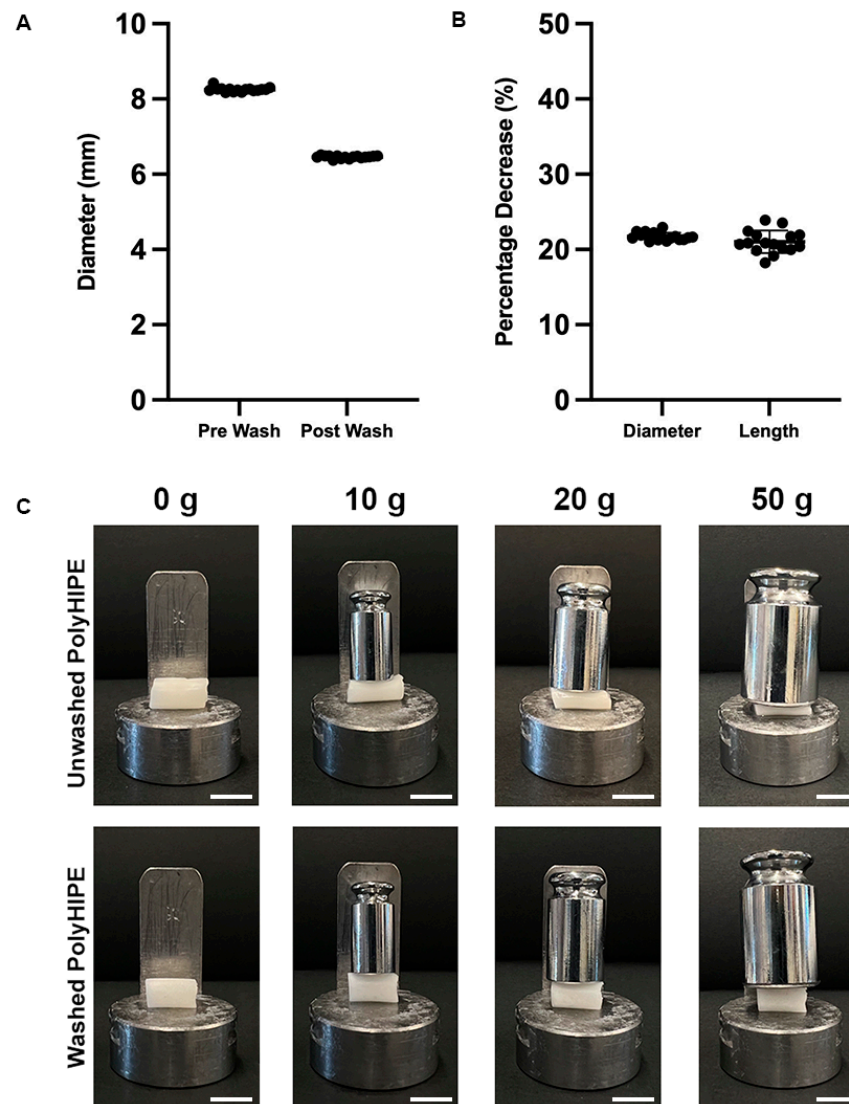
Figure 4. The effects of the post-processing washing cycles on PCL–M polyHIPEs, (**A**) the decrease in diameter and (**B**) the percentage decrease in diameter and length of cylindrical scaffolds (*n* = 16, black dots represent data points). (**C**) The significant changes in stiffness of PCL–M polyHIPEs following post-processing washing cycles could be visually observed when loads ranging from 0–50 g were applied (scale bar = 1 cm).

Table 1. High-resolution XPS scan data for the different surface treatments, (i) untreated, (ii) air-plasma-treated, (iii) acrylic-acid-plasma-coated, (iv) fibronectin-coated, (v) air-plasma-treated and fibronectin-coated, and (vi) acrylic-acid-plasma-coated and fibronectin-coated.

C1s	C-C/C-H at% (285 eV)	C-O/C-N at% (286.2 eV)	(C,N)-C=O at% (288.2 eV)	HO-C=O at% (288.9 eV)
Untreated	67.6 ± 0.1	19.1 ± 0.3	2.1 ± 0.2	11.3 ± 0.1
Air plasma	62.8 ± 3.0	22.4 ± 2.4	1.8 ± 0.4	13.1 ± 1.0
AAc plasma	56.3 ± 1.7	28.0 ± 2.0	1.2 ± 0.1	14.6 ± 0.2
Untreated and fibronectin	61.4 ± 0.3	23.6 ± 0.3	4.1 ± 0.2	10.9 ± 0.9
Air plasma and fibronectin	52.7 ± 2.6	29.3 ± 2.7	6.1 ± 0.1	11.8 ± 0.1
AAc plasma and fibronectin	55.6 ± 0.4	28.7 ± 0.3	6.2 ± 0.6	9.6 ± 0.5
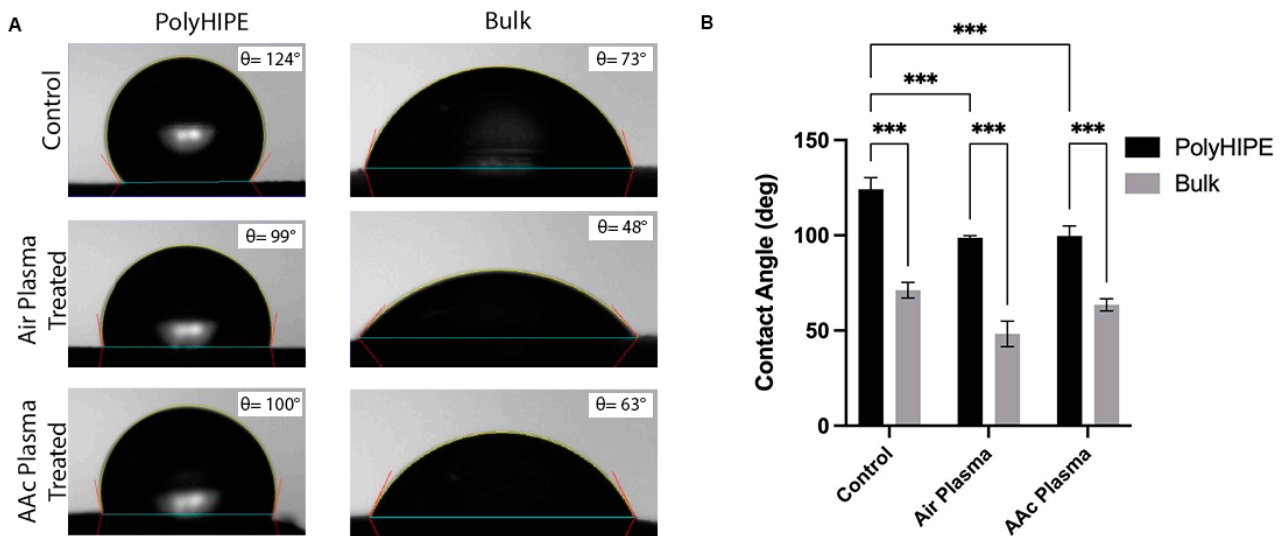
Figure 5. (**A**) The effect of air and acrylic acid plasma treatment on the contact angle of polyHIPE and bulk PCL–M surfaces. (**B**) The mean $\pm$ SD of the effect air and AAc plasma treatment on the wettability of polyHIPE and bulk PCL–M ($n = 3$, *** $p < 0.001$).

4.6. Interaction of PCL–M polyHIPEs with a Vascular Network Using an Ex Ovo CAM Assay

The CAM assay is an established *ex ovo* model able to assess the initial interactions of a biomaterial within a well-established vascularised tissue [33,42–44]. The assay investigated the biocompatibility of PCL–M polyHIPEs with and without surface functionalisation via air and AAc plasma treatment (Figure 6A). There is no significant change in vessel density surrounding the polyHIPE scaffolds (Figure 6B).
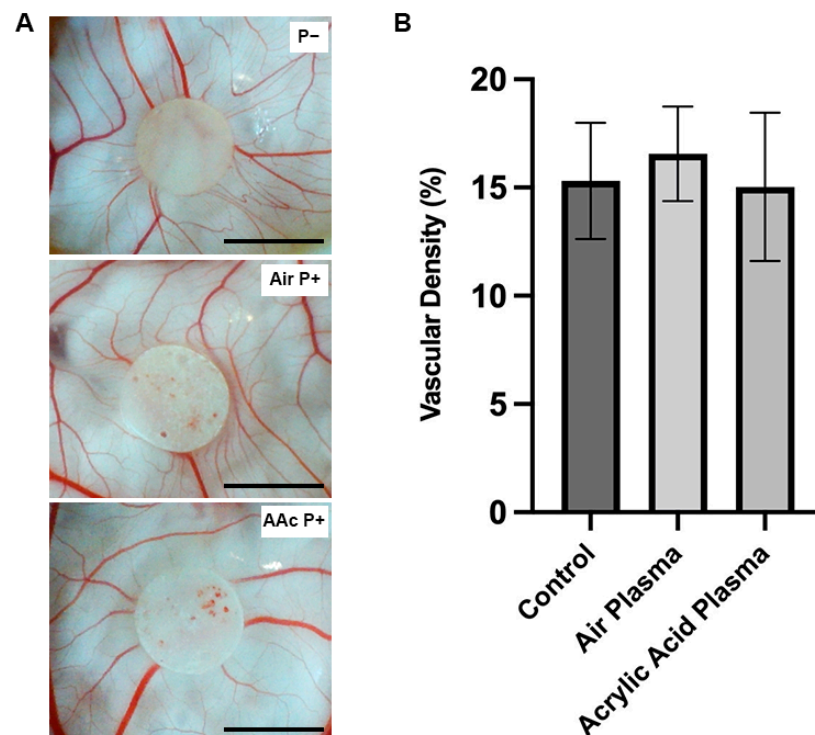
Figure 6. Assessment of PCL–M polyHIPE biocompatibility. (**A**) Images of PCL–M polyHIPEs functionalised with air and acrylic acid plasma treatment on chorioallantoic membrane (CAM) at day 11 (scale bar represents 5 mm). (**B**) The vascular density of the vessels surrounding the polyHIPE scaffolds ($n = 5$).

4.7. Activity and Interaction of MDA-MB-231 Cells on PCL–M Scaffolds

A seven-day study using Resazurin reduction was used to determine the metabolic activity and cell proliferation on PCL–M scaffolds. PCL–M scaffolds under three different plasma treatment conditions were analysed. The results show a consistently significant increase in metabolic activity between the control and three treatment conditions through days 1, 3, and 7 (Figure 7A). There is a significant difference at day 1 between untreated scaffolds (P−) and the air-plasma-treated scaffolds (air P+). At all other time points and between all conditions, P−, air P+, and acrylic acid plasma treatment (AAc P+), there is no significant difference between metabolic activity. However, air P+ and AAc P+ scaffolds show slightly increased metabolic activity at day 1 and 3 compared to P− scaffolds. Also, via comparison to the 2D control at the day 1 timepoint of the resazurin reduction assay, the adhesion of MDA-MB-231 cells can be approximated. Following seeding, approximately 50% of cells adhere to P− scaffolds and 68% adhere to air and AAc P+.
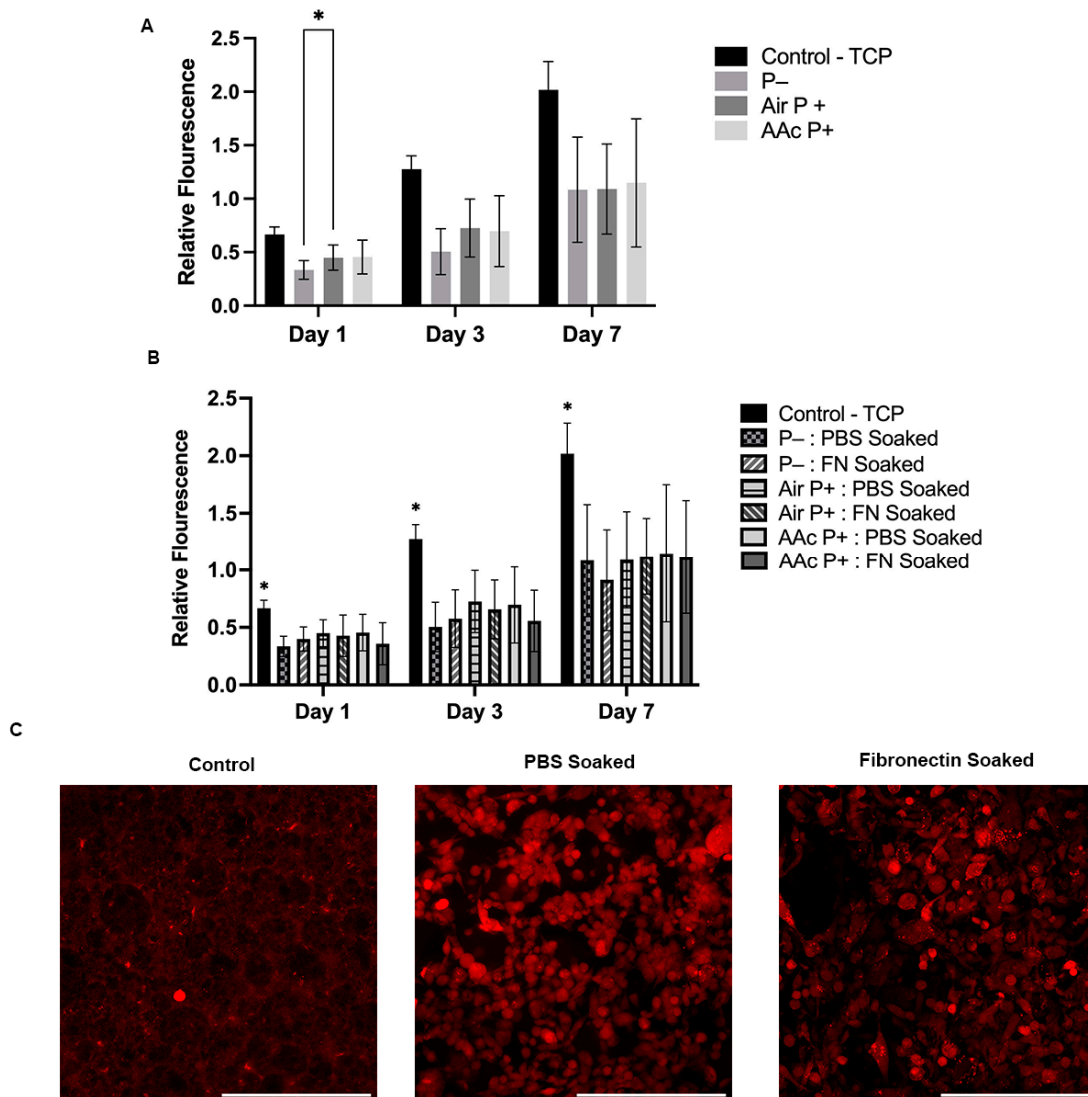
Figure 7. Biological assessment of PCL–M polyHIPEs. The metabolic activity of MDA-MB-231 cells via a resazurin reduction assay across 7 days on (**A**) untreated PCL–M scaffolds (P−) or scaffolds functionalised with air and acrylic acid (AAc) plasma treatment (P+) and (**B**) preconditioned with fibronectin (N = 3, *n* = 5, * *p* < 0.033). (**C**) Confocal images of MDA-MB-231 cells transduced with mStrawberry following 7 days cultured on PCL–M scaffolds pre-soaked in PBS or fibronectin (scalebar represents 200 µm).

Furthermore, the effect on metabolic activity and cellular interaction by coating the surfaces with fibronectin was investigated. A seven-day resazurin reduction assay measures no significant difference between the fibronectin-soaked scaffolds and the control PBS-soaked scaffolds through all plasma treatment conditions (Figure 7B). At day 7, the samples were fixed and further analysed via confocal. As shown in the images, there is little difference in the presence and morphology of MDA-MD-231 cells observed on scaffolds that are soaked in fibronectin compared to scaffolds that are PBS soaked (Figure 7C). Low background autofluorescence is observed on the control cell-free scaffold, with a small number of brighter auto-fluorescent artefacts.

5. Discussion

An open porous interconnected architecture is vitally important within scaffolds for tissue engineering applications. Interconnections through pores provide transport channels for cell migration, mass transport of cell nutrients and waste, and support cell signalling [45,46]. Open-surface porosity is also important for cell ingrowth, which is affected by the surface of the polyHIPE when it is in contact during photopolymerisation. Contact with a mould can cause a reduction in open porous morphology at the interfaces of the emulsion and the moulds [32]. Therefore, to utilise the inner open, interconnected porous morphology of the polyHIPE structure, it was decided to section bulk cylinders of polyHIPE, as described in Section 3.3.

When investigating the effect of mixing speed on polyHIPE structure, a reciprocal relationship is observed, as the mixing speed increases the pore sizes, and window sizes decrease (Figure 2A,B), in line with previous studies [26,27,47–49]. These findings demonstrate the ability to easily tune the internal structure of polyHIPEs via simple manufacturing adjustments. A high variability in both pore and window size is observed in the PCL–M polyHIPE scaffolds when 200 and 400 rpm mixing speeds are used as the internal phase (water) is added (Figure 2B).

A dynamic range in pore size is beneficial as it can provide multiple elements necessary to form a functioning biomimetic scaffold. It has been reported that micro-pores (100 nm–5 μm) enable cell attachment, medium-size pores (5–250 μm) enable cell infiltration, whilst macro-pores (>250 μm) support neo-vascularisation and, thus, scaffold vascularisation [46,50,51]. The larger interconnections provide micro-features and further support cell infiltration and transport of nutrients and waste through the scaffold. Smaller interconnections provide nano-features, with Smith et al. [46] reporting enhanced cell attachment and ECM formation within scaffolds.

Moreover, Bružauskaitė et al. [52] demonstrate that smaller pores are required for smaller cell types (e.g., fibroblasts) to enhance cell attachment by reducing unwanted cell migration. In addition, large pore sizes can reduce intracellular signalling [53], further demonstrating the importance of being able to tune the porosity of a chosen scaffold to the required application.

As described by Poltavets et al. [54], it has been identified that cancer cell behaviour is driven by biomechanical signals of the tumour microenvironment. Within breast cancer tissue, the presence of organised collagen fibres results in an increase in tissue stiffness compared to surrounding tissue, enhancing tumour progression and metastasis [55,56]. The Young's modulus of the material is measured at 2.38 MPa, resulting in stiff scaffolds that are easily handled. The scaffolds provide an environment in which cells can lay down ECM with a stiffness suitable for the specific cell type. To enhance this process, the scaffolds could be combined with a hydrogel substrate within the structure, to provide a predefined ECM surrounding the cells [57].

Surprisingly, the stiffness of the washed PCL–M polyHIPE, which has an internal phase volume of 83%, is only three-fold less than bulk PCL–M, demonstrating the advantageous characteristics of using a high-molecular-weight PCL–M polyHIPE structure, achieving relatively high stiffness with high-internal-phase volumes. On the other hand, the ultimate tensile strength (UTS) of the polyHIPE scaffold compared to the bulk material decreases

nearly eight-fold from bulk to washed polyHIPE scaffolds. Interestingly, the structure of the polyHIPE has no significant effect on the maximum elongation of the scaffolds when compared to the bulk material.

During the post-processing of the polyHIPEs, methanol and water washing cycles were used. These washing stages are important to remove remaining surfactant, photoinitiator, and solvent from the scaffold. Interestingly, during the process it is observed that the post-processing affects the structural and mechanical properties of the scaffolds (Figure 4C). Before washing, the scaffolds show higher elasticity, while scaffold stiffness is lacking. Post-washing, the maximum elongation halves but there is an 80-fold increase in stiffness. In addition, isotropic shrinking of the scaffold by 20% is observed. Through the washing process, this change in stiffness and size is most noticeable following the water wash cycle compared to the methanol wash cycle. Thus, it is deduced that the change in properties occurs due to the removal of excess solvent within the scaffold, which act as a plasticiser of the produced thermoset polymer construct. This finding corresponds well with the findings of Dikici et al. [42]. The study used ethanol to expand a PCL polyHIPE tube. After insertion of an electrospun layer, a PBS wash was used to remove excess solvent, resulting in shrinkage of the polyHIPE tube. This also indicates that the mechanical properties can be used as a simple test for the efficiency of solvent removal.

In previous studies, the significant impact of dry and wet conditions on the mechanical properties of polymer scaffolds was reported, demonstrating a significant decrease in stiffness, maximum elongation, and UTS from dry to wet conditions [32,58,59]. As tissue-engineered constructs and models are commonly used within fluidic systems to recapitulate *in vivo* conditions, tensile tests were conducted using wet polyHIPE samples in this study.

One of the most significant disadvantages of using PCL in tissue engineering constructs is its hydrophobicity. The degree of hydrophobicity is observed to significantly increase from bulk to polyHIPE PCL–M (Figure 5). These findings correspond to the Wenzel model, which describes how surface roughness enhances hydrophobicity characteristics due to the chemistry of the surface [60]. Thus, if a material is hydrophobic, surface roughness enhances the degree of hydrophobicity further. The micropores within the surface of the polyHIPE discs increase the surface roughness, therefore, enhancing the degree of hydrophobicity of the surface compared to bulk PCL–M.

Many studies functionalise the surface of materials using a range of plasma treatments to produce more hydrophilic surfaces. Far et al. highlighted an increase in hydroxyl moieties on polyglycerol sebacate (PGS) surfaces after air plasma treatment, which was correlated with a reduction in water contact angle [61]. The results from this study concur with these findings, identifying significant reductions in surface contact angle when treating the PCL–M polyHIPE with air or acrylic acid plasma. Furthermore, plasma polymerisation of a surface is a common technique used to produce biomaterials with chemically reactive surfaces, which improve cell proliferation, and interacts and permanently binds with biologically active molecules [62,63]. Depending on the specific plasma treatment utilised, high concentrations of specific functional groups are deposited on the surface of the substrate [61,64]. Different functional groups interact differently with biological molecules and cells. For example, Cools et al. [65] observed a positive effect on the generation of glycosaminoglycans matrix when plasma coating via helium and acrylic acid; however, acrylic acid plasma treatment further stimulated cell migration through scaffolds.

Air and acrylic acid plasma treatments lead to the formation of hydroxyl and carboxyl functional groups, respectively, on the surface of the treated material [64], which is also confirmed by the high-resolution XPS results (Table 1). Plasma treatment clearly decreases the amount of aliphatic carbon (R/H-C) and increases the amount of oxidised carbon moieties (C-OR and COOH) at the surface. Functionalisation via the formation of hydroxyl and carboxylic groups are two of the most common methods used within biomedical applications [66,67]. Thus, the effect of air and acrylic acid plasma treatments on cell and biological molecule (fibronectin) interaction was investigated. The high-resolution XPS scan reveals there is an increase of up to 5 at% of the 288.2 eV peak, which can be attributed

to the amide carbon, and is a clear indication of protein binding. Surprisingly, there is no significant difference in cell metabolic activity when pre-soaking the scaffolds in fibronectin compared to PBS. In addition, there is no significant difference in cell metabolic activity between the air- and acrylic-acid-treated scaffolds, and the control, non-treated scaffolds. However, similar findings with air plasma treatment were published by Aldemir Dikici et al. [32] for PCL polyHIPE scaffolds.

Furthermore, there is little difference in the cell morphology on the surface of scaffolds when pre-soaked with PBS compared to the same scaffolds pre-soaked with fibronectin (Figure 7C). Overall, the metabolic activity of the cells on the scaffolds increases approximately three-fold in 7 days, indicating that PCL–M polyHIPE scaffolds are viable options for cell growth and proliferation. Rabionet et al. [68] observed similar findings when culturing MDA-MB-231 cells on electrospun PCL scaffolds, additionally presenting improved metabolic activity on electrospun scaffolds when increasing the pore area from 0.24 μm^2 to 0.84 μm^2. Furthermore, fibronectin-soaking and/or plasma-treating the scaffolds did does yield any further improvement in cell adhesion or proliferation compared to untreated PCL–M polyHIPE scaffolds.

The CAM assay is an established *ex ovo* model used within many studies to determine cell infiltration and material capability to support vascularization. In addition, the CAM assay has been documented as a tool to investigate material biocompatibility [69,70], with Ribatti et al. [71] describing the CAM assay as an integral part of biocompatibility testing process for the development of biomaterials. Mangir et al. [44] reported that average embryo survival rates for intermediate users is 68%. In this study, the embryo survival rate is 69%, demonstrating the material does not have an adverse effect on embryo survival. In conjunction with the resazurin reduction assay, demonstrating increasing cell metabolic activity across 7 days, PCL–M polyHIPEs can be classed as biocompatible. Furthermore, the consistency in vessel density surrounding the polyHIPE scaffolds demonstrates that PCL–M scaffolds are bioinert regardless of surface functionalisation via air and acrylic acid plasma treatment. Importantly, surface functionalisation via air and AAc plasma treatment does not adversely affect scaffold biocompatibility, while not greatly enhancing the vessel or cell growth either, identifying that this processing step could be omitted for these PCL-based polyHIPE scaffolds.

Whilst the current model uses a porous scaffold to increase the diffusional mass transfer limit and enhance cell attachment, advancements in the model could include vascularisation of a polyHIPE scaffold by co-culturing with endothelial cells [42] within an active perfusion system, as previously successfully demonstrated [72]. Pore sizes around 250 μm have been reported to be suitable for vascularisation [73]. However, there are a number of studies that report successful vascular invasion within smaller pore sizes. Chiu et al. [74] demonstrated no significant difference in vascular invasion after 3 weeks into the bulk of scaffolds with pore sizes ranging from 100–150 μm and 50–100 μm. Moreover, Artel et al. [75] show that vascularisation to the centre of a porous polymer scaffold can occur through pores ranging 40–270 μm in diameter, however, the time for vascularisation to the centre increases as average pore diameter decreases. Thus, these findings would suggest both the PCL–M polyHIPEs manufactured with mixing speeds of 200 and 400 rpm could be suitable candidates for future *in vitro* vascularisation models.

6. Conclusions

In this study, we fabricated a polyHIPE scaffold using photocurable high-molecular-weight four-arm PCL–M. By altering the mixing speed during emulsion fabrication, we demonstrate that the structural properties of the resulting polyHIPE can be tuned for a specific application and cell type. Lower mixing speeds (200 and 400 rpm) produce scaffolds with larger pores and interconnections, which are a more suitable environment for cell adhesion, infiltration, and vascularisation. Interestingly, whilst the polyHIPE structure provides a high-internal-phase volume, the mechanical properties are relatively comparable to bulk PCL–M. Surface functionalisation of the polyHIPEs via plasma treatment and fibronectin

adsorption shows little improvement in cell adhesion and morphology. Furthermore, this study demonstrates the biocompatibility and bioinert properties of PCL–M polyHIPEs regardless of surface modifications via fibronectin adsorption and/or air and acrylic acid plasma treatment. In conclusion, we demonstrate that high-molecular-weight PCL–M polyHIPE is a good candidate for TE scaffolds with potential for vascularisation and active perfusion.

References

1. Brown, L.M.; Hebert, K.L.; Gurrala, R.R.; Byrne, C.E.; Burow, M.; Martin, E.C.; Lau, F.H. Modeling Breast Cancer in Human Breast Tissue using a Microphysiological System. *J. Vis. Exp.* **2021**, *2021*, e62009.
2. Siegel, R.L.; Miller, K.D.; Fuchs, H.E.; Jemal, A. Cancer statistics, 2022. *CA Cancer J. Clin.* **2022**, *72*, 7–33. [CrossRef]
3. Welsh, J.E. Animal Models for Studying Prevention and Treatment of Breast Cancer. In *Animal Models for the Study of Human Disease*; Academic Press: Cambridge, MA, USA, 2013; pp. 997–1018. ISBN 9780124158948.
4. Wolf, K.; Friedl, P. Mapping proteolytic cancer cell-extracellular matrix interfaces. *Clin. Exp. Metastasis* **2009**, *26*, 289–298. [CrossRef]
5. Bersini, S.; Jeon, J.S.; Moretti, M.; Kamm, R.D. In vitro models of the metastatic cascade: From local invasion to extravasation. *Drug Discov. Today* **2014**, *19*, 735–742. [CrossRef]
6. Rijal, G.; Bathula, C.; Li, W. Application of Synthetic Polymeric Scaffolds in Breast Cancer 3D Tissue Cultures and Animal Tumor Models. *Int. J. Biomater.* **2017**, *2017*, 8074890. [CrossRef]
7. Knight, E.; Murray, B.; Carnachan, R.; Przyborski, S. Alvetex®: Polystyrene Scaffold Technology for Routine Three Dimensional Cell Culture. In *Methods in Molecular Biology*; Clifton, N.J., Ed.; Humana Press: Totowa, NJ, USA, 2011; Volume 695, pp. 323–340.
8. Hutmacher, D.W. Scaffold design and fabrication technologies for engineering tissues–State of the art and future perspectives. *J. Biomater. Sci. Polym. Ed.* **2001**, *12*, 107–124. [CrossRef]
9. Bokhari, M.; Carnachan, R.J.; Przyborski, S.A.; Cameron, N.R. Emulsion-templated porous polymers as scaffolds for three dimensional cell culture: Effect of synthesis parameters on scaffold formation and homogeneity. *J. Mater. Chem.* **2007**, *17*, 4088–4094. [CrossRef]
10. Bokhari, M.; Carnachan, R.J.; Cameron, N.R.; Przyborski, S.A. Novel cell culture device enabling three-dimensional cell growth and improved cell function. *Biochem. Biophys. Res. Commun.* **2007**, *354*, 1095–1100. [CrossRef]
11. Hayman, M.W.; Smith, K.H.; Cameron, N.R.; Przyborski, S.A. Growth of human stem cell-derived neurons on solid three-dimensional polymers. *J. Biochem. Biophys. Methods* **2005**, *62*, 231–240. [CrossRef] [PubMed]
12. Chan, B.P.; Leong, K.W. Scaffolding in tissue engineering: General approaches and tissue-specific considerations. *Eur. Spine J.* **2008**, *17*, 479. [CrossRef]
13. Lu, P.; Weaver, V.M.; Werb, Z. The extracellular matrix: A dynamic niche in cancer progression. *J. Cell Biol.* **2012**, *196*, 395–406. [CrossRef]
14. Egeblad, M.; Rasch, M.G.; Weaver, V.M. Dynamic interplay between the collagen scaffold and tumor evolution. *Curr. Opin. Cell Biol.* **2010**, *22*, 697–706. [CrossRef]
15. Dong, C.; Lv, Y. Application of collagen scaffold in tissue engineering: Recent advances and new perspectives. *Polymer* **2016**, *8*, 42. [CrossRef] [PubMed]

16. Khan, Y.; Yaszemski, M.J.; Mikos, A.G.; Laurencin, C.T. Tissue Engineering of Bone: Material and Matrix Considerations. *J. Bone Jt. Surg.-Am. Vol.* **2008**, *90*, 36–42. [CrossRef] [PubMed]

17. Abdulghani, S.; Mitchell, G.R. Biomaterials for in situ tissue regeneration: A review. *Biomolecules* **2019**, *9*, 750. [CrossRef] [PubMed]

18. Hsu, S.H.; Hung, K.C.; Chen, C.W. Biodegradable polymer scaffolds. *J. Mater. Chem. B* **2016**, *4*, 7493–7505. [CrossRef]

19. Loh, Q.L.; Choong, C. Three-Dimensional Scaffolds for Tissue Engineering Applications: Role of Porosity and Pore Size. *Tissue Eng. Part B Rev.* **2013**, *19*, 485. [CrossRef]

20. Eltom, A.; Zhong, G.; Muhammad, A. Scaffold Techniques and Designs in Tissue Engineering Functions and Purposes: A Review. *Adv. Mater. Sci. Eng.* **2019**, *2019*, 3429527. [CrossRef]

21. Hutmacher, D.W.; Woodfield, T.B.F.; Dalton, P.D. Scaffold Design and Fabrication. In *Tissue Engineering*; Elsevier: Amsterdam, The Netherlands, 2014; pp. 311–346. ISBN 9780124201453.

22. Zhao, P.; Gu, H.; Mi, H.; Rao, C.; Fu, J.; Turng, L.-S. Fabrication of scaffolds in tissue engineering: A review. *Front. Mech. Eng.* **2018**, *13*, 107–119. [CrossRef]

23. Aldemir Dikici, B.; Sherborne, C.; Reilly, G.C.; Claeyssens, F. Emulsion templated scaffolds manufactured from photocurable polycaprolactone. *Polymer* **2019**, *175*, 243–254. [CrossRef]

24. Cameron, N.R. High internal phase emulsion templating as a route to well-defined porous polymers. *Polymer* **2005**, *46*, 1439–1449. [CrossRef]

25. Silverstein, M.S. PolyHIPEs: Recent advances in emulsion-templated porous polymers. *Prog. Polym. Sci.* **2014**, *39*, 199–234. [CrossRef]

26. Aldemir Dikici, B.; Claeyssens, F. Basic Principles of Emulsion Templating and Its Use as an Emerging Manufacturing Method of Tissue Engineering Scaffolds. *Front. Bioeng. Biotechnol.* **2020**, *8*, 875. [CrossRef] [PubMed]

27. Moglia, R.S.; Holm, J.L.; Sears, N.A.; Wilson, C.J.; Harrison, D.M.; Cosgriff-Hernandez, E. Injectable PolyHIPEs as High Porosity Bone Grafts. *Biomacromolecules* **2011**, *12*, 3621. [CrossRef]

28. Busby, W.; Cameron, N.R.; Jahoda, C.A.B. Emulsion-Derived Foams (PolyHIPEs) Containing Poly(E-caprolactone) as Matrixes for Tissue Engineering. *Biomacromolecules* **2001**, *2*, 154–164. [CrossRef]

29. Woodruff, M.A.; Hutmacher, D.W. The return of a forgotten polymer–Polycaprolactone in the 21st century. *Prog. Polym. Sci.* **2010**, *35*, 1217–1256. [CrossRef]

30. Brannigan, R.P.; Dove, A.P. Synthesis, properties and biomedical applications of hydrolytically degradable materials based on aliphatic polyesters and polycarbonates. *Biomater. Sci.* **2016**, *5*, 9–21. [CrossRef]

31. Diba, M.; Fathi, M.H.; Kharaziha, M. Novel forsterite/polycaprolactone nanocomposite scaffold for tissue engineering applications. *Mater. Lett.* **2011**, *65*, 1931–1934. [CrossRef]

32. Dikici, B.A.; Dikici, S.; Reilly, G.C.; MacNeil, S.; Claeyssens, F. A novel bilayer polycaprolactone membrane for guided bone regeneration: Combining electrospinning and emulsion templating. *Materials* **2019**, *12*, 2643. [CrossRef] [PubMed]

33. Ramos-rodriguez, D.H.; Macneil, S.; Claeyssens, F.; Asencio, I.O. Delivery of Bioactive Compounds to Improve Skin Cell Responses on Microfabricated Electrospun Microenvironments. *Bioengineering* **2021**, *8*, 105. [CrossRef]

34. Annabi, N.; Fathi, A.; Mithieux, S.M.; Martens, P.; Weiss, A.S.; Dehghani, F. The effect of elastin on chondrocyte adhesion and proliferation on poly (ε-caprolactone)/elastin composites. *Biomaterials* **2011**, *32*, 1517–1525. [CrossRef] [PubMed]

35. Gniesmer, S.; Brehm, R.; Hoffmann, A.; Cassan, D.; Menzel, H.; Hoheisel, A.; Glasmacher, B.; Willbold, E.; Reifenrath, J.; Wellmann, M.; et al. In vivo analysis of vascularization and biocompatibility of electrospun polycaprolactone fibre mats in the rat femur chamber. *J. Tissue Eng. Regen. Med.* **2019**, *13*, 1190–1202. [CrossRef] [PubMed]

36. Farr, N.T.H.; Klosterhalfen, B.; Noé, G.K. Characterization in respect to degradation of titanium-coated polypropylene surgical mesh explanted from humans. *J. Biomed. Mater. Res. B. Appl. Biomater.* **2023**, *111*, 1142–1152. [CrossRef]

37. Barbetta, A.; Cameron, N.R. Morphology and surface area of emulsion-derived (PolyHIPE) solid foams prepared with oil-phase soluble porogenic solvents: Span 80 as surfactant. *Macromolecules* **2004**, *37*, 3188–3201. [CrossRef]

38. Sigma Aldrich Authenticated MDA-MB-231 Cell Line. Available online: https://www.sigmaaldrich.com/GB/en/product/sigma/cb_92020424 (accessed on 12 August 2022).

39. English, W.R.; Lunt, S.J.; Fisher, M.; Lefley, D.V.; Dhingra, M.; Lee, Y.-C.; Bingham, K.; Hurrell, J.E.; Lyons, S.K.; Kanthou, C.; et al. Differential Expression of VEGFA Isoforms Regulates Metastasis and Response to Anti-VEGFA Therapy in Sarcoma. *Cancer Res.* **2017**, *77*, 2633–2646. [CrossRef]

40. Sandoval-Castellanos, A.M.; Claeyssens, F.; Haycock, J.W. Bioactive 3D Scaffolds for the Delivery of NGF and BDNF to Improve Nerve Regeneration. *Front. Mater.* **2021**, *8*, 466. [CrossRef]

41. Zhang, Y.; Ouyang, H.; Chwee, T.L.; Ramakrishna, S.; Huang, Z.M. Electrospinning of gelatin fibers and gelatin/PCL composite fibrous scaffolds. *J. Biomed. Mater. Res. Part B Appl. Biomater.* **2005**, *72*, 156–165. [CrossRef]

42. Dikici, S.; Aldemir Dikici, B.; Bhaloo, S.I.; Balcells, M.; Edelman, E.R.; MacNeil, S.; Reilly, G.C.; Sherborne, C.; Claeyssens, F. Assessment of the Angiogenic Potential of 2-Deoxy-D-Ribose Using a Novel in vitro 3D Dynamic Model in Comparison with Established in vitro Assays. *Front. Bioeng. Biotechnol.* **2020**, *7*, 20. [CrossRef]

43. Naik, M.; Brahma, P.; Dixit, M. A cost-effective and efficient chick ex-ovo cam assay protocol to assess angiogenesis. *Methods Protoc.* **2018**, *1*, 19. [CrossRef]

44. Mangir, N.; Dikici, S.; Claeyssens, F.; Macneil, S. Using ex Ovo Chick Chorioallantoic Membrane (CAM) Assay to Evaluate the Biocompatibility and Angiogenic Response to Biomaterials. *ACS Biomater. Sci. Eng.* **2019**, *5*, 3190–3200. [CrossRef]

45. Dhandayuthapani, B.; Yoshida, Y.; Maekawa, T.; Kumar, D.S. Polymeric scaffolds in tissue engineering application: A review. *Int. J. Polym. Sci.* **2011**, *2011*, 290602. [CrossRef]

46. Smith, I.O.; Liu, X.H.; Smith, L.A.; Ma, P.X. Nanostructured polymer scaffolds for tissue engineering and regenerative medicine. *Wiley Interdiscip. Rev. Nanomed. Nanobiotechnol.* **2009**, *1*, 226–236. [CrossRef] [PubMed]

47. Huš, S.; Krajnc, P. PolyHIPEs from Methyl methacrylate: Hierarchically structured microcellular polymers with exceptional mechanical properties. *Polymer* **2014**, *55*, 4420–4424. [CrossRef]

48. Paterson, T.E.; Gigliobianco, G.; Sherborne, C.; Green, N.H.; Dugan, J.M.; Macneil, S.; Reilly, G.C.; Claeyssens, F. *Porous microspheres* support mesenchymal progenitor cell ingrowth and stimulate angiogenesis. *APL Bioeng.* **2018**, *2*, 026103. [CrossRef] [PubMed]

49. Mravljak, R.; Bizjak, O.; Podlogar, M.; Podgornik, A. Effect of polyHIPE porosity on its hydrodynamic properties. *Polym. Test.* **2021**, *93*, 106590. [CrossRef]

50. Zhang, K.; Fan, Y.; Dunne, N.; Li, X. Effect of microporosity on scaffolds for bone tissue engineering. *Regen. Biomater.* **2018**, *5*, 115–124. [CrossRef] [PubMed]

51. Vagaská, B.; Bačáková, L.; Filová, E.; Balík, K. Osteogenic cells on bio-inspired materials for bone tissue engineering. *Physiol. Res.* **2010**, *59*, 309–322. [CrossRef]

52. Bružauskaitė, I.; Bironaitė, D.; Bagdonas, E.; Bernotienė, E. Scaffolds and cells for tissue regeneration: Different scaffold pore sizes—Different cell effects. *Cytotechnology* **2016**, *68*, 355–369. [CrossRef]

53. Mbundi, L.; González-Pérez, M.; González-Pérez, F.; Juanes-Gusano, D.; Rodríguez-Cabello, J.C. Trends in the Development of Tailored Elastin-Like Recombinamer–Based Porous Biomaterials for Soft and Hard Tissue Applications. *Front. Mater.* **2021**, *7*, 1–27. [CrossRef]

54. Poltavets, V.; Kochetkova, M.; Pitson, S.M.; Samuel, M.S. The role of the extracellular matrix and its molecular and cellular regulators in cancer cell plasticity. *Front. Oncol.* **2018**, *8*, 431. [CrossRef]

55. Northey, J.J.; Barrett, A.S.; Acerbi, I.; Hayward, M.K.; Talamantes, S.; Dean, I.S.; Mouw, J.K.; Ponik, S.M.; Lakins, J.N.; Huang, P.J.; et al. Stiff stroma increases breast cancer risk by inducing the oncogene ZNF217. *J. Clin. Investig.* **2020**, *130*, 5721–5737. [CrossRef] [PubMed]

56. Provenzano, P.P.; Eliceiri, K.W.; Campbell, J.M.; Inman, D.R.; White, J.G.; Keely, P.J. Collagen reorganization at the tumor-stromal interface facilitates local invasion. *BMC Med.* **2006**, *4*, 38. [CrossRef]

57. Katt, M.E.; Placone, A.L.; Wong, A.D.; Xu, Z.S.; Searson, P.C. In vitro tumor models: Advantages, disadvantages, variables, and selecting the right platform. *Front. Bioeng. Biotechnol.* **2016**, *4*, 12. [CrossRef] [PubMed]

58. Wu, L.; Zhang, J.; Jing, D.; Ding, J. "Wet-state" mechanical properties of three-dimensional polyester porous scaffolds. *J. Biomed. Mater. Res. Part A* **2006**, *76*, 264–271. [CrossRef]

59. Tran, T.T.; Hamid, Z.A.; Cheong, K.Y. A Review of Mechanical Properties of Scaffold in Tissue Engineering: Aloe Vera Composites. *J. Phys. Conf. Ser.* **2018**, *1082*, 012080. [CrossRef]

60. Kwok, Y.K. Wettability on Different Surfaces. In *21st Century Surface Science—A Handbook*; Pham, P., Goel, P., Kumar, S., Yadav, K., Eds.; IntechOpen: London, UK, 2020; ISBN 978-1-78985-200-4.

61. Farr, N.; Thanarak, J.; Schäfer, J.; Quade, A.; Claeyssens, F.; Green, N.; Rodenburg, C.; Farr, N.; Thanarak, J.; Claeyssens, F.; et al. Understanding Surface Modifications Induced via Argon Plasma Treatment through Secondary Electron Hyperspectral Imaging. *Adv. Sci.* **2021**, *8*, 2003762. [CrossRef]

62. Puleo, D.A.; Kissling, R.A.; Sheu, M.S. A technique to immobilize bioactive proteins, including bone morphogenetic protein-4 (BMP-4), on titanium alloy. *Biomaterials* **2002**, *23*, 2079–2087. [CrossRef]

63. Morra, M.; Cassinelli, C.; Cascardo, G.; Cahalan, P.; Cahalan, L.; Fini, M.; Giardino, R. Surface engineering of titanium by collagen immobilization. Surface characterization and in vitro and in vivo studies. *Biomaterials* **2003**, *24*, 4639–4654. [CrossRef]

64. Friedrich, J.; Kühn, G.; Mix, R.; Fritz, A.; Schönhals, A. Polymer surface modification with monofunctional groups of variable types and densities. *J. Adhes. Sci. Technol.* **2012**, *17*, 1591–1617. [CrossRef]

65. Cools, P.; Mota, C.; Lorenzo-Moldero, I.; Ghobeira, R.; De Geyter, N.; Moroni, L.; Morent, R. Acrylic Acid Plasma Coated 3D Scaffolds for Cartilage tissue engineering applications. *Sci. Rep.* **2018**, *8*, 3830. [CrossRef]

66. Xing, H.; Li, R.; Wei, Y.; Ying, B.; Li, D.; Qin, Y. Improved Osteogenesis of Selective-Laser-Melted Titanium Alloy by Coating Strontium-Doped Phosphate With High-Efficiency Air-Plasma Treatment. *Front. Bioeng. Biotechnol.* **2020**, *8*, 367. [CrossRef] [PubMed]

67. Carton, O.; Ben Salem, D.; Bhatt, S.; Pulpytel, J.; Arefi-Khonsari, F. Plasma Polymerization of Acrylic Acid by Atmospheric Pressure Nitrogen Plasma Jet for Biomedical Applications. *Plasma Process. Polym.* **2012**, *9*, 984–993. [CrossRef]

68. Rabionet, M.; Yeste, M.; Puig, T.; Ciurana, J. Electrospinning PCL Scaffolds Manufacture for Three-Dimensional Breast Cancer Cell Culture. *Polymers* **2017**, *9*, 328. [CrossRef] [PubMed]

69. Moreno-Jiménez, I.; Kanczler, J.M.; Hulsart-Billstrom, G.; Inglis, S.; Oreffo, R.O.C. *The Chorioallantoic Membrane Assay for Biomaterial Testing in Tissue Engineering: A Short-Term In Vivo Preclinical Model. *Tissue Eng. Part C Methods* **2017**, *23*, 938–952. [CrossRef]

70. Baiguera, S.; Macchiarini, P.; Ribatti, D. Chorioallantoic membrane for in vivo investigation of tissue-engineered construct biocompatibility. *J. Biomed. Mater. Res.-Part B Appl. Biomater.* **2012**, *100*, 1425–1434. [CrossRef]

71. Ribatti, D.; Annese, T.; Tamma, R. The use of the chick embryo CAM assay in the study of angiogenic activiy of biomaterials. *Microvasc. Res.* **2020**, *131*, 104026. [CrossRef]
72. Bahmaee, H.; Owen, R.; Boyle, L.; Perrault, C.M.; Garcia-Granada, A.A.; Reilly, G.C.; Claeyssens, F. Design and Evaluation of an Osteogenesis-on-a-Chip Microfluidic Device Incorporating 3D Cell Culture. *Front. Bioeng. Biotechnol.* **2020**, *8*, 1042. [CrossRef]
73. Rouwkema, J.; Rivron, N.C.; van Blitterswijk, C.A. Vascularization in tissue engineering. *Trends Biotechnol.* **2008**, *26*, 434–441. [CrossRef]
74. Chiu, Y.C.; Cheng, M.H.; Engel, H.; Kao, S.W.; Larson, J.C.; Gupta, S.; Brey, E.M. The role of pore size on vascularization and tissue remodeling in PEG hydrogels. *Biomaterials* **2011**, *32*, 6045–6051. [CrossRef]
75. Artel, A.; Mehdizadeh, H.; Chiu, Y.C.; Brey, E.M.; Cinar, A. An agent-based model for the investigation of neovascularization within porous scaffolds. *Tissue Eng.-Part A* **2011**, *17*, 2133–2141. [CrossRef]

CHAPTER 3. Surfactant-Free Gelatin-Stabilised Biodegradable Polymerised High Internal Phase Emulsions with Macroporous Structures

Supplementary information for this article is available in Appendix A.

Check for updates

Surfactant-free gelatin-stabilised biodegradable polymerised high internal phase emulsions with macroporous structures

Rachel Furmidge[1,2†], Caitlin E. Jackson[1,2†],
María Fernanda Velázquez de la Paz[1,2], Victoria L. Workman[1,2],
Nicola H. Green[1,2], Gwendolen C. Reilly[1,2], Vanessa Hearnden[1,2]
and Frederik Claeyssens[1,2]*

[1]Materials Science and Engineering, The Kroto Research Institute, University of Sheffield, Sheffield, United Kingdom, [2]Insigneo Institute for In Silico Medicine, University of Sheffield, Sheffield, United Kingdom

High internal phase emulsion (HIPE) templating is a well-established method for the generation of polymeric materials with high porosity (>74%) and degree of interconnectivity. The porosity and pore size can be altered by adjusting parameters during emulsification, which affects the properties of the resulting porous structure. However, there remain challenges for the fabrication of polyHIPEs, including typically small pore sizes (~20−50 μm) and the use of surfactants, which can limit their use in biological applications. Here, we present the use of gelatin, a natural polymer, during the formation of polyHIPE structures, through the use of two biodegradable polymers, polycaprolactone-methacrylate (PCL-M) and polyglycerol sebacate-methacrylate (PGS-M). When gelatin is used as the internal phase, it is capable of stabilising emulsions without the need for an additional surfactant. Furthermore, by changing the concentration of gelatin within the internal phase, the pore size of the resulting polyHIPE can be tuned. 5% gelatin solution resulted in the largest mean pore size, increasing from 53 μm to 80 μm and 28 μm to 94 μm for PCL-M and PGS-M respectively. In addition, the inclusion of gelatin further increased the mechanical properties of the polyHIPEs and increased the period an emulsion could be stored before polymerisation. Our results demonstrate the potential to use gelatin for the fabrication of surfactant-free polyHIPEs with macroporous structures, with potential applications in tissue engineering, environmental and agricultural industries.

KEYWORDS

polyHIPE, gelatin, surfactant-free, polycaprolactone, poly(glycerol sebacate), porous polymers, emulsion templating

1 Introduction

Various polymer applications benefit from having highly porous structures with a high degree of openness and interconnectivity. For example, in tissue engineering this enables cell ingrowth; in filters, interconnectivity facilitates mass transport and for electrode substrates and catalysts high surface areas result in a better current and substrate conversion, respectively (Chong et al., 2019; Elango et al., 2021; Fager et al., 2021; Vásquez et al., 2021; Maksoud et al., 2022; Mravljak et al., 2022). There are numerous methods of introducing porous geometries

86

within polymers, including bioprinting, particulate leaching, freeze drying, electrospinning and emulsion templating (Eltom et al., 2019; Sharma et al., 2022). Emulsion templating is a relatively simple technique that can be easily tuned to control and influence the resulting structures. Additionally, the internal phase can easily be removed from the polymerised structure via washing and/or dissolving, unlike techniques such as salt/particulate leaching where there is a risk that the presence of residual particles may negatively affect biocompatibility (Maksoud et al., 2022; Montanheiro et al., 2022).

Emulsion templating is performed via the mixing of two immiscible fluids, commonly in the presence of a surfactant, to form a water-in-oil (w/o) or oil-in-water (o/w) emulsion (Foudazi, 2021). During mixing droplets of the internal phase are dispersed within the external phase. The external phase is then solidified, with the internal phase droplets acting as templates for the formation of pores. The internal phase is then removed, resulting in a porous structure. Emulsion templating techniques can be easily tuned by altering parameters such as temperature, surfactant type and concentration, stirring speed and the volume fraction of the internal phase (Aldemir Dikici and Claeyssens, 2020). Emulsions with an internal phase volume >74% are classified as high internal phase emulsions (HIPEs) (Mert and Mert, 2022). Following the polymerisation of these HIPEs (polyHIPEs), a porous structure is fabricated with a high degree of porosity and interconnectivity (Aldemir Dikici and Claeyssens, 2020). Interconnectivity in polyHIPEs occurs when the external phase ruptures at the thinnest sections between the densely packed droplets of the internal phase. This results in the formation of "windows," providing interconnections between pores (Menner and Bismarck, 2006; Silverstein, 2014).

The optimal pore size of a polyHIPE varies greatly depending on the specific application. For example, within tissue engineering, the optimal pore size for angiogenesis has been reported as 160–270 μm (Artel et al., 2011), whereas pore sizes of 11 μm have been reported as optimal for the infiltration of dermal fibroblasts into elastin scaffolds (Rnjak-Kovacina et al., 2011). In membrane filtration systems for conventional particle filtration for water purification, there are a range of optimal pore sizes (5–1,000 μm) for the capture of different particle types (e.g., > 25 μm for sand, 10–100 μm for pollen and <50 μm for atmospheric dust) (Lee et al., 2016). For other filtration applications, such as oil recovery, optimal pore sizes between 82.3 and 145.6 μm have been reported (Zhang and Guo, 2017; Sherborne and Claeyssens, 2021). Despite the advantages of HIPE templating, the pore size of surfactant-stabilised polyHIPEs is typically quite small, <50 μm (Barbetta and Cameron, 2004; Dikici et al., 2019), with smaller windows (1–10 μm) forming interconnections between pores (Silverstein, 2014; Sun et al., 2019). Given the ranges of pore sizes required for these different applications, it is beneficial to be able to alter the pore size of polyHIPE materials.

A known mechanism for increasing the pore size of emulsion-templated materials is via the modulation of emulsion stability (Dhavalikar et al., 2021). Emulsions are thermodynamically unstable, and as such, it is energetically favourable for the surface area of the internal droplets to be reduced if the interfacial tension is too high. This mechanism occurs through the coalescence of droplets, increasing droplet size to reduce surface area, thus resulting in increased pore size of the polymerised emulsion

(polyHIPE) (Bokhari et al., 2007; Ravera et al., 2021). Through this principle, reducing emulsion stability can be used to increase the pore size of emulsion-templated materials. Previous attempts have been made to reduce the stability of emulsions, for example, Kent and Saunders reported the use of magnesium sulphate within w/o emulsions to reduce the adsorption of surfactant, thus increasing the droplet size within the emulsion (Kent and Saunders, 2001; Aldemir Dikici and Claeyssens, 2020). Concerning emulsion-templated biomaterials, Choi et al. (2010) created porous poly (D, L-lactide-co-glycolide) (PLGA) beads using gelatin, with tuneable pore size, controlled through the use of phase-separated emulsions. To increase pore size within the beads, fractions of the emulsion with reduced stability were used during bead fabrication (Choi et al., 2010).

As previously mentioned, surfactant type and concentration are also important parameters in the fabrication of emulsions and play a key role in the resulting pore size of the polyHIPE. Surfactants used to create polyHIPEs are commonly amphiphilic, consisting of a hydrophilic head group and a hydrophobic tail. The surfactant forms a barrier between the droplet and the surrounding phase, reducing the surface tension and facilitating the interaction between the two phases. However, due to the synthetic nature of most commonly used surfactants, their use can lead to cytotoxicity, and/or a series of lengthy and costly washing steps. The use of surfactant-free templating methods, such as Pickering HIPEs (e.g., soft and Janus particles) (Venkataramani et al., 2020) as well as biologically-based surfactants (Wang et al., 2020; Chen et al., 2021) have been previously explored. Biologically-based surfactants of plant and microbial origin have been explored by the agricultural, chemical, and cosmetics industries (Duprat-De-Paule et al., 2018; Deotale et al., 2019; Moldes et al., 2021; Gayathiri et al., 2022). However, one of their main challenges is high production costs (Farias et al., 2021).

Gelatin is a natural polymer formed by the denaturation of collagen via partial hydrolysis (Zhang et al., 2020). Gelatin undergoes a sol-gel transition when dissolved in water at temperatures between 35°C and 37°C, wherein cooling of the gelatin solution induces the formation of triple helices stabilised by intermolecular hydrogen bonds (Haug et al., 2009), allowing the reversible formation of gels (Chen and Vyazovkin, 2009). Gelatins have reportedly been used as an emulsifier for many different applications, commonly in the food industry, where they serve as foaming, emulsifying and wetting agents to improve the quality of various foods and improve their stabilisation (Karim and Bhat, 2009; Zhang et al., 2020). Gelatin exhibits amphiphilic behaviour and can decrease interfacial tension by migrating from the water phase to the oil/water interface (Ding et al., 2020). However, gelatin is viewed as a weak stabiliser, especially when compared to other surfactants commonly used to make polyHIPEs, such as Span80, Hypermer B246 and polyglycerol polyricinoleate (PGPR) (Aldemir Dikici and Claeyssens, 2020; Zhang et al., 2020). Due to the emulsification properties of gelatin, we postulated that gelatin could be used to fabricate surfactant-free polyHIPEs, and, as the emulsifying ability of gelatin is weak, these polyHIPEs would have large pore sizes (>50 μm).

This study utilises gelatin solutions as the internal phase in polymer-based emulsions to fabricate surfactant-free polyHIPEs. We assessed the pore geometry and characteristics of the resulting

TABLE 1 Emulsion Formulations. Emulsions were fabricated either with or without surfactant, with water or gelatin of varying concentrations as the internal phase.

Emulsion	Gelatin solution concentration (%)	Surfactant (weight (%) of polymer weight)
G0S10	0	10
G5S10	5	10
G7S10	7	10
G10S10	10	10
G0S0	0	0
G5S0	5	0
G7S0	7	0
G10S0	10	0

polyHIPEs compared to conventional polyHIPEs fabricated with water as the internal phase. The concentration of gelatin was varied to assess the effect on polyHIPE structure. In addition, we investigated the effect of using gelatin in combination with a commonly used surfactant (Hypermer B246) to further elucidate the behaviour of gelatin as a stabiliser.

For these experiments, we have used two synthetic biodegradable polymers, polycaprolactone-methacrylate (PCL-M) and poly(glycerol sebacate)-methacrylate (PGS-M). PCL is FDA-approved and the photocurable form, PCL-M, has been extensively researched within our group for bone and nerve tissue engineering applications (Aldemir Dikici et al., 2020; Field et al., 2021; Aldemir Dikici et al., 2022a). PGS is an emergent material that has been well-documented as being softer than most traditionally used synthetic polymers (Pashneh-Tala et al., 2018; Vogt et al., 2021). PCL-M and PGS-M were selected as both materials are biodegradable and biocompatible, whilst having different chemical and mechanical profiles (Labet and Thielemans, 2009; Rai et al., 2012).

The long-term stability of the fabricated emulsions was assessed over the course of 2 months, and the resulting polyHIPEs were characterised using scanning electron microscopy (SEM). Finally, the effect of using gelatin during polyHIPE fabrication on the mechanical properties of the polyHIPEs was investigated. Overall, this investigation highlights the potential use of gelatin as a surfactant-free method to generate polyHIPEs with large pore sizes in polymeric constructs.

2 Materials

Photoinitiator (2,4,6-Trimethylbenzoyl Phosphine Oxide/2-Hydroxy-2- Methylpropiophenone blend), glycerol (99%), sebacic acid (99%), 4-methoxyphenol (99%), trimethylamine (99.5%), methacrylic anhydride (94%, MEA) and type A gelatin from porcine skin (300 g Bloom) were purchased from Sigma Aldrich. Chloroform (99%), toluene (99.5%), ethanol (99%), dichloromethane (99%, DCM), hydrochloric acid (37%) and glacial acetic acid (99%) were purchased from Fisher Scientific. The surfactant, Hypermer B246 (98%) was received as a sample from Croda (Goole, United Kingdom). High molecular weight 4-arm methacrylated polycaprolactone [PCL-M, 95% degree of

methacrylation, M_w = 20,331 g/mol, Supplementary Figures S1C, E) was synthesised in the laboratory [a general synthesis method is given in Aldemir Dikici et al. (2019)].

3 Methods

3.1 PGS-M synthesis

PGS pre-polymer was synthesised via methods previously described (Pashneh-Tala et al., 2018; Singh et al., 2018; Becerril-Rodriguez and Claeyssens, 2022). Briefly, glycerol and sebacic acid in an equimolar ratio were stirred and heated to 120°C with nitrogen gas at a flow rate of 1 L/min applied to the system for 24 h to prevent oxygen contamination. After 24 h, a vacuum, at a pressure of 9 mbar, was applied for a further 24 h to remove excess water from the system following the polycondensation reaction.

To methacrylate PGS to enable photocuring, PGS prepolymer was dissolved in DCM 1:4 (w/v) and 1 mg of the accelerator 4-methoxyphenol was added per gram of PGS-prepolymer to increase the initial rate and extent of polymerisation. The system was then surrounded by an ice bath (0°C) to slow reaction kinetics, and triethylamine was added at a concentration of 0.8 mol/mol of PGS pre-polymer OH groups (for a theoretical 80% degree of methacrylation), followed by an equimolar amount of MEA which was added dropwise. Following the addition of MEA, the temperature was allowed to rise to room temperature over the following 24 h. The actual degree of methacrylation following characterization was 75%, and the molecular weight was 2,065 g/mol (Supplementary Figures S1D, E).

After 24 h, an additional 1 mg 4-methoxyphenol per gram of PGS prepolymer was added to stop the reaction. To remove any residual reagents used during methacrylation, the yielded PGS-M pre-polymer was washed with 30 mM hydrochloric acid. Vacuum filtration through a 6 μm pore cellulose filter (Whatman—Grade 3, GE Healthcare Life Sciences, United Kingdom) was used to remove any potential residual solids before the residual solvent was removed via rotary evaporation for 3 h under a vacuum at a pressure of 9 mbar at approximately 10°C. The residual PGS-M pre-polymer was then removed and stored at −20°C before use.

3.2 PCL-M polyHIPE fabrication

0.4 g PCL-M and 0.04 g surfactant were heated to melt the surfactant and PCL-M. 0.6 g of a 60 wt% chloroform and 40 wt% toluene solvent mixture (0.24 and 0.28 mL respectively) and 0.03 g photoinitiator were added to the PCL-M-surfactant mixture respectively. The contents were mixed (250 rpm) using a magnetic stirrer (20 mm × 7 mm) for 3 min at 37°C. Once homogeneous, 2 mL of internal phase (deionized water or gelatin solution) was added dropwise at a rate of approximately 1 droplet/s and the emulsion was further mixed for 5 min.

3.3 PGS-M polyHIPE fabrication

0.5 g PGS-M pre-polymer with 0.05 g surfactant was heated to melt the surfactant and reduce polymer viscosity. 0.5 g toluene was then added and then mixed for a minimum of 3 min at 37°C at 250 rpm using a magnetic stirrer (20 mm × 7 mm). Once homogenous, 4 mL of the internal phase (deionised water or gelatin solution) was added into the stirring mixture dropwise at a rate of approximately 1 droplet/s. The mixture was stirred for 3 min to allow the emulsion to thicken before adding 0.05 g of photoinitiator and stirring for a further 2 min.

The internal phase, heated to 37°C before addition to the emulsion, consisted of either deionised water, or a solution of gelatin (5, 7, 10 wt/v%), and emulsions were made either with or without 10 wt/wt% surfactant. The composition of the various emulsions tested can be seen in Table 1.

3.4 Polymerisation of PCL-M and PGS-M HIPEs

Emulsions were polymerised via radical polymerisation (Supplementary Figure S2) in a transparent 2 mL syringe. All samples were cured using ultraviolet (UV) light for 5 min on both sides using the OmniCure Series 1,000 system (100 W, Lumen Dynamics, Canada), with 18 W/cm^2 reported light density and spectral output from 250 to 600 nm. The resulting polyHIPEs were removed from the syringe and washed in 100% ethanol for 2 days, changing the ethanol after a 24 h period. Following this, ethanol was replaced daily for 3 days, rehydrating the polyHIPEs through a series of ethanol dilutions; 70%, 50%, and 25% before placing the polyHIPEs into deionised water. PolyHIPEs were rehydrated gradually in order to prevent severe structural changes due to changes in surface tension during washing. All polyHIPE samples were washed and stored at room temperature. PolyHIPE length and diameter were measured post-curing and after washing to determine the shrinkage of the constructs following the washing process.

To analyse the effect of gelatin on the pore structure of the polymer alone, rather than in the presence of gelatin, before scanning electron microscopy (SEM), helium pycnometry and mechanical testing, polyHIPEs (including those fabricated without gelatin) were washed twice in 99% glacial acetic acid for 15 min at 37°C to remove gelatin before the washing steps outlined above. Following completion of washing, samples were freeze-dried (Lyotrap, LTE Scientific Ltd., United Kingdom) for 24 h to dehydrate the samples before characterisation.

3.5 Assessment of polyHIPE pore structure via SEM

To observe and analyse the microstructure of the polyHIPE samples, constructs polymerised within the 2 mL syringe were manually sliced into approximately 1 mm thick discs using a scalpel. The morphology of the polyHIPEs was analysed using a scanning electron microscope (SEM, Inspect F, FEI, United States). Samples were subject to the deposition of gold coating. To avoid surface charging and damage to the sample a low accelerating voltage of 5 kV with a spot size of 3 and a typical vacuum pressure of 10^{-5} mbar at a working distance of 10 mm was applied. The SEM images were used to calculate the average pore size and distribution. Across three micrographs, 60 pores were randomly selected (20 per image) and measured using ImageJ v. 1.48 from the National Institutes of Health (NIH, Bethesda, MD, United States). The pores were selected by placing a 30-square grid over the image and measuring the diameter of each pore that was in contact with each cross-section of the grid. A correction factor (Dhavalikar et al., 2021) was applied to adjust for the assumption that each pore had not been exactly bisected (Barbetta and Cameron, 2004).

3.6 Helium pycnometry

The porosity of the PCL-M and PGS-M polyHIPEs produced using different emulsion formulations was determined using a helium pycnometer (AccuPyc 1,340, Micromeritics, United States). In this study, porosity refers to the percentage of void space in the material. Constructs were prepared and freeze-dried as described previously in Section 3.4. The length and diameter of the dry constructs were then measured using digital callipers, which were used to calculate the bulk volume of the polyHIPEs, without factoring in the internal porosity. The polyHIPEs were then placed within a 1 cm^3 chamber insert within the pycnometer before the chamber was pressurised at 19,500 psi with helium, and the volume of the chamber occupied by the polyHIPE was measured, factoring in the internal porosity. This was the true volume of the constructs, including the porosity, denoted as the "pycnometric volume". The following equation (Eq. 1) was used to determine the construct porosity:

$$Porosity\ (\%) = \frac{V_b - V_p}{V_b} * 100 \qquad (1)$$

where V_b was the bulk volume, and V_p was the pycnometric volume. Theoretical porosity was calculated using the following formula (Eq. 2):

$$Porosity\ (\%) = \frac{V_i}{V_i + V_e} \qquad (2)$$

where V_i and V_e represent the volume of the internal phase (water or gelatin solution) and external phase (PGS-M pre-polymer, surfactant and photoinitiator) respectively. Solvent volume was excluded from internal phase volume as it is presumed that solvent would evaporate following polymerisation of the HIPEs, and thus would not form part of the solid volume.

89

3.7 Long-term stability

G0S10, G5S10, and G5S0 emulsions were fabricated (as described previously, Section 3.2 and Section 3.3) and sealed in an air-tight vial (to maintain humidity), covered in aluminium foil and stored at room temperature. Emulsions were then polymerised using UV light (as described previously, Section 3.4) on day 1, day 7, day 14, and day 56. Following polymerisation all the samples were washed in 100% ethanol for 2 days, changing the ethanol after a 24 h period. Following this, ethanol was replaced daily, rehydrating the polyHIPEs through a series of ethanol dilutions; 70%, 50%, and 25% before placing the polyHIPEs into deionised water. All polyHIPE samples were washed and stored at room temperature. To prepare the samples for SEM analysis, the samples were further washed twice in 99% glacial acetic acid for 15 min at 37°C to remove gelatin before repeating the ethanol and water washing procedure as outlined above.

3.8 Mechanical characterisation

The compressive modulus of the PCL-M and PGS-M polyHIPEs was calculated using compressive mechanical testing (MultiTest 2.5–dV, Mecmesin, Slinford, United Kingdom), using the 250 N load cell at room temperature and 40% humidity. Samples were cut into cylinders approximately 1 cm in length before their exact length and diameters were measured using digital callipers for calculating mechanical properties. The polyHIPEs were then placed between two compression plates, and compressive tests were performed on each sample at a rate of 1 N/s until the maximum load of 250 N was reached. The stiffness was calculated from the gradient of the initial linear region of the stress-strain curve for each sample.

3.9 Statistical analysis

Statistical analysis was carried out using statistical analysis software (GraphPad Prism, Version 9.4.1, CA, United States). A normality test was used to determine if data was normally distributed. Normally distributed data were analysed using a one-way Brown-Forsythe and Welch analysis of variance (ANOVA) followed by Dunnet's T3 multiple comparison test. Non-normally distributed data were analysed using a Kruskal–Wallis test with Dunn's multiple comparisons test. Error bars on graphs indicate standard deviation and the number of technical repeats (n) are given in figure captions where applicable. Statistical significance on graphs is represented as p-value <0.033 (*), 0.002 (**), and 0.001 (***).

4 Results

4.1 Manufacturing and assessment of polyHIPE pore structure

HIPEs made with 3%–15% gelatin solution with or without surfactant were assessed. Formulations with <5% gelatin solution without surfactant were not able to form emulsions. In addition, without the presence of gelatin or surfactant, emulsions could not

form, thus further assessment of these HIPEs was excluded. Gelatin solutions ≥15% resulted in highly viscous solutions that rapidly gelled, preventing the fabrication of reproducible emulsions. Therefore, stable HIPEs were fabricated using 5, 7%, and 10% gelatin solutions as the internal phase, with and without the addition of surfactant. HIPEs fabricated with gelatin solution as the internal phase appeared to have increased viscosity compared to surfactant-only HIPEs.

Overall, the inclusion of gelatin in the internal phase of the HIPE without the use of additional surfactant increased the pore size of PCL-M and PGS-M polyHIPEs compared to those fabricated with surfactant. A visual change in polyHIPE structure was observed, where there was an increased number of large pores, occupying a greater proportion of the field of view (Figures 1A, B).

Increasing the concentration of gelatin in surfactant-free polyHIPEs resulted in a large distribution of pore sizes (Supplementary Figures S3, S4) which did not yield a statistically significant change in the mean pore size. However, there were trends in the data that correlate to the visual observations from the SEM images. For PCL-M, increasing the concentration of the gelatin solution in surfactant-free polyHIPEs from 5% to 7% resulted in a decrease in mean pore size (79.9 ± 42.9 μm to 60.6 ± 25.4 μm respectively) (Figure 1C). However, further increasing the gelatin concentration from 7% to 10% led to an increase in mean pore size from 60.6 ± 25.4 μm to 70.5 ± 36.5 μm respectively. For PGS-M polyHIPEs, the mean pore size significantly decreased from 94.3 ± 70.0 μm to 51.8 ± 32.6 μm from 5% to 7% gelatin, respectively, and increased from 51.8 ± 32.6 μm to 59.0 ± 37.2 μm from 7% to 10%, respectively (Figure 1D).

With the inclusion of surfactant in the HIPE, increasing the concentration of the gelatin solution had no significant effect on the mean pore size of PCL-M or PGS-M polyHIPEs. Furthermore, there was no significant difference between surfactant-only and surfactant and gelatin polyHIPEs (Figures 1C, D).

For both PCL-M and PGS-M, 5% gelatin solution without additional surfactant resulted in the largest mean pore size (79.9 ± 42.9 μm and 94.3 ± 70.0 μm respectively), which are both significantly larger than conventional surfactant-only polyHIPEs (53.0 ± 18.7 μm and 27.7 ± 13.0 μm respectively) which are comparable to pore sizes of surfactant stabilised polyHIPEs commonly reported in literature (Kramer et al., 2021). Thus, all further analysis was completed on polyHIPE constructs fabricated using a 5% gelatin solution.

4.2 Porosity of polyHIPEs

All polyHIPEs had a reduced porosity compared to the theoretically predicted porosity of 82.1% and 88.4% for PCL-M and PGS-M respectively, with the largest decrease in porosity observed in surfactant-free, 5% gelatin polyHIPEs (Table 2).

4.3 Mechanical characterisation of polyHIPEs

The inclusion of gelatin with or without surfactant in the formation of PCL-M and PGS-M polyHIPEs led to significantly
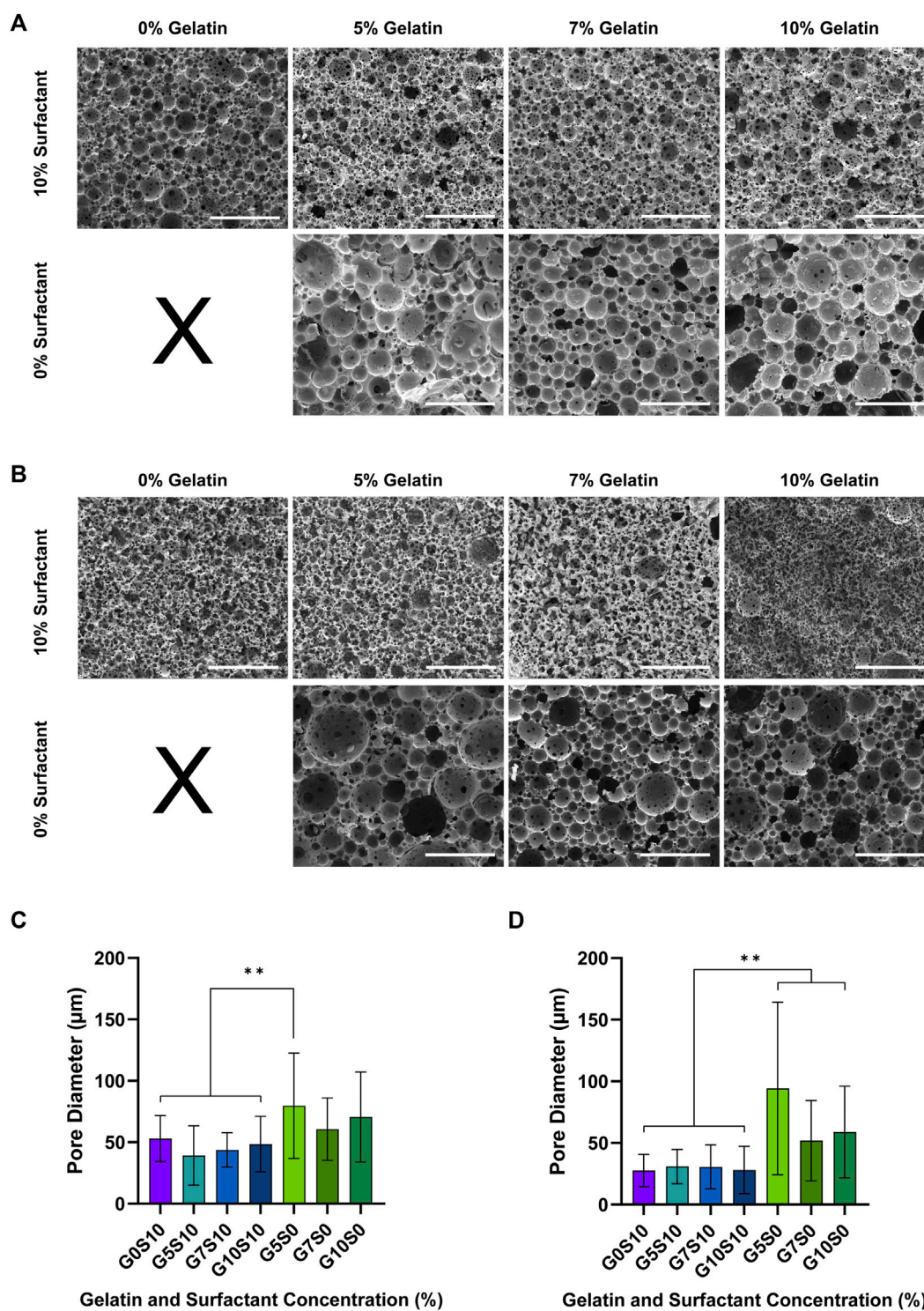
90

FIGURE 1
PCL-M and PGS-M polyHIPEs were fabricated using different concentrations of gelatin with or without surfactant. Scanning electron micrographs of **(A)** PCL-M and **(B)** PGS-M polyHIPEs fabricated using 0, 5, 7%, and 10% gelatin solution with or without 10% surfactant (scale bar = 200 µm). Varying the concentration of gelatin within the internal phase of the emulsions affects the resulting pore size of **(C)** PCL-M and **(D)** PGS-M polyHIPEs (mean $\pm$ SD, $n =$ 60, $**p < 0.002$). Histograms showing relative frequency and distribution of pore sizes can be found in Supplementary Figures S3, S4 for PCL-M and PGS-M respectively.

higher stiffness than surfactant-only polyHIPEs (Figures 2A–D; Supplementary Table S1). There was no significant effect on stiffness with the addition of surfactant within gelatin constructs.

Following deformation, all of the PCL-M polyHIPEs assessed exhibited little elastic recovery (Figure 2E). On the other hand, surfactant-only PGS-M polyHIPEs exhibited full elastic recovery

TABLE 2 Porosity of PCL-M and PGS-M polyHIPEs, as measured via helium pycnometry. Porosity is expressed as a percentage of the total volume of the construct. The bottom row shows the theoretical porosity of all polyHIPEs fabricated (based on the volumes of liquids added to the initial emulsion) calculated using the ratio of internal phase volume to total emulsion volume.

Emulsion	PCL-M measured porosity (%)	PGS-M measured porosity (%)
G0S10	73	82
G5S10	74	78
G5S0	72	76
Theoretical (based on emulsion composition)	82	88

following deformation, whereas PGS-M polyHIPEs fabricated with 5% gelatin solution exhibited reduced elastic recovery following deformation (Figure 2F).

4.4 Effect of washing on polyHIPE structures

The polyHIPEs undergo several post-processing washing steps to remove excess solvent, surfactant and photoinitiator from within the structure. It was observed that through this post-processing cycle, the polyHIPEs significantly decreased in size, which was assumed to further cause a decrease in pore size (Figure 3). For both PCL-M and PGS-M surfactant-containing polyHIPEs the addition of gelatin did not significantly affect the degree of shrinkage following the washing process. However, for surfactant-free gelatin PCL-M, there was a significant reduction in shrinkage compared to surfactant-containing polyHIPEs (Figure 3A), whilst for surfactant-free gelatin PGS-M there was a significant increase in shrinkage compared to surfactant-containing polyHIPEs (Figure 3B).

4.5 Long-term stability of PCL-M and PGS-M emulsions

The amount of time an emulsion can remain stable without separating is affected by many factors such as surfactant type, concentration and emulsion composition, including that of the internal phase. PCL-M and PGS-M emulsions fabricated with 5% gelatin and stored at room temperature remained visibly stable for up to 56 days whereas surfactant-only emulsions stored at room temperature were stable for 24 h (Table 3). Visual stability was defined when there was no phase separation, flocculation or coalescence observed within the sealed storage vial which can usually be seen when instability occurs in emulsions (Tian et al., 2022) (Supplementary Figure S6). After storage at room temperature, the stable 5% gelatin emulsions became very viscous but were still able to be transferred into a mould for curing. However, after storage at 37°C for 24 h the 5% gelatin emulsions destabilised and phase separation was observed (data not shown).

The stable emulsions were cured and the micro-structures were further analysed via SEM. PCL-M and PGS-M emulsions cured after 24 h–56 days demonstrated typical porous polyHIPE structure in the resulting polyHIPE (Figures 4A, B). There was a decrease in mean pore size for both PCL-M and PGS-M polyHIPEs from day 1 to day 7 (Figures 4C, D). However, there was no significant

difference between the pore sizes of polyHIPEs that were cured after being stored for 7, 14, and 56 days for both PCL-M and PGS-M surfactant-free gelatin polyHIPEs.

5 Discussion

This study investigated the effect of using a solution of gelatin as the internal phase in PCL-M and PGS-M polyHIPEs. Our findings indicate that gelatin can act as an emulsifier, and when used as the sole stabilising agent in the emulsion, it can generate polyHIPEs with large pore sizes (80–200 μm). This allows for the fabrication of surfactant-free polyHIPEs, whilst additionally providing a method of preloading the internal pores of polyHIPEs with gelatin. In addition, the use of gelatin impacts the mechanical properties of the polyHIPEs, resulting in a significant increase in stiffness. This effect was independent of the use of an additional surfactant (Hypermer B246) alongside gelatin. Furthermore, by adding gelatin to the internal phase, the emulsions can be stored for longer periods before curing compared to conventional emulsions. The resulting polyHIPEs fabricated from these stored emulsions retain their porous structure after curing, further enabling the potential applications of these gelatin-based emulsions.

The amphiphilic properties of gelatin have previously been harnessed to stabilise emulsions for the fabrication of polyHIPEs (Oh et al., 2015). Oh et al. (2015) used gelatin grafted onto poly (N-isopropyl-acrylamide) as the external phase of an o/w emulsion, with p-xylene as the internal oil phase, without additional surfactant. The grafted poly (N-isopropyl-acrylamide) side chains on the gelatin allowed the external phase of the emulsion to be solidified. These emulsions formed gelatinous scaffolds with macroporous structures. However, the study found that only the gelatin copolymer could stabilise the emulsion, not gelatin itself. It was also observed that the interfacial tension between grafted gelatin and p-xylene was lower than that between non-grafted gelatin and p-xylene. This may indicate that if the interfacial tension between the gelatin solution and the opposing phase is too high, gelatin may no longer act as an effective stabiliser.

Varying the concentration of gelatin within surfactant-free polyHIPEs allowed control over pore size. Using the lowest concentration of gelatin, 5%, conferred the largest mean pore size. When considering the pore size of polyHIPEs, it is worth noting that the constructs were imaged in dry conditions. PolyHIPEs can shrink following drying, in particular when they are formulated with porogenic solvents (Pierre et al., 2006; Murphy et al., 2017; Jackson et al., 2023). In this study, all constructs
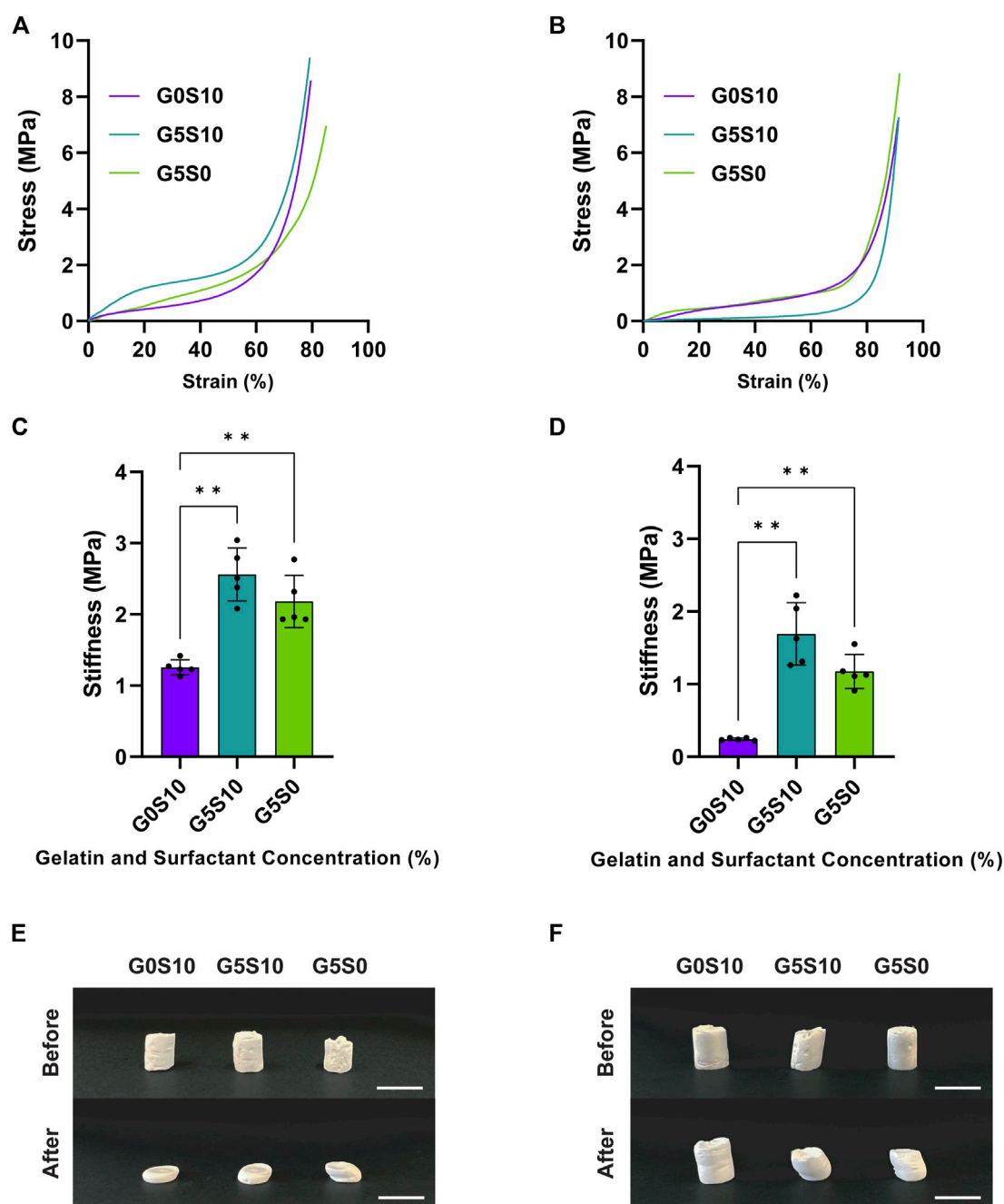
FIGURE 2
Representative stress-strain curves of **(A)** PCL-M and **(B)** PGS-M polyHIPEs following the removal of gelatin via acetic acid and freeze-drying with the corresponding mean stiffness of the **(C)** PCL-M and **(D)** PGS-M polyHIPEs (mean ± SD, $n = 5$, **$p < 0.002$). **(E)** PCL-M and **(F)** PGS-M polyHIPEs before and after mechanical compression under a 250 N load. PolyHIPEs from left to right are G0S10, G5S10, and G5S0 respectively (scale bar = 1 cm).

exhibited shrinkage following freeze drying (Supplementary Figure S5), so it should be considered that pore sizes in these dehydrated polyHIPEs may be smaller than if the polyHIPEs were hydrated.

As previously mentioned, the pore size of a polyHIPE can be controlled through emulsion stability, and as such, increasing surfactant concentration during polyHIPE fabrication increases stability and leads to a reduction in pore size. Following this principle, as gelatin behaves as a stabiliser (albeit a weak one), increasing the concentration of gelatin should lead to reduced

polyHIPE pore size. This effect was observed in surfactant-free gelatin polyHIPEs, where the mean pore size from 5% to 7% gelatin decreased for PCL-M and PGS-M polyHIPEs. However, this trend was not maintained following an increase in gelatin concentration from 7% to 10% gelatin, where the pore size instead increased slightly. As increasing gelatin concentration increases the viscosity of the gelatin solution (Sancakli et al., 2021), the increase in pore size between 7% and 10% gelatin may be due to increased viscosity of the internal phase. Increased internal
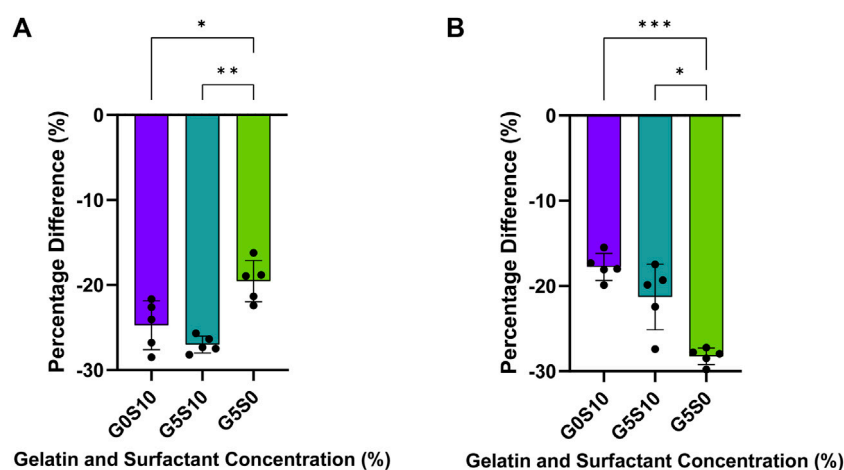
93

FIGURE 3
The percentage difference in the size of **(A)** PCL-M and **(B)** PGS-M polyHIPEs following the post-processing washing cycle (mean $\pm$ SD, $n = 5$, $*p < 0.033$, $**p < 0.002$, $***p < 0.001$).

TABLE 3 Long-term stability of G5S0 emulsions, fabricated and stored at room temperature prior to curing after 1 day, 7 days, 14 days, and 56 days. A conventional HIPE (G0S10) was used as a control. Emulsions were described as stable when no visible separation occurred and the emulsion could be transferred to a mould and photocrosslinked.

Polymer	Emulsion composition	Emulsion storage time			
		1 Day	7 Days	14 Days	56 Days
PCL-M	10% surfactant, 0% gelatin	Stable	Separation observed	Separation observed	Separation observed
	0% surfactant, 5% gelatin	Stable	Stable	Stable	Stable
PGS-M	10% surfactant, 0% gelatin	Stable	Separation observed	Separation observed	Separation observed
	0% surfactant, 5% gelatin	Stable	Stable	Stable	Stable

phase viscosity compared to external phase viscosity has been shown to inhibit efficient mixing (Busby et al., 2001; Kataruka and Hutchens, 2019). Reduced mixing efficiency reduces droplet transport and distribution throughout the emulsion, preventing droplet breakup from collision with the stirrer (Sajjadi, 2006; Ashrafizadeh and Kamran, 2010). In addition, with reduced mixing efficiency, droplets undergo reduced shear forces (Moglia et al., 2014), which in turn may reduce droplet dispersal, leading to increased droplet size and subsequently larger pore sizes. The effect of reduced mixing efficiency and subsequent droplet breakup may also be exacerbated by the low mixing speed used within this study of 250 rpm (Moglia et al., 2011; Jackson et al., 2023). Thus, increasing gelatin concentration and its stabilising ability leads to a reduction in droplet size, however, when a critical viscosity of gelatin solution is reached, viscosity has a greater influence on polyHIPE pore size than increasing gelatin concentration.

Whilst pore size is a key factor in construct design, another important parameter is porosity, which is the percentage of void space within the material. Here we investigated the porosity of gelatin polyHIPEs using helium pycnometry. It was observed that the measured porosity was less than the theoretical porosity. All the emulsions had the same volume of internal phase added, therefore any decrease in measured porosity of the resulting polyHIPEs from the

theoretical value is not likely due to a reduction in internal pores, but instead a reduction in interconnectivity. This is further supported by the SEM characterisation (Figures 1A, B), where more interconnects are visible in the surfactant-stabilised polyHIPEs compared to the gelatin-stabilised polyHIPEs. Any closed pores within the polyHIPE will reduce the measured porosity. The relationship between interconnectivity and porosity in polyHIPEs has been previously reported (O'Brien, 2011; Aldemir Dikici and Claeyssens, 2020). For example, Owen et al. (2016) observed a linear relationship between porosity and degree of openness (interconnectivity). While the incorporation of gelatin in the internal phase during polyHIPE fabrication slightly reduced porosity in PCL-M and PGS-M polyHIPEs, the materials remained highly porous (>70%).

PolyHIPEs are commonly subjected to several post-processing steps to remove unreacted monomer, excess solvent, surfactant and photoinitiator from within the structure. These steps are especially important for tissue engineering applications to prevent the leaching of cytotoxic chemicals. Washing of polyHIPEs can cause shrinkage or swelling, depending on the material composition as well as the medium used for washing (Aldemir Dikici and Claeyssens, 2020). For design and manufacturing purposes, it is important to know the degree of swelling or shrinkage of a certain polyHIPE, so that size of moulds can be scaled to account for the change in construct size.
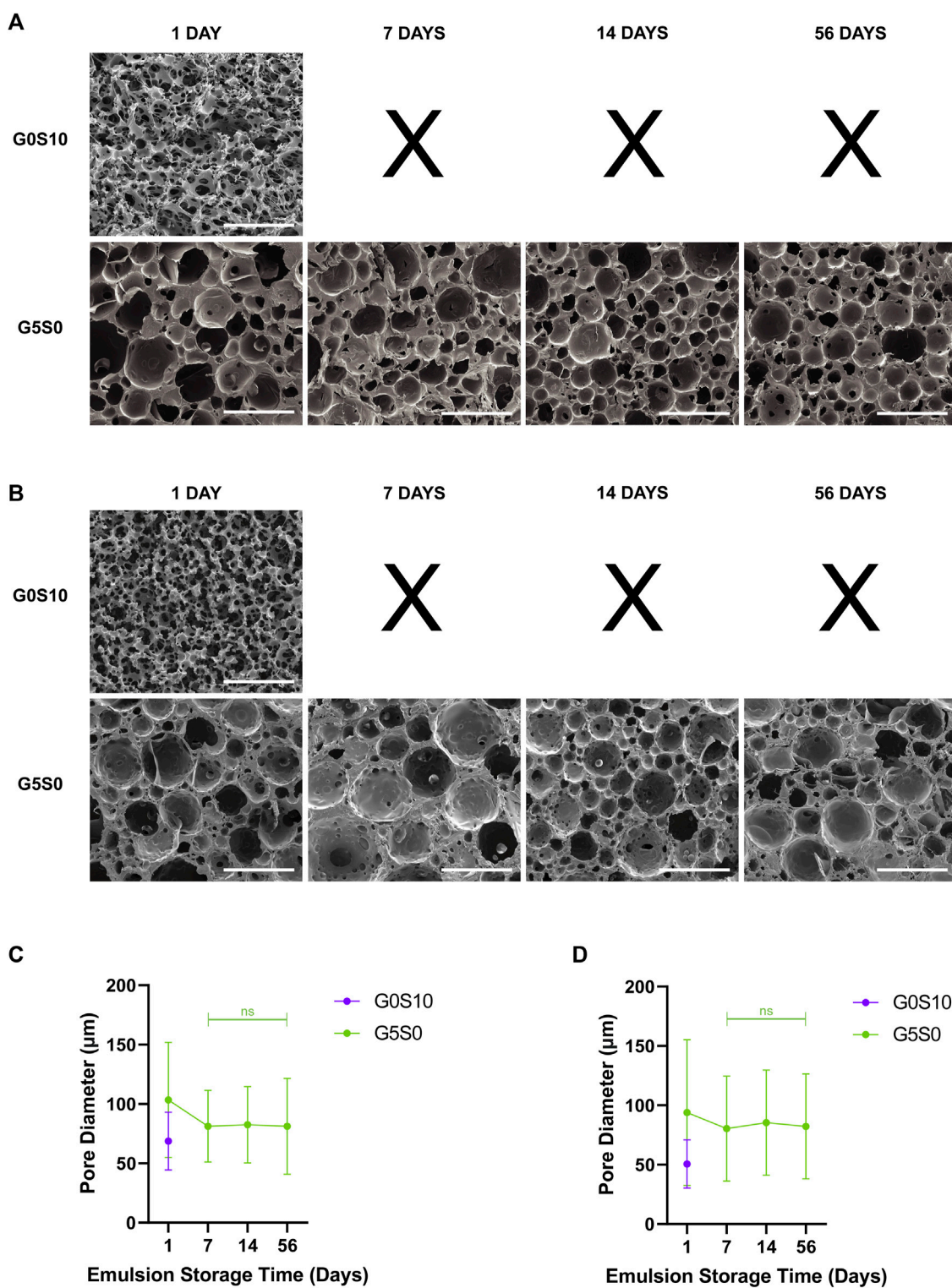
94

FIGURE 4
Scanning electron micrographs of **(A)** PCL-M and **(B)** PGS-M polymerised emulsions (polyHIPEs) fabricated with water and surfactant (G0S10) or with gelatin and no surfactant (G5S0), following storage of emulsions for 1 day, 7 days, 14 days, and 56 days, prior to curing (scale bar = 200 μm). Emulsions not containing gelatin were not fabricated and stored for more than 7 days following emulsion separation observed on day 7. The pore size of the resulting **(C)** PCL-M and **(D)** PGS-M surfactant-free gelatin polyHIPEs did not change significantly following storage of the emulsions from 7 days up to 56 days (mean $\pm$ SD, n = 60, ns = not significant).

95

A degree of shrinkage was observed across all polyHIPEs between the fabrication of the polyHIPE and after the post-processing steps (Figure 3). These steps consisted of an acetic acid wash to remove gelatin, followed by washing and rehydration of the polyHIPE through a series of ethanol dilutions and water. It has been reported that polyHIPEs can reduce in size due to pore collapse following the removal of solvent (Woodward et al., 2017). However, the SEM images of the washed samples did not reveal that the gelatin polyHIPEs exhibited structural collapse following washing, indicating that their shrinkage may instead be due to the elution of the solvent during water washes. This principle has been previously utilised by Dikici et al. (2020), where the shrinkage of polyHIPEs was used to aid in the assembly of a bilayer tube. Many reports have focused on the shrinkage of polyHIPEs due to drying (Hobiger et al., 2021), although there has been less focus on shrinkage during washing. However, shrinkage and swelling have been noted for gels and colloids during washing (Nussinovitch and Peleg, 1990).

Mechanical strength is an important characteristic, as it determines the ability of a material to withstand external forces and loads without failure. Overall, the inclusion of gelatin as the internal phase during the fabrication of polyHIPEs increased the compressive mechanical strength compared to conventional surfactant-stabilised polyHIPEs (G0S10) (Figure 2). It is well established within the literature that for conventional polyHIPEs, larger pore sizes confer greater mechanical strength than smaller pore sizes, usually due to the increased thickness of the walls between pores (Jiang et al., 2007; Lin-Gibson et al., 2007; Huš and Krajnc, 2014; Aldemir Dikici et al., 2019; Kovačič et al., 2019). However, concerning the use of co-emulsifiers, Wu et al. (2010) report that the inclusion of co-emulsifying silica nanoparticles alongside a surfactant increased mechanical strength compared to conventional polyHIPEs, despite a reduction in pore size. Therefore, we might expect that the use of both surfactant (hypermer) and gelatin as co-emulsifiers would lead to a synergistic emulsifying effect, resulting in smaller pore sizes and increased mechanical strength. However, we observed that the inclusion of gelatin and surfactant did not change mean pore size compared to conventional polyHIPEs (Figures 1C, D), despite an increase in stiffness (Figure 2). Furthermore, G5S10 and G5S0 polyHIPEs had similar mechanical properties, whilst having different pore sizes. This may indicate that the inclusion of gelatin during fabrication had a larger overarching effect on mechanical properties than the change in pore size.

In the literature, several methods have been established to alter the mechanical properties of polyHIPEs, which can be divided into three categories; modifications to the emulsion parameters, modification of the polymerisation and post-processing modifications. During emulsification, internal phase volume (Aldemir Dikici and Claeyssens, 2020), surfactant type and concentration (Aldemir Dikici et al., 2022b), mixing speed (Jackson et al., 2023), diluting solvent type and ratio (Aldemir Dikici et al., 2019), and the inclusion of reinforcing agents or particles in the external phase (Wu et al., 2010) can all alter the mechanical properties of the resulting polyHIPE. However, these mechanisms also alter the pore size of the polyHIPE, which may limit their benefit for some applications. The polymerisation process can also be modified. For example, Luo et al. (2012) used reversible addition-fragmentation chain transfer polymerisation to increase the mechanical properties of styrene and divinylbenzene polyHIPEs 3-fold compared to conventional radical polymerisation techniques. However, this resulted in varying pore morphology. Finally, post-processing steps can be performed on polyHIPEs to increase their mechanical properties. For example, electroless nickel plating has been used to coat the surface of polyHIPEs, conferring a >4-fold increase in stiffness (Sengokmen-Ozsoz et al., 2023). However, this leads to reduced surface porosity and increases the complexity of fabrication with additional processing steps. In comparison to the above-mentioned techniques, using the methodology presented in this study, combining surfactant and gelatin, we provide a simple technique to increase mechanical strength whilst maintaining the pore size. This method does not require alteration to the composition of the external phase, or the polymerisation reaction or necessitate additional post-processing steps. Emulsions are typically metastable, stabilised by surfactants or particles to lower the interfacial tension, however, they eventually undergo phase separation. The lifetime for which an emulsion can remain stable (referred to in this study as long-term stability) depends on the formulation of the emulsion. The final "breaking" of the emulsion occurs through various mechanisms which have been widely studied such as creaming, flocculation, Ostwald ripening and coalescence (Ostwald, 1901; Friberg et al., 1976; Pays et al., 2010; McClements and Jafari, 2018).

The ability to store uncured emulsions for a long time may be beneficial for use as an inherently porous photocurable resin, allowing an emulsion to be fabricated, transported, stored and later cured into a desired shape by the end user. However, the long-term stability of polymeric emulsions can be short-lived and thus may be insufficient for this purpose (Pays et al., 2010). When 5% gelatin solution was used as the internal phase, emulsions were stable for 56 days, whereas a conventional emulsion without gelatin was unstable by day 7. Given that gelatin solution transitions to a gel state at lower temperatures, after fabrication of the emulsions at 37°C, gelatin solidifies, and therefore the droplets of the internal phase are no longer in a liquid state. Therefore, it is no longer as energetically favourable for the gelatin droplets to coalesce, and the solid droplets remain suspended and stable in the viscous emulsion, unlike a standard emulsion where both phases remain liquid. Oh et al. (2015) observed a similar effect in emulsions fabricated using a gelatin copolymer as the external phase. Following cooling of the emulsions to 4°C, the viscosity of the emulsions increased and they did not flow any more, remaining kinetically stable; this was attributed to the gelation of gelatin.

The internal phase of w/o emulsions is most commonly composed of water (Cameron, 2005), and, following this study, it may be the case that by simply substituting this water for a solution of gelatin and allowing it to cool, the storage time of these emulsions before curing could be increased. This enhanced long-term stability could also provide further opportunities for polyHIPE fabrication, such as the solidification of polyHIPEs without the need for polymerisation. Polymerisation-free polyHIPE solidification is a process based on solvent evaporation, and is usually limited by the long solidification process, which can take 24–48 h (Samanta et al., 2016; Yang et al., 2017), and thus requires stability to be maintained over this period. However, with gelatin as the internal

96

phase, stability could be maintained, even if the initial stability of the emulsion before cooling was weak.

In this study, gelatin was removed from the polyHIPEs before characterisation. We aimed to investigate how using gelatin during polyHIPE fabrication impacted the resulting structure of the polymer, rather than study the composite polymer-gelatin structure. However, for some applications, it may be beneficial to retain the gelatin within the structure, for example, if used as a bioprinting ink with the inclusion of living cells within the gelatin solution. Retaining the gelatin within polyHIPEs may have environmental applications. Gelatin has been utilised to treat wastewater used for irrigation, to prevent the accumulation of pollutant heavy metal ions in agricultural soil (Chen et al., 2014; Li et al., 2016). In this instance, amino groups in gelatin bind to the metal ions via chelation. Using gelatin as the internal phase of polyHIPEs may be a simple fabrication method to create "sponges" that can be used within wastewater filtration systems to absorb pollutants, preventing soil contamination. Furthermore, gelatin has been shown to provide a source of nitrogen, acting as a biostimulant seed treatment, improving plant performance (Wilson et al., 2018). Incorporation of gelatin within a polymer matrix such as a polyHIPE could provide ease of handling and structural integrity, as well as protect the gelatin from degradation via external factors such as UV light. Over time, the polymer would degrade, slowly releasing the gelatin in a manner which could be controlled by tailoring the degradation rate of the polymer. Whilst there are more cost-effective traditional fertilisers available, there are other beneficial factors of a polyHIPE delivery system, including, controlled release and reduction in fertiliser run-off.

Gelatin is commonly used as a coating for tissue engineering scaffolds as it contains the arginine–glycine–aspartic acid (RGD) sequence, a key molecule for the formation of interactions between integrins on the cell surface and the surrounding extracellular matrix (Kim et al., 2017). In addition, most polymers used in conventional w/o polyHIPEs are hydrophobic (Cameron, 2005), which can reduce cell adhesion on the material. These hydrophobic polymers commonly require surface modification or coating to improve their hydrophilicity (Qin et al., 2022). Gelatin is a hydrophilic molecule, and if used as the internal phase for a polyHIPE made from a hydrophobic polymer, it could potentially improve initial cell attachment, and provide a simple method for internally pre-coating the pores of a scaffold for tissue engineering purposes. In addition, the gelatin could be loaded to release bioactive factors to promote tissue-specific cellular responses such as cell proliferation and differentiation (Santoro et al., 2014).

Similarly, gelatin-loaded polyHIPEs could be used to create sustained-release drug delivery systems where the gelatin acts as a drug carrier (Milano et al., 2023) For example, Toyama et al. (2012) have performed a clinical trial using cisplatin-loaded gelatin microspheres to treat liver carcinoma, with a 100% success rate. By using emulsion templating to incorporate the gelatin into the pores of a polyHIPE, the material could be pre-loaded with gelatin. The external polymer could provide mechanical strength and stability to the drug delivery system, and the internal gelatin could provide the functional aspect of drug delivery. However, the safety and efficacy of gelatin drug delivery systems needs to be established.

6 Conclusion

In summary, in this study, we demonstrated that gelatin solution can be used as the internal phase of w/o HIPEs. The gelatin within the internal phase has the ability to stabilise the emulsion, and thus, PCL-M and PGS-M emulsions can be fabricated without the need for an additional surfactant. The resultant polyHIPEs had significantly increased pore size, which could be altered by changing the concentration of the gelatin solution. Furthermore, the utilisation of gelatin within the internal phase increased the mechanical properties of the polyHIPEs, while maintaining a high porosity of 72% and 76% for PCL-M and PGS-M respectively. Despite gelatin being a weak stabilising agent, gelatin-containing emulsions displayed improved long-term stability at room temperature compared to conventional emulsions, which we attribute to an increase in the viscosity of gelatin as a result of the gelation of gelatin at lower temperatures. These findings suggest that gelatin has great potential to be used as a stabiliser for the production of surfactant-free polyHIPEs with tuneable macroporous structures. Surfactant-free gelatin polyHIPEs may hold promise in numerous applications, and highlight the potential use of amphiphilic natural polymers as an alternative stabiliser for the generation of polyHIPE constructs with large pore structures.

Data availability statement

The raw data supporting the conclusion of this article will be made available by the authors, without undue reservation.

Author contributions

Funding

Acknowledgments

97

Conflict of interest

The authors declare that the research was conducted in the absence of any commercial or financial relationships that could be construed as a potential conflict of interest.

Publisher's note

All claims expressed in this article are solely those of the authors and do not necessarily represent those of their affiliated organizations, or those of the publisher, the editors and the reviewers. Any product that may be evaluated in this article, or claim that may be made by its manufacturer, is not guaranteed or endorsed by the publisher.

Supplementary material

The Supplementary Material for this article can be found online at: https://www.frontiersin.org/articles/10.3389/fchem.2023.1236944/full#supplementary-material

References

Aldemir Dikici, B., and Claeyssens, F. (2020). Basic principles of emulsion templating and its use as an emerging manufacturing method of tissue engineering scaffolds. *Front. Bioeng. Biotechnol.* 8, 875. doi:10.3389/fbioe.2020.00875

Aldemir Dikici, B., Dikici, S., and Claeyssens, F. (2022b). Synergistic effect of type and concentration of surfactant and diluting solvent on the morphology of emulsion templated matrices developed as tissue engineering scaffolds. *React. Funct. Polym.* 180, 105387. doi:10.1016/j.reactfunctpolym.2022.105387

Aldemir Dikici, B., Malayeri, A., Sherborne, C., Dikici, S., Paterson, T., Dew, L., et al. (2022a). Thiolene-and polycaprolactone methacrylate-based polymerized high internal phase emulsion (PolyHIPE) scaffolds for tissue engineering. *Biomacromolecules* 23 (3), 720–730. doi:10.1021/acs.biomac.1c01129

Aldemir Dikici, B., Reilly, G. C., and Claeyssens, F. (2020). Boosting the osteogenic and angiogenic performance of multiscale porous polycaprolactone scaffolds by *in vitro* generated extracellular matrix decoration. *ACS Appl. Mater Interfaces* 12 (11), 12510–12524. doi:10.1021/acsami.9b23100

Aldemir Dikici, B., Sherborne, C., Reilly, G. C., and Claeyssens, F. (2019). Emulsion templated scaffolds manufactured from photocurable polycaprolactone. *Polym. Guildf.* 175, 243–254. doi:10.1016/j.polymer.2019.05.023

Artel, A., Mehdizadeh, H., Chiu, Y. C., Brey, E. M., and Cinar, A. (2011). An agent-based model for the investigation of neovascularization within porous scaffolds. *Tissue Eng. Part A* 17 (17–18), 2133–2141. doi:10.1089/ten.tea.2010.0571

Ashrafizadeh, S. N., and Kamran, M. (2010). Emulsification of heavy crude oil in water for pipeline transportation. *J. Pet. Sci. Eng.* 71 (3–4), 205–211. doi:10.1016/j.petrol.2010.02.005

Barbetta, A., and Cameron, N. R. (2004). Morphology and surface area of emulsion-derived (PolyHIPE) solid foams prepared with oil-phase soluble porogenic solvents: Span 80 as surfactant. *Macromolecules* 37 (9), 3188–3201. doi:10.1021/ma0359436

Becerril-Rodriguez, I. C., and Claeyssens, F. (2022). Low methacrylated poly(glycerol sebacate) for soft tissue engineering. *Polym. Chem.* 13 (23), 3513–3528. doi:10.1039/d2py00212d

Bokhari, M., Carnachan, R. J., Przyborski, S. A., and Cameron, N. R. (2007). Emulsion-templated porous polymers as scaffolds for three dimensional cell culture: Effect of synthesis parameters on scaffold formation and homogeneity. *J. Mater Chem. [Internet]* 17 (38), 4088–4094. doi:10.1039/b707499a

Busby, W., Cameron, N. R., and Jahoda, C. A. B. 2001. Emulsion-Derived foams (PolyHIPEs) containing poly(ε-caprolactone) as matrixes for tissue engineering. *Biomacromolecules* 2(164):154–164. doi:10.1021/bm0000889

Cameron, N. R. (2005). High internal phase emulsion templating as a route to well-defined porous polymers. *High Intern. phase emulsion templating as a route well-defined porous Polym.* 46, 1439–1449. doi:10.1016/j.polymer.2004.11.097

Chen, G., Qiao, C., Wang, Y., and Yao, J. (2014). Synthesis of magnetic gelatin and its adsorption property for Cr(VI). *Ind. Eng. Chem. Res.* 53, 15576–15581. doi:10.1021/ie502709u

Chen, K., and Vyazovkin, S. (2009). Temperature dependence of sol-gel conversion kinetics in gelatin-water system. *Macromol. Biosci.* 9 (4), 383–392. doi:10.1002/mabi.200800214

Chen, Q., Tai, X., Li, J., Li, C., and Guo, L. (2021). High internal phase emulsions solely stabilized by natural oil-based nonionic surfactants as tea tree oil transporter. *Colloids Surfaces A Physicochem Eng. Asp.* 616, 126320. doi:10.1016/j.colsurfa.2021.126320

Choi, S. W., Yeh, Y. C., Zhang, Y., Sung, H. W., and Xia, Y. (2010). Uniform beads with controllable pore sizes for biomedical applications. *Small* 6 (14), 1492–1498. doi:10.1002/smll.201000544

Chong, P., Erable, B., and Bergel, A. (2019). Effect of pore size on the current produced by 3-dimensional porous microbial anodes: A critical review. *Bioresour. Technol.* 289, 121641. doi:10.1016/j.biortech.2019.121641

Deotale, S. M., Dutta, S., Moses, J. A., and Anandharamakrishnan, C. (2019). Coffee oil as a natural surfactant. *Food Chem.* 295, 180–188. doi:10.1016/j.foodchem.2019.05.090

Dhavalikar, P., Shenoi, J., Salhadar, K., Chwatko, M., Rodriguez-Rivera, G., Cheshire, J., et al. (2021). Engineering toolbox for systematic design of polyhipe architecture. *Polym. (Basel)* 13 (9), 1479. doi:10.3390/polym13091479

Dikici, B. A., Dikici, S., Reilly, G. C., MacNeil, S., and Claeyssens, F. (2019). A novel bilayer polycaprolactone membrane for guided bone regeneration: Combining electrospinning and emulsion templating. *Mater. (Basel)* 12 (16), 2643. doi:10.3390/ma12162643

Dikici, S., Aldemir Dikici, B., Bhaloo, S. I., Balcells, M., Edelman, E. R., MacNeil, S., et al. (2020). Assessment of the angiogenic potential of 2-deoxy-D-ribose using a novel *in vitro* 3D dynamic model in comparison with established *in vitro* assays. *Front. Bioeng. Biotechnol.* 7 (451), 451. doi:10.3389/fbioe.2019.00451

Ding, M., Zhang, T., Zhang, H., Tao, N., Wang, X., and Zhong, J. (2020). Gelatin molecular structures affect behaviors of fish oil-loaded traditional and Pickering emulsions. *Food Chem.* 309, 125642. doi:10.1016/j.foodchem.2019.125642

Duprat-De-Paule, S., Guilbot, J., Roso, A., Cambos, S., Seppic, P., and Bellini, T. (2018). Augmented bio-based lipids for cosmetics. *OCL* 25 (5), D503. doi:10.1051/ocl/2018036

Elango, R., Nadeina, A., Cadiou, F., De Andrade, V., Demortière, A., Morcrette, M., et al. (2021). Impact of electrode porosity architecture on electrochemical performances of 1 mm-thick LiFePO4 binder-free Li-ion electrodes fabricated by Spark Plasma Sintering. *J. Power Sources* 488, 229402. doi:10.1016/j.jpowsour.2020.229402

Eltom, A., Zhong, G., and Muhammad, A. (2019). Scaffold techniques and designs in tissue engineering functions and purposes: A review. *Adv. Mater Sci. Eng.* 2019, 1–13. doi:10.1155/2019/3429527

Fager, C., Gebäck, T., Hjärtstam, J., Röding, M., Olsson, A., Lorén, N., et al. (2021). Correlating 3D porous structure in polymer films with mass transport properties using FIB-SEM tomography. *Chem. Eng. Sci. X* 12, 100109. doi:10.1016/j.cesx.2021.100109

Farias, C. B. B., Almeida, F. C. G., Silva, I. A., Souza, T. C., Meira, H. M., Soares da Silva, R. de C. F., et al. (2021). Production of green surfactants: Market prospects. *Electron. J. Biotechnol.* 51, 28–39. doi:10.1016/j.ejbt.2021.02.002

Field, J., Haycock, J. W., Boissonade, F. M., and Claeyssens Tuneable, F. A. (2021). A tuneable, photocurable, poly(caprolactone)-based resin for tissue engineering—synthesis, characterisation and use in stereolithography. *Mol* 26 (5), 1199. doi:10.3390/molecules26051199

Foudazi, R. (2021). HIPEs to polyHIPEs. *React. Funct. Polym.* 164, 104917. doi:10.1016/j.reactfunctpolym.2021.104917

Friberg, S., Jansson, P. O., and Cederberg, E. (1976). Surfactant association structure and emulsion stability. *J. Colloid Interface Sci.* 55 (3), 614–623. doi:10.1016/0021-9797(76)90072-2

Gayathiri, E., Prakash, P., Karmegam, N., Varjani, S., Awasthi, M. K., and Ravindran, B. (2022). Biosurfactants: Potential and eco-friendly material for sustainable agriculture and environmental safety—a review. *Agron* 12 (3), 662. doi:10.3390/agronomy12030662

Haug, I. J., and Draget, K. I. (2009). "Gelatin," in *Handbook of hydrocolloids*. Editors G. O. Phillips and P. A. Williams (Cambridge: Woodhead Publishing Limited). Available from: https://www.academia.edu/44785184/Handbook_of_hydrocolloids_Second_edition_Edited_by

Hobiger, V., Zahoranova, A., Baudis, S., Liska, R., and Krajnc, P. (2021). Thiol-ene cross-linking of poly(ethylene glycol) within high internal phase emulsions: Degradable hydrophilic PolyHIPEs for controlled drug release. *Macromolecules* 54 (22), 10370–10380. doi:10.1021/acs.macromol.1c01240

Huš, S., and Krajnc, P. (2014). PolyHIPEs from Methyl methacrylate: Hierarchically structured microcellular polymers with exceptional mechanical properties. *Polym. Guildf.* 55 (17), 4420–4424. doi:10.1016/j.polymer.2014.07.007

98

Jackson, C. E., Ramos-Rodriguez, D. H., Farr, N. T. H., English, W. R., Green, N. H., and Claeyssens, F. (2023). Development of PCL PolyHIPE substrates for 3D breast cancer cell culture. *Bioeng* 10 (5), 522. doi:10.3390/bioengineering10050522

Jiang, B., Wang, Z., and Zhao, N. (2007). Effect of pore size and relative density on the mechanical properties of open cell aluminum foams. *Screen. Mater* 56 (2), 169–172. doi:10.1016/j.scriptamat.2006.08.070

Karim, A. A., and Bhat, R. (2009). Fish gelatin: Properties, challenges, and prospects as an alternative to mammalian gelatins. *Food Hydrocoll.* 23 (3), 563–576. doi:10.1016/j.foodhyd.2008.07.002

Kataruka, A., and Hutchens, S. B. (2019). PDMS polymerized high internal phase emulsions (polyHIPEs) with closed-cell, aqueous-filled microcavities. *Soft Matter* 15 (47), 9665–9675. doi:10.1039/c9sm01732a

Kent, P., and Saunders, B. R. (2001). The role of added electrolyte in the stabilization of inverse emulsions. *J. Colloid Interface Sci.* 242 (2), 437–442. doi:10.1006/jcis.2001.7792

Kim, A. Y., Kim, Y., Lee, S. H., Yoon, Y., Kim, W. H., and Kweon, O. K. (2017). Effect of gelatin on osteogenic cell sheet formation using canine adipose-derived mesenchymal stem cells. *Cell. Transpl.* 26 (1), 115–123. doi:10.3727/096368916X693338

Kovačič, S., Žagar, E., and Slugovc, C. (2019). Strength versus toughness of emulsion templated Poly(Dicyclopentadiene) foams. *Polym. Guildf.* 169, 58–65. doi:10.1016/j.polymer.2019.02.045

Kramer, S., Cameron, N. R., and Krajnc, P. (2021). Porous polymers from high internal phase emulsions as scaffolds for biological applications. *Polym. (Basel)* 13 (11), 1786. doi:10.3390/polym13111786

Labet, M., and Thielemans, W. (2009). Synthesis of polycaprolactone: A review. *Chem. Soc. Rev. [Internet* 38 (12), 3484–3504. doi:10.1039/b820162p

Lee, A., Elam, J. W., and Darling, S. B. (2016). Membrane materials for water purification: Design, development, and application. *Environ. Sci. Water Res. Technol.* 2 (1), 17–42. doi:10.1039/c5ew00159e

Li, B., Zhou, F., Huang, K., Wang, Y., Mei, S., Zhou, Y., et al. (2016). Highly efficient removal of lead and cadmium during wastewater irrigation using a polyethylenimine-grafted gelatin sponge. *Sci. Rep.* 6, 33573. doi:10.1038/srep33573

Lin-Gibson, S., Cooper, J. A., Landis, F. A., and Cicerone, M. T. (2007). Systematic investigation of porogen size and content on scaffold morphometric parameters and properties. *Biomacromolecules* 8 (5), 1511–1518. doi:10.1021/bm061139q

Luo, Y., Wang, A. N., and Gao, X. (2012). Pushing the mechanical strength of PolyHIPEs up to the theoretical limit through living radical polymerization. *Soft Matter* 8 (6), 1824–1830. doi:10.1039/c1sm06756g

Maksoud, F. J., Velázquez de la Paz, M. F., Hann, A. J., Thanarak, J., Reilly, G. C., Claeyssens, F., et al. (2022). Porous biomaterials for tissue engineering: A review. *J. Mater Chem. B* 10, 8111–8165. doi:10.1039/d1tb02628c

McClements, D. J., and Jafari, S. M. (2018). Improving emulsion formation, stability and performance using mixed emulsifiers: A review. *Adv. Colloid Interface Sci.* 251, 55–79. doi:10.1016/j.cis.2017.12.001

Menner, A., and Bismarck, A. (2006). New evidence for the mechanism of the pore formation in polymerising high internal phase emulsions or why polyHIPEs have an interconnected pore network structure. *Macromol. Symp.* 242 (1), 19–24. doi:10.1002/masy.200651004

Mert, H. H., and Mert, E. H. (2022). "Emulsion templated hierarchical macroporous polymers," in *Advanced functional porous materials* (Berlin, Germany: Springer), 43–86. doi:10.1007/978-3-030-85397-6_3

Milano, F., Masi, A., Madaghiele, M., Sannino, A., Salvatore, L., and Gallo, N. (2023). Current trends in gelatin-based drug delivery systems. *Pharmaceutics* 15 (5), 1499. doi:10.3390/pharmaceutics15051499

Moglia, R. S., Holm, J. L., Sears, N. A., Wilson, C. J., Harrison, D. M., and Cosgriff-Hernandez, E. (2011). Injectable polyHIPEs as high-porosity bone grafts. *Biomacromolecules* 12 (10), 3621–3628. doi:10.1021/bm2008839

Moglia, R. S., Whitely, M., Dhavalikar, P., Robinson, J., Pearce, H., Brooks, M., et al. (2014). Injectable polymerized high internal phase emulsions with rapid *in situ* curing. *Biomacromolecules* 15 (8), 2870–2878. doi:10.1021/bm500754r

Moldes, A. B., Rodríguez-López, L., Rincón-Fontán, M., López-Prieto, A., Vecino, X., and Cruz, J. M. (2021). Synthetic and bio-derived surfactants versus microbial biosurfactants in the cosmetic industry: An overview. *Int. J. Mol. Sci.* 22 (5), 2371. doi:10.3390/ijms22052371

Montanheiro, T. L. D. A., Schatkoski, V. M., de Menezes, B. R. C., Pereira, R. M., Ribas, R. G., de Freitas, A. de S. M., et al. (2022). Recent progress on polymer scaffolds production: Methods, main results, advantages and disadvantages. *Express Polym. Lett.* 16 (2), 197–219. doi:10.3144/expresspolymlett.2022.16

Mravljak, R., Božič, B., Podlogar, M., and Podgornik, A. (2022). Tubular catalytic polyHIPE reactor with deposited silver nanoplate nanoparticles. *Chem. Eng. J.* 449, 137869. doi:10.1016/j.cej.2022.137869

Murphy, A. R., Ghobrial, I., Jamshidi, P., Laslett, A., O'Brien, C. M., and Cameron, N. R. (2017). Tailored emulsion-templated porous polymer scaffolds for iPSC-derived human neural precursor cell culture. *Polym. Chem.* 8 (43), 6617–6627. doi:10.1039/c7py01375b

Nussinovitch, A., and Peleg, M. (1990). An empirical model for describing weight changes in swelling and shrinking gels. *Food Hydrocoll.* 4 (1), 69–76. doi:10.1016/s0268-005x(09)80329-9

O'Brien, F. J. (2011). Biomaterials & scaffolds for tissue engineering. *Biomaterials Scaffolds Tissue Eng.* 14, 88–95. doi:10.1016/s1369-7021(11)70058-x

Oh, B. H. L., Bismarck, A., and Chan-Park, M. B. (2015). Injectable, interconnected, high-porosity macroporous biocompatible gelatin scaffolds made by surfactant-free emulsion templating. *Macromol. Rapid Commun.* 36 (4), 364–372. doi:10.1002/marc.201400524

Ostwald, W. (1901). Blocking of Ostwald ripening allowing long-term stabilization. *Z. Für Phys. Chem.* 37, 385.

Owen, R., Sherborne, C., Paterson, T., Green, N. H., Reilly, G. C., and Claeyssens, F. (2016). Emulsion templated scaffolds with tunable mechanical properties for bone tissue engineering. *J. Mech. Behav. Biomed. Mater* 54, 159–172. doi:10.1016/j.jmbbm.2015.09.019

Pashneh-Tala, S., Owen, R., Bahmaee, H., Rekštyte, S., Malinauskas, M., and Claeyssens, F. (2018). Synthesis, characterization and 3D micro-structuring via 2-photon polymerization of poly(glycerol sebacate)-methacrylate-an elastomeric degradable polymer. *Front. Phys.* 6 (MAY), 41. doi:10.3389/fphy.2018.00041

Pays, K., Mabille, C., Schmitt, V., Leal-Calderon, F., and Bibette, J. (2010). Understanding the stability and lifetime of emulsions. *J. Dispers. Sci. Technol.* 23, 175–186. doi:10.1080/01932690208984198

Pierre, S. J., Thies, J. C., Dureault, A., Cameron, N. R., Van Hest, J. C. M., Carette, N., et al. (2006). Covalent enzyme immobilization onto photopolymerized highly porous monoliths. *Adv. Mater [Internet* 18 (14), 1822–1826. doi:10.1002/adma.200600293

Qin, X., Wu, Y., Liu, S., Yang, L., Yuan, H., Cai, S., et al. (2022). Surface modification of polycaprolactone scaffold with improved biocompatibility and controlled growth factor release for enhanced stem cell differentiation. *Front. Bioeng. Biotechnol.* 9, 802311. doi:10.3389/fbioe.2021.802311

Rai, R., Tallawi, M., Grigore, A., and Boccaccini, A. R. (2012). Synthesis, properties and biomedical applications of poly(glycerol sebacate) (PGS): A review. *Prog. Polym. Sci.* 37 (8), 1051–1078. doi:10.1016/j.progpolymsci.2012.02.001

Ravera, F., Dziza, K., Santini, E., Cristofolini, L., and Liggieri, L. (2021). Emulsification and emulsion stability: The role of the interfacial properties. *Adv. Colloid Interface Sci.* 288, 102344. doi:10.1016/j.cis.2020.102344

Rnjak-Kovacina, J., Wise, S. G., Li, Z., Maitz, P. K. M., Young, C. J., Wang, Y., et al. (2011). Tailoring the porosity and pore size of electrospun synthetic human elastin scaffolds for dermal tissue engineering. *Biomaterials* 32 (28), 6729–6736. doi:10.1016/j.biomaterials.2011.05.065

Sajjadi, S. (2006). Effect of mixing protocol on formation of fine emulsions. *Chem. Eng. Sci.* 61 (9), 3009–3017. doi:10.1016/j.ces.2005.10.071

Samanta, A., Nandan, B., and Srivastava, R. K. (2016). Morphology of electrospun fibers derived from high internal phase emulsions. *J. Colloid Interface Sci.* 471, 29–36. doi:10.1016/j.jcis.2016.03.012

Sancakli, A., Basaran, B., Arican, F., and Polat, O. (2021). Effects of bovine gelatin viscosity on gelatin-based edible film mechanical, physical and morphological properties. *SN Appl. Sci.* 3 (1), 8–11. doi:10.1007/s42452-020-04076-0

Santoro, M., Tatara, A. M., and Mikos, A. G. (2014). Gelatin carriers for drug and cell delivery in tissue engineering. *J. Control Release* 190, 210–218. doi:10.1016/j.jconrel.2014.04.014

Sengokmen-Ozsoz, N., Boston, R., and Claeyssens, F. (2023). Investigating the potential of electroless nickel plating for fabricating ultra-porous metal-based lattice structures using PolyHIPE templates. *ACS Appl. Mater Interfaces* 15, 30769–30779. doi:10.1021/acsami.3c04637

Sharma, V., Agrawal, A., Singh, O., Goyal, R., Sarkar, B., Gopinathan, N., et al. (2022). A comprehensive review on the synthesis techniques of porous materials for gas separation and catalysis. *Can. J. Chem. Eng.* 100 (9), 2653–2681. doi:10.1002/cjce.24507

Sherborne, C., and Claeyssens, F. (2021). Considerations using additive manufacture of emulsion inks to produce respiratory protective filters against viral respiratory tract infections such as the COVID-19 virus. *Int. J. Bioprinting* 7 (1), 316. doi:10.18063/ijb.v7i1.316

Silverstein, M. S. (2014). PolyHIPEs: Recent advances in emulsion-templated porous polymers. *Prog. Polym. Sci.* 39 (1), 199–234. doi:10.1016/j.progpolymsci.2013.07.003

Singh, D., Harding, A. J., Albadawi, E., Boissonade, F. M., Haycock, J. W., and Claeyssens, F. (2018). Additive manufactured biodegradable poly(glycerol sebacate methacrylate) nerve guidance conduits. *Acta Biomater.* 78, 48–63. doi:10.1016/j.actbio.2018.07.055

Sun, P., Yang, S., Sun, X., Wang, Y., Jia, Y., Shang, P., et al. (2019). Preparation of PolyHIPE scaffolds for 3D cell culture and the application in cytotoxicity evaluation of cigarette smoke. *Polym. (Basel)* 11 (6), 959. doi:10.3390/polym11060959

Tian, Y., Zhou, J., He, C., He, L., Li, X., and Sui, H. (2022). The Formation, stabilization and separation of oil–water emulsions: A review. *Process* 10(4):738. doi:10.3390/pr10040738

99

Toyama, T., Nitta, N., Ohta, S., Tanaka, T., Nagatani, Y., Takahashi, M., et al. (2012). Clinical trial of cisplatin-conjugated gelatin microspheres for patients with hepatocellular carcinoma. *Jpn. J. Radiol.* 30 (1), 62–68. doi:10.1007/s11604-011-0010-2

Vásquez, L., Davis, A., Gatto, F., Ngoc An, M., Drago, F., Pompa, P. P., et al. (2021). Multifunctional PDMS polyHIPE filters for oil-water separation and antibacterial activity. *Sep. Purif. Technol.* 255, 117748. doi:10.1016/j.seppur.2020.117748

Venkataramani, D., Tsulaia, A., and Amin, S. (2020). Fundamentals and applications of particle stabilized emulsions in cosmetic formulations. *Adv. Colloid Interface Sci.* 283, 102234. doi:10.1016/j.cis.2020.102234

Vogt, L., Ruther, F., Salehi, S., and Boccaccini, A. R. (2021). Poly(Glycerol sebacate) in biomedical applications—a review of the recent literature. *Adv. Healthc. Mater [Internet]* 10 (9), 2002026. doi:10.1002/adhm.202002026

Wang, Z., Yao, S., Song, K., Gong, X., Zhang, S., Gao, S., et al. (2020). A bio-based benzoxazine surfactant from amino acids. *Green Chem. [Internet]* 22 (11), 3481–3488. doi:10.1039/d0gc00218f

Wilson, H. T., Amirkhani, M., and Taylor, A. G. (2018). Evaluation of gelatin as a biostimulant seed treatment to improve plant performance. *Front. Plant Sci.* 9, 1006. doi:10.3389/fpls.2018.01006

Woodward, R. T., Jobbe-Duval, A., Marchesini, S., Anthony, D. B., Petit, C., and Bismarck, A. (2017). Hypercrosslinked polyHIPEs as precursors to designable, hierarchically porous carbon foams. *Polym. Guildf.* 115, 146–153. doi:10.1016/j.polymer.2017.03.042

Wu, R., Menner, A., and Bismarck, A. (2010). Tough interconnected polymerized medium and high internal phase emulsions reinforced by silica particles. *J. Polym. Sci. Part A Polym. Chem.* 48, 1979–1989. doi:10.1002/pola.23965

Yang, T., Hu, Y., Wang, C., and Binks, B. P. (2017). Fabrication of hierarchical macroporous biocompatible scaffolds by combining pickering high internal phase emulsion templates with three-dimensional printing. *ACS Appl. Mater Interfaces* 9, 22950–22958. doi:10.1021/acsami.7b05012

Zhang, T., and Guo, Q. (2017). Continuous preparation of polyHIPE monoliths from ionomer-stabilized high internal phase emulsions (HIPEs) for efficient recovery of spilled oils. *Chem. Eng. J.* 307, 812–819. doi:10.1016/j.cej.2016.09.024

Zhang, T., Xu, J., Zhang, Y., Wang, X., Lorenzo, J. M., and Zhong, J. (2020). Gelatins as emulsifiers for oil-in-water emulsions: Extraction, chemical composition, molecular structure, and molecular modification. *Trends Food Sci. Technol.* 106, 113–131. doi:10.1016/j.tifs.2020.10.005

100

CHAPTER 4. Gelatin-containing Porous Polycaprolactone PolyHIPEs as Substrates for 3D Breast Cancer Cell Culture and Vascular Infiltration

Supplementary information for this article is available in Appendix B.

frontiers | Frontiers in Bioengineering and Biotechnology

Gelatin-containing porous polycaprolactone PolyHIPEs as substrates for 3D breast cancer cell culture and vascular infiltration

Caitlin E. Jackson[1,2], Iona Doyle[1], Hamood Khan[1],
Samuel F. Williams[3], Betül Aldemir Dikici[4],
Edgar Barajas Ledesma[5], Helen E. Bryant[6], William R. English[7],
Nicola H. Green[1,2] and Frederik Claeyssens[1,2]*

[1]The Kroto Research Institute, Materials Science and Engineering, University of Sheffield, Sheffield,
United Kingdom, [2]Insigneo Institute for in Silico Medicine, The Pam Liversidge Building, University of
Sheffield, Sheffield, United Kingdom, [3]Department of Infection, Immunity and Cardiovascular Disease,
Royal Hallamshire Hospital, The University of Sheffield, Sheffield, United Kingdom, [4]Department of
Bioengineering, Izmir Institute of Technology, Urla, Türkiye, [5]Department of Chemistry, The University of
Sheffield, Sheffield, United Kingdom, [6]School of Medicine and Population Health, University of Sheffield,
Sheffield, United Kingdom, [7]Norwich Medical School, University of East Anglia, Norwich, United Kingdom

Tumour survival and growth are reliant on angiogenesis, the formation of new blood vessels, to facilitate nutrient and waste exchange and, importantly, provide a route for metastasis from a primary to a secondary site. Whilst current models can ensure the transport and exchange of nutrients and waste via diffusion over distances greater than 200 μm, many lack sufficient vasculature capable of recapitulating the tumour microenvironment and, thus, metastasis. In this study, we utilise gelatin-containing polymerised high internal phase emulsion (polyHIPE) templated polycaprolactone-methacrylate (PCL-M) scaffolds to fabricate a composite material to support the 3D culture of MDA-MB-231 breast cancer cells and vascular ingrowth. Firstly, we investigated the effect of gelatin within the scaffolds on the mechanical and chemical properties using compression testing and FTIR spectroscopy, respectively. Initial *in vitro* assessment of cell metabolic activity and vascular endothelial growth factor expression demonstrated that gelatin-containing PCL-M polyHIPEs are capable of supporting 3D breast cancer cell growth. We then utilised the chick chorioallantoic membrane (CAM) assay to assess the angiogenic potential of cell-seeded gelatin-containing PCL-M polyHIPEs, and vascular ingrowth within cell-seeded, surfactant and gelatin-containing scaffolds was investigated via histological staining. Overall, our study proposes a promising composite material to fabricate a substrate to support the 3D culture of cancer cells and vascular ingrowth.

102

1 Introduction

Angiogenesis is the process through which new vasculature is formed from an existing network and is a key process to ensure cell survival and maintenance, facilitating oxygen and nutrient delivery, and waste removal (Adair and Montani, 2010; Rouwkema and Khademhosseini, 2016). Moreover, angiogenesis is critical for tumour survival, maintenance and growth, as well as providing a route for cancer cell metastasis (Nishida et al., 2006; Lugano et al., 2020). However, many current *in vitro* models lack sufficient vasculature to fully recapitulate tumour-driven angiogenesis, tumour growth and metastasis. Therefore, there is a need to design improved *in vitro* culture substrates to support tumour cell culture and growth whilst additionally facilitating tumour-driven angiogenesis and vascular ingrowth.

Substrates for *in vitro* culture are commonly fabricated using polymers, either natural or synthetic (Langer and Tirrell, 2004; Kohane and Langer, 2008; Place et al., 2009). Whilst natural polymers, such as collagen and Matrigel, better recapitulate the architecture of the microenvironment (Habanjar et al., 2021) and lend themselves to optical microscopy analysis techniques better than synthetic polymers, they are often fabricated as hydrogels, and as such, the resultant mechanical properties of the gels can cause challenges in scaffold handling. Synthetic polymers can be fabricated consistently, at low cost, are easier to produce and can often be chemically or mechanically tuned, producing scaffolds which can be easily handled (Rijal et al., 2017; Donnaloja et al., 2020; Reddy et al., 2021). Thus, a substrate fabricated with a combination of natural and synthetic polymers could provide a better solution for improved *in vitro* cell culture, resulting in a substrate which has architecture recognisable by cells whilst still easily handled.

We have previously reported on the use of gelatin to both chemically and mechanically tune porous polymer substrates (Furmidge, 2023). Gelatin is a biodegradable and biocompatible polymer with low toxicity that is a molecular derivative of type I collagen, therefore, it has the capability to biologically perform similarly to collagen and is a suitable substitute (Bello et al., 2020). Furthermore, gelatin is readily available, can be extracted from multiple sources and is more cost-effective than extracellular matrix (ECM) proteins such as collagen, laminin and fibronectin (Bello et al., 2020; Lukin et al., 2022).

Due to the amphiphilic properties of gelatin, it has been previously utilised as a surfactant, albeit a weak surfactant and is capable of stabilising emulsions (Aldemir Dikici and Claeyssens, 2020; Zhang et al., 2020; Furmidge et al., 2023) via lowering the interfacial energy of the oil-water interface.

Our previous study demonstrated how the inclusion of gelatin within the internal phase of PCL polyHIPEs led to a significant increase in pore size of the resulting scaffold (Table 1) (Furmidge et al., 2023). Thus, we hypothesised that such increases in the pore size could enable increased vessel ingrowth. Therefore, this study investigates the use of gelatin-containing polyHIPEs as a substrate to support 3D breast cancer cell growth and facilitate angiogenesis. We initially assessed the impact of gelatin within the scaffold on mechanical properties and the cancer cell metabolic activity before using the pre-existing vascular network from an *ex ovo* chick chorioallantoic membrane (CAM) assay to assess the vascular ingrowth of the CAM vessels. Furthermore, we combined 3D cancer cell culture on the substrates as a tumour tissue mimic within the CAM assay, assessing the validity of our approach using a porous polymer substrate to recapitulate angiogenesis surrounding tumour tissue.

2 Materials

Photoinitiator (2,4,6-Trimethylbenzoyl Phosphine Oxide/2-Hydroxy-2- Methylpropiophenone blend), Dulbecco's modified Eagle media (DMEM), fetal bovine serum (FBS), pencillin/streptomycin (PS), L-glutamine, trypsin, formaldehyde, resazurin sodium salt, type A gelatine from porcine skin, isopentane and haematoxylin solution were purchased from Sigma Aldrich. Chloroform, toluene, ethanol, acetone and methanol were purchased from Fisher Scientific. The surfactant, Hypermer B246 was received as a sample from Croda (Goole, United Kingdom). The optimal cutting temperature-tissue freezing medium (OCT-TFM) was purchased from CellPath, the VectaMount aqueous mounting medium was purchased from Vector and the eosin solution was purchased from Acros Organics. High molecular weight 4-arm methacrylated polycaprolactone (PCL-M, 20,331 g/mol, 95% methacrylated) was synthesised in the laboratory [a general synthesis method is given in Aldemir Dikici et al. (2019)].

3 Methods

3.1 PCL-M PolyHIPE fabrication

0.4 g PCL-M and 10 wt% surfactant were heated to melt the surfactant and PCL-M. 0.6 g of 60 wt% chloroform and 40 wt% toluene solvent mixture and 0.03 g photoinitiator were added to the PCL-M-surfactant mixture respectively. The contents were mixed (250 rpm) using a magnetic stirrer (20 mm × 7 mm) for 3 min at 37°C. Once homogeneous, 2 mL of the internal phase (water or 5% gelatin solution prepared with water (wt/v)) was added dropwise and the emulsion was mixed for 5 min. Three compositions were prepared: i) 10 wt% surfactant with water as an internal phase

TABLE 1 The pore size (Furmidge et al., 2023) and stiffness of PCL-M polyHIPEs fabricated with different combinations of 10% surfactant and 5% gelatin (mean ± SD).

PCL-M PolyHIPE	Pore size (µm) (Furmidge et al., 2023)	Stiffness (MPa)
G0S10	53 ± 19	0.91 ± 0.23
G5S10	39 ± 24	2.68 ± 0.60
G5S0	80 ± 43	1.52 ± 0.20

103

(G0S10), ii) 10 wt% surfactant with 5% gelatin solution as an internal phase (G5S10) and iii) 0 wt% surfactant with 5% gelatin solution as an internal phase (G5S0).

3.2 Polymerisation of PCL-M HIPEs

Emulsions were polymerised in a transparent 2 mL syringe. All samples were cured using ultraviolet (UV) light for 5 min on both sides using the OmniCure Series 1,000 system (100 W, Lumen Dynamics, Canada), with 18 W/cm² reported light density and spectral output from 250–600 nm. The resulting polyHIPEs were removed from the syringe and washed in 100% ethanol for 24 h before washing in 70% ethanol for 48 h, changing the ethanol after each 24 h period. Following this, ethanol was gradually replaced with deionised water for 3 days, changing the water after each 24 h period. All polyHIPE samples were washed and stored in dH_2O at room temperature.

3.3 Mechanical characterisation

The compressive modulus of the PCL-M polyHIPEs was calculated by compressive mechanical testing (MultiTest 2.5–dv, Mecmesin, Slinford, United Kingdom), using the 250 N load cell at room temperature. Samples were cut into approximately 1 cm cylinders using a scalpel and placed between two compression plates. The compressive tests were performed on each sample at a rate of 1 N/s until the maximum load of 250 N was reached. The stiffness was calculated from the gradient of the initial linear region of the stress-strain curve for each sample.

3.4 Chemical characterisation using fourier transform infrared spectroscopy (FTIR)

Measurements were collected using an Agilent 4300 spectrometer fitted with a diamond 3-Bounce-2-Pass attenuated total reflection (ATR) crystal and a mercury cadmium telluride detector (Agilent Technologies, Santa Clara CA, United Kingdom). Data between 4000 cm^{-1} and $1,000 \text{ cm}^{-1}$ was obtained by collecting 32 scans at 4 cm^{-1} resolution. All spectra were normalised to the PCL peak (1722 cm^{-1}). Spectral processing was conducted using Spectragryph (v1.2.15, 2020).

3.5 General cell culture

MDA-MB-231 cells (Aldrich, 2023) were used to evaluate the proliferation of cancer cells within gelatin-containing PCL-M polyHIPEs. The MDA-MB-231 cells were purchased from Merck (ECACC) and transduced to express luciferase2 and mStrawberry by transfection with a transposon and the transposase PiggyBac using methodology developed previously (English et al., 2017). The cells were transduced and selected with puromycin and stocks frozen within 5 passages and then used within 30 passages of receipt from ECACC. The cells were thawed, transferred to media (DMEM supplemented with 10% FBS, 1% PS, 1% L-glutamine) and centrifuged at 95 g for 5 min. The cell pellet was resuspended in

fresh media with 1 μg/mL puromycin and cultured until 90% confluence with media changes every 3 days. Puromycin was removed from the media 24 h before each experiment.

3.6 MDA-MB-231 cell seeding on PCL-M polyHIPE scaffolds

To initially characterise cell-scaffold interactions, polyHIPE discs (8 mm diameter and 1 mm depth) were used. To sterilise, all scaffolds were washed in ethanol followed by dH_2O. Once reaching 90% confluency, cells were detached from the cell culture flask using trypsin. After 4 min the trypsin was neutralised with cell culture media (ratio of 1:2 respectively), followed by centrifugation ($95 \times g$ for 5 min) and resuspended in fresh media before counting using the trypan blue exclusion method to assess cell viability. For cell viability and CAM assays, 25 μL of MDA-MB-231 cells at 2×10^6 cells/mL were transferred onto each scaffold and left for 30 min in the incubator ($37°C$ and 5% CO_2) to allow for cell attachment. After 30 min, fresh media was placed in each well and incubated for 7 days with fresh media replaced every 2–3 days.

3.7 Cell viability on PCL-M polyHIPE scaffolds

The viability of cells on the scaffold was assessed using the resazurin reduction (RR) assay. 1 mM resazurin stock solution was diluted in cell culture media to form a 10% v/v resazurin working solution. The media was removed and discarded from each well and a further 0.5 mL of the working solution was added to each well. The well plate was protected from light and incubated for 4 h at $37°C$. An orbital rocker (30 rpm) was used in the incubator to ensure full penetration of the resazurin working solution. 150 μL was taken, in triplicate, from each scaffold and transferred to a 96 well plate. A fluorescence microplate reader (BioTek FLx800, Agilent BioTek, Santa Clara, CA, United States) was used to read the fluorescence of each well at an excitation wavelength of 540 nm and an emission wavelength of 630 nm. The working solution was removed from the scaffolds, and each scaffold was further washed with PBS three times before adding fresh cell culture media and continuing incubation. The assay was performed at days 1, 3 and 7.

3.8 VEGF ELISA

The concentration of VEGF in the supernatant of cell-seeded scaffolds was determined using the Human VEGF ELISA kit, according to the manufacturer's instructions (Abcam, United Kingdom). The optical density was measured on an absorbance microplate reader (BioTek ELx800, Agilent BioTek, Santa Clara, CA, United States) set to 450 nm.

3.9 CAM assay

The *ex ovo* CAM assay, as described by Mangir et al. (2019) was used to study the vascularisation of gelatin-containing, cell-seeded

104

polyHIPEs. Briefly, pathogen-free fertilised eggs (*Gallus domesticus*), obtained from Med Eggs (Fakenham, United Kingdom), were cleaned with 20% v/v industrial methylated spirits (IMS) before incubating in humidified (45%) hatching incubators (Rcom King Suro Max-20, P&T Poultry, Powys, Wales) at 38°C and for 3 days. After 3 days the eggs were cracked into sterile 100 mL weigh boats with 3 mL of PBS + 1% v/v penicillin–streptomycin solution (100 IU/mL–100 mg/mL) (Supplementary Figure S1). The eggs were further incubated at 38°C in a cell culture incubator (Binder, Tuttlingen, Germany). At day 7 of embryonic development, 500 μm polyHIPE discs sectioned using a vibratome (5100 mz, Campden Instruments, Loughborough, United Kingdom), seeded as described in Section 3.6, were implanted within the boundaries of the CAM and incubated for a further 6 days. The scaffolds were placed with the non-seeded surface in contact with the CAM to create a chemotactic gradient through the polyHIPE scaffold from the CAM surface. At day 13 of embryonic development, the CAM was imaged using a digital camera and MicroCapture software (version 2.0). Body lotion (Extracts, Tesco, Welwyn Garden City, UK) was injected into the surrounding area of the sample to provide contrast between blood vessels and the sample (Supplementary Figure S2). Following imaging, all embryos were sacrificed by the end of day 13 of embryonic development. Within each condition, initially 8 scaffolds were placed within the boundary of the CAM of individual eggs. This allowed for compensation when the foetus became unviable or for when the scaffold was not in an optimal position for imaging and analysis following the growth of the foetus. For each condition, the 3 scaffolds which were most optimally positioned were used for image analysis and data collection.

3.10 Morphometric quantification of the angiogenesis

Three images from each group were quantified using IKOSA software (CAM Assay, KML Vision GmbH) to assess the total vessel length and area and the number of branching points. Furthermore, a modified version of a well-established method (Barnhill and Ryan, 1983; Eke et al., 2017; Mangir et al., 2019; Dikici et al., 2020; Dikici et al., 2021) was used to assess the number of vessels. Briefly, the following parameters were set to all images in Adobe Photoshop (PS) to improve the ability to discern between the blood vessels; brightness and contrast; −50/10, unsharp; 50/10/0, smart sharpen; 100/5 with Gaussian blur, reduced noise; 5/0/0/50, contrast; 100, and contrast; 20-100. A new layer was created in PS, and all discernible vessels touching the scaffolds were drawn digitally using a Wacom Intuos Pro Medium Tablet with a 2 pixels size-hard round brush. The number of blood vessels was calculated by counting the total count of the vessels touching the border of the scaffolds (Aldemir Dikici et al., 2020).

3.11 Haematoxylin and Eosin (H&E) staining

On day 13, following the CAM assay the polyHIPE scaffolds and a surrounding area of tissue were excised from the membrane and were fixed with 3.7% w/v formaldehyde for 30 min at room temperature. The samples were further washed with PBS and stored in 70% ethanol. The excess CAM tissue was trimmed from the edges of the scaffold, and the scaffold was sectioned into 2 semi-circular sections before placing the sections in the cryo-mould with OTC-TFM and freezing in isopentane. The cryo-moulds were placed in liquid nitrogen for 7 min before sectioning on a cryostat (CM 1900, Leica, Germany), 16 μm slices were mounted onto the surface of Thermo SuperFrost® Plus slides. For H&E staining, samples were air dried for 2 h before freezing in a 50% v/v acetone and methanol mixture for 15 min. The slides were washed in PBS for 1 min followed by a wash in H_2O for 3 min. Slides were stained in haematoxylin for 15 s, rinsed for 10 min in H_2O and dehydrated in 70% and 90% ethanol for 1 min each. Slides were further stained in eosin for 8 s before washing in 100%, 95% and 70% ethanol for 1 min each and mounted using aquamount medium.

3.12 Statistical analysis

Statistical analysis was carried out using the analysis software GraphPad Prism (Version 9.4.1, CA, United States). All data was analysed using one-way or two-way analysis of variance (ANOVA) followed by Dunnett T3 ($n < 50$) multiple comparisons test. Error bars on graphs indicate standard deviation, and all n values are given in figure captions where relevant. Statistical significance on graphs is represented as p-value < 0.033 (*), 0.002 (**) and 0.001 (***).

4 Results

4.1 Mechanical characterisation

The compression tests were conducted under wet conditions, in which the scaffolds had been washed and pre-soaked in deionised water before the experiment. The inclusion of gelatin within the internal phase of the polyHIPE resulted in a significant increase in stiffness independent of whether the scaffold was fabricated with additional surfactant (Table 1; Figure 1A). The stress-strain curves of the gelatin-containing scaffolds demonstrated a deviation in the curve at ~60% strain, resulting in an S-shaped curve compared to the smooth J-shaped curve observed in the control surfactant-only polyHIPE (G0S10) (Figure 1B).

4.2 Biological characterisation

Attenuated total reflection Fourier transform infrared (ATR-FTIR) spectroscopy was used to verify the presence of gelatin in the scaffolds post-processing and before cell seeding. The spectra of all PCL-M polyHIPE samples show characteristic bands for 4 arm PCL, observed at 2,940 cm^{-1} and 2,860 cm^{-1} (Figure 2A), caused by asymmetric and symmetric CH_2 stretching, respectively. The fingerprint region also shows strong absorption peaks attributed to PCL at 1722 cm^{-1} (ester carbonyl stretching), 1,290 cm^{-1} (C-O and C-C stretching), 1,240 cm^{-1}, (asymmetric C-O-C stretching) and 1,170 cm^{-1} (symmetric C-O-C stretching). Furthermore, the fingerprint region of the spectra of the gelatin-containing polyHIPEs (G5S10 and G5S0) also include peaks at 1,630 cm^{-1} (C=O stretching vibration), corresponding to the amide I band.
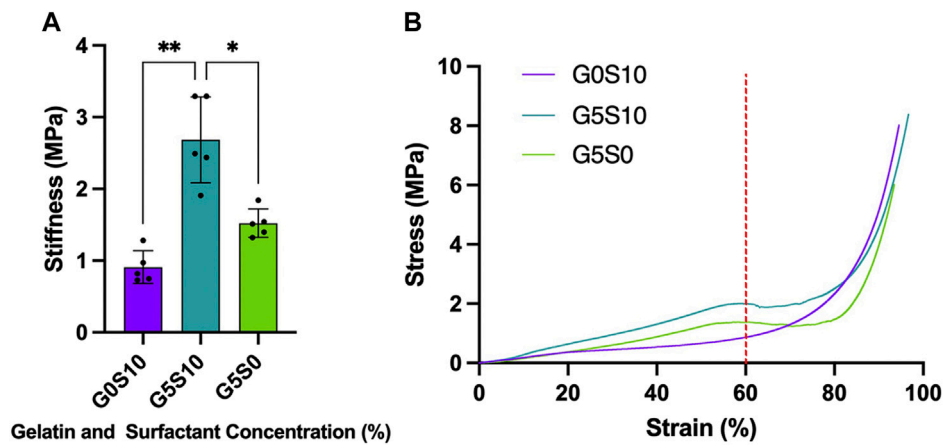
FIGURE 1
Stiffness of PCL-M polyHIPEs fabricated with different combinations of 10% surfactant and 5% gelatin displaying **(A)** the mean stiffness $\pm$ SD (n = 5, * p < 0.033, ** p < 0.002) and **(B)** representative stress-strain curves of each PCL-M polyHIPE condition (red dotted line indicates 60% strain).
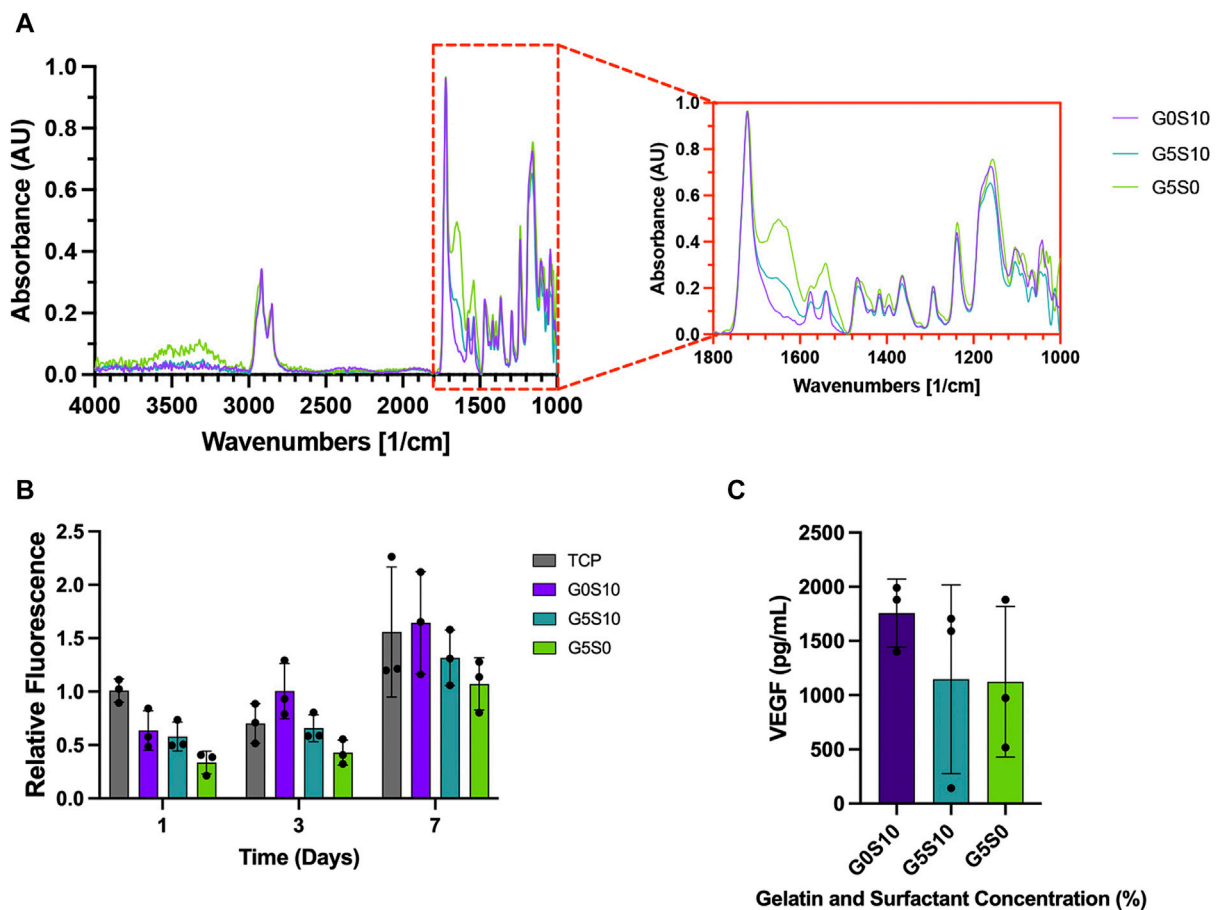

FIGURE 2
Chemical and biological assessment of PCL−M polyHIPEs containing gelatin. **(A)** The mid-infrared spectrum of PCL-M polyHIPEs containing gelatin, the red callout indicates the fingerprint region. **(B)** The metabolic activity of MDA-MB-231 cells via a resazurin reduction assay across 7 days (mean $\pm$ SD, N = 3, n = 3). **(C)** The concentration of VEGF expressed by MDA-MB-231 cells following 7 days of culture on PCL-M polyHIPEs containing gelatin (mean $\pm$ SD, N = 3, n = 2).

106

FIGURE 3

Assessment of the angiogenic potential of PCL-M polyHIPEs. **(A)** Digital Images of surfactant-only (G0S10), surfactant and gelatin-containing (G5S10) and gelatin-only (G5S0) PCL-M polyHIPEs prepared in control (PBS soaked), media soaked and cell seeded conditions on chick chorioallantoic membrane (CAM) at day 13 (scalebar represents 5 mm) with quantitative assessment describing **(B)** the total vessel area, **(C)** the total vessel length, **(D)** the number of branching points and **(E)** the number of blood vessels surrounding the PCL-M polyHIPE scaffolds (Mean $\pm$SD, $N = 3$).

The intensity of the amide I bands is higher and more prominent in the spectrum of the gelatin-only PCL-M polyHIPE.

A 7-day resazurin reduction assay was utilised to assess the metabolic activity of MDA-MB-231 cells on PCL-M scaffolds containing gelatin. There was a significant increase in metabolic activity across the 7-day period for all PCL-M polyHIPE scaffolds (Figure 2B). Furthermore, at each time point, there was no significant difference between the PCL-M polyHIPE scaffolds and
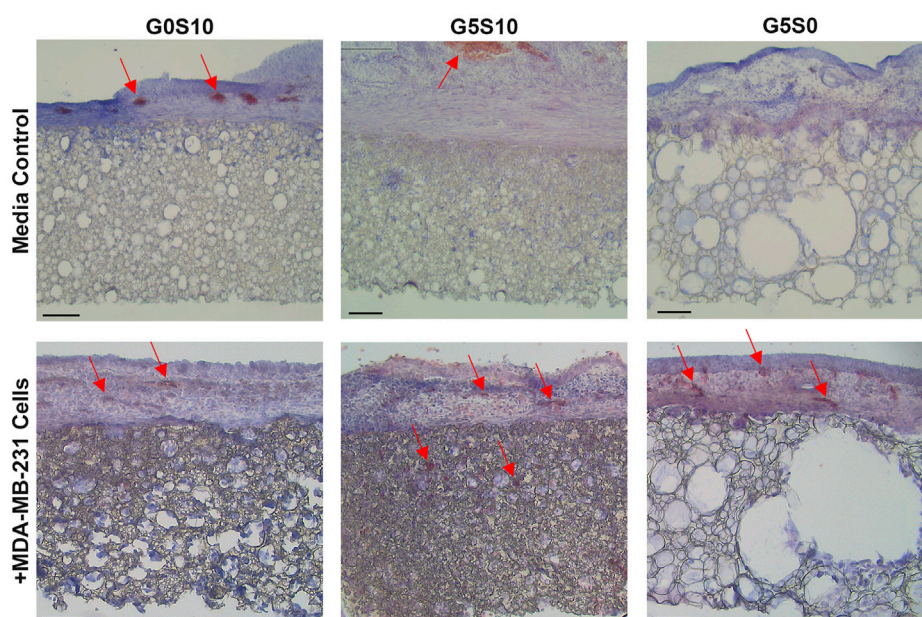
107

FIGURE 4
Haematoxylin and Eosin staining to analyse the angiogenic potential of surfactant-only (G0S10), surfactant and gelatin-containing (G5S10) and gelatin-only (G5S0) PCL-M polyHIPEs prepared in media soaked and cell-seeded conditions on chick chorioallantoic membrane (CAM) at day 13 (scalebar represents 100 μm, red arrows indicate blood vessels).

the control condition (tissue culture plastic, TCP). A VEGF ELISA was used to quantify the concentration of VEGF expressed by MDA-MB-231 cells following 7 days of culture on PCL-M polyHIPEs. There was no significant difference in the expression of VEGF between the different PCL-M polyHIPEs containing gelatin ± surfactant and standard surfactant-only PCL-M polyHIPEs (Figure 2C).

4.3 Ex ovo chorioallantoic membrane assay to assess angiogenic potential

The *ex ovo* CAM assay was utilised to assess the angiogenic potential of PCL-M polyHIPEs seeded with MDA-MB-231 breast cancer cells. Visually, we observed no negative impact of the gelatin-containing scaffolds ± cancer cells on the viability of the chick embryos or vascular network (Figure 3A). We observed increased directionality of the vessels towards the scaffold when seeded with MDA-MB-231 cells. To further investigate this finding, we quantified the vessels, defining the total vessel area and length, number of branching points and the number of vessels surrounding the scaffolds. There was no significant difference in the total vessel area and length or number of branching points between the conditions (Figures 3B–D). There was a significant increase in the number of vessels surrounding the scaffold gelatin-only cell-seeded polyHIPE compared to the surfactant-containing cell-seeded polyHIPEs (Figure 3E).

Haematoxylin and Eosin (H&E) staining was used to further assess the integration of the CAM vasculature within the gelatin-containing PCL-M polyHIPEs (Figure 4). Blood vessels (indicated by red arrows) were observed in the CAM tissue on the polyHIPE

scaffolds, with more vessels present in the CAM tissue on the cell-seeded gelatin-containing scaffolds. Moreover, additional blood vessels were observed within the cell-seeded surfactant and gelatin-containing polyHIPE scaffolds.

5 Discussion

Within this study, we demonstrate the use of gelatin-containing PCL-M polyHIPEs that can support 3D breast cancer cell culture, whilst maintaining the key functionality of expressing vascular endothelial growth factor (VEGF) to promote angiogenesis. We used an *ex ovo* CAM assay to validate the capability of these gelatin-containing cell-seeded polyHIPEs for vascular ingrowth. Our study presents a potential substrate, with tuneable mechanical properties for use within microphysiological systems (MPS) that can successfully support 3D breast cancer cell culture and vascular ingrowth.

Firstly, we assessed the stiffness of the polyHIPE scaffolds to better understand the mechanical environment around the cells cultured within the substrates. We assessed the stiffness of the polyHIPEs in wet conditions with gelatin remaining in the scaffold to be more physiologically relevant, as has been discussed in previous studies (Aldemir Dikici et al., 2019; Jackson et al., 2023). Interestingly, when compared to our previous study in which PCL-M polyHIPE constructs were compressed in dry conditions with the gelatin removed prior to testing, we observe little difference in the stiffness of the resulting polyHIPEs (Figure 1A). Therefore, this suggests that the fabrication technique, utilising gelatin in the internal phase and the resulting effect it has on the polyHIPE structure is responsible for the change

in stiffness rather than the condition of the scaffolds during testing (wet/dry ± gelatin).

When further analysing the stress-strain curves, all the polyHIPE samples demonstrated typical linear elastic behaviour at low strain with a final region of rapidly increasing stress at high strain, this is likely due to material densifying (Sun et al., 2016). The standard surfactant-only PCL-M polyHIPE displayed standard viscoelastic behaviour, as observed in our previous study (Furmidge et al., 2023). However, the addition of gelatin into the scaffolds alters the response of the polyHIPE to compressive loads, observing a deviation in the curve at 60% strain before increasing to a maximum (Figure 1B). The S-shaped curve observed, indicates elastic instability. Up to 60% strain we observed the stiffness due to the composition of the pores and the gelatin which results in a higher stiffness than the surfactant PCL-M polyHIPE (G0S10). 60%–75% strain is where we observed elastic instability, this is likely due to the gelatin being extruded from scaffold through the collapsed pores. We observed this difference visually, finding that the gelatin-containing polyHIPEs structurally failed following compression, with large sections of gelatin protruding from the broken body of the scaffold compared to surfactant-only polyHIPEs, which remained intact (Supplementary Figure S3). Moreover, gelatin has its own viscoelastic properties which differ from PCL-M, and as such, this may introduce a difference in energy dissipation and the resulting deformation (Guarino et al., 2017; Moučka et al., 2023). At 75% strain onwards the stiffness observed is due to the bulk of the PCL-M in which the gelatin-containing polyHIPE scaffolds demonstrate a similar stiffness to surfactant-only PCL-M polyHIPE scaffolds. In our previous study, compression of gelatin polyHIPE constructs in which the gelatin was removed prior to compression testing did not result in the S-shaped curve observed in this study (Furmidge et al., 2023). This would further suggest it is the gelatin remaining in the scaffold that causes the complex response to the compression rather than any physical changes to the structure of the polyHIPE when using a gelatin solution as the internal phase.

To ensure the presence of gelatin within the scaffolds following the post-processing washing steps and prior to cell seeding we used ATR-FTIR to identify the attributed peaks (Figure 2A). In both samples containing gelatin, amide I peaks were evident and interestingly, sample G5S0 shows the highest absorption in this region, which ties well with the fact that this sample contains gelatin only. Gelatin is widely used in biomaterials due to its cell adhesive properties and capability to provide a more ECM-like environment for cell growth (Bello et al., 2020; Lukin et al., 2022; Asim et al., 2023). Interestingly, the presence of gelatin did not have any significant effect on the metabolic activity of the cells compared to the surfactant-only polyHIPE (Figure 2B), these finding are similar to previous studies in which common coating techniques, such as fibronectin and plasma coating did not yield any significant improvement in 3D cell culture within PCL-M polyHIPEs (Dikici et al., 2019; Jackson et al., 2023). In this study the potential improvement in cell attachment might be mitigated by the lower amount of surface area or the potential for the cells to fall through the pores when being seeded in the larger pore scaffolds. However, this technique, which utilises a cost-effective, biocompatible protein, provides a simple and effective method to alter pore size and stiffness whilst supporting 3D cell culture. Thus, these scaffolds could be used in combination with each other within an MPS cancer model to

achieve a diverse range of mechanical cues and environments to influence different stages of the metastatic cascade.

Vascular endothelial growth factor (VEGF) is a factor secreted by tumour cells, including the MDA-MB-231 breast cancer cell line used in this study. Expression of VEGF is a key factor for angiogenesis, promoting the proliferation of vascular endothelial cells. Using a VEGF ELISA kit, we confirmed the expression of VEGF from MDA-MB-231 cells cultured on surfactant-only and gelatin-containing PCL-M polyHIPEs (Figure 2C). There is variation within these results, and it is most likely due to the inefficiency of cell adhesion which arises from using a manual seeding technique. Further improvements in the seeding technique using automation would be beneficial in the future to reduce such variability. The concentration of VEGF expressed is comparable with previous studies which have used similar cell numbers (Matsui et al., 2008; Sohn et al., 2018). This further suggests that PCL-M polyHIPEs (surfactant-only and gelatin-containing) are suitable substrates for 3D cell culture of breast cancer.

It is well documented in the literature that gelatin is a suitable biomaterial to replicate the mechanical properties of breast tissue and has been commonly used to fabricate breast tissue phantoms (McGarry et al., 2020; Cannatà et al., 2021; Amiri et al., 2022). Therefore, whilst the stiffness of the PCL-M scaffolds does not replicate that seen in soft tissue *in vivo,* the gelatin within the structure can provide a more mimetic environment for the breast cancer cells. Furthermore, it has been widely reported that gelatin sponges implanted on CAM assays demonstrate good levels of angiogenesis (Ribatti et al., 1997; Ribatti et al., 2006; Dreesmann et al., 2007). The gelatin sponges used in many previous studies provide a permissive substrate for cell attachment, migration and proliferation resulting in vastly improved rates of angiogenesis compared to commercial collagen sponges. However, it is often difficult to handle and manipulate hydrogels. The combination of gelatin within a PCL-M polyHIPE scaffold provides a synthetic polymer scaffold, which is easily handled and manipulated, and a hydrogel to promote angiogenesis and vascular invasion within the bulk of the scaffold. Similarly, Tan et al. used PCL/gelatin electrospun scaffolds combined with induced pluripotent stem-cell derived endothelial cells (iPSC-ECs) (Tan et al., 2018). When implanted *in vivo* it was observed the iPSC-ECs survived a further 3 days once implanted and there was improved blood perfusion and host-angiogenic responses compared to when the iPSC-ECs were implanted without the composite PCL/gelatin scaffold.

In this study we seeded MDA-MB-231 cells on to gelatin-containing PCL-M polyHIPEs to further support angiogenesis by the expression of VEGF from the triple negative breast cancer cell line. Wang et al. have shown how the addition of VEGF to a PCL/gelatin electrospun scaffold can improve endothelial cell proliferation *in vitro* and enhanced vascularisation *in vivo* (Wang et al., 2015). Sustained release of VEGF was achieved by functionalising the gelatin by heparin immobilisation, creating a binding site for VEGF. Similarly, Del Gaudio et al. functionalised gelatin by crosslinking with genipin, resulting in improved angiogenesis (Del Gaudio et al., 2013). Alternatively, Jiang et al. combined PCL nanofibers with gelatin encapsulated VEGF to enhance angiogenesis of endothelial cells (Jiang et al., 2018). In this study, we simplify the scaffold processing steps, removing the

109

need for gelatin functionalisation or encapsulation by utilising the innate ability of MDA-MB-231 cells to express VEGF.

To validate the use of gelatin-containing PCL-M polyHIPEs to support vascular invasion and growth, we used the *ex ovo* CAM assay, assessing the effect of cell-seeded PCL-M polyHIPEs on angiogenesis from an established, pre-existing vascular network. The CAM assay has been well documented to study the angiogenic capability of biomaterial scaffolds (Naik et al., 2018; Ribatti et al., 2020). Due to the biological nature of the CAM assay, it is common to see variation within datasets as shown in previous studies which utilise the CAM assay (Aldemir Dikici et al., 2020; Samourides et al., 2020). We report visually increased directionality of the vessels towards the cell-seeded polyHIPE scaffolds (Figure 3). We suggest this observation is due to the expression of VEGF from the breast cancer cells promoting directed vessel growth around the circumference of the scaffolds. This is further supported in literature, in which VEGF is identified as one of the main factors for vascular growth regulation in the CAM (Chen et al., 2021), with many studies observing an increase in scaffold integration and number of blood vessels when the scaffolds were loaded with VEGF (Cidonio et al., 2019a; Cidonio et al., 2019b; He et al., 2019; Marshall et al., 2020). Moreover, similar directional vessel growth has been observed by Guerra et al. in response to varying VEGF concentrations (Guerra et al., 2021). They identified that increased levels of VEGF resulted in vessel growth with increased vessel density towards the VEGF-loaded hydrogel.

There was a statistically significant increase in the number of vessels surrounding the cell-seeded gelatin-only polyHIPE scaffolds (Figure 3E). This was also observed in the H&E staining, we observed there were more vessels present in the CAM tissue on the cell-seeded gelatin-only polyHIPE scaffold compared to the media-soaked gelatin-only polyHIPE scaffold (Figure 4). A study investigating porous poly(glycerol sebacate urethane) scaffolds observed a significant increase in the number of vessels surrounding scaffolds which had larger pores (Samourides et al., 2020). This correlates to the significance observed in this study in which the gelatin-only scaffolds have significantly larger pores than the surfactant-containing polyHIPEs. The average pore sizes have been previously reported, as 80 μm for the gelatin-only scaffold, 39 μm for the gelatin and surfactant scaffold, and 53 μm for the surfactant-only scaffold (Furmidge et al., 2023). On the other hand, whilst we observed a greater number of vessels in the CAM tissue around the gelatin-only scaffolds, we did not observe vessels within the scaffold. The H&E staining of these scaffolds showed the CAM tissue forming a distinct layer on the scaffold with limited integration. This lack of integration was further pronounced when preparing the samples for histological assessment, and the layer of CAM tissue was easily separated from the scaffold, as previously described by Mangir et al. (2019). This lack of integration is likely due to the larger pores in the gelatin-only PCL-M polyHIPEs. Whilst large pores are favourable for vascular invasion and integration, for cell attachment and migration they may need to be significantly smaller. The ingrowing CAM cells are likely fibroblasts, and it is reported that fibroblast ingrowth occurs with scaffold pore sizes of 5–15 μm (Yang et al., 2001). Interestingly, on multiple occasions in the cell-seeded surfactant and gelatin-containing PCL-M polyHIPEs, we observed the CAM membrane starting to grow over and envelop the scaffold (Figure 3. G5S10 +MDA-MB-231; Supplementary Figure S4). This phenomenon has been observed

previously as an indicator of tissue/scaffold integration and angiogenesis (Baiguera et al., 2012; Totonelli et al., 2012; Orlando et al., 2013). Interestingly, these studies use ECM-derived matrices to fabricate decellularised scaffolds. Thus, it is likely the gelatin, a heterogenous mixture of peptides which are derived from Collagen, which is one of the most abundant ECM proteins, alongside the expression of VEGF from the MDA-MB-231 cells within the PCL-M polyHIPEs is responsible for stimulating the envelopment of these scaffolds. The H&E staining provided further evidence of vascular integration, where we observed the presence of blood vessels within the surfactant and gelatin-containing scaffold (Figure 4). Whilst these scaffolds have smaller pores [mean = 39 μm (Furmidge et al., 2023)], vascular invasion was observed. Similarly, Paterson et al. demonstrated vascular invasion occurred within emulsion-templated microspheres with small pores (median pore size = 21 μm) however, only in combination with human embryonic stem cell-derived mesenchymal progenitor cells (Paterson et al., 2018). Furthermore, they suggest the expression of VEGF from the cells may be partially responsible for the induction of the angiogenic response. Furthermore, Baker et al. observed vascular ingrowth within porous PCL scaffolds with a similar range of pore sizes as the scaffolds used in this study (Baker et al., 2011). The study also identified that the infiltrating vascular network preferentially aligned along micro-fractures in the structure. Therefore, any similar fractures or weaknesses within the polyHIPE structure could provide additional support for vascular alignment and infiltration and is a possible design feature to investigate in the future to further improve the vascularisation of gelatin-containing PCL polyHIPEs.

6 Conclusion

In this study, we demonstrated the use of gelatin-containing PCL-M polyHIPEs to support 3D breast cancer cell culture by assessing the cell metabolic activity and the expression of VEGF. Furthermore, we validated the use of these substrates to support vascular invasion and growth using the CAM assay. Via combining breast cancer cells with the gelatin-containing polyHIPE substrates, we observed a significant increase in the number of blood vessels surrounding the scaffold and improved tissue integration. Thus, we present gelatin-containing PCL-M polyHIPEs as a promising composite material for MPS substrates to support both 3D cancer cell culture and vascular ingrowth.

Data availability statement

The raw data supporting the conclusions of this article will be made available by the authors, without undue reservation.

Ethics statement

Ethical approval was not required for the studies on humans in accordance with the local legislation and institutional requirements because only commercially available established cell lines were used. Ethical approval was not required for the study involving animals in accordance with the local legislation and institutional requirements

110

because the work was completed in *ex ovo* conditions under the 14 days threshold set out by the UK Home Office.

Author contributions

CJ: Data curation, Formal Analysis, Investigation, Methodology, Writing–original draft, Writing–review and editing. ID: Data curation, Formal Analysis, Investigation, Writing–original draft. HK: Data curation, Investigation, Methodology, Writing–review and editing. SW: Data curation, Formal Analysis, Investigation, Methodology, Writing–original draft, Writing–review and editing. BA: Formal Analysis, Writing–original draft, Writing–review and editing. EB: Supervision, Writing–review and editing. HB: Supervision, Writing–review and editing. WE: Supervision, Writing–review and editing. NG: Supervision, Writing–review and editing. FC: Conceptualization, Supervision, Writing–review and editing.

Funding

Acknowledgments

Conflict of interest

The authors declare that the research was conducted in the absence of any commercial or financial relationships that could be construed as a potential conflict of interest.

Publisher's note

All claims expressed in this article are solely those of the authors and do not necessarily represent those of their affiliated organizations, or those of the publisher, the editors and the reviewers. Any product that may be evaluated in this article, or claim that may be made by its manufacturer, is not guaranteed or endorsed by the publisher.

Supplementary material

The Supplementary Material for this article can be found online at: https://www.frontiersin.org/articles/10.3389/fbioe.2023.1321197/full#supplementary-material

References

Adair, T. H., and Montani, J. P. (2010). "Overview of angiogenesis," in *Angiogenesis* (San Rafael (CA): Morgan and Claypool Life Sciences). Available from: https://www.ncbi.nlm.nih.gov/books/NBK53238/.

Aldemir Dikici, B., and Claeyssens, F. (2020). Basic principles of emulsion templating and its use as an emerging manufacturing method of tissue engineering scaffolds. *Front. Bioeng. Biotechnol.* 8, 875. doi:10.3389/fbioe.2020.00875

Aldemir Dikici, B., Reilly, G. C., and Claeyssens, F. (2020). Boosting the osteogenic and angiogenic performance of multiscale porous polycaprolactone scaffolds by *in vitro* generated extracellular matrix decoration. *ACS Appl. Mater Interfaces* 12 (11), 12510–12524. doi:10.1021/acsami.9b23100

Aldemir Dikici, B., Sherborne, C., Reilly, G. C., and Claeyssens, F. (2019). Emulsion templated scaffolds manufactured from photocurable polycaprolactone. *Polym. Guildf.* 175, 243–254. doi:10.1016/j.polymer.2019.05.023

Aldrich, S. (2023). *Authenticated MDA-MB-231 cell line*. Available from: https://www.sigmaaldrich.com/GB/en/product/sigma/cb_92020424.

Amiri, S. A., Berckel, P. V., Lai, M., Dankelman, J., and Hendriks, B. H. W. (2022). Tissue-mimicking phantom materials with tunable optical properties suitable for assessment of diffuse reflectance spectroscopy during electrosurgery. *Biomed. Opt. Express* 13 (5), 2616–2643. doi:10.1364/boe.449637

Asim, S., Tabish, T. A., Liaqat, U., Ozbolat, I. T., and Rizwan, M. (2023). Advances in gelatin bioinks to optimize bioprinted cell functions. *Adv. Healthc. Mater* 12 (17), 2203148. doi:10.1002/adhm.202203148

Baiguera, S., Macchiarini, P., and Ribatti, D. (2012). Chorioallantoic membrane for *in vivo* investigation of tissue-engineered construct biocompatibility. *J. Biomed. Mater Res. B Appl. Biomater.* 100 B (5), 1425–1434. doi:10.1002/jbm.b.32653

Baker, S. C., Rohman, G., Hinley, J., Stahlschmidt, J., Cameron, N. R., and Southgate, J. (2011). Cellular integration and vascularisation promoted by a resorbable, particulate-leached, cross-linked poly(ε-caprolactone) scaffold. *Macromol. Biosci.* 11 (5), 618–627. doi:10.1002/mabi.201000415

Barnhill, R. L., and Ryan, T. J. (1983). Biochemical modulation of angiogenesis in the chorioallantoic membrane of the chick embryo. *J. Investigative Dermatology* 81 (6), 485–488. doi:10.1111/1523-1747.ep12522728

Bello, A. B., Kim, D., Kim, D., Park, H., and Lee, S. H. (2020). Engineering and functionalization of gelatin biomaterials: from cell culture to medical applications. *Tissue Eng. Part B Rev.* 26 (2), 164–180. doi:10.1089/ten.teb.2019.0256

Cannatà, A., Meo, S. Di, Morganti, S., Matrone, G., and Pasian, M. (2021). "Gelatin-Based tissue-mimicking materials for breast phantoms: dielectric and mechanical characterization," in *2021 XXXIVth general assembly and scientific symposium of the international union of radio science* (Rome, Italy: URSI GASS), 1–3.

Chen, L., Wang, S., Feng, Y., Zhang, J., Du, Y., Zhang, J., et al. (2021). Utilisation of chick embryo chorioallantoic membrane as a model platform for imaging-navigated biomedical research. *Cells* 10 (2), 463. doi:10.3390/cells10020463

Cidonio, G., Alcala-Orozco, C. R., Lim, K. S., Glinka, M., Mutreja, I., Kim, Y. H., et al. (2019b). Osteogenic and angiogenic tissue formation in high fidelity nanocomposite Laponite-gelatin bioinks. *Biofabrication* 11 (3), 035027. doi:10.1088/1758-5090/ab19fd

Cidonio, G., Cooke, M., Glinka, M., Dawson, J. I., Grover, L., and Oreffo, R. O. C. (2019a). Printing bone in a gel: using nanocomposite bioink to print functionalised bone scaffolds. *Mater Today Bio* 4, 100028. doi:10.1016/j.mtbio.2019.100028

Del Gaudio, C., Baiguera, S., Boieri, M., Mazzanti, B., Ribatti, D., Bianco, A., et al. (2013). Induction of angiogenesis using VEGF releasing genipin-crosslinked electrospun gelatin mats. *Biomaterials* 34 (31), 7754–7765. doi:10.1016/j.biomaterials.2013.06.040

Dikici, B. A., Dikici, S., Reilly, G. C., MacNeil, S., and Claeyssens, F. (2019). A novel bilayer polycaprolactone membrane for guided bone regeneration: combining electrospinning and emulsion templating. *Materials* 12 (16), 2643. Available from:. doi:10.3390/ma12162643

Dikici, S., Aldemir Dikici, B., Bhaloo, S. I., Balcells, M., Edelman, E. R., MacNeil, S., et al. (2020). Assessment of the angiogenic potential of 2-deoxy-D-ribose using a novel

111

in vitro 3D dynamic model in comparison with established *in vitro* assays. *Front. Bioeng. Biotechnol.* 7, 451. doi:10.3389/fbioe.2019.00451

Dikici, S., Aldemir Dikici, B., Macneil, S., and Claeyssens, F. (2021). Decellularised extracellular matrix decorated PCL PolyHIPE scaffolds for enhanced cellular activity, integration and angiogenesis. *Biomater. Sci.* 9 (21), 7297–7310. doi:10.1039/d1bm01262b

Donnaloja, F., Jacchetti, E., Soncini, M., and Raimondi, M. T. (2020). Natural and synthetic polymers for bone scaffolds optimization. *Polym. (Basel)* 12 (4), 905. doi:10.3390/polym12040905

Dreesmann, L., Ahlers, M., and Schlosshauer, B. (2007). The pro-angiogenic characteristics of a cross-linked gelatin matrix. *Biomaterials* 28 (36), 5536–5543. doi:10.1016/j.biomaterials.2007.08.040

Eke, G., Mangir, N., Hasirci, N., MacNeil, S., and Hasirci, V. (2017). Development of a UV crosslinked biodegradable hydrogel containing adipose derived stem cells to promote vascularization for skin wounds and tissue engineering. *Biomaterials* 129, 188–198. doi:10.1016/j.biomaterials.2017.03.021

English, W. R., Lunt, S. J., Fisher, M., Lefley, D. V., Dhingra, M., Lee, Y. C., et al. (2017). Differential expression of VEGFA isoforms regulates metastasis and response to anti-VEGFA therapy in sarcoma. *Cancer Res.* 77 (10), 2633–2646. doi:10.1158/0008-5472.can-16-0255

Furmidge, R., Jackson, C. E., Velázquez de la Paz, M. F., Workman, V. L., Green, N. H., Reilly, G. C., et al. (2023). Surfactant-free gelatin-stabilised biodegradable polymerised high internal phase emulsions with macroporous structures. *Front. Chem.* 11, 11. doi:10.3389/fchem.2023.1236944

Guarino, V., Gentile, G., Sorrentino, L., and Ambrosio, L. (2017). Polycaprolactone: synthesis, properties, and applications. *Encycl. Polym. Sci. Technol.* 1–36, 1–36. doi:10.1002/0471440264.PST658

Guerra, A., Belinha, J., Mangir, N., MacNeil, S., and Natal Jorge, R. (2021). Simulation of the process of angiogenesis: quantification and assessment of vascular patterning in the chicken chorioallantoic membrane. *Comput. Biol. Med.*, 136, 104647. doi:10.1016/j.compbiomed.2021.104647

Habanjar, O., Diab-Assaf, M., Caldefie-Chezet, F., and Delort, L. (2021). 3D cell culture systems: tumor application, advantages, and disadvantages. *Int. J. Mol. Sci.* 22 (22), 12200. doi:10.3390/ijms222212200

He, D., Zhao, A. S., Su, H., Zhang, Y., Wang, Y. N., Luo, D., et al. (2019). An injectable scaffold based on temperature-responsive hydrogel and factor-loaded nanoparticles for application in vascularization in tissue engineering. *J. Biomed. Mater Res. A* 107 (10), 2123–2134. doi:10.1002/jbm.a.36723

Jackson, C. E., Ramos-Rodriguez, D. H., Farr, N. T. H., English, W. R., Green, N. H., and Claeyssens, F. (2023). Development of PCL PolyHIPE substrates for 3D breast cancer cell culture. *Bioengineering* 10 (5), 522. doi:10.3390/bioengineering10050522

Jiang, Y. C., Wang, X. F., Xu, Y. Y., Qiao, Y. H., Guo, X., Wang, D. F., et al. (2018). Polycaprolactone nanofibers containing vascular endothelial growth factor-encapsulated gelatin particles enhance mesenchymal stem cell differentiation and angiogenesis of endothelial cells. *Biomacromolecules* 19 (9), 3747–3753. doi:10.1021/acs.biomac.8b00870

Kohane, D. S., and Langer, R. (2008). Polymeric biomaterials in tissue engineering. *Pediatr. Res.* 63 (5), 487–491. doi:10.1203/01.pdr.0000305937.26105.e7

Langer, R., and Tirrell, D. A. (2004). Designing materials for biology and medicine. *Nature* 428, 487–492. doi:10.1038/nature02388

Lugano, R., Ramachandran, M., and Dimberg, A. (2020). Tumor angiogenesis: causes, consequences, challenges and opportunities. *Cell. Mol. Life Sci.* 77 (9), 1745–1770. doi:10.1007/s00018-019-03351-7

Lukin, I., Erezuma, I., Maeso, L., Zarate, J., Desimone, M. F., Al-Tel, T. H., et al. (2022). Progress in gelatin as biomaterial for tissue engineering. *Pharmaceutics* 14 (6), 1177. doi:10.3390/pharmaceutics14061177

Mangir, N., Dikici, S., Claeyssens, F., and Macneil, S. (2019). Using ex ovo chick chorioallantoic membrane (CAM) assay to evaluate the biocompatibility and angiogenic response to biomaterials. *ACS Biomater. Sci. Eng.* 5 (7), 3190–3200. doi:10.1021/acsbiomaterials.9b00172

Marshall, K. M., Kanczler, J. M., and Oreffo, R. O. C. (2020). Evolving applications of the egg: chorioallantoic membrane assay and *ex vivo* organotypic culture of materials for bone tissue engineering. *J. Tissue Eng.*, 11. doi:10.1177/2041731420942734

Matsui, J., Funahashi, Y., Uenaka, T., Watanabe, T., Tsuruoka, A., and Asada, M. (2008). Multi-kinase inhibitor E7080 suppresses lymph node and lung metastases of human mammary breast tumor MDA-MB-231 via inhibition of vascular endothelial growth factor-receptor (VEGF-R) 2 and VEGF-R3 kinase. *Clin. Cancer Res.* 14 (17), 5459–5465. doi:10.1158/1078-0432.CCR-07-5270

McGarry, C. K., Grattan, L. J., Ivory, A. M., Leek, F., Liney, G. P., Liu, Y., et al. (2020). Tissue mimicking materials for imaging and therapy phantoms: a review. *Phys. Med. Biol.* 65 (23), 23TR01. doi:10.1088/1361-6560/abbd17

Moučka, R., Sedláčik, M., and Pátíková, Z. (2023). Fractional viscoelastic models of porcine skin and its gelatin-based surrogates. *Mech. Mater.* 177, 104559. doi:10.1016/j.mechmat.2023.104559

Naik, M., Brahma, P., and Dixit, M. (2018). A cost-effective and efficient chick ex-ovo cam assay protocol to assess angiogenesis. *Methods Protoc.* 1 (2), 19–9. doi:10.3390/mps1020019

Nishida, N., Yano, H., Nishida, T., Kamura, T., and Kojiro, M. (2006). Angiogenesis in cancer. *Vasc. Health Risk Manag.* 2 (3), 213–219. doi:10.2147/vhrm.2006.2.3.213

Orlando, G., Booth, C., Wang, Z., Totonelli, G., Ross, C. L., Moran, E., et al. (2013). Discarded human kidneys as a source of ECM scaffold for kidney regeneration technologies. *Biomaterials* 34 (24), 5915–5925. doi:10.1016/j.biomaterials.2013.04.033

Paterson, T. E., Gigliobianco, G., Sherborne, C., Green, N. H., Dugan, J. M., Macneil, S., et al. (2018). Porous microspheres support mesenchymal progenitor cell ingrowth and stimulate angiogenesis. *Apl. Bioeng.* 2 (2), 026103. doi:10.1063/1.5008556

Place, E. S., George, J. H., Williams, C. K., and Stevens, M. M. (2009). Synthetic polymer scaffolds for tissue engineering. *Chem. Soc. Rev.* 38 (4), 1139–1151. doi:10.1039/b811392k

Reddy, M. S. B., Ponnamma, D., Choudhary, R., and Sadasivuni, K. K. (2021). A comparative review of natural and synthetic biopolymer composite scaffolds. *Polym. (Basel)* 13 (7), 1105. doi:10.3390/polym13071105

Ribatti, D., Annese, T., and Tamma, R. (2020). The use of the chick embryo CAM assay in the study of angiogenic activiy of biomaterials. *Microvasc. Res.*, 131, 104026. doi:10.1016/j.mvr.2020.104026

Ribatti, D., Gualandris, A., Bastaki, M., Vacca, A., Iurlaro, M., Roncali, L., et al. (1997). New model for the study of angiogenesis and antiangiogenesis in the chick embryo chorioallantoic membrane: the gelatin sponge/chorioallantoic membrane assay. *J. Vasc. Res.* 34 (6), 455–463. doi:10.1159/000159256

Ribatti, D., Nico, B., Vacca, A., and Presta, M. (2006). The gelatin sponge–chorioallantoic membrane assay. *Nat. Protoc.* 1 (1), 85–91. doi:10.1038/nprot.2006.13

Rijal, G., Bathula, C., and Li, W. (2017). Application of synthetic polymeric scaffolds in breast cancer 3D tissue cultures and animal tumor models. *Int. J. Biomater.* 2017, 1–9. doi:10.1155/2017/8074890

Rouwkema, J., and Khademhosseini, A. (2016). Vascularization and angiogenesis in tissue engineering: beyond creating static networks. *Trends Biotechnol.* 34 (9), 733–745. doi:10.1016/j.tibtech.2016.03.002

Samourides, A., Browning, L., Hearnden, V., and Chen, B. (2020). The effect of porous structure on the cell proliferation, tissue ingrowth and angiogenic properties of poly(glycerol sebacate urethane) scaffolds. *Mater. Sci. Eng. C* 108, 110384. doi:10.1016/j.msec.2019.110384

Sohn, E. J., Jung, D. B., Lee, H. J., Han, I., Lee, J., Lee, H., et al. (2018). CNOT2 promotes proliferation and angiogenesis via VEGF signaling in MDA-MB-231 breast cancer cells. *Cancer Lett.* 412, 88–98. doi:10.1016/j.canlet.2017.09.052

Sun, Y., Amirrasouli, B., Razavi, S. B., Li, Q. M., Lowe, T., and Withers, P. J. (2016). The variation in elastic modulus throughout the compression of foam materials. *Acta Mater* 110, 161–174. doi:10.1016/j.actamat.2016.03.003

Tan, R. P., Chan, A. H. P., Lennartsson, K., Miravet, M. M., Lee, B. S. L., Rnjak-Kovacina, J., et al. (2018). Integration of induced pluripotent stem cell-derived endothelial cells with polycaprolactone/gelatin-based electrospun scaffolds for enhanced therapeutic angiogenesis. *Stem Cell. Res. Ther.* 9 (1), 70. doi:10.1186/s13287-018-0824-2

Totonelli, G., Maghsoudlou, P., Garriboli, M., Riegler, J., Orlando, G., Burns, A. J., et al. (2012). A rat decellularized small bowel scaffold that preserves villus-crypt architecture for intestinal regeneration. *Biomaterials* 33 (12), 3401–3410. doi:10.1016/j.biomaterials.2012.01.012

Wang, K., Chen, X., Pan, Y., Cui, Y., Zhou, X., Kong, D., et al. (2015). Enhanced vascularization in hybrid PCL/gelatin fibrous scaffolds with sustained release of VEGF. *Biomed. Res. Int.* 2015, 1–10. doi:10.1155/2015/865076

Yang, S., Leong, K. F., Du, Z. M. E., and Chua, C. K. (2001). The design of scaffolds for use in tissue engineering. Part I. Traditional factors. *Tissue Eng.* 7 (6), 679–689. doi:10.1089/107632701753337645

Zhang, T., Xu, J., Zhang, Y., Wang, X., Lorenzo, J. M., and Zhong, J. (2020). Gelatins as emulsifiers for oil-in-water emulsions: extraction, chemical composition, molecular structure, and molecular modification. *Trends Food Sci. Technol.* 106, 113–131. doi:10.1016/j.tifs.2020.10.005

112

CHAPTER 5. Development of an in vitro vascularised tumour model for oncology applications.

Supplementary information for this article is available in Appendix C.

Development of an *in vitro* vascularised tumour model for oncology applications.

C. E. Jackson[1*], N. L. Lam[2], C. E. Macdougall[3], T. S. P. Grandhi[2], H. Chenoweth[3], B. R. Miller[4], R. Kasprowicz[5], T. L. Gales[6], P. L. Candarlioglu[2§]

[1] The Kroto Research Institute, Materials Science and Engineering, University of Sheffield, Sheffield, UK

[2] Complex In Vitro Models, GlaxoSmithKline, Stevenage, Hertfordshire, UK

[3] Oncology Cell Therapy, GlaxoSmithKline, Stevenage, Hertfordshire, UK

[4] Research Statistics, GlaxoSmithKline, Stevenage, Hertfordshire, UK

[5] Screening, Profiling and Mechanistic Biology, GlaxoSmithKline, Stevenage, Hertfordshire, UK

[6] In Vitro In Vivo Translation, GlaxoSmithKline, Stevenage, Hertfordshire, UK

[§] now in 3D and 3Rs Ltd.

* Correspondence:
Caitlin E. Jackson
cejackson1@sheffield.ac.uk

Keywords: Vascularisation, Spheroid, tumour-on-chip, colorectal cancer, oncology, cell therapy

Abstract

Cancer is a leading cause of mortality in modern society and there is a significant demand to provide relevant translational preclinical models to reduce the attrition rate of oncology therapies in the clinic. Recent advances in the complex *in vitro* models field have presented an opportunity to overcome previous limitations of traditional static *in vitro* models to recapitulate the tumour microenvironment (TME). However, current models lack integration of an organised, stable vascular network that provides key architectural components of the TME whilst enabling the exchange of essential nutrients and removal of waste. Here, we describe a perfusable tumour-on-chip model designed to recapitulate the solid TME via integrating a vascular network with a tumour spheroid. We characterised colon adenocarcinoma (HT29) spheroids for use in the model, assessing parameters including spheroid growth, proliferative regions within spheroids and hypoxic characteristics for up to 10 days. We utilised the Mimetas OrganoReady system to support the co-culture of large spheroids (>200 μm diameter) and vasculature, observing spheroid/vascular connection 4 days post co-culture. Furthermore, following successful integration of spheroids and vasculature we investigated two

potential oncological applications to assess the effect of antibody-based anti-angiogenic cancer therapies and the efficacy of CAR-T cell therapy treatments.

1   Introduction

Using broad-spectrum cytotoxic chemotherapies may have reached its therapeutic plateau in certain cancers (1) and cell therapies show promising success in haematological cancers and could be the hope if replicated in solid tumours (2). Therefore, to develop effective cell therapies in this space, more translational *in vitro* models are required for clinical success (3).

Recently, significant advances were achieved in the complex *in vitro* models field, particularly the development of advanced microfluidic models. These models aim to recapitulate the tumour microenvironment (TME) more holistically by incorporating key pathophysiological characteristics such as tissue-tissue interfaces, fluid flow, leaky vasculature and mechanical cues (4), which can incorporate and support the growth of larger cellular structures such as organoids and spheroids (5). These larger structures enhance translatability by recapitulating features of solid tumours such as architecture, physiological response, metabolic activity such as low oxygen and more anaerobic glycolysis, secretion of soluble factors and drug resistance mechanisms. Consequently, a more biologically-relevant understanding of cell-cell, cell-ECM and tumour-drug interactions can be achieved (6,7).

However, previous models have been limited by the lack of integration of an organised, stable vascular network to allow the exchange of oxygen, nutrients and waste, whilst also providing key architectural components of the TME (8). Despite the advances in the tumour-on-chip field (9–11), there is capacity to improve the modelling of the large tumour mass and it's interaction with vasculature. Thus, enabling the efficacy evaluation of newer therapeutic modalities such as cell therapies or antibody based anti-cancer treatments.

We present a perfusable microphysiological system (MPS) designed to mimic the solid TME with a hypoxic core, integrated vascularisation and proliferation behaviour of tumours *in vivo*. Using the Mimetas OrganoReady Graft system we developed an *in vitro* vascularised solid tumour model composed of a single human adenocarcinoma colorectal (HT29) spheroid on top of a collagen gel matrix, integrated with a dense vascular network. Following spheroid/vascular connection, we demonstrated two potential applications of this novel model in therapeutics development; efficacy

assessment of antibody-based anti-angiogenic tumour therapy and cell therapy treatments. This model highlights key characteristics and challenges not yet addressed during previous MPS research.

2 Materials and Methods

2.1 Production of GFP tagged HT29 cell line

1×10^5 HT29 cells (ATCC, HTB-38) were plated in a 6-well plate in McCoys 5A media supplemented with 2mM glutamine and 10% foetal bovine serum (FBS). After 24h, the pLEX-CMV-eGFP virus was added at a MOI=5 with 8 µg/mL of polybrene in a total of 1.5 mL. After 24h of virus addition the media was refreshed with 5 mL McCoys 5A media supplemented with 2mM glutamine and 10% FBS and 1 µg/mL of puromycin (InvivoGen, France). The puromycin-containing media was replaced every 48h up to 6 days. The top 15% of GFP-positive cells were sorted (Flow sorting, MA900, Sony, Japan) and further expanded. The resulting GFP-transduced and sorted cells will be further referred to as HT29-GFP.

2.2 General Cell Culture

HT29-GFP cells were cultured in McCoys 5A + GlutaMAX (Sigma, USA) supplemented with 10% FBS (Sigma, USA) and puromycin (1 µg/ml, InvivoGen, France) and used between passage 7-15 through all experiments. Cells were incubated in a humidified incubator (5% CO_2 and 37˚C) and media was replaced every 2-3 days.

2.3 Spheroid Generation

Upon confluency, HT29-GFP cells were dissociated from the flask using TrypLE Express Enzyme (Gibco, USA) for 7min. TrypLE was neutralised with McCoys media and centrifuged at 300 g for 5min. The pellet was resuspended in complete Tumorsphere (Promocell, Germany). Cell counts and viability were assessed via an automated cell counter (NC-202, Chemometec, UK). 100µl of cell suspension (25,000 or 50,000 cells/ml to generate 2500 or 5000 cell spheroids, respectively) was transferred into individual wells of an ultra-low attachment (ULA) 96-well plate (Nunclon-Sphera, Thermo, USA), centrifuged at 100 g for 10min and placed into a humidified incubator (5% CO2 and 37˚C).

2.4 Histology of Spheroids

Spheroids were collected at day 3 and day 8 post generation. Hypoxia was evaluated by immunohistochemistry using the Hypoxyprobe-PAb27 kit (Hypoxyprobe, Inc., Burlington, USA). Briefly, spheroid cultures treated with pimondazole for 3h and untreated controls were collected. All samples were fixed for 24h in 10% neutral buffered formalin (Sigma, USA), embedded in Histogel (ThermoFisher, USA) and processed to paraffin blocks. Serial 5 μm sections were prepared using a rotary microtome and collected on charged glass slides for immunohistochemical staining using a Ventana Discovery Ultra autostainer (Roche, USA). Briefly, sections were deparaffinized, subjected to heat induced epitope retrieval (32min in EDTA buffer, pH 9.0), blocked to reduce non-specific staining, incubated for 32min with primary antibody (Ki67, Abcam 231172, clone Sp6, 0.4 ug/ml or Pab27HAP, rabbit anti-pimonidazole antibody, diluted 1:750 for proliferation and hypoxia staining, respectively). Slides were then incubated with secondary antibodies and amplification polymers (DAB chromogen, Roche, USA), and counterstained with hemotoxylin. Stain specificity was assessed by substitution of primary antibody with species- and concentration-matched isotype control immunoglobulins. Positive and negative tissue control sections were included to assess each staining procedure and results evaluated microscopically by a veterinary pathologist.

2.5 VEGF ELISA

VEGF levels in HT29-GFP supernatants were determined using the Human VEGF Quantikine ELISA kit, according to the manufacturer's instructions (R&D systems, USA). The optical density was measured on a SpectraMax i3 MiniMax 300 Imaging Cytometer (Molecular Devices, USA) set to 450 nm, with wavelength correction set to 540 nm.

2.6 Spheroid Characterisation

To assess the size and growth of the HT29 spheroids across an 8-day period, a CellTiter Glo assay (Promega, Belgium) was used. For this, individual spheroids in 100 μL of media were added to 100 μL of CellTiter Glo buffer (Promega, Belgium) and shaken for 5min at 600 rpm before equilibrating statically for 25min. The luminescence was measured using a SpectraMax i3 MiniMax 300 Imaging Cytometer. Luminenscence was compared to a standard curve of known cell numbers to interpolate number of cells per spheroid.

To assess GFP signal, at day 3 post spheroid generation the 96-well ULA plates were transferred to the IncuCyte® cell imaging system (Sartorius, Germany) and analysed in Sartorius software. First, spectral unmixing was performed using single stained controls. A mask of the GFP cells was generated with images representative of the range of conditions. The optimised spheroid mask was used over all wells at all time points, and data and images were exported and analysed using GraphPad (Prism, Version 5.04, USA).

2.7 3D cell culture in microfluidic device (Preparation of tumour-on-chip)

OrganoReady (Mimetas, Netherlands) was utilised for microfluidic cell culture (12). The OrganoReady is composed of 2 channels either side of central Graft chamber with phase guides between each compartment. Upon arrival of the primary Human Umbilical Vein Endothelial Cells (HUVEC) pre-seeded microfluidic plate, the plate was incubated for 1h (5% CO_2 and 37˚C) to liquify the transport medium. Following liquification, the transport medium was replaced with 50 μL of supplemented EGM-2 media (Lonza, Switzerland) in the perfusion inlet and outlets and graft chamber. The plate was placed on a rocker (OrganoFlow L, Mimetas, Netherlands) in a humidified incubator h (5% CO_2 and 37˚C) at an inclination of ±14˚ with an 8min interval and media was replaced every 2-3 days.

2.8 Vascular sprout formation, live cell staining and spheroid connection

Angiogenic sprouting of the HUVEC tubules into the central Graft chamber was induced by the addition of 50 μL sprouting initiation mix to the Graft chamber (Mimetas, Netherlands). The plate was returned to the incubator and the sprouting mix was replaced every 2-3 days.

Prior to spheroid addition, the vasculature was stained with NucBlue (2 drops/mL, Invitrogen, USA) and anti-CD31-APC (1:100, Invitrogen, USA) in HUVEC-CM (HUVEC channel media, MIMETAS, Netherlands) for 1h on the rocker (5% CO_2 and 37˚C, inclination of ±14˚ with 8min interval). After a PBS wash, EGM-2 media and Tumorsphere were replaced in the perfusion channels and Graft chambers, respectively. Spheroids were transferred to the Graft chamber 3 days post-generation via automation (Bravo, Agilent, USA). Inaccurate transfer of spheroids was corrected manually. The plate was incubated in the same conditions as detailed above.

2.9 Barrier Integrity following sprout initiation

Barrier integrity of the HUVEC tubules and sprouts before and after the addition of sprouting initiation mix was assessed using EGM-2 containing 50 μg/mL Cascade blue Dextran (3 KDa, Invitrogen, USA). 50 μL of the EGM-2 containing the tracer was added to the perfusion inlet and outlet of one of the perfusion channels. 50 μL of EGM-2 only was added to the Graft chamber and the remaining perfusion channel. Following 24h incubation (5% CO_2 and 37˚C) the chips were imaged using the Revolve fluorescent microscope (ECHO, USA).

2.10 Quantification of spheroid-infiltrating vessels

Spheroid/vascular network formation was monitored at days 1, 4 and 8 post spheroid transfer using a CellVoyager 8000 (10x objective, Yokogawa, USA). Quantification of spheroid volumes and the volumes of spheroid-infiltrating vessels was performed in Vision4D (Arivis, Germany). The first analysis pipeline segmented and assigned the spheroid with an object tag, while the second pipeline exclusively detected vessels within the spheroid object tag (**Figure. S1**).

2.11 Modelling the effect of anti-angiogenic targeting tumour therapy on OrganoReady

HUVEC vessels were pre-treated with anti-VEGF-A antibody Bevacizumab (4 μg/mL, R&D systems, USA) or anti-VEGF-R2 antibody Ramucirumab (5 μg/mL, Selleckchem, USA), 1 day prior to spheroid addition (**Figure 3A&B**). Human isotype control (IgG1, 5 μg/mL, Eurobio Scientific, UK) was used as a control. Barrier permeability was assessed using EGM-2 containing 50 μg/mL Rhodamine B Dextran (10 KDa, Invitrogen, USA). 50 μL of the EGM-2 containing the tracer was added to the perfusion inlet and outlet of one of the perfusion channels. 50 μL of EGM-2 only was added to the Graft chamber and the remaining perfusion channel. Following 24h, 20 μL of media from each well was transferred to a 384-imaging plate (Greiner Bio-one, UK) and the fluorescence was measured using a SpectraMax i3 MiniMax 300 Imaging Cytometer with the excitation and emission set at 400 and 425 nm respectively.

2.12 CAR-T Efficacy Assays

CAR-T cells (with matching and non-matching antigen as target or control groups) were provided by GSK. All CAR-T cells were activated and rested to increase CAR-T cell efficacy *in vitro* using a proprietary media and protocol. Before addition to the Mimetas OrganoReady, the CAR-T cells were stained using CellTracker Violet (Invitrogen, USA) following the manufacturer's instructions. CAR-

T cells were resuspended in EGM-2 media and 50 μL of CAR-T cell suspension was added either to a ULA plate containing a single spheroid per well and incubated (5% CO_2 and 37˚C). Alternatively, CAR-T cells were added to the OrganoReady Graft model via the perfusion inlet for all conditions, except for direct addition control chip. Where 50 μL of CAR-T cell suspension was added directly to the graft chamber and 50 μL of EGM-2 media was added to the perfusion inlet. Following CAR-T addition 50 μL of EGM-2 was added to the remaining perfusion outlets and 100 μL of EGM-2 to the graft chambers. The plate was incubated as the same conditions detailed above. Tumour spheroid GFP signal was measured by IncuCyte® cell imaging system (Sartouris, Germany), data was analysed as previously described.

2.13 Statistical Analysis

For spheroid characterisation, statistical analysis was performed in GraphPad. VEGF concentration was analysed using one-way analysis of variance (ANOVA) and Tukey's multiple comparison test (**Figure 1D**); cell number and GFP signal were analysed using two-way ANOVA and Bonferroni's multiple comparison test (**Figure 1C&1E**). Statistical significance was attributed to values of $p < 0.05$. Error bars on graphs indicate standard error of mean (SE) and all n values are indicated in the figure captions where relevant. To maintain consistency with previous published analyses, no data transformations were applied.

For CAR-T efficacy, data was plotted in GraphPad Prism displaying means and SEs (**Figure 4A&4B**). Statistical analysis was performed for spheroids within the Mimetas OrganoReady model in R (version 3.6.1). To analyse the effect of effector or control CAR-T cells on GFP signal, a linear mixed effects model was fit, with fixed effects for the interaction between CAR-T cell type (effector or control), effector:target (E:T) ratio (1:1, 1:5, or 1:20), and time point (factor coded), and random intercepts for well and row to account for potential well-to-well and row-to-row differences. The endpoint, GFP signal, was log10 transformed prior to analysis to ensure homoscedasticity. Analysis was restricted to time points ≤ 78h.

3   Results

3.1   Spheroid Characterisation

After 3 days, HT29 spheroids formed that were transferred into an imaging well plate (**Figure 1A).** H&E and Ki67 staining revealed that day 3 spheroids generated using 2500 cells had minimal cell

necrosis in the centre and low proliferation. At day 8, the same spheroids had an outer proliferating cell layer with increased cell necrosis of the central core of the spheroid (**Figure 1A**).
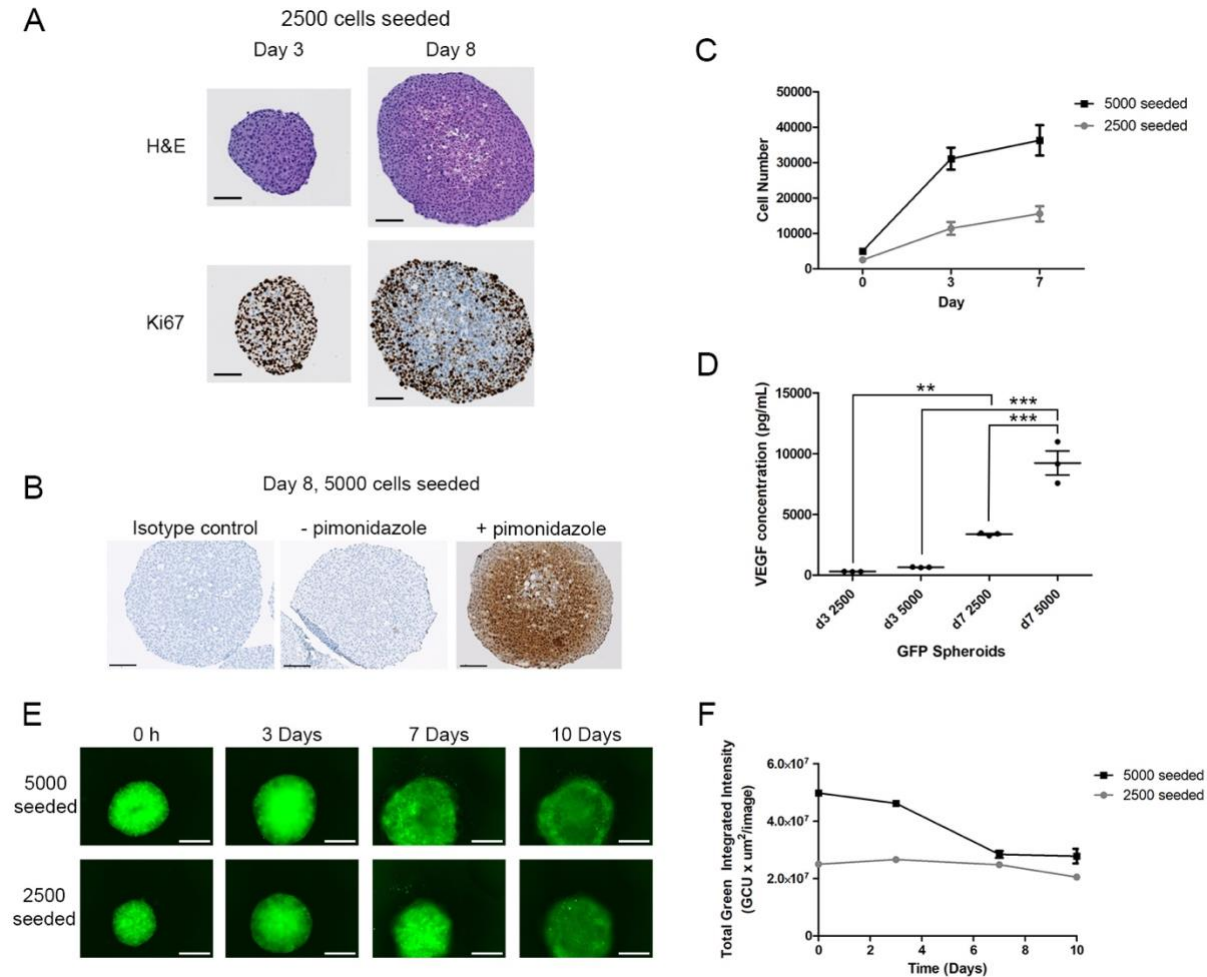

Figure 1. Spheroid Characterisation. HT29 spheroids (2500 cells seeded) were cultured within a ultra-low adhesion plate model assessing; **(A)** spheroid proliferation from day 3 to day 8 (scale bar: 100 μm) using Formalin-Fixed Paraffin-Embedded (FFPE) sections that were generated and stained with H&E or anti-ki67 (brown) where nuclei were counterstained with haematoxylin., **(B)** regions of hypoxia (scale bar: 100 μm), using FFPE sections that were generated and stained with pimonidazole, **(C)** growth rate of the spheroids from day 0 to 7 (N=3, n=6, mean ± SE), **(D)** VEGF production from spheroids at day 3 and day 7 post generation (n=3, mean ± SE) and **(E)** fluorescent images of the GFP signal of the spheroids up to day 10 (scalebar: 400 μm), **(F)** further quantified using IncuCyte masking (n=3, mean ± SE).

Pimonidazole staining was used to identify regions of hypoxia within spheroids. On day 8 post generation, we detected endogenous levels of hypoxia within spheroids seeded with 5000 cells

initially and treated with pimonidazole for 3h (**Figure 1B**). The non-staining areas consist of cellular loss as well as vacuolation of cells that are in the process of necrosis. There was no hypoxia detected with pimonidazole in spheroids 3 days post generation.

Across a 7-day period, spheroids generated with 2500 and 5000 cells proliferated to 11421 (SE = 1802) and 31120 cells (SE = 3094) at day 3, and 15555 (SE = 2143) and 36309 cells (SE = 4281) at day 7 respectively (**Figure 1C**). Furthermore, there is a proportional increase in VEGF secretion in line with cell numbers in the spheroids from day 3 to day 7 post generation (**Figure 1D**). The VEGF expression of spheroids generated with 2500 cells increased from 293 (SE = 6) pg/mL to 642 (SE = 11) pg/mL from day 3 to 7, whereas spheroids generated with 5000 cells increased from 3369 (SE = 65) pg/mL to 9234 (SE = 988) pg/mL. The GFP signal of spheroids generated with 2500 cells remained consistent over 7 days at 2.5×10^7 GCUxμm^2/image with a small decrease to 2.1×10^7 GCUxμm^2/image by 10 days (**Figure 1E&F**). Rapid proliferation at the spheroid border with large necrotic core of the 5000-cell group (**Figure 1B**) prevented representative viability readings with CellTiter-Glo (**Figure 1E&F**). Therefore, the integrated intensity of the GFP signal of the spheroids was used to improve rapid analysis of spheroid viability and a measure for CAR-T mediated killing. The integrated intensity of the GFP signal accounts for the total GFP signal relative to the area of the spheroid which enabled rapid assessment of the viability of spheroids. GFP signal of spheroids generated with 5000 cells decreased from 5.0×10^7 GCUxμm^2/image to 4.6×10^7 GCUxμm^2/image across 3 days and then further dropped to 2.8×10^7 GCUxμm^2/image at day 7 before plateauing until day 10. Stable signal was observed in 2500 cell spheroids whereas there was a drop in signal for 5000 cell spheroids, whilst the area of the spheroids increased there is a reduction in signal to area, correlating to the development of a necrotic core. As a result, spheroids seeded with 2500 cells were used in downstream assays.

3.2 Establishing vascular and spheroid connection

Cascade Blue dextran tracer identified a tight endothelial barrier before sprouting initiation by containment of the tracer in the endothelial tubule. Following 6 days of sprouting initiation, the tracer perfuses throughout the microfluidic device and leaked to the graft chamber, indicating the development of vascular sprouts providing a pathway for perfusion from the endothelial tubules to the centre graft chamber of the microfluidic chip (**Figure 2A&B**).
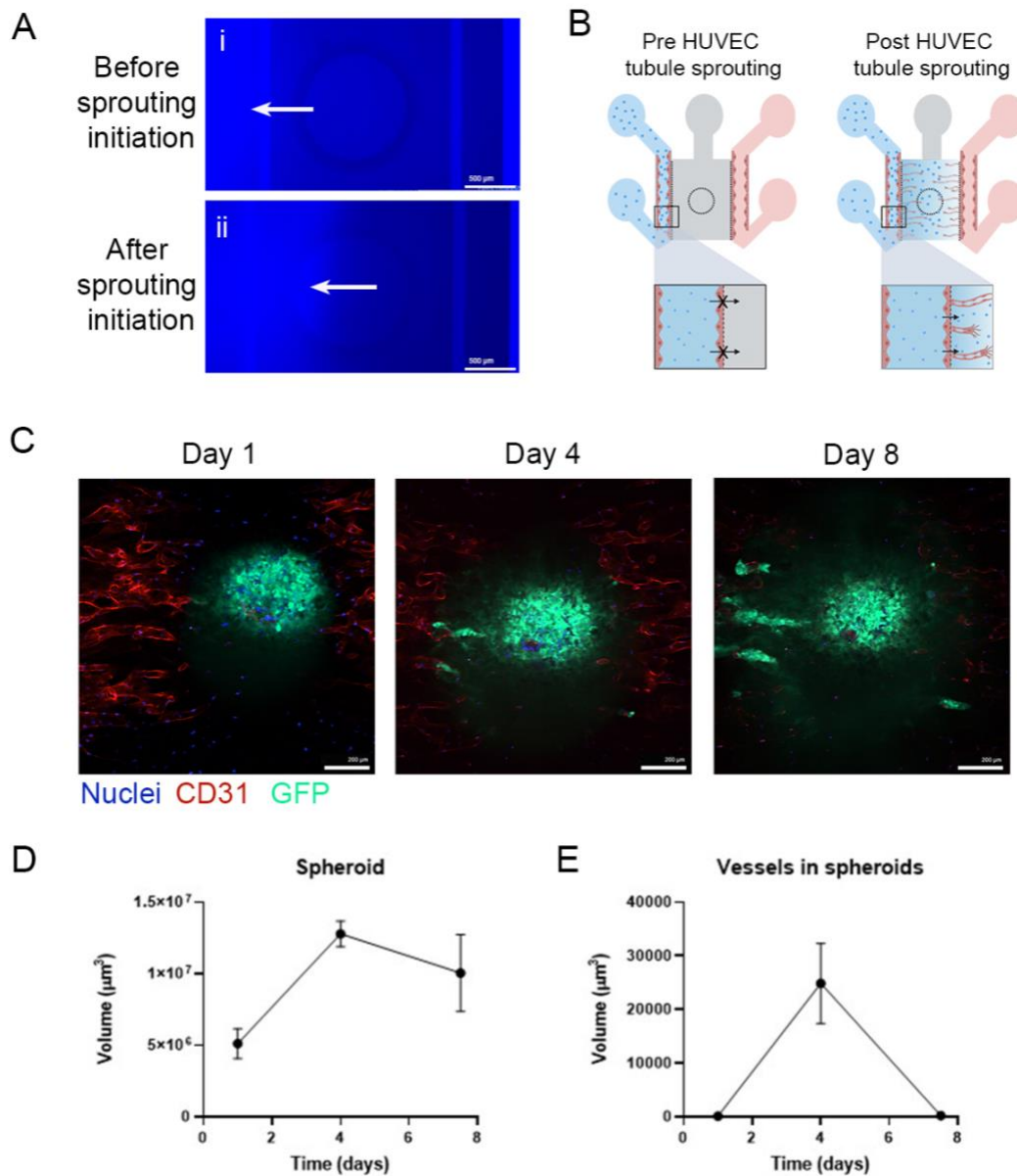
Figure 2. Establishing vascular and spheroid connection. **(A)** Fluorescent images of 3 KDa Cascade Blue tracer perfusing through **(i)** a chip with tight endothelial tubules with no sprouting and **(ii)** a chip post tubule sprouting, white arrows indicate localisation of Cascade Blue tracer (Scale bar: 500 μm) **(B)** Cascade Blue tracer perfuses more rapidly in chips with sprouted vessels due to morphological restructuring of the endothelial tubule when sprout formation occurs (created with BioRender.com). HUVEC sprouts invade HT29-GFP spheroids by day four and spheroid destabilisation occurs at later timepoints. HT29-GFP cells were seeded at 2500 cells/well in ultra-low attachment **(**ULA) plates and formed spheroids over a 3-day period. (**C**) HT29-GFP spheroids (green) were transferred to an OrganoReady Graft plate following live-cell staining of the HUVECs

with NucBlue (blue) and anti-CD31-APC (red). Representative images are shown at days 1, 4 and 8. (Scale bar: 200 μm) (**D**) Spheroid and (**E**) Spheroid-infiltrating vessel volumes were quantified using Vision4D (Arivis) (N=2, *n*=4-6, mean ± SE).

Vascular and spheroid connection was visualised at 4 days post co-culture (**Figure 2C**). Spheroid destabilisation occurred by day 8 as indicated by a decrease in spheroid volume (**Figure 2D**). Consequently, there was sharp decrease in vessel volume as spheroids destabilised (**Figure 2E**).

3.3   Modelling the effect of anti-angiogenic targeting tumour therapy on OrganoReady

Following treatment with anti-VEGF blockade (Bevacizumab and Ramucirumab) the permeability of vessels to Rhodamine B Dextran tracer from the dosing channel to the graft chamber was reduced compared to using an IgG treatment (**Figure 3C**). This suggests the anti-VEGF blockade stabilises the vascular network, reducing leaky vasculature.
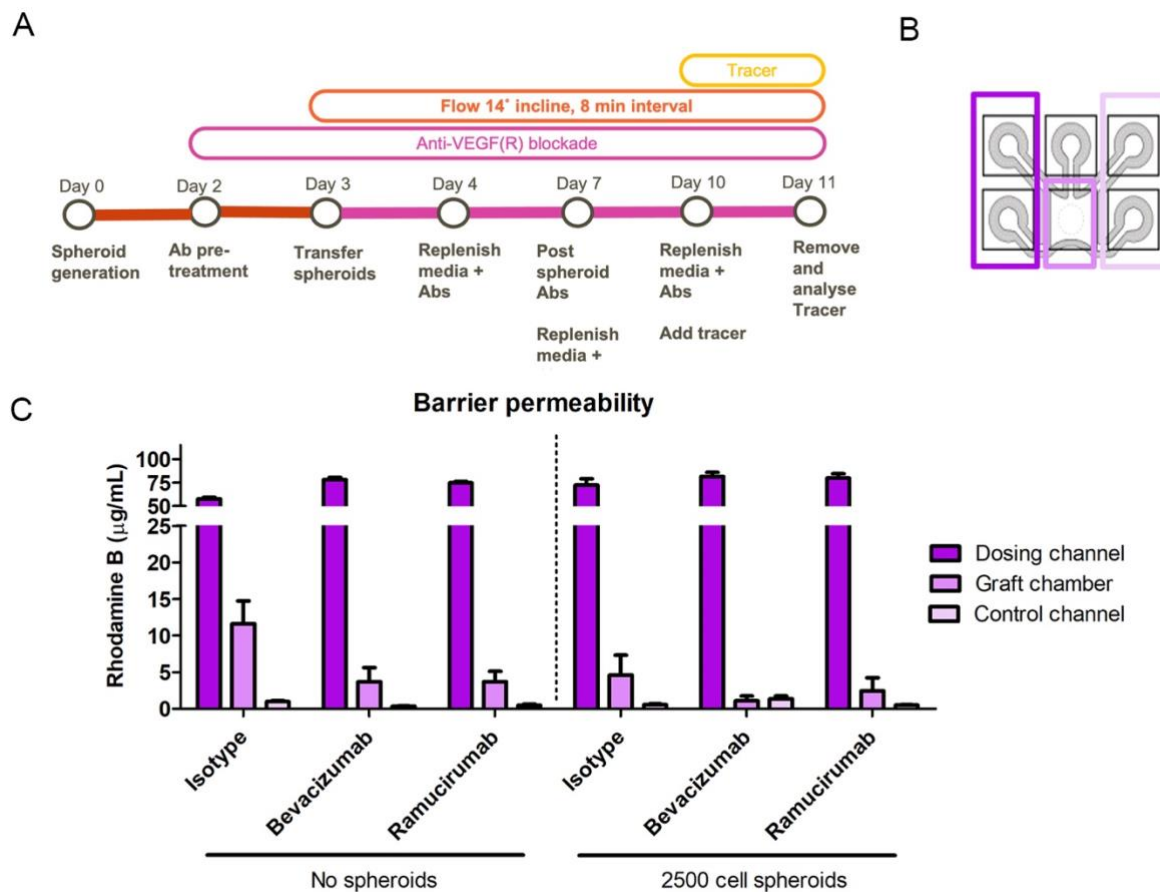

Figure 3. The addition of anti-angiogenic monoclonal antibodies, Bevacizumab and Ramucirumab, stabilised leaky vessels as observed by the reduction in dextran leaking into the

central graft chamber compared to the isotype control. In addition, this trend is more apparent following vascular/spheroid connection. (A) HT29-GFP cells were seeded at 2500 cells/well in ultra-low attachment **(**ULA) plates and formed spheroids over a 3-day period. The vascular networks were treated with anti-angiogenic monoclonal antibodies starting 24 h before spheroid transfer, replenishing the treatment every 2-3 days thereafter. **(B)** At day 10, 10 KDa Rhodamine B labelled dextran was added to the dosing channel (chambers highlighted in dark purple). **(C)** Following 24 h the resulting concentrations of Rhodamine B across the chip were quantified (n=4, mean ± SE).

3.4   CAR-T Efficacy Assay

Firstly, CAR-T cell activity was assessed within an ULA plate assay. Effector CAR-T cells were co-cultured with spheroids 3 days post generation, with effector CAR-T cells showing the highest killing occurring at 72h, as evident by the reduction in tumour cell GFP signal compared to the co-cultures with control CAR-T cells (**Figure 4A**). The effector CAR-T cells demonstrated a targeted killing pattern when co-cultured with HT29-GFP spheroids. Initial cell activity resulted in an increase in GFP signal, peaking at 24h before decreasing to 0 by 72h. In comparison, the GFP signal when co-cultured with the control CAR-Ts remained consistent throughout the experiment similar to the spheroid only control. However, when co-culturing the effector CAR-T with spheroids 7 days post generation, the decreased viability of the spheroids affected the integrity of the spheroid and thereby the size-based quantification of the killing, thus the targeted killing by the effector CAR-T cells cannot be distinguished from the untargeted allogenic-induced killing by the control CAR-T cells (**Figure 4B**). The reduced viability at the beginning of the experiment in the day 7 post generation 5000 cell seeded spheroids is evident by the lower brightness of the GFP signal in the images (**Figure 4C**). All spheroids had a reduction in GFP signal over 72h whether co-cultured with the effector or control CAR-T cells.
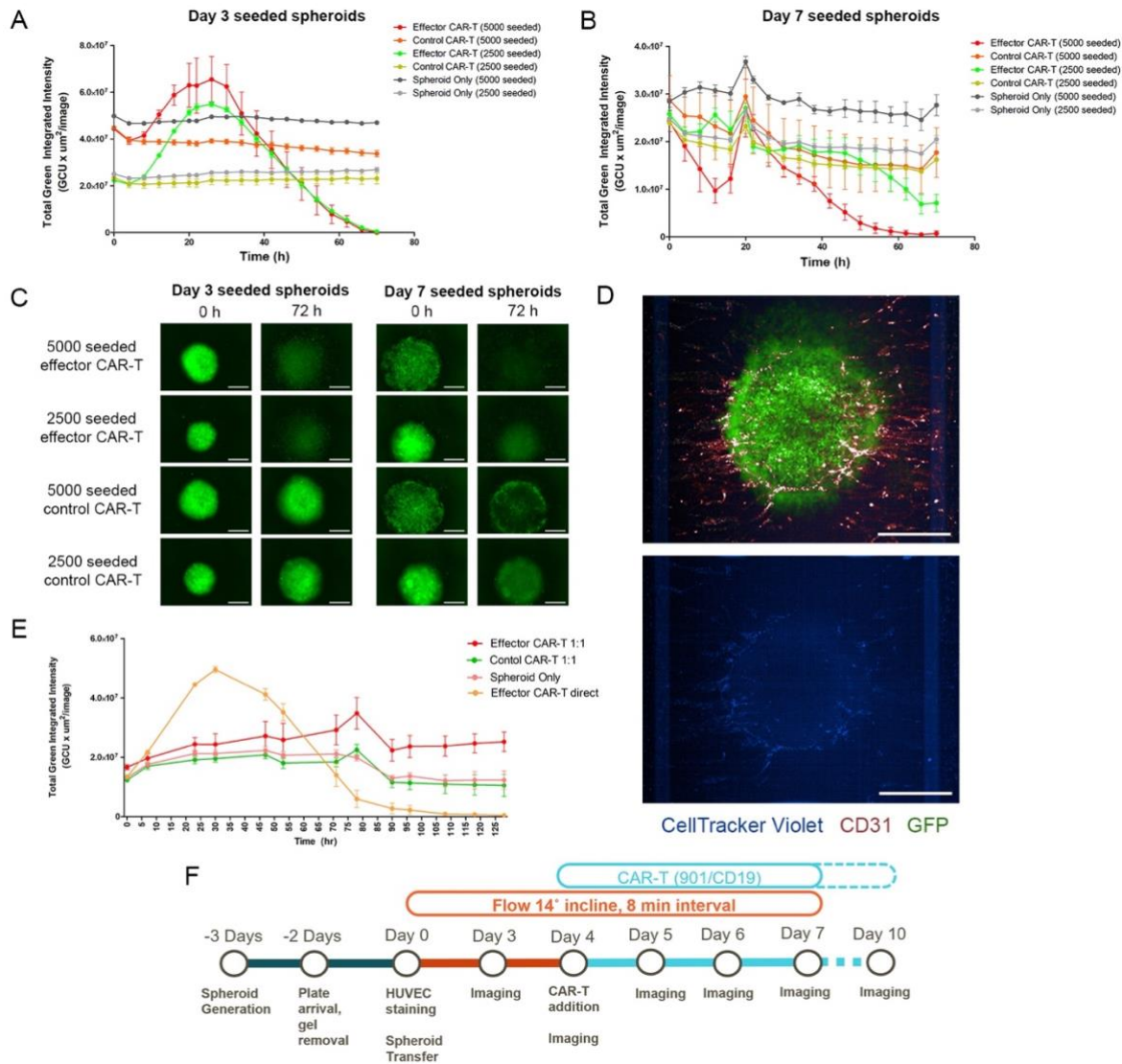
Figure 4. Addition of 2 sets of CAR-T (with matching and non-matching antigen as target or control groups) cells to ultra-low attachment (ULA) and Mimetas OrganoReady HT29 spheroid models. The total integrated intensity of the spheroids GFP signal in the ULA model was used to assess the killing pattern of the effector and control CAR-T cell groups when added to spheroid cultures at **(A)** day 3 and **(B)** day 7 post spheroid generation (n=3, mean ± SE). 0 h indicates a GFP measurement taken immediately after CAR-T addition. **(C)** Fluorescent images of the GFP signal of spheroids (2500 and 5000 seeded) before and 72 h post CAR-T addition (scalebar: 400 μm). Further, HT29-GFP cells were seeded at 2500 cells/well in ULA plates and formed spheroids over a 3-day period. **(D)** HT29-GFP spheroids (green) were transferred to an OrganoReady Graft plate following live-cell staining of the HUVECs with anti-CD31-APC (red), CAR-T cells (blue) were added 4 days post spheroid addition. Representative fluorescent images at day 3 post CAR-T addition are shown (scalebar: 500 μm). **(E)** Total integrated intensity of the spheroids GFP signal were

126

quantified using IncuCyte masking in which an effector:target (E:T) ratio of 1:1 was used (*n*=4, mean ± SE). 0 h indicates a GFP measurement taken immediately after CAR-T addition. **(F)** Schematic diagram detailing the experimental timeline of the CAR-T inclusion in the Mimetas OrganoReady model.

Effector or control CAR-T cells were successfully dosed into our established microfluidic model through the perfusion ports. Following a 48h delay, the CellTracker violet-labelled CAR-T cells were observed in the vasculature connecting to the spheroid and on the spheroid (**Figure 4D**). The control chip with direct addition of the effector CAR-T to the graft chamber, used as a control to overcome the kinetics associated with migration and infiltration, resulted in a killing pattern similar to the simplistic co-culture experiment (**Figure 4A&E**). The GFP signal peaked at 24h and decreased until 72h before further slowly decreasing to 0 (**Figure 4E**). The GFP signal of the effector CAR-T added through the perfusion inlets shows initial characteristics of this killing pattern of the direct addition control at a delayed rate. The GFP signal which correlates with the CAR-T killing increases from 48h to 72h before starting to decrease, suggesting the peak killing had been reached.

After normalising to baseline differences, statistical analysis identified that when comparing the effector and control CAR-T cells: i) GFP signal of the control CAR-T is significantly higher in the 1:1 dose at 7h (p = 0.005), and in the 1:5 dose at 53h (p = 0.022) and ii) the GFP signal of the effector CAR-T is significantly higher in the 1:1 dose at 71h (p = 0.026) and in the 1:20 dose at 78h (p = 0.003, **Figure S3**).

4   Discussion

There is an unmet need for translational oncology models to improve the success rate in the clinic (13–15). Microfluidic-based tissue models may offer an improved predictivity by implementing a holistic approach to emulate the key parameters of cancer *in vitro* (10,11,16). Hence, we developed a tumour-on-chip model to recapitulate zonal proliferation characteristics of tumours with vascularisation, up to 10 days. We then used the efficacy of anti-angiogenic agents and CAR-T cell therapies to determine translational utility of this tumour-on-chip.

The stability of the 2500-cell spheroids enabled connection with the vascular network in the chip by one week when transferred 3 days post generation (**Figure 1A**). 4 days following spheroid transfer, vascular connections started to form (spheroid day 7), as reported previously (17) which occur through the activation of hypoxia signalling initiated via the necrotic core of the spheroid (**Figure**

1A)(18). Once matured, the model with a vascularised hypoxic spheroid captured key features of TME (19). The increase in VEGF production from day 3 to 7 spheroids (**Figure 1D**) further suggests the spheroids will induce aberrant VEGF sprouting in the system, further supporting the phenomenon demonstrated by Bonanini et al. that the presence of a hepatic spheroid alone was sufficient to induce vascular sprouting (20).

To track the vessel sprouting, we utilised a vessel quantification method which detects and analyses large objects. However, throughout the experiment, spheroids underwent morphological changes, such as fragmentation and invasion into the collagen gel, becoming less spherical which led to a sharp decrease in the infiltrating vessel volume quantified by day 8. Additionally, the design of the OrganoGraft chip where the spheroid and vasculature not on the same plane may have contributed to this decline since the area of contact between the spheroid (located on top of the ECM gel) and the vasculature (located within the ECM gel) is much smaller than the whole spheroid surface.

Following successful integration and connection of the tumour spheroid with the vasculature, the tumour-on-chip was used to demonstrate two potential therapeutic applications. Firstly, we modelled the effect of antibody based anti-angiogenic tumour therapy on the vascular components within the tumour-on-chip, using Bevacizumab and Ramucirumab. These two anti-angiogenic monoclonal antibodies are used in the clinic and target VEGF-A and VEGF receptor-2, respectively (21). Following treatment with these antibodies, we observed a stabilisation of the leaky vessels connected to the spheroids, a hallmark of cancer pathophysiology, as evidenced by the reduction in Rhodamine B tracer perfusing into the central graft chamber. However, the effect of the Bevacizumab and Ramucirumab were overall less pronounced in the absence of a spheroid as the vessel network was not fully connected. Therefore, the endothelial tubules and vascular sprouts continue to undergo morphological restructuring, resulting in leakage of tracer where the tight junctions between endothelial cells have been compromised due to these structural changes.

Secondly, we utilised CAR-T cells with matching and non-matching antigen as target or control groups to assess the potential of the tumour-on-chip to evaluate the immune cell infiltration and efficacy of cell therapies. Introducing immune cells through an endothelial barrier connected to a 3D tumour recapitulates the cell-cell interactions and physical barriers that immune cells encounter in a more physiologically relevant manner (22,23). When multiple doses of E:T ratios were tested to evaluate the relevance of a dose response, only 1:1 of the effector CAR-T cells resulted in a significant change in GFP signal compared to the control CAR-T at one of the later timepoints. This

group of CAR-Ts showed the initial characteristic of the killing pattern in the GFP signal of the spheroids which was observed in direct addition of effector CAR-T cells to the spheroids. Interestingly, this response was delayed and reduced compared to 2D, with incomplete spheroid killing due to too few effector CAR-T cells reaching the spheroid. We also observed arrested migration of CAR-T cells within the vascular sprouts connected to the spheroid (data not shown). These findings are comparable to *in vivo* clinical data, where T-cell exhaustion leading to insufficient tracking and expansion at the target site is a well-documented clinical challenge (24–27).

As previously highlighted, the spheroid and vasculature lie on different planes, leading to vessels reaching upwards with decreasing shear stress. Shear stress is known to be a mechanical activator of the T-cell and thus the lack of it may explain CAR-T cell exhaustion through reduced activation (28). We also observed IP10 (CXCL10) expression from spheroids day 7 post generation (data not shown) which induces T-cell migration driven by cognate receptor CXCR3 (29). This further suggests that the reduced shear stress is an overriding stimulus for the CAR-T cell migration in the chip. It is unique to be able to capture these physical challenges of the T-cell migration in an *in vitro* model, which also explains the lack of any discernible killing effects on the tumour by the lower E:T ratios. Furthermore, E:T ratios become irrelevant when the same CAR-Ts are evaluated *in vivo* models. Therefore, one can argue these highly complex *in vitro* models possess the similar physiological barriers as *in vivo* models, and E:T ratios may be less relevant. Instead, the CAR-T loading capacity may be determined by the number of the immune cells that will not disrupt the endothelial barrier where we observed such disruption with CAR-T cell numbers $>1x10^5$ cell/mL.

Albeit there is a tremendous utility in a T-cell exhaustion-on-chip model, efficacy of the model can be improved by transferring the spheroids encapsulated in a collagen gel to improve vascular connection (17), using pre-vascularised spheroids for increased connection (20) or changing the design where the vascular network and the tumour are in the same plane. Thus, it is necessary to consider the specific scientific question being investigated when choosing a platform. The tumour-on-chip presented in this study can accommodate large spheroids (>200µm diameter) within an established perfusable vascular network that may have clear utility to evaluate the infiltration and exhaustion potential of different CAR designs, as well as investigating the effect of anti-angiogenesis targeting oncotherapies.

5   Conflict of Interest

6   Author Contributions

C.E.J. contributed significantly to the manuscript with critical review and editing completed by P.L.C. P.L.C. and C.E.M. conceived the project. P.L.C., C.E.M., C.E.J. and N.L.L. designed the study; P.L.C. and C.E.M. provided leadership for the whole project. C.E.J. and N.L.L. contributed to spheroid and chip preparation and maintenance. T.S.P.G. and T.L.G. contributed to histology sample preparation and analysis. C.E.M. and H.C. contributed to CAR-T preparation and maintenance. C.E.J., N.L.L. and R.K. contributed to image analysis. B.R.M. contributed to statistical analysis.

All authors contributed to manuscript revision, read and approved the submitted version.

7   Funding

8   Acknowledgments

9   Data Availability Statement

All analysed data and materials are available in the main text.

10   References

1.   Schiller JH, Harrington D, Belani CP, Langer C, Sandler A, Krook J, et al. Comparison of four chemotherapy regimens for advanced non-small-cell lung cancer. N Engl J Med [Internet]. 2002 Jan 10 [cited 2023 Oct 12];346(2):92–8. Available from: https://pubmed.ncbi.nlm.nih.gov/11784875/

2.   Guzman G, Reed MR, Bielamowicz K, Koss B, Rodriguez A. CAR-T Therapies in Solid Tumors: Opportunities and Challenges. Curr Oncol Rep [Internet]. 2023 May 1 [cited 2023 Oct 12];25(5):479. Available from: /pmc/articles/PMC10110629/

3.   Zugazagoitia J, Guedes C, Ponce S, Ferrer I, Molina-Pinelo S, Paz-Ares L. Current Challenges in Cancer Treatment. Clin Ther [Internet]. 2016 Jul 1 [cited 2023 Oct 12];38(7):1551–66. Available from: https://pubmed.ncbi.nlm.nih.gov/27158009/

4.   Sontheimer-Phelps A, Hassell BA, Ingber DE. Modelling cancer in microfluidic human organs-on-chips. Nat Rev Cancer [Internet]. 2019 Feb 1 [cited 2023 Oct 12];19(2):65–81. Available from: https://pubmed.ncbi.nlm.nih.gov/30647431/

5.   Mehta P, Rahman Z, ten Dijke P, Boukany PE. Microfluidics meets 3D cancer cell migration. Trends Cancer [Internet]. 2022 Aug 1 [cited 2023 Oct 12];8(8):683–97. Available from: https://pubmed.ncbi.nlm.nih.gov/35568647/

6.   Costa EC, Moreira AF, de Melo-Diogo D, Gaspar VM, Carvalho MP, Correia IJ. 3D tumor spheroids: an overview on the tools and techniques used for their analysis. Biotechnol Adv [Internet]. 2016 Dec 1 [cited 2023 Oct 12];34(8):1427–41. Available from: https://pubmed.ncbi.nlm.nih.gov/27845258/

7.   Fennema E, Rivron N, Rouwkema J, van Blitterswijk C, De Boer J. Spheroid culture as a tool for creating 3D complex tissues. Trends Biotechnol [Internet]. 2013 Feb [cited 2023 Oct 12];31(2):108–15. Available from: https://pubmed.ncbi.nlm.nih.gov/23336996/

8.   Grebenyuk S, Ranga A. Engineering organoid vascularization. Front Bioeng Biotechnol. 2019 Mar 19;7(MAR):435621.

9.   Marx U, Andersson TB, Bahinski A, Beilmann M, Beken S, Cassee FR, et al. Biology-inspired microphysiological system approaches to solve the prediction dilemma of substance testing. ALTEX [Internet]. 2016 [cited 2023 Oct 12];33(3):272–321. Available from: https://pubmed.ncbi.nlm.nih.gov/27180100/

10.   Trujillo-de Santiago G, Flores-Garza BG, Tavares-Negrete JA, Lara-Mayorga IM, González-Gamboa I, Zhang YS, et al. The Tumor-on-Chip: Recent Advances in the Development of Microfluidic Systems to Recapitulate the Physiology of Solid Tumors. Materials 2019, Vol 12, Page 2945 [Internet]. 2019 Sep 11 [cited 2023 Oct 12];12(18):2945. Available from: https://www.mdpi.com/1996-1944/12/18/2945/htm

11.   Liu X, Fang J, Huang S, Wu X, Xie X, Wang J, et al. Tumor-on-a-chip: from bioinspired design to biomedical application. Microsystems & Nanoengineering 2021 7:1 [Internet]. 2021 Jun 21 [cited 2023 Oct 12];7(1):1–23. Available from: https://www.nature.com/articles/s41378-021-00277-8

12.   Mimetas - OrganoPlate® Graft Automated Tissue Placement [Internet]. [cited 2023 Oct 12]. Available from: https://www.mimetas.com/files/Protocols/OrganoPlate%20Graft%20Automated%20Tissue%20Placement%20V1.0.pdf

13.   Seyhan AA. Lost in translation: the valley of death across preclinical and clinical divide – identification of problems and overcoming obstacles. Translational Medicine Communications 2019 4:1 [Internet]. 2019 Nov 18 [cited 2023 Oct 12];4(1):1–19. Available from: https://transmedcomms.biomedcentral.com/articles/10.1186/s41231-019-0050-7

14.   Sun D, Gao W, Hu H, Zhou S. Why 90% of clinical drug development fails and how to improve it? Acta Pharm Sin B [Internet]. 2022 Jul 1 [cited 2023 Oct 12];12(7):3049. Available from: /pmc/articles/PMC9293739/

15.   Wong CH, Siah KW, Lo AW. Estimation of clinical trial success rates and related parameters. Biostatistics [Internet]. 2019 Apr 1 [cited 2023 Oct 12];20(2):273–86. Available from: https://pubmed.ncbi.nlm.nih.gov/29394327/

16.   Zhang X, Karim M, Hasan MM, Hooper J, Wahab R, Roy S, et al. Cancer-on-a-Chip: Models for Studying Metastasis. Cancers (Basel) [Internet]. 2022 Feb 1 [cited 2023 Oct 12];14(3). Available from: https://pubmed.ncbi.nlm.nih.gov/35158914/

17. Nashimoto Y, Hayashi T, Kunita I, Nakamasu A, Torisawa YS, Nakayama M, et al. Integrating perfusable vascular networks with a three-dimensional tissue in a microfluidic device. Integr Biol (Camb) [Internet]. 2017 Jun 1 [cited 2023 Oct 12];9(6):506–18. Available from: https://pubmed.ncbi.nlm.nih.gov/28561127/

18. Karsch-Bluman A, Feiglin A, Arbib E, Stern T, Shoval H, Schwob O, et al. Tissue necrosis and its role in cancer progression. Oncogene [Internet]. 2019 Mar 14 [cited 2023 Oct 12];38(11):1920–35. Available from: https://pubmed.ncbi.nlm.nih.gov/30390074/

19. Bartlett R, Everett W, Lim S, Natasha G, Loizidou M, Jell G, et al. Personalized In Vitro Cancer Modeling — Fantasy or Reality? Transl Oncol [Internet]. 2014 [cited 2023 Oct 12];7(6):657. Available from: /pmc/articles/PMC4311045/

20. Bonanini F, Kurek D, Previdi S, Nicolas A, Hendriks D, de Ruiter S, et al. In vitro grafting of hepatic spheroids and organoids on a microfluidic vascular bed. Angiogenesis [Internet]. 2022 Nov 1 [cited 2023 Oct 12];25(4):455–70. Available from: https://pubmed.ncbi.nlm.nih.gov/35704148/

21. Xiao B, Wang W, Zhang D. Risk of bleeding associated with antiangiogenic monoclonal antibodies bevacizumab and ramucirumab: a meta-analysis of 85 randomized controlled trials. Onco Targets Ther [Internet]. 2018 [cited 2023 Oct 12];11:5059–74. Available from: https://pubmed.ncbi.nlm.nih.gov/30174444/

22. Augustine TN. Analysis of Immune-Tumor Cell Interactions Using a 3D Co-culture Model. Methods in molecular biology [Internet]. 2020 [cited 2023 Oct 12];2184:103–10. Available from: https://pubmed.ncbi.nlm.nih.gov/32808221/

23. Boucherit N, Gorvel L, Olive D. 3D Tumor Models and Their Use for the Testing of Immunotherapies. Front Immunol [Internet]. 2020 Dec 10 [cited 2023 Oct 12];11. Available from: https://pubmed.ncbi.nlm.nih.gov/33362787/

24. Kosti P, Maher J, Arnold JN. Perspectives on chimeric antigen receptor T-cell immunotherapy for solid tumors. Front Immunol. 2018 May 22;9(MAY):365321.

25. Morgan MA, Schambach A. Engineering CAR-T Cells for Improved Function Against Solid Tumors. Front Immunol. 2018 Oct 29;9:417530.

26. Schmidts A, Maus M V. Making CAR T Cells a Solid Option for Solid Tumors. Front Immunol [Internet]. 2018 Nov 8 [cited 2023 Oct 12];9(NOV):2593. Available from: /pmc/articles/PMC6235951/

27. Delgoffe GM, Xu C, Mackall CL, Green MR, Gottschalk S, Speiser DE, et al. The role of exhaustion in CAR T cell therapy. Cancer Cell [Internet]. 2021 Jul 12 [cited 2023 Oct 12];39(7):885–8. Available from: https://pubmed.ncbi.nlm.nih.gov/34256903/

28. Hope JM, Dombroski JA, Pereles RS, Lopez-Cavestany M, Greenlee JD, Schwager SC, et al. Fluid shear stress enhances T cell activation through Piezo1. BMC Biol [Internet]. 2022 Dec 1 [cited 2023 Oct 12];20(1):1–13. Available from: https://bmcbiol.biomedcentral.com/articles/10.1186/s12915-022-01266-7

29. Tokunaga R, Zhang W, Naseem M, Puccini A, Berger MD, Soni S, et al. CXCL9, CXCL10, CXCL11/CXCR3 axis for immune activation - A target for novel cancer therapy. Cancer Treat Rev [Internet]. 2018 Feb 1 [cited 2023 Oct 12];63:40–7. Available from: https://pubmed.ncbi.nlm.nih.gov/29207310/

CHAPTER 6. Overall conclusions and future work

Microphysiological systems (MPS) are rapidly developing to model a range of both healthy and diseased tissues, including cancer and more specifically the metastatic cascade. There are a vast number of models being developed to focus on many aspects of cancer [1], [2], [3], [4], [5], including cancer type, progression, and different parts of the metastatic cascade (invasion, intravasation, circulation, extravasation and colonisation) [6], [7], [8], [9], [10]. Currently, there is no singular model that can incorporate and fully recapitulate all aspects of cancer and therefore many studies focus on using a reductionist approach. This approach focuses on developing a model for a specific application and function. Therefore, within this thesis the main focus of the model development was on creating a substrate which could support a stable vascular network to further study the intravasation or extravasation of cancer cells within an MPS. Specifically aiming to develop a substrate that could support the 3D culture of MDA-MB-231 triple-negative breast cancer cells, which have been shown to be invasive and spontaneously metastasise and are a well-defined cancer cell line that is widely used to model late-stage breast cancer [11], [12], [13], [14]. To achieve this highly porous 4-arm polycaprolactone-methacrylate (PCL-M) scaffolds were fabricated using emulsion templating techniques, resulting in cell culture substrates which show promise in supporting 3D cancer cell culture and vascular infiltration. Within this chapter the advantages and limitations of this work are highlighted. Furthermore, suggestions of how future improvements could be made to overcome the limitations are described in regard to techniques used in other MPS of intravasation and extravasation in literature.

In the first chapter, it was demonstrated how varying the parameters during the emulsion templating process can impact the resulting PCL-M polyHIPE scaffold. The study identified the effect of mixing speed during emulsion fabrication on the resulting pore size, interconnectivity and mechanical properties of PCL-M polyHIPEs. Additionally, the study showed how increasing the hydrophilicity of the PCL-M polyHIPEs using plasma and fibronectin coating did not affect cell adhesion and proliferation. Whilst this chapter demonstrated that PCL-M polyHIPEs can be a suitable substrate for the 3D culture of MDA-MB-231 cells, there is a need for additional investigation to explore the capability of the PCL-M substrate to support other cell types commonly used in microfluidic models, such as endothelial cells, fibroblasts or immune cells. The presence of such cell types can often

change the interactions and behaviour of cancer cells and the progression of metastasis. For example, Gadde et al. used a simplistic microfluidic model to investigate the initial steps of breast cancer cell intravasation from an ECM into a singular central vessel [15]. The model used inflammatory breast cancer cells to successfully stimulate and model *in vivo* events of sprouting of the endothelium of the vessel encircling clusters of the cells. However, this model lacked additional stomal or immune cell types. Therefore, Gadde et al. further developed this model to include tumour associated macrophages [16]. Due to the inclusion of these macrophages there was an increase of ECM porosity, increased vascular sprouting and enhanced permeability of the endothelium. Importantly, the addition of tumour associated macrophages led to the successful intravasation of the breast cancer cells into the vessels.

Likewise, Silvestri et al. developed a similar simple MPS to study tumour-vessel interactions and breast cancer intravasation [17]. The model consisted of a central microvessel within a collagen gel. Within the model they observed cancer cell-vessel interactions, including mosaic vessel formation, a process that is associated with intravasation of cancer cells, as the cells physically displaced the endothelial cells in the vessel wall to migrate through into the vessel lumen in clusters. Linville et al. continued to develop the model to study the tumour-vessel interactions in the blood tumour barrier [18]. Brain microvascular endothelial-like cells were used to create the central vessel within a collagen and Matrigel combined hydrogel further which was seeded with breast cancer spheroids and macrophages. Whilst this model was able to study tumour-vessel interactions, it was also capable of investigating the further effects of immune cells on these interactions, creating a model which recapitulates the significant effect of macrophages on brain metastases *in vivo*.

Whilst these models were used to study intravasation, there are significantly less models developed for extravasation which include supporting cell types. However, Crippa et al. developed a microphysiological system to model the early metastatic niche to investigate breast cancer cell extravasation and the impact that the presence of platelets has on the system [19]. The model was able to monitor the upregulation of cancer cell transendothelial migration due to the presence of platelets and neutrophils. Moreover, it was observed that the inclusion of platelets led to an increase of expression of EMT markers and thus the use of a clinically approved antiplatelet drug led to reduced expression of EMT markers as observed *in vivo*. This model shows promise in providing a platform in which extravasation can be monitored and assessed whilst importantly incorporating blood cell types which, as

demonstrated in this study, can significantly affect the efficiency of cancer cell metastasis. The development of these models demonstrates the importance of including additional cell types within microfluidic models to better recapitulate the tumour microenvironment to successfully model events of the metastatic cascade. Furthermore, exploring other cell types which PCL-M polyHIPEs could support could vastly expand the applicability of these scaffolds within other areas of tissue engineering.

Following previous studies which show closed morphology on the surface of moulded emulsions [20], [21], all the PCL-M scaffolds that were used within this chapter and throughout the thesis were polymerised in a syringe and discs were cut using either a scalpel or vibratome to ensure there was open morphology on the surface for cell seeding and adhesion and vascular infiltration. However, further investigation to improve pore morphology in moulded emulsions is needed. Such a technique would be highly beneficial, allowing researchers to mould emulsions to meet the requirements of any application. Furthermore, for the *in vitro* and *ex ovo* studies all the scaffolds were sterilised using either methanol or ethanol solution to reduce the risk of infection. Sterilisation via autoclaving was also investigated and whilst polyHIPE pore morphology remained consistent compared to ethanol sterilised PCL-M polyHIPEs (**Appendix D, Figure S1**), after 7 days in culture there was a significant reduction in cell metabolic activity (97%) on the polyHIPEs sterilised via autoclaving compared to ethanol (**Appendix D, Figure S2**). Iqbal et al. investigated the effect of autoclaving on polymer coatings and observed a 15º increase in contact angle [22]. PCL-M polyHIPEs have a mean contact angle of 124º and thus any further increase in contact angle could lead to PCL-M polyHIPEs very nearly becoming a superhydrophobic material which is likely to lead to a reduction in cell adhesion. However, there is a need to further investigate this relationship to understand how the autoclaving process alters the chemical and mechanical properties of PCL-M polyHIPEs to cause such an extreme effect on cell adhesion.

From the initial studies in the first chapter, the average pore size of the PCL-M polyHIPEs was 55 and 29 μm when the emulsion was mixed at 200 and 400 rpm respectively. Within literature, it is often stated that the pore size required for vascularisation is >100 μm [23], [24], [25]. Hence, we investigated if changing an alternative parameter to mixing speed in the fabrication process of emulsion templating would lead to pore sizes within this range. It is well documented that the type of surfactant used within the emulsion templating process can affect the resulting pore size [26]. Therefore, we investigated if gelatin, a biocompatible, natural

polymer, which has been reported as weak surfactant [27], could stabilise PCL-M polyHIPEs. Thus, the second chapter reports on the development of gelatin-containing polymer polyHIPEs via the incorporation of gelatin within the internal phase of the emulsion which resulted in increased pore sizes and mechanical properties. Moreover, the study showed that different concentrations of gelatin could be used to further tune the resulting polyHIPE pore size and mechanical properties. Within the discussion of this study, the use of gelatin containing polyHIPEs for drug delivery was explored. The use of a PCL electrospun scaffold to deliver a controlled release of heparin via a heparin loaded gelatin coating has been demonstrated to enhance bone regeneration by Lee et al. [28]. Similarly, Jiang et al. combined PCL nanofibres with VEGF loaded gelatin to enhance angiogenesis [29]. Therefore, I feel this could be a very interesting application for these gelatin polyHIPEs and as such the capability of these polyHIPEs to deliver drugs via slow release should be further studied. Initial assessments would include biodegradation studies of both the PCL-M polyHIPE and gelatin and the corresponding drug release following such degradation.

In the third chapter the gelatin-containing PCL-M polyHIPEs were assessed for their potential to support 3D cancer cell culture alongside vascular infiltration. This study showed promising results to indicate that gelatin-containing PCL-M polyHIPEs are capable of both and therefore are a promising solution as natural/synthetic polymer composite for 3D cell culture substrates that can be used within vascularised microphysiological systems (MPS). Interestingly, this work highlighted that whilst there was no significant difference in the metabolic activity of the MDA-MB-231 cells due to different pore sizes within the gelatin-containing PCL-M scaffolds, there was an effect on the vascular infiltration. It was observed that the gelatin-containing PCL-M scaffolds fabricated with additional surfactant (mean pore size = 39 μm) had improved vascular infiltration than the gelatin-containing PCL-M scaffolds fabricated without additional surfactant (mean pore size = 80 μm). However, there was a greater number of vessels observed surrounding the gelatin-containing PCL-M scaffolds fabricated without additional surfactant. This is likely due to the pore sizes being too large for the migration of fibroblasts from the CAM vessels into the scaffold as Yang et al. report that fibroblast ingrowth occurs with scaffold pore sizes of 5–15 μm [30]. Additionally due to the large size of the pores, vessel infiltration may be harder to quantify via histology due to such a small area of the sample imaged in each slice. Therefore, further analysis is required to quantify the invasion of the vessels more accurately throughout the larger pores and the depth of the scaffold. Techniques such as confocal microscopy could be a solution however whilst

CAM vessels express CD31 which is a commonly used biomarker for blood vessel identification there are no known antibodies which react against chick CD31 antigens thus further investigation is required to find a suitable biomarker for the CAM vessels.

Whilst it was observed that vascular infiltration into the surfactant and gelatin-containing PCL-M occurred, further optimisation is required to assess whether different concentrations of surfactant and gelatin could improve the volume of vascularisation into the scaffold. Moreover, the future work following on from this study is to transition from the *ex ovo* chick chorioallontoic membrane (CAM) assay, which was utilised to generate a proof of concept with a pre-existing vascular network, to a purely *in vitro* model. This work would include assessing the capability of PCL-M polyHIPEs to act as a substrate incorporated into an MPS to investigate its function in comparison to widely used substrates such as hydrogels.

A key advantage of many of the current models which utilise hydrogels is the capability of imaging the system to capture the mechanisms of intravasation and extravasation. Throughout this project, there was difficulty in imaging the PCL-M polyHIPE scaffolds. Firstly, it was observed that PCL-M polyHIPEs scaffolds autofluoresce when using fluorescence microscopy techniques, such as confocal microscopy. Images could be obtained however post processing of the images was required to reduce the background autofluorescence to identify the fluorescent signal from the cells. Sudan Black has been recently used within our research group with PGS-M to reduce this phenomenon following a similar method reported by Sharaf et al., in which the polymer samples are dipped in a Sudan Black solution [31]. However, this technique did not perform to the same level as alternative techniques such as UV-bleaching. Flamourakis et al. have reported the use of Sudan Black as a photoinitiator in the fabrication of 3D polymer constructs followed by dipping the samples in a solution of Sudan Black [32]. This combination of treatment resulted in the elimination of autofluorescence from the 3D polymer sample. It would be interesting to expand this work and investigate if similar methods using Sudan Black could also be used to reduce the background fluorescence of PCL-M polyHIPE scaffolds, improving the fluorescence imaging ease and quality. Alternative analysis techniques, such as histology were also investigated within this project. When processing the PCL-M polyHIPE samples for analysis the common method of wax embedding could not be utilised as the xylene used within the process dissolves the PCL-M scaffolds. Therefore, the scaffolds were processed and sectioned using the cryostat. The processing of the samples via this technique was difficult and samples had to be frozen using extreme temperatures which

was achieved via a liquid nitrogen bath. Using the methods described in chapter 4 section 3.11 we were able to achieve sections of a minimum thickness of 16 µm. Whilst these sections could be imaged and used to obtain results it would be beneficial to further optimise the protocol to decrease the section thickness to achieve clearer images in which key features in samples can be more easily identified and analysed.

Due to these difficulties, current models which use hydrogels have a significant advantage over the PCL-M scaffolds presented in this project due to the ease of imaging the model to observe and analyse the system in real-time. For example, Nagaraju et al. developed a model to study intravasation composed of three concentric channels separated by microposts in which MDA-MB-231 cells had to migrate through a collagen stromal layer before intravasating into the outer vasculature [13]. The vascular component of the model comprised of a spontaneously assembled network of HUVECs which more closely resembled capillaries *in vivo*. The invasion of the cancer cells into the stromal layer increased in the presence of the vascular network, in response the cancer cells induced morphological changes to the vascular network, resulting in thinner and more permeable vessels. This model is successful in observing responses similar to those seen in *in vivo* and could provide real-time analysis of single-cell intravasation. An MPS which is capable of similar levels of imaging and real-time analysis for extravasation has also been developed by Chen et al. [33]. The model is composed of three parallel channels, in which human microvascular networks are formed over 4-5 days. The model utilises standard confocal techniques to monitor the extravasation of MDA-MB-231 cells, observing morphological changes in both tumour and endothelial cells. To achieve such high-resolution imaging this model confines the vascular network to one plane, therefore does not wholly recapitulate the characteristics of a thick 3D tissue. However, the model has been developed with a capacity of up to 36 devices per experiment, increasing the model's throughput capabilities, which is a rising demand to advance the use of MPS within clinical studies.

There are a number of methods to improve model throughput, one such method is via MPS which are designed with multiple chips on a standard well plate. These designs increase throughput whilst also improving the integration of the model with current standardised imaging techniques as most microscopy equipment are capable of imaging a standard well plate. The final experimental chapter demonstrates the development of a vascularised tumour model using a commercially available chip design which features 64 chips on a standard 384

well plate. The study highlights two proof of concept studies for which the model could be utilised, assessing antibody-based anti-angiogenic cancer therapies and the efficacy of CAR-T cell therapy. Whilst the models showed promising indications in the proof of concept studies there are many parameters that need to be optimised to establish a reliable model. When assessing CAR-T therapy the number of CAR-T cells added to the system needs further investigation, adding more than 1×10^5 cell/mL led to a disruption in the endothelial barrier and too few resulted in no therapeutic impact on the tumour spheroid. Therefore, there is need to optimise this parameter and further assess the clinical relevance of the dose used in the model versus the dose used within a clinical *in vivo* setting. Furthermore, additional investigations to improve the model include encasing the spheroid in the collagen gel to increase the vascular connection over a larger volume of the spheroid, as demonstrated by Nashimoto et al. [34], better recapitulating the vascular connection of a tumour *in vivo*. Alternatively, Bonanini et al. improved vascular-spheroid connection within the same MPS by using a pre-vascularised spheroid [35]. In addition, further improvements could be achieved by altering the formulation of the gel the spheroid rests on. In a similar model, Agrawal et al. demonstrated the use of a combined fibrin, Matrigel and collagen gel to improve cellular interactions and cross talk [36]. The study found the combination of gels led to improved vascularisation of HT-29 tumour spheroids with intravasation events of the cancer cells observed in the combined gel, identifying strands of cancer cells asymmetrically growing and infiltrating from the tumour spheroid to the nearest microvasculature.

By using a multi-chip design that came pre-loaded with vascular networks that had previously undergone rigorous quality testing we were able to improve the reliability of the model than using a single chip design or culturing the system from the beginning. However, factors such as chip location on the well-plate, chips located on the edge vs. the centre of the plate, and blanket use of growth factors across chips are likely to have impacted cell behaviour and thus our results. Oliver et al. presents a combined approach using artificial intelligence (AI) alongside an MPS to provide a more robust technique to produce a more reliable, clinically applicable model [37]. The blood brain niche MPS in combination with AI is capable of identifying the extravasation potential of cancer cells via minute differences in cell phenotype. The use of AI allows for the continual improvement and training of the model as they expand the number of patient samples used in the future.

To avoid overuse of growth factors within MPS Meng et al. developed a model in which the release of vascular endothelial and epidermal growth factors could be reliably released via a laser [38], giving greater control and regulation of the concentration of growth factors and thus the directional stimulation of angiogenesis within the system. The model consists of a central vessel within a fibroblast-laden hydrogel matrices which contained a tumour cell droplet and 3D bioprinted stimuli-responsive microcapsules containing the growth factors. The model used EGF and VEGF to stimulate cancer cell migration and angiogenic sprouting respectively. At 9-12 days cancer cells could be observed within the main vessel, demonstrating cancer cell intravasation had occurred. Furthermore, these cells could be observed travelling within the fluid flow as CTCs and as such could be collected in chambers and analysed. Whilst the concentration of growth factors could be reliably controlled, this artificial release of growth factors does not recapitulate the *in vivo* mechanisms for the controlled release of growth factors by the cells in the tumour microenvironment.

Alongside low throughput and poor reliability of MPS, the lack of automation is another factor that limits the use of MPS within clinic studies, greatly affecting the uptake of models at a larger scale. Automation of cell culture protocols is rapidly expanding and improving. Throughout this project all the PCL-M polyHIPEs were manually cell seeded, this seeding technique could lead to variability in results as the droplet of cells may be incorrectly placed and thus the cell suspension would not absorb into the scaffold and instead could fall off the scaffold into the culture well. Therefore, automating the cell seeding could greatly benefit the cell seeding efficiency and accuracy, reducing human error and standardising the operating procedure between researchers.

Automation was used within the model presented in chapter 5, in which we were able to transfer the spheroids from the ultra-low adhesion well plate to the Mimetas Organograft. The use of automation removed human error in the transfer of spheroids and as such the associated complications, such as skewed spheroid growth and spheroid damage which could lead to a spheroid breaking into multiple pieces and the chip becoming unfeasible. However, we were only able to achieve a 50% success rate of transfer and any spheroids that did not or incorrectly transferred had to be corrected manually, reintroducing the complications mentioned earlier. Therefore, further optimisation of the protocol is needed. This is common complication across MPS, as technology, such as automation, is striving to keep up with the

advances in models and thus the industry is rapidly learning how to repurpose existing technology to help advance MPS.

Overall, with the current understanding and technology available it is impossible to recapitulate the full complexities of the 3D tumour microenvironments, with all the biological, mechanical and chemical components, within a single model, that is reproducible, easy to use by trained researchers and with high enough throughput to provide a reportable dataset. In addition, with such variation between not only different cancer types but within a subset of cancers the best method to design models currently is with a reductionist approach [6]. An approach which utilises advantages from both natural and synthetic materials to create models with specific applications and features and acknowledging the limitations of each model whilst technology and model development advances towards a more wholistic MPS. The work described in this thesis is a crucial part of this journey the research field is on. This research identified and analysed the use of a synthetic material, providing advantages such as high porosity and interconnectivity, reproducibility and reduced batch to batch variation, as an alternative to or combined with commonly used natural substrates to support 3D cell growth and vascular invasion. Whilst there is still further optimisation required, specifically on understanding how best to image these polyHIPE substrates, the studies within this thesis set the foundation for polyHIPEs to be utilised within MPS systems, capable of incorporating vascular ingrowth and thus hold promise in the use of polyHIPEs to study intravasation or extravasation of metastatic cancer cells.

References

[1]   Z. Wu, D. Huang, J. Wang, Y. Zhao, W. Sun, and X. Shen, "Engineering Heterogeneous Tumor Models for Biomedical Applications," *Advanced Science*, vol. 11, no. 1, p. 2304160, Jan. 2024, doi: 10.1002/ADVS.202304160.

[2]   H. F. Tsai and et al., "Tumour-on-a-chip: microfluidic models of tumour morphology, growth and microenvironment," *J. R. Soc. Interface*, vol. 14, 2017.

[3]   A. Sontheimer-Phelps and et al., "Modelling cancer in microfluidic human organs-on-chips," *Nat. Rev. Cancer*, vol. 19, pp. 65–81, 2019.

[4]   X. Liu *et al.*, "Tumor-on-a-chip: from bioinspired design to biomedical application," *Microsystems & Nanoengineering 2021 7:1*, vol. 7, no. 1, pp. 1–23, Jun. 2021, doi: 10.1038/s41378-021-00277-8.

[5]   K. Seaman, · Yu Sun, and · Lidan You, "Recent advances in cancer-on-a-chip tissue models to dissect the tumour microenvironment," *Med-X 2023 1:1*, vol. 1, no. 1, pp. 1–28, Oct. 2023, doi: 10.1007/S44258-023-00011-1.

[6] A. Malandrino, R. D. Kamm, and E. Moeendarbary, "In Vitro Modeling of Mechanics in Cancer Metastasis," *ACS Biomater Sci Eng*, vol. 4, no. 2, pp. 294–301, Feb. 2018, doi: 10.1021/ACSBIOMATERIALS.7B00041/ASSET/IMAGES/LARGE/AB-2017-000418_0002.JPEG.

[7] J. S. Jeon *et al.*, "Human 3D vascularized organotypic microfluidic assays to study breast cancer cell extravasation," *Proc Natl Acad Sci U S A*, vol. 112, no. 1, pp. 214–219, Jan. 2015, doi: 10.1073/PNAS.1417115112.

[8] J. J. F. Sleeboom and et al., "Metastasis in context: modeling the tumor microenvironment with cancer-on-a-chip approaches," *Dis. Model. Mech.*, vol. 11, 2018.

[9] M. Jouybar, C. M. de Winde, K. Wolf, P. Friedl, R. E. Mebius, and J. M. J. den Toonder, "Cancer-on-chip models for metastasis: importance of the tumor microenvironment," *Trends Biotechnol*, 2023, doi: 10.1016/J.TIBTECH.2023.10.001/ATTACHMENT/FC599FB3-8F72-42E0-B68D-42282B5852CD/MMC1.DOCX.

[10] X. Zhang *et al.*, "Cancer-on-a-Chip: Models for Studying Metastasis," *Cancers (Basel)*, vol. 14, no. 3, Feb. 2022, doi: 10.3390/CANCERS14030648.

[11] S. Bersini, J. S. Jeon, M. Moretti, and R. D. Kamm, "In vitro models of the metastatic cascade: from local invasion to extravasation.," *Drug Discov Today*, vol. 19, no. 6, pp. 735–42, Jun. 2014, doi: 10.1016/j.drudis.2013.12.006.

[12] G. Rijal, C. Bathula, and W. Li, "Application of Synthetic Polymeric Scaffolds in Breast Cancer 3D Tissue Cultures and Animal Tumor Models," *Int J Biomater*, vol. 2017, 2017, doi: 10.1155/2017/8074890.

[13] S. Nagaraju, D. Truong, G. Mouneimne, and M. Nikkhah, "Microfluidic Tumor–Vascular Model to Study Breast Cancer Cell Invasion and Intravasation," *Adv Healthc Mater*, vol. 7, no. 9, p. 1701257, May 2018, doi: 10.1002/ADHM.201701257.

[14] E. Fröhlich, "The Variety of 3D Breast Cancer Models for the Study of Tumor Physiology and Drug Screening," *Int J Mol Sci*, vol. 24, no. 8, Apr. 2023, doi: 10.3390/IJMS24087116.

[15] M. Gadde *et al.*, "In vitro vascularized tumor platform for modeling tumor-vasculature interactions of inflammatory breast cancer," *Biotechnol Bioeng*, vol. 117, no. 11, pp. 3572–3590, Nov. 2020, doi: 10.1002/BIT.27487.

[16] M. Gadde, M. Mehrabi-Dehdezi, B. G. Debeb, W. A. Woodward, and M. N. Rylander, "Influence of Macrophages on Vascular Invasion of Inflammatory Breast Cancer Emboli Measured Using an In Vitro Microfluidic Multi-Cellular Platform," *Cancers 2023, Vol. 15, Page 4883*, vol. 15, no. 19, p. 4883, Oct. 2023, doi: 10.3390/CANCERS15194883.

[17] V. L. Silvestri, E. Henriet, R. M. Linville, A. D. Wong, P. C. Searson, and A. J. Ewald, "A tissue-engineered 3d microvessel model reveals the dynamics of mosaic vessel formation in breast cancer," *Cancer Res*, vol. 80, no. 19, pp. 4288–4301, Oct. 2020, doi: 10.1158/0008-5472.CAN-19-1564/653770/AM/A-TISSUE-ENGINEERED-3D-MICROVESSEL-MODEL-REVEALS.

[18] R. M. Linville *et al.*, "A tissue-engineered model of the blood-tumor barrier during metastatic breast cancer," *Fluids Barriers CNS*, vol. 20, no. 1, pp. 1–17, Dec. 2023, doi: 10.1186/S12987-023-00482-9/FIGURES/6.

[19] M. Crippa *et al.*, "A microphysiological early metastatic niche on a chip reveals how heterotypic cell interactions and inhibition of integrin subunit β3 impact breast cancer cell extravasation," *Lab Chip*, vol. 21, no. 6, pp. 1061–1072, Mar. 2021, doi: 10.1039/D0LC01011A.

[20] B. A. Dikici, S. Dikici, G. C. Reilly, S. MacNeil, and F. Claeyssens, "A Novel Bilayer Polycaprolactone Membrane for Guided Bone Regeneration: Combining Electrospinning and Emulsion Templating," *Materials*, vol. 12, no. 16, p. 2643, 2019, doi: 10.3390/MA12162643.

[21] N. R. Cameron, "High internal phase emulsion templating as a route to well-defined porous polymers," *Polymer (Guildf)*, vol. 46, no. 5, pp. 1439–1449, Feb. 2005, doi: 10.1016/J.POLYMER.2004.11.097.

[22] Z. Iqbal, W. Moses, S. Kim, E. J. Kim, W. H. Fissell, and S. Roy, "Sterilization Effects on Ultrathin Film Polymer Coatings for Silicon-based Implantable Medical Devices," *J Biomed Mater Res B Appl Biomater*, vol. 106, no. 6, p. 2327, Aug. 2018, doi: 10.1002/JBM.B.34039.

[23] K. Zhang, Y. Fan, N. Dunne, and X. Li, "Effect of microporosity on scaffolds for bone tissue engineering," *Regen Biomater*, vol. 5, no. 2, pp. 115–124, Mar. 2018, doi: 10.1093/rb/rby001.

[24] I. Bružauskaitė, D. Bironaitė, E. Bagdonas, and E. Bernotienė, "Scaffolds and cells for tissue regeneration: different scaffold pore sizes—different cell effects," *Cytotechnology*, vol. 68, no. 3, pp. 355–369, 2016, doi: 10.1007/s10616-015-9895-4.

[25] Y.-C. Chiu *et al.*, "The role of pore size on vascularization and tissue remodeling in PEG hydrogels," *Biomaterials*, vol. 32, no. 26, pp. 6045–6051, Sep. 2011, doi: 10.1016/j.biomaterials.2011.04.066.

[26] B. Aldemir Dikici and F. Claeyssens, "Basic Principles of Emulsion Templating and Its Use as an Emerging Manufacturing Method of Tissue Engineering Scaffolds," *Front Bioeng Biotechnol*, vol. 8, p. 875, Aug. 2020, doi: 10.3389/FBIOE.2020.00875/BIBTEX.

[27] T. Zhang, J. Xu, Y. Zhang, X. Wang, J. M. Lorenzo, and J. Zhong, "Gelatins as emulsifiers for oil-in-water emulsions: Extraction, chemical composition, molecular structure, and molecular modification," *Trends Food Sci Technol*, vol. 106, pp. 113–131, 2020, doi: 10.1016/J.TIFS.2020.10.005.

[28] S. S. Lee, M. Santschi, and S. J. Ferguson, "A Biomimetic Macroporous Hybrid Scaffold with Sustained Drug Delivery for Enhanced Bone Regeneration," *Biomacromolecules*, vol. 22, no. 6, pp. 2460–2471, Jun. 2021, doi: 10.1021/ACS.BIOMAC.1C00241/ASSET/IMAGES/LARGE/BM1C00241_0006.JPEG.

[29] Y. C. Jiang *et al.*, "Polycaprolactone Nanofibers Containing Vascular Endothelial Growth Factor-Encapsulated Gelatin Particles Enhance Mesenchymal Stem Cell Differentiation and Angiogenesis of Endothelial Cells," *Biomacromolecules*, vol. 19, no. 9, pp. 3747–3753, Sep. 2018, doi: 10.1021/ACS.BIOMAC.8B00870.

[30] S. Yang, K.-F. Leong, Z. M. E. Du, and C.-K. Chua, "The Design of Scaffolds for Use in Tissue Engineering. Part I. Traditional Factors," Mary Ann Liebert, Inc, 2001.

[31] A. Sharaf, J. P. Frimat, G. J. Kremers, and A. Accardo, "Suppression of auto-fluorescence from high-resolution 3D polymeric architectures fabricated via two-photon polymerization for cell biology applications," *Micro and Nano Engineering*, vol. 19, p. 100188, Jun. 2023, doi: 10.1016/J.MNE.2023.100188.

[32] G. Flamourakis *et al.*, "Low-autofluorescence, transparent composite for multiphoton 3D printing," *Optical Materials Express, Vol. 11, Issue 3, pp. 801-813*, vol. 11, no. 3, pp. 801–813, Mar. 2021, doi: 10.1364/OME.418269.

[33] M. B. Chen, J. A. Whisler, J. Fröse, C. Yu, Y. Shin, and R. D. Kamm, "On-chip human microvasculature assay for visualization and quantification of tumor cell extravasation dynamics," *Nature Protocols 2017 12:5*, vol. 12, no. 5, pp. 865–880, Mar. 2017, doi: 10.1038/nprot.2017.018.

[34] Y. Nashimoto *et al.*, "Integrating perfusable vascular networks with a three-dimensional tissue in a microfluidic device," *Integr Biol (Camb)*, vol. 9, no. 6, pp. 506–518, Jun. 2017, doi: 10.1039/C7IB00024C.

[35] F. Bonanini *et al.*, "In vitro grafting of hepatic spheroids and organoids on a microfluidic vascular bed," *Angiogenesis*, vol. 25, no. 4, pp. 455–470, Nov. 2022, doi: 10.1007/S10456-022-09842-9.

[36] A. Agrawal, S. Shahreza, Y. Javanmardi, N. Szita, and E. Moeendarbary, "The tumour microenvironment modulates cancer cell intravasation," *Organs-on-a-Chip*, vol. 4, p. 100024, Dec. 2022, doi: 10.1016/J.OOC.2022.100024.

[37] C. R. Oliver *et al.*, "A platform for artificial intelligence based identification of the extravasation potential of cancer cells into the brain metastatic niche," *Lab Chip*, vol. 19, no. 7, pp. 1162–1173, Mar. 2019, doi: 10.1039/C8LC01387J.

[38] F. Meng, C. M. Meyer, D. Joung, D. A. Vallera, M. C. McAlpine, and A. Panoskaltsis-Mortari, "3D Bioprinted In Vitro Metastatic Models via Reconstruction of Tumor Microenvironments," *Advanced Materials*, vol. 31, no. 10, p. 1806899, Mar. 2019, doi: 10.1002/ADMA.201806899.

Appendix

A. Supplementary Information for Chapter 3

Supplementary Material

Surfactant-Free Gelatin-Stabilised Biodegradable Polymerised High Internal Phase Emulsions with Macroporous Structures

Rachel Furmidge[1,2†], Caitlin E. Jackson[1,2†], María Fernanda Velázquez de la Paz[1,2], Victoria L. Workman[1,2], Nicola H. Green[1,2], Gwendolen C. Reilly[1,2], Vanessa Hearnden[1,2], Frederik Claeyssens[1,2]*

* Correspondence: Corresponding Author: f.claeyssens@sheffield.ac.uk

1.   Supplementary Methods, Figures and Tables

1   Characterisation of PCL-M and PGS-M using gel permeation chromatography (GPC)

Gel permeation chromatography (GPC) was used to determine the molecular weights of PCL-M and PGS-M. The samples were dissolved in tetrahydrofuran (0.10 mg/mL) and injected at a flow rate of 1 mL/min into a Viscotek GPCmax (VE2001), with a differential refractive index detector (Waters 410). Toluene was added as a reference and samples were analysed in a 650 mm PLgel 3 μm mixed E column at 40°C. Chromatogram peaks were analysed to determine the molecular weight average (Mw) and the polydispersity index (PD).

2   Characterisation of PCL-M and PGS-M by proton nuclear magnetic resonance (NMR) spectroscopy

The methacrylation of PCL-M and PGS-M was determined using proton (1H) nuclear magnetic resonance (NMR) spectroscopy. The spectrometer (Burker AVIIIHD 400 NMR spectrometer) frequency was set at 400MHz and data was recorded using a 30° pulse for excitation, 64k acquisition points over a spectral width of 20.5 ppm, 64 transients and a relaxation delay of 2 s. Samples were dissolved in 1 mL of deuterated chloroform at 1% w/v. Chemical shifts were referenced to the deuterated chlorofrom at 7.27 ppm. Spectra were analysed using MestReNova software (Version 11.0.4-18998, Mestrelab Research). The degree of methacrylation of PCL-M was determined by comparing the integrals of the methacrylate group peaks (5.5 and 6 ppm) to the peaks of the hydroxyl groups (3.6 ppm). The degree of methacrylation for PGS-M was determined by comparing the integrals of the methacrylate group peaks (1.9, 5.6 and 6.2 ppm) to the sebacic acid peak (1.3 ppm).
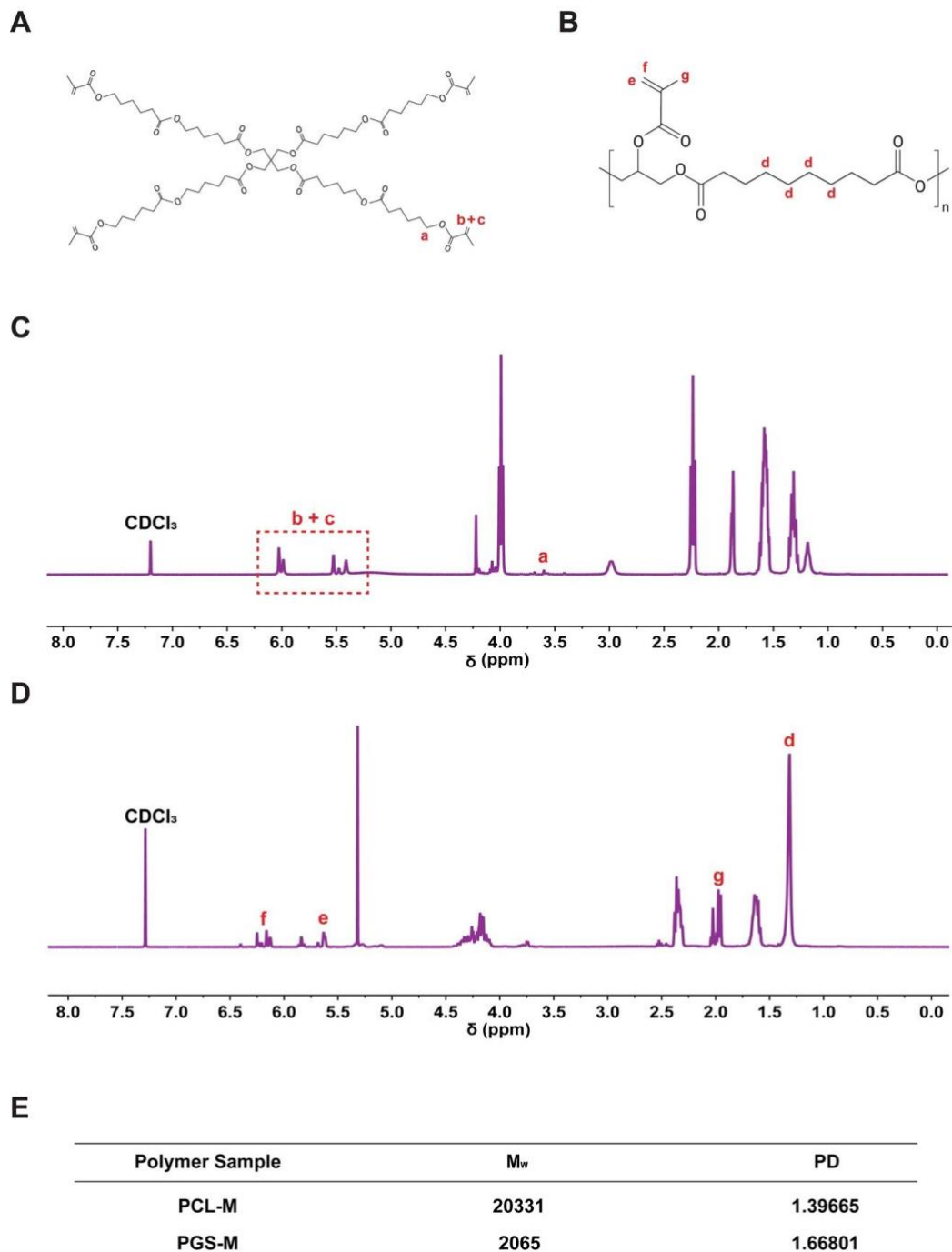
SUPPLEMENTARY FIGURE 1. Chemical structures of (A) PCL-M and (B) PGS-M, respectively. Created with BioRender.com. 1H+ NMR spectra of (C) PCL-M and (D) PGS-M. For PCL-M, peaks at 3.6 ppm represent (a) hydroxyl groups and peaks at 6 and 5.5 represent (b,c) methacrylate groups. For PGS-M, peaks at 1.3 ppm represent (d) sebacic acid and at 5.6, 6.2 and 1.9 ppm represent (e-g) methacrylate group peaks. (E) Molecular weight (Mw) and polydispersity index (PD) of PCL-M and PGS-M as measured by gel permeation chromatography (GPC).
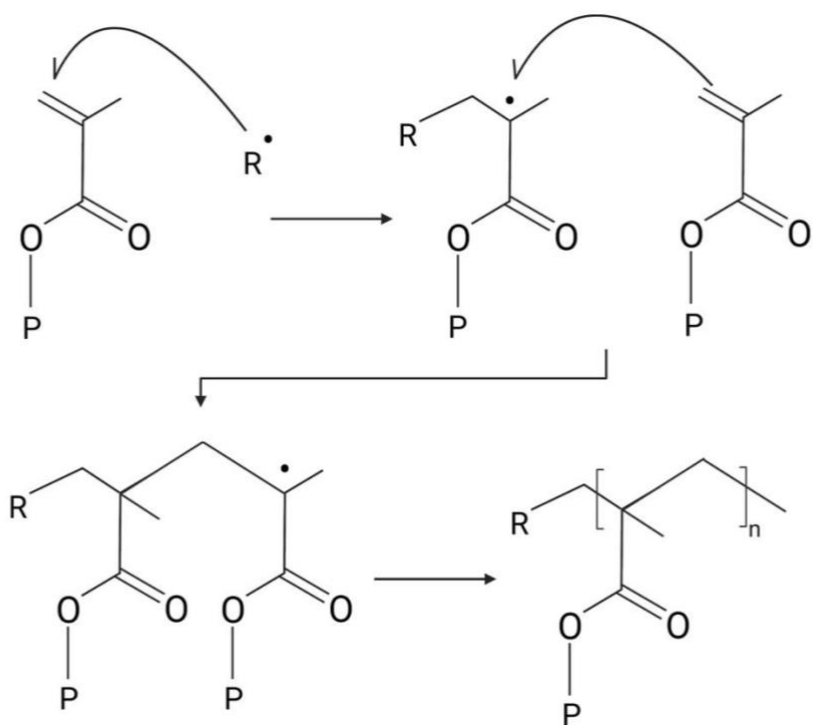
SUPPLEMENTARY FIGURE 2. Free radical polymerisation of PCL-M and PGS-M (P) methacrylate, Created with BioRender.com
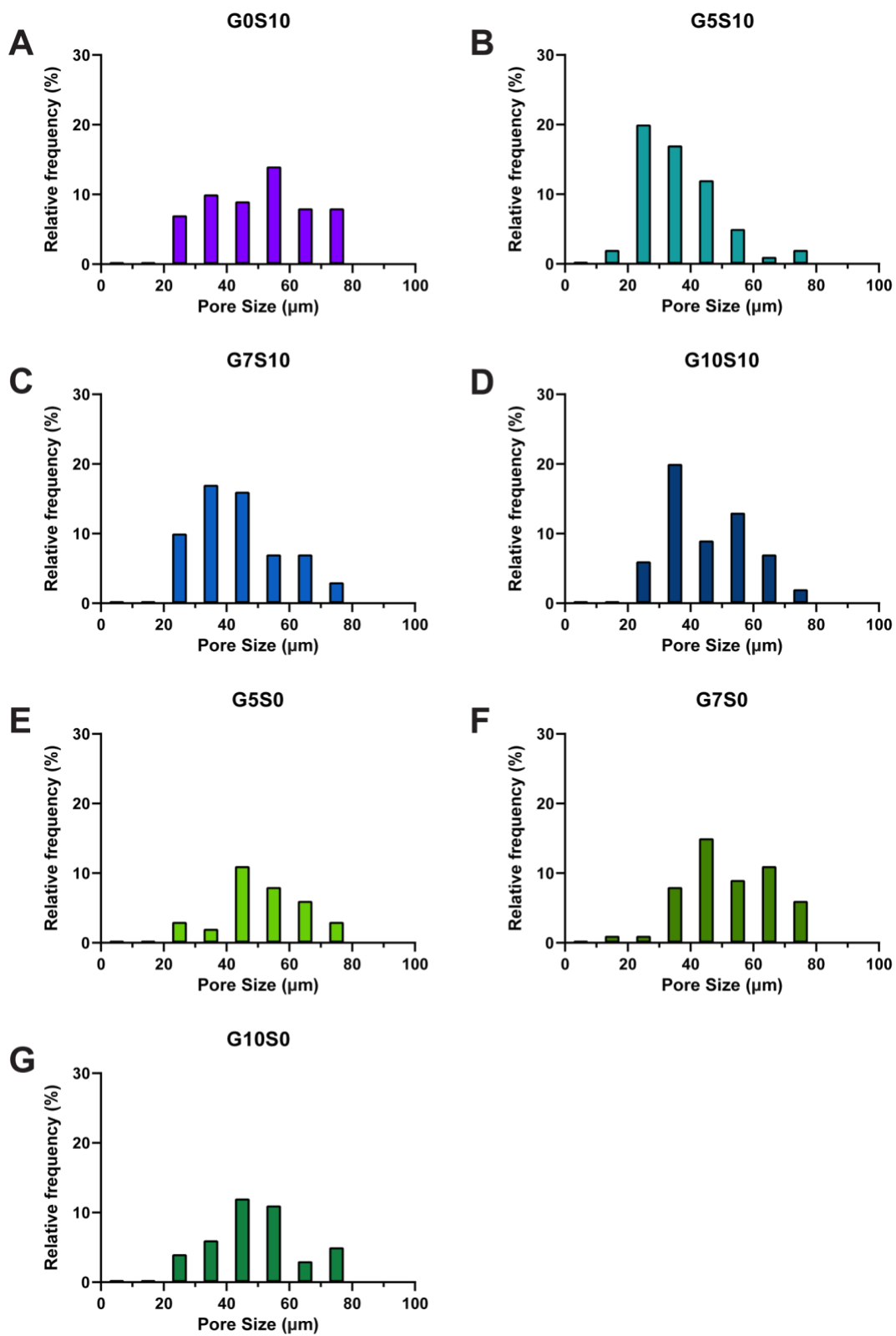
SUPPLEMENTARY FIGURE 3. Relative frequency and distribution of pore sizes in PCL-M polyHIPEs fabricated using different concentrations of gelatin ± surfactant.
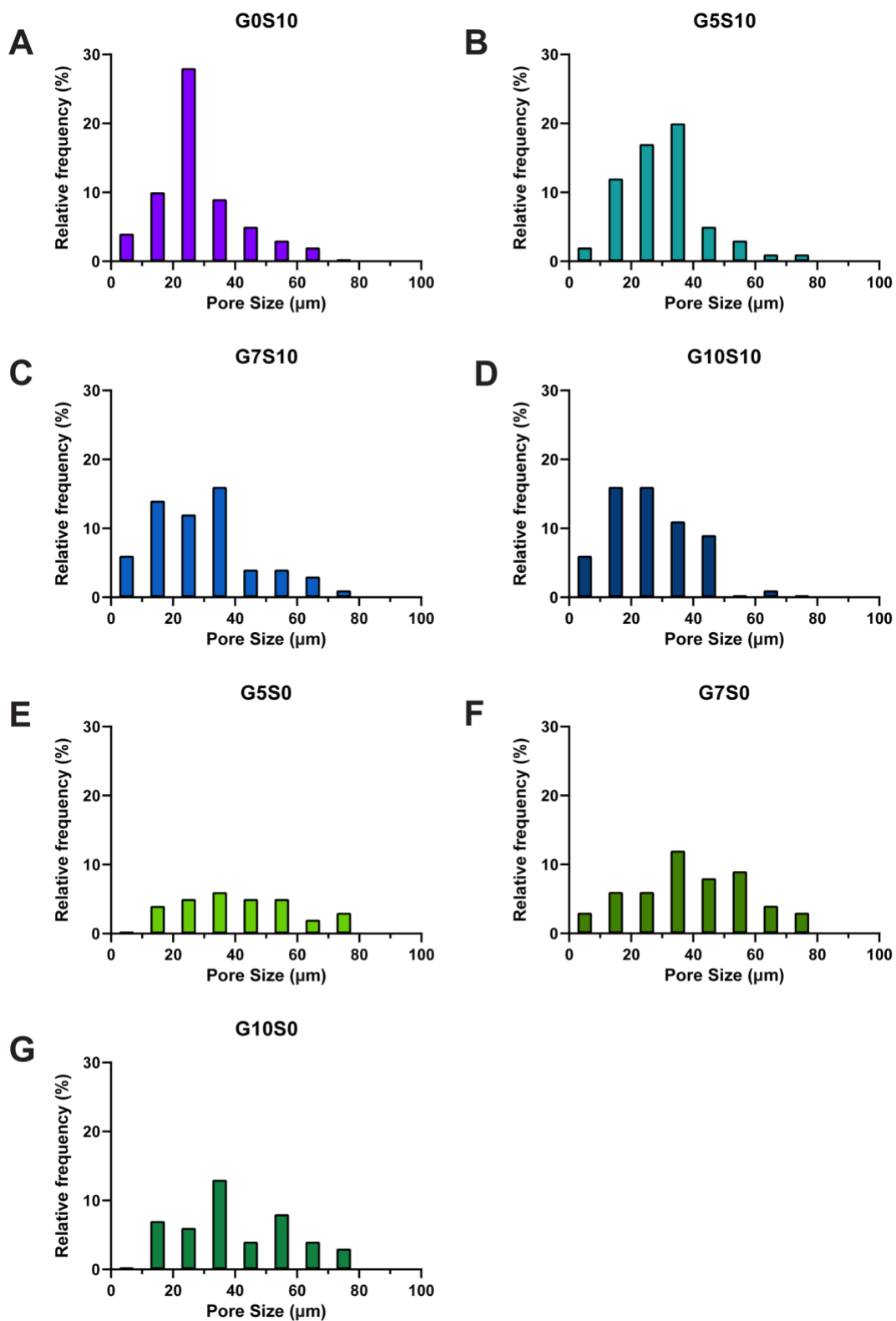
SUPPLEMENTARY FIGURE 4. Relative frequency and distribution of pore sizes in PGS-M polyHIPEs fabricated using different concentrations of gelatin ± surfactant.

SUPPLEMENTARY TABLE 1. Mean (± SD) stiffness of PCL-M and PGS-M polyHIPEs following the removal of gelatin via acetic acid and freeze drying ($n = 5$).

Emulsion	Mean Stiffness (MPa)	
	PCL	PGS
G0S10	1.26 ± 0.11	0.24 ± 0.018
G5S10	2.56 ± 0.37	1.69 ± 0.43
G5S0	2.18 ± 0.37	1.18 ± 0.23
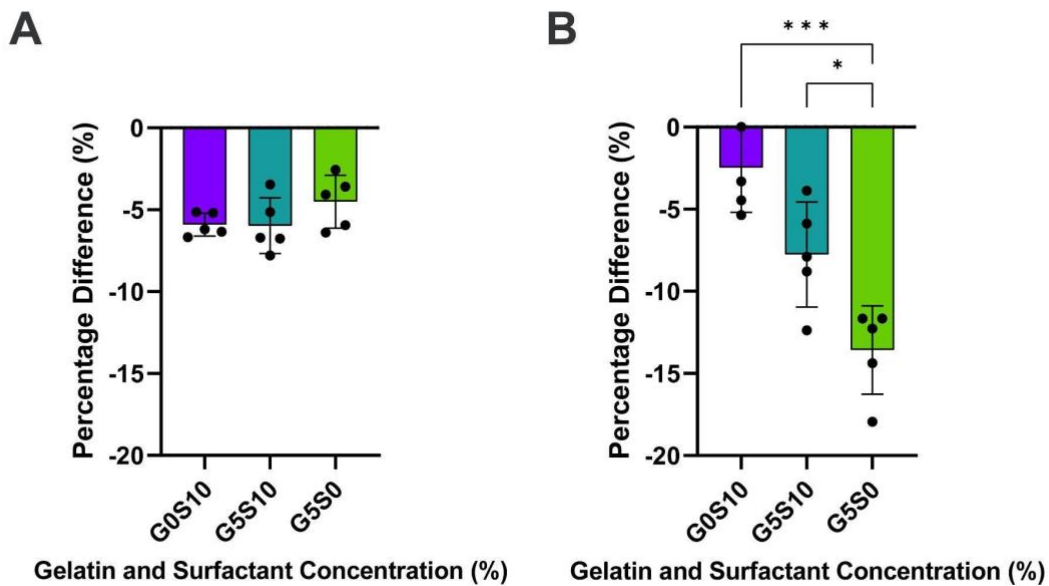
SUPPLEMENTARY FIGURE 5. The percentage difference in the size of **(A)** PCL-M and **(B)** PGS-M polyHIPEs from a wet to dry state following freeze drying (mean ± SD, $n = 5$, $* p < 0.033$, $*** p < 0.001$).
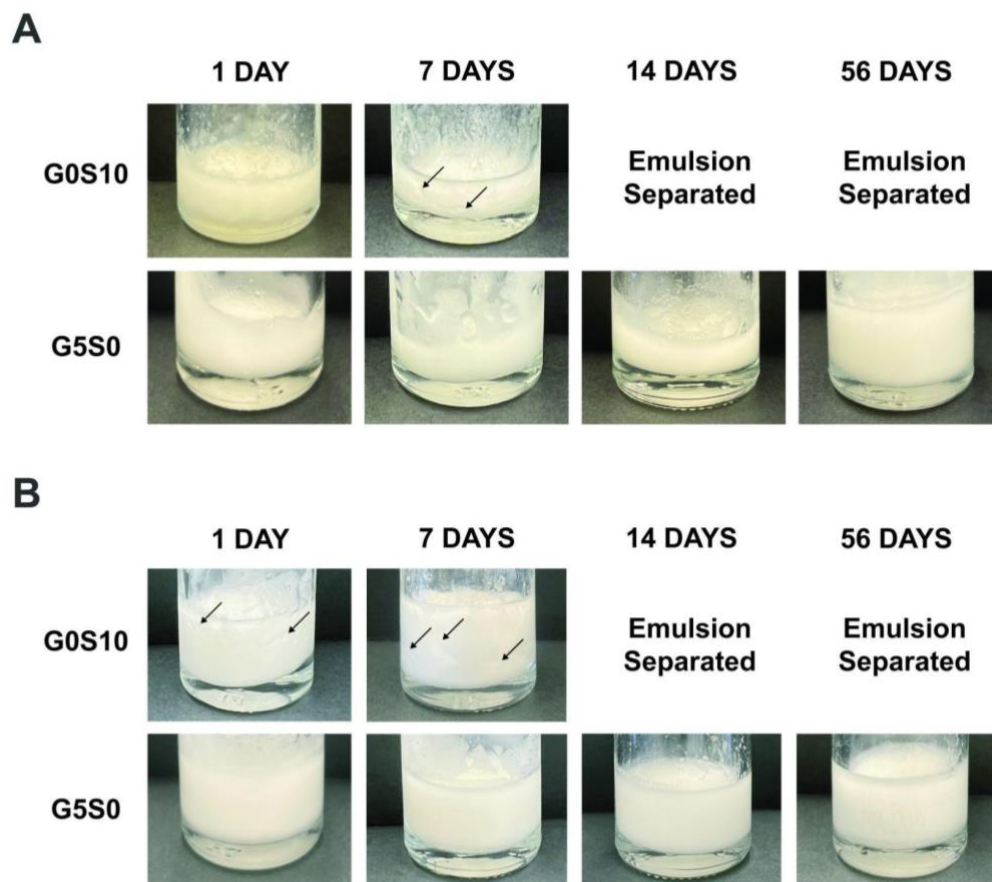
SUPPLEMENTARY FIGURE 6. (A) PCL-M and **(B)** PGS-M emulsions fabricated with water and surfactant (G0S10) or with gelatin and no surfactant (G5S0), following storage for 1 day, 7 days, 14 days and 56 days. Arrows indicate areas of visible phase separation. Emulsions not containing gelatin were not fabricated and stored for more than 7 days following emulsion separation observed at day 7.

B. Supplementary Information for Chapter 4

Supplementary Material

Gelatin-containing Porous Polycaprolactone PolyHIPEs as Substrates for 3D Breast Cancer Cell Culture and Vascular Infiltration

Caitlin E. Jackson[1,2], Iona Doyle[1], Hamood Khan[1], Samuel F. Williams[3], Betul Aldemir Dikici[4], Edgar Barajas Ledesma[1], Helen E. Bryant[5], William R. English[6], Nicola H. Green[1,2], Frederik Claeyssens[1,2]*

* Correspondence: f.claeyssens@sheffield.ac.uk
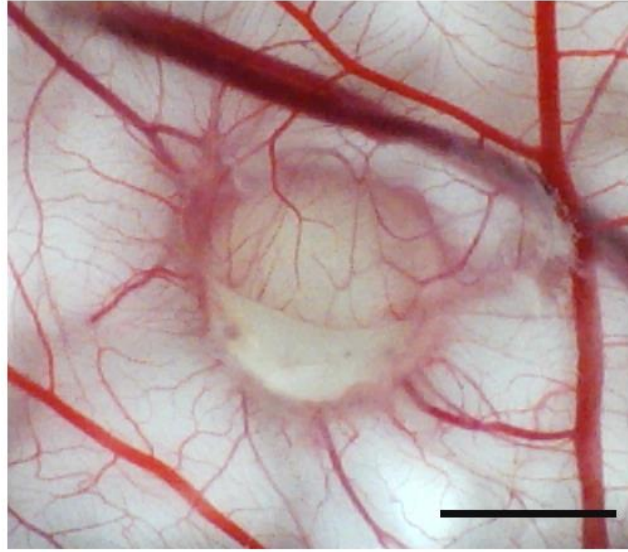
Supplementary Figures
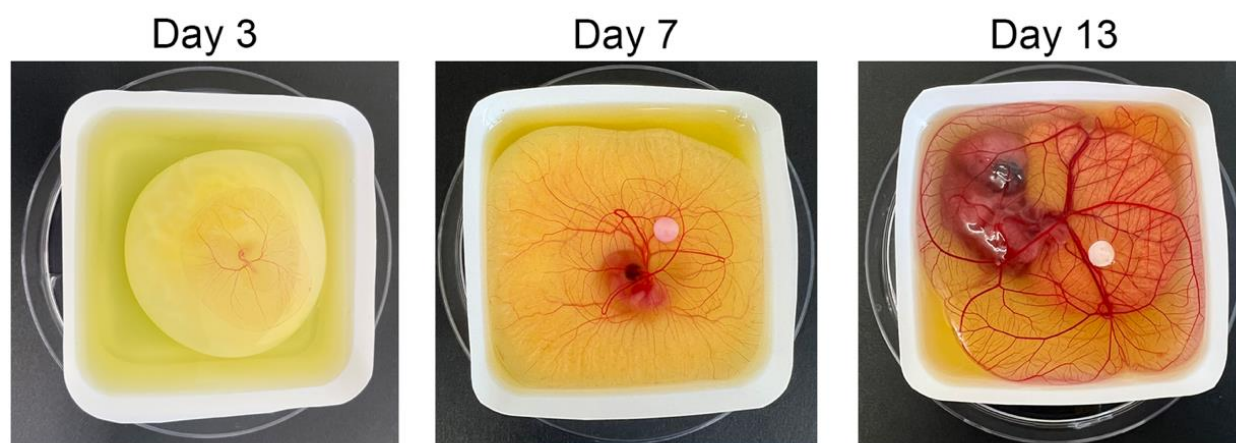
SUPPLEMENTARY FIGURE 1. The growth of the chick foetus and chorioallantoic membrane from cracking (day 3), to scaffold placement (day 7), to imaging (day 13).
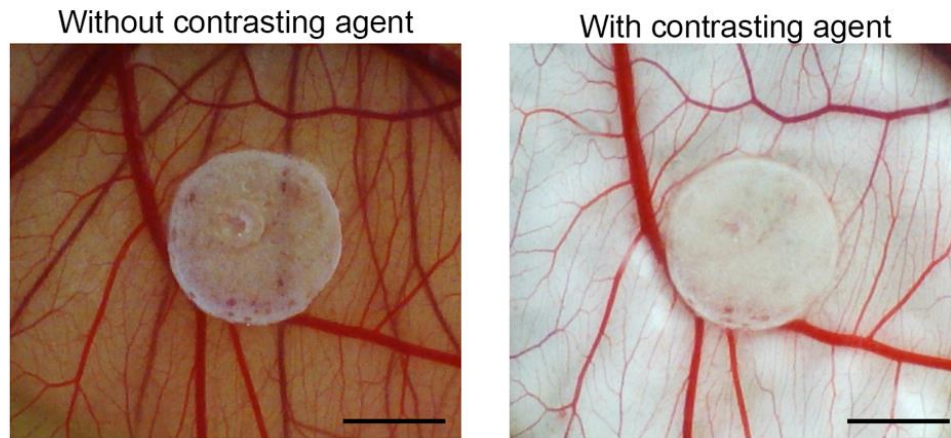
SUPPLEMENTARY FIGURE 2. Digital images demonstrating the effect of using a contrasting agent to improve the clarity of the vessels lying directly under the PCL-M polyHIPE scaffolds.
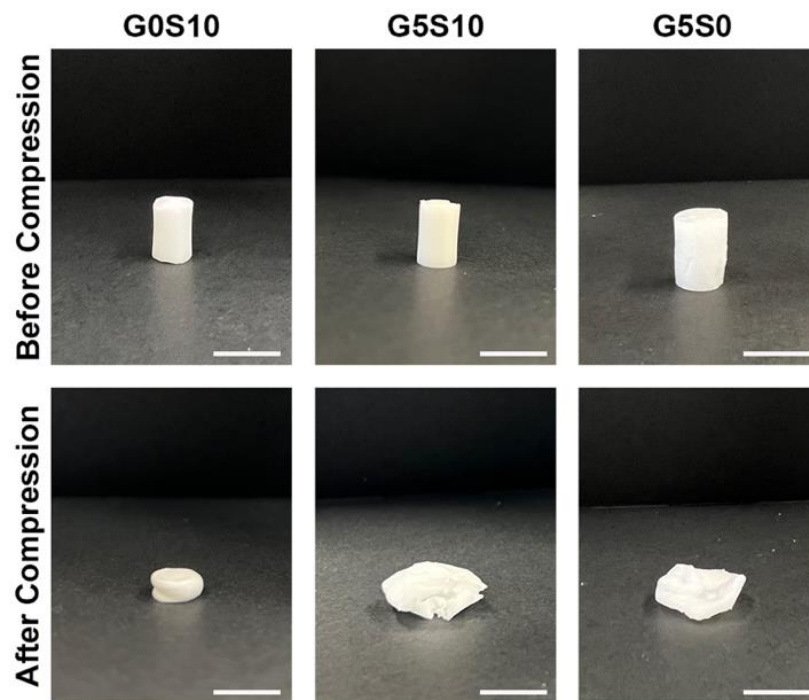
SUPPLEMENTARY FIGURE 3. Digital images, demonstrating the physical deformation experienced by PCL-M polyHIPEs containing gelatin following mechanical compression.

SUPPLEMENTARY FIGURE 4. Surfactant and gelatin-containing PCL-M polyHIPE enveloped by the chorioallantoic membrane (CAM).
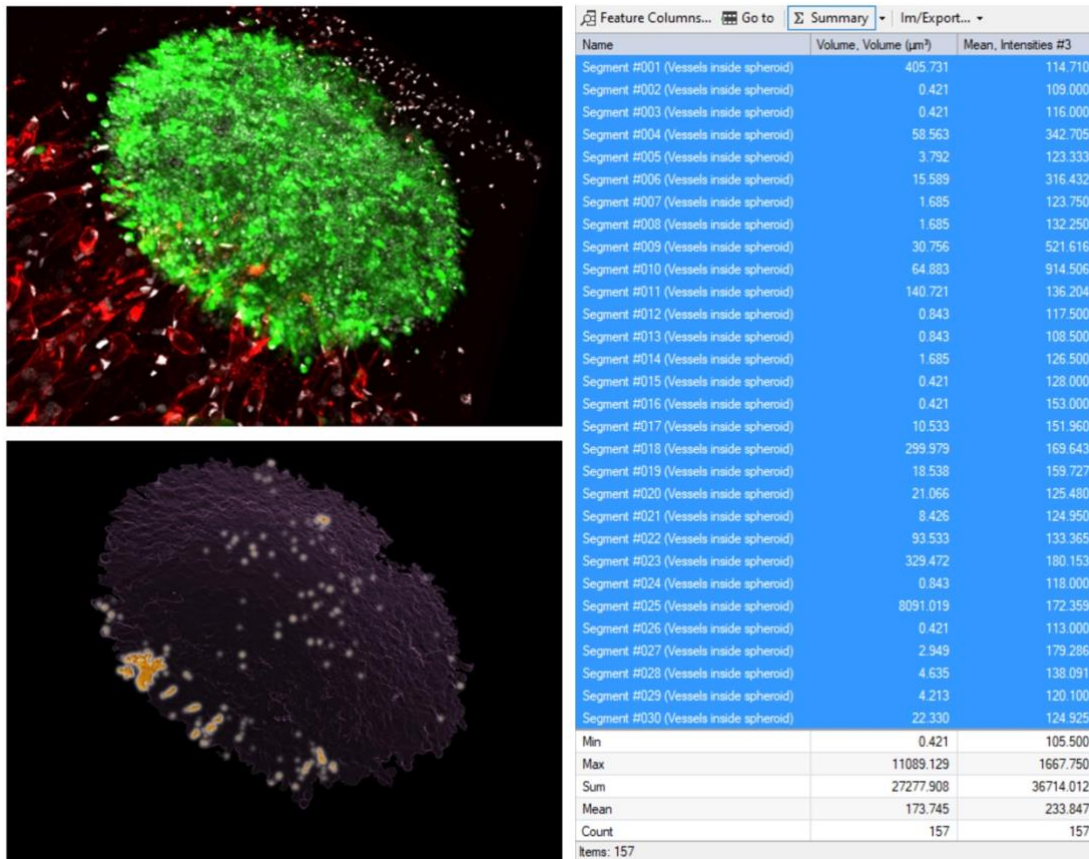
C. Supplementary Information for Chapter 5

Supplementary Material

Development of an *in vitro* vascularised tumour model for oncology applications.

C. E. Jackson[1*], N. L. Lam[2], C. E. Macdougall[3], T. S. P. Grandhi[2], H. Chenoweth[3], B. R. Miller[4], R. Kasprowicz[5], T. L. Gales[6], P. L. Candarlioglu[2§]

* Correspondence: cejackson1@sheffield.ac.uk
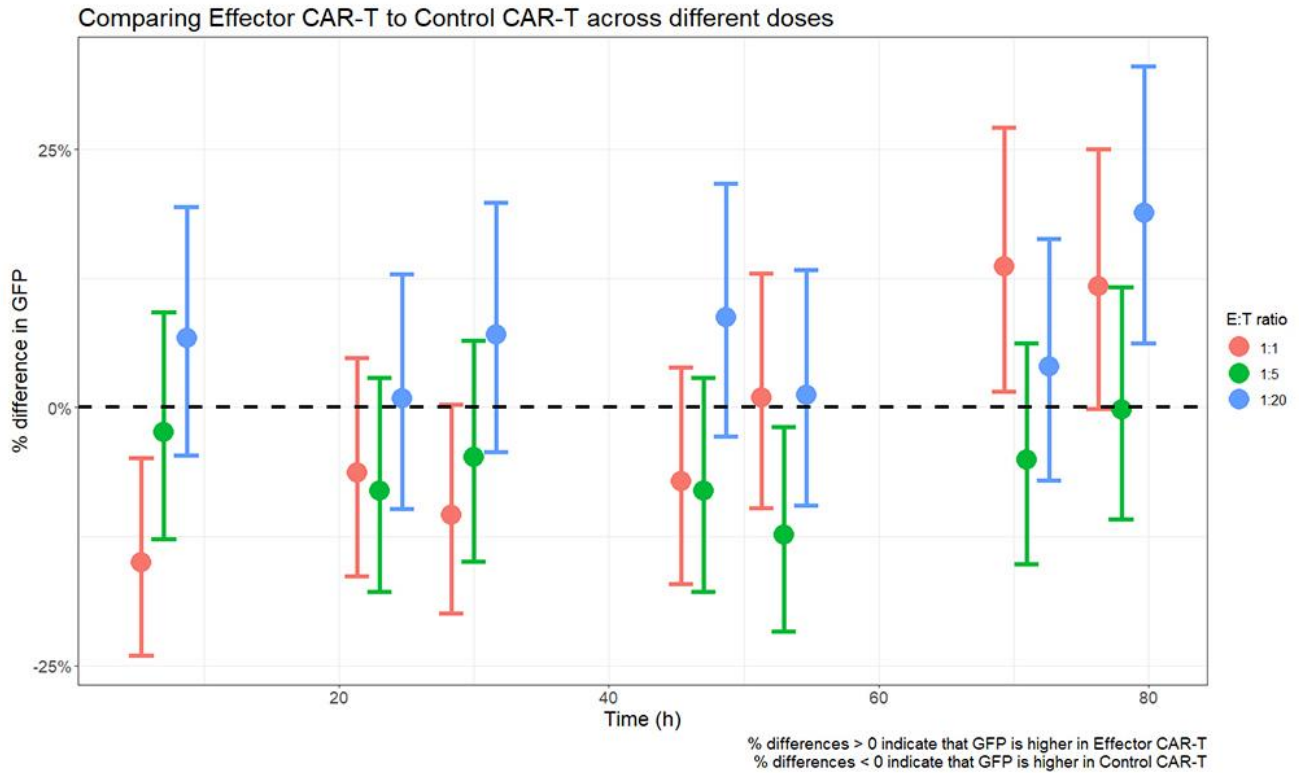
1.   Supplementary Figures and Tables

SUPPLEMENTARY FIGURE 1. Quantification of spheroid-infiltrating vessels using Vision4D (Arivis). Spheroids were segmented based on intensity and cell aggregates were excluded based on size. Spheroids were assigned with an object tag and volumes calculated. Following deionising and background correction, vessels were segmented within the spheroid object tag and sum of volumes calculated.
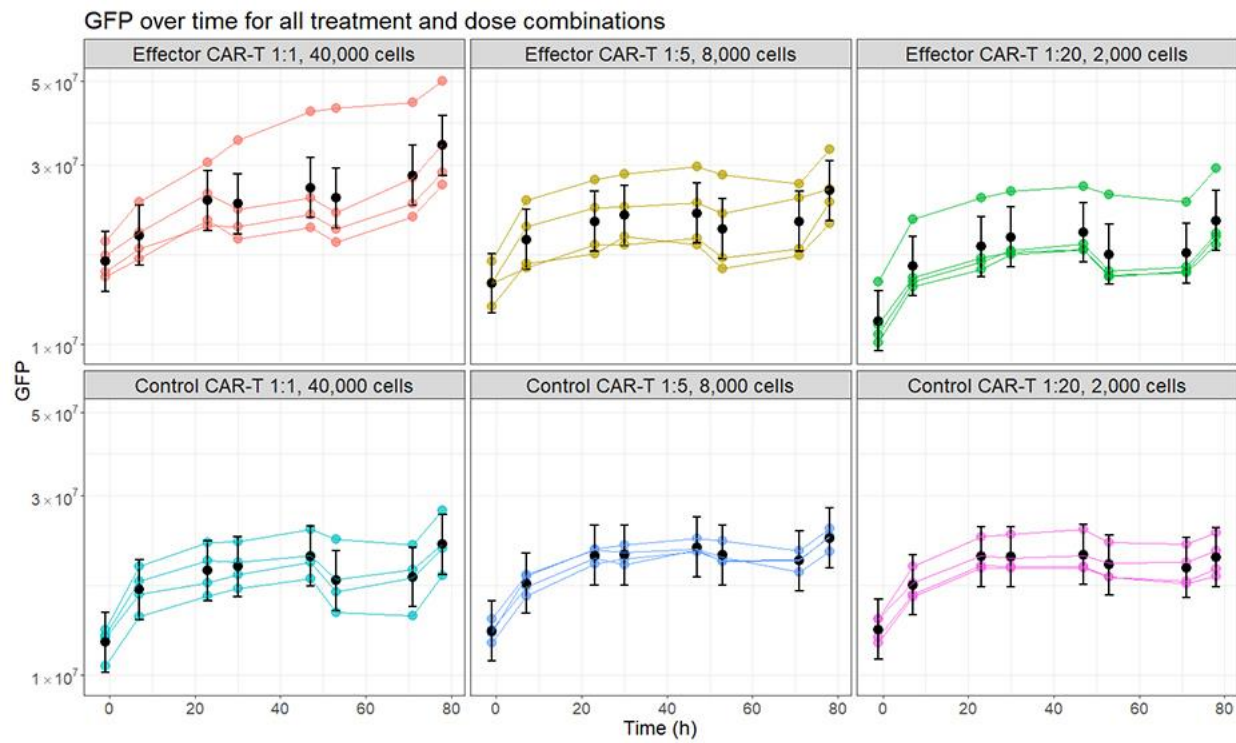
SUPPLEMENTARY FIGURE 2. Estimated mean GFP signal and corresponding 95% confidence intervals for all combinations of CAR-T cell types and effector:target ratio at each time point.

SUPPLEMENTARY FIGURE 3. Mean percentage differences (and corresponding 95% confidence intervals) in log10 GFP signal, comparing Effector CAR-T to Control CAR-T across all three effector:target ratios at each time point. As baseline differences are observed at -1 h, we decide to normalise to these baseline differences when carrying out the linear contrasts. As treatment is aliased with column in the plate plan, baseline differences may represent a column effect, similar to the row effect that was observed and accounted for in the statistical model. Here, normalising to treatment baseline is equivalent to normalising to column baseline, statistically accounting for any potential column effect. Additionally, a table showing all percentage changes and corresponding p-values is shown in Table S1.

SUPPLEMENTARY TABLE 1. Mean percentage differences and corresponding 95% confidence intervals in log10 GFP signal, comparing Effector CAR-T to Control CAR-T across all three effector:target ratios at each time point. Additionally, an uncorrected p-value is displayed which tests the hypothesis that mean GFP signal is equal across Effector and Control CAR-T cells.

Linear contrast	% difference in log10 GFP	95% confidence interval	p-value
1:1, 7 hours	-14.974%	(-24.017%, -4.854%)	0.005
1:5, 7 hours	-2.389%	(-12.771%, 9.228%)	0.671
1:20, 7 hours	6.741%	(-4.612%, 19.445%)	0.253
1:1, 23 hours	-6.348%	(-16.308%, 4.798%)	0.251
1:5, 23 hours	-8.074%	(-17.851%, 2.867%)	0.141
1:20, 23 hours	0.894%	(-9.837%, 12.902%)	0.876
1:1, 30 hours	-10.382%	(-19.914%, 0.284%)	0.056
1:5, 30 hours	-4.823%	(-14.946%, 6.505%)	0.386
1:20, 30 hours	7.1%	(-4.291%, 19.847%)	0.230
1:1, 47 hours	-7.186%	(-17.058%, 3.86%)	0.192
1:5, 47 hours	-8.047%	(-17.827%, 2.897%)	0.142
1:20, 47 hours	8.764%	(-2.804%, 21.708%)	0.142
1:1, 53 hours	0.982%	(-9.758%, 13%)	0.864
1:5, 53 hours	-12.338%	(-21.662%, -1.905%)	0.022
1:20, 53 hours	1.249%	(-9.52%, 13.299%)	0.827
1:1, 71 hours	13.633%	(1.547%, 27.157%)	0.026
1:5, 71 hours	-5.051%	(-15.15%, 6.249%)	0.363

Supplementary Material

Linear contrast	% difference in log10 GFP	95% confidence interval	p-value
1:20, 71 hours	3.956%	(-7.101%, 16.328%)	0.496
1:1, 78 hours	11.771%	(-0.117%, 25.073%)	0.052
1:5, 78 hours	-0.253%	(-10.862%, 11.619%)	0.965
1:20, 78 hours	18.888%	(6.244%, 33.038%)	0.003

D. Supplementary Information for Chapter 6

Supplementary Material

The effect of sterilisation techniques on MDA-MB-231 cell metabolic activity

Supplementary Methods and Figures

1.   Assessment of polyHIPE pore structure

To analyse the effect of ethanol and autoclave sterilization techniques on the microstructure of PCL-M polyHIPEs, scaffolds discs (8 mm diameter and 1 mm depth) were sterilised in 70% ethanol followed by dH_2O or autoclaved (121°C for 15 min). The pore morphology was analysed using a scanning electron microscope (SEM, Inspect F, FEI, United States). Samples were subject to the deposition of gold coating. To avoid surface charging and damage to the sample a low accelerating voltage of 5kV with a spot size of 3 and a typical vacuum pressure of 10−5 mbar at a working distance of 10 mm was applied.

2.   MDA-MB-231 cell seeding on PCL-M polyHIPE scaffolds

To initially characterise the effect of sterilisation techniques on cell-scaffold interactions, polyHIPE discs (8 mm diameter and 1 mm depth) were used. All scaffolds were either sterilised in 70% ethanol followed by dH_2O or autoclaved (121°C for 15 min). Once reaching 90% confluency, cells were detached from the cell culture flask using trypsin. After 4 min the trypsin was neutralised with cell culture media (ratio of 1:2 respectively), followed by centrifugation (95 × g for 5 min) and resuspended in fresh media before counting using the trypan blue exclusion method to assess cell viability. 25 µL of MDA-MB-231 cells at 2×10^6 cells/mL was transferred onto each scaffold and left for 30 min in the incubator (37ºC and 5% CO_2) to allow for cell attachment. After 30 min, fresh media was placed in each well and incubated for 7 days.

### 3.   Cell Viability on PCL-M polyHIPE scaffolds

The viability of cells on the scaffold was assessed using the resazurin reduction (RR) assay. 1 mM resazurin stock solution was diluted in cell culture media to form a 10% v/v resazurin working solution. The media was removed and discarded from each well and a further 0.5 ml of the working solution was added to each well. The well plate was protected from light and incubated for 4 h at 37ºC. An

orbital rocker (30 rpm) was used in the incubator to ensure full penetration of the resazurin working solution. 150 µL was taken, in triplicate, from each scaffold and transferred to a 96 well plate. A fluorescence microplate reader (BioTek FLx800, Agilent BioTek, Santa Clara, CA, USA) was used to read the fluorescence of each well at an excitation wavelength of 540 nm and an emission wavelength of 630 nm. The working solution was removed from the scaffolds and each scaffold was further washed with PBS three times before adding fresh cell culture media and continuing incubation. The assay was performed at day 1 and repeated at day 3 and 7.

4.   Statistical Analysis

Statistical analysis was carried out using analysis software GraphPad Prism (Version 9.4.1, CA, USA). All data was analysed using a two-way analysis of variance (ANOVA) followed by Tukeys multiple comparisons test. Error bars on graphs indicate standard deviation and significance on the graph is represented as p-value < 0.033 (*) and 0.001 (***).
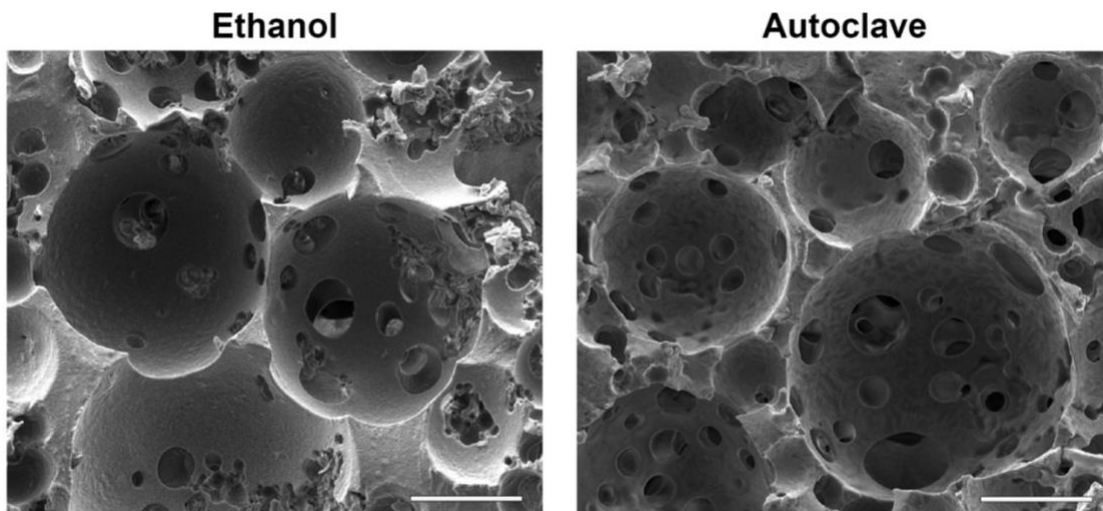
SUPPLEMENTARY FIGURE 1. Scanning electron micrographs of PCL-M polyHIPEs sterilised in 70% ethanol or autoclaved (scale bar = 25 µm).
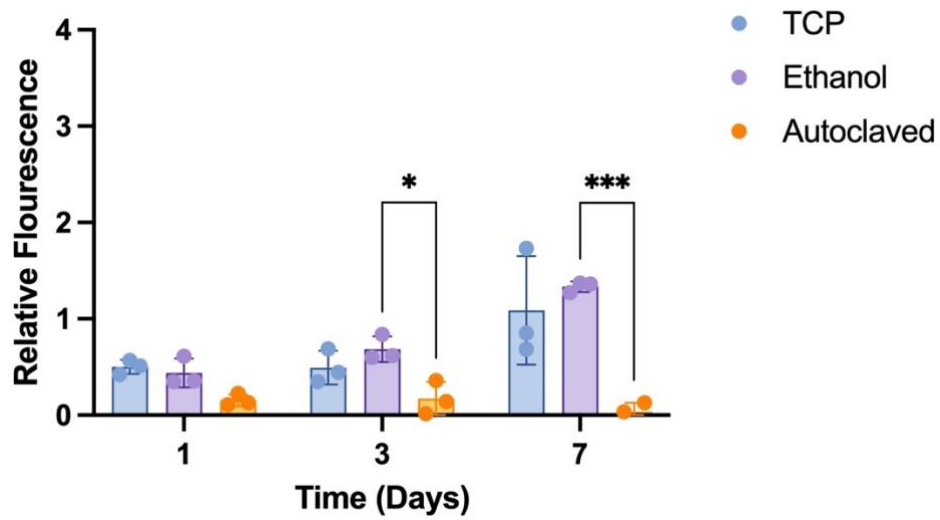
SUPPLEMENTARY FIGURE 2. Biological assessment of PCL–M polyHIPEs sterilised by 70% ethanol or autoclaved with tissue culture plastic (TCP) control, evaluating the metabolic activity of MDA-MB-231 cells via a resazurin reduction assay across 7 days (mean ± SD, N=3, $n = 3$).

E. RRI Plan

D.1 Briefly outline your research project

Cancer is a becoming a huge social and economic burden on society, being the most significant barrier to life expectancy in the 21st century. One of the most significant difficulties to finding efficient therapies for specific cancers, such as breast cancer, is the efficiency and ease of drug development and testing. Micro-physiological systems (MPS) are under development to mimic the structural and biological complexity of human tissue, thus, becoming increasingly popular as an alternative to animal testing for pharmaceuticals. However, the lack of a system for perfusion within current models remains a challenge.

This project will utilise high internal phase emulsions templating techniques to create an *in vitro* vascularised tissue via fabrication of a porous PCL polyHIPE scaffold. The porous network will allow for vascular ingrowth to occur in a scaffold in which cells can be seeded. This will be developed to overcome the short comings in current models and provide an *in vitro* alternative to *in vivo* testing platforms and will be used to explore cancer models, mainly focussing on metastatic breast cancer.

D.2 Are there any major controversial concerns relating to this work? If so, how are they being considered?

My project was based on providing an alternative method testing platform for drug testing. Therefore, there are no major controversial concerns that are associated with the project. Throughout, the project I used the chick chorioallantoic membrane (CAM) assay to investigate biocompatibility and potential for vascular ingrowth. This utilises the vascular network of a chick foetus, all work was undertaken and the chick was sacrificed before the chick has developed a nervous system. Furthermore, this work was completed following the guidelines of the Home Office, UK.

D.3 Anticipate, Reflect, Engage, Act

D.3.1 Public/Stakeholder engagement

Some of our CDT and project stakeholders include the external advisory board, directors and individual project supervisors. As a cohort we planned a mini-conference which showcased our projects and the progress to date. Ideally, the conference would have been held in person but due to social distancing restrictions we adapted the proceeding to an online conference. My

supervisors are very important stakeholders in my project and as such I will be in contact with them at least every two weeks if not every week.

As part of public engagement of my project I completed a blog post that was available for the public to read, relating to life as CDT student. I have also attended and presented at many conferences sharing my work and gaining opportunities to engage with other researchers and industry members, learning how my work could be best suited and adapted to their needs.

Within my project I was able to work with GlaxoSmithKline with their research team. Throughout this experience I was able to connect and network with many people within the pharmaceutical industry, learning the current needs and requirements within the industry. The outcome of my project would be to reduce the need for animal testing and thus pharmaceutical companies could be viewed as potential stakeholders.

D.3.2 Science Education

As a cohort we took part in an outreach programme in March 2020 at the Whitworth gallery. This activity included helping to teach the children about plants (part of their curriculum) whilst using engineering tools such as 3D printer doodle pens and microscopes. During COVID there we were not able to deliver in person outreach activities. To overcome this, I presented a why study video, aimed at secondary school children, explaining my journey into science, why I love research and trying to inspire the next generation of scientists. Following becoming a STEM ambassador, I was able to take part in the North Star outreach day. This day involved guiding year 8/9 students round multiple STEM activities, showing them numerous future routes into science that they could follow.

D.3.3 Equality, Diversity and Inclusion

Through the duration of my project, I did not interact with patients or members of public in any trials. However, when working in a collaboration with other PhD students, post docs or supervisors I aimed to ensure the EDI values were in place. I worked within a diverse team guaranteeing the inclusion of all people however it was also beneficial to my work as a more diverse range of ideas were pooled. When organising events as part of the CDT EDI Social Calendar project we ensured EDI was always taken into account for all attendees, ensuring it was open to all in an accessible, friendly environment which was comfortable for all.

D.3.4 Open Access

Throughout my PhD I have been fortunate enough to publish my work. Each publication has been published via open access to ensure that my work is publicly available for other researchers to access and hopefully help further research within the area at a quicker rate.

D.3.5 Ethics

When completing any CAM assays, I ensured that the Home Office guidelines were met and the paperwork associated with each experiment was kept up to standard for official records. When conducting my research, all reporting of my data was ethical and I ensured there was no misrepresentation of data or results and all data was presented in full, with complete honesty. By completing a data management plan, I had an organised plan in place to store my data in a safe and secure place which can also be accessed by supervisors for complete transparency in my work. I endeavour to follow the University's good research and innovation practises (GRIP) guidance. This document outlines the expectations for ethically undertaking research.

D.3.6 Governance

I ensured that I followed all rules and regulations that surrounded my work and work environment. Within my PhD, due to social distancing, there was increased restrictions on training, these complications were overcome by following the additional guidelines, however it did impact the timeline for my work, increasing the time taken to train on equipment. Being part of committees within the CDT such as the outreach committee and representing my CDT cohort at management committee meeting allowed me to take part and shape the governance of the CDT.

D.3.7 Sustainability

I worked with biodegradable polymers, therefore any waste or used polymer will biodegrade in approximately a year. However, the involved lab work of my project contributes to chemical and plastic waste. I could not remove this waste from my project however, I aimed to reduce waste by thoroughly planning the correct number of experiments and using the correct amount of reagents each time so little was wasted. Using glassware that can be cleaned and reused was an additional method to reduce waste.